
Doctoral

Tourism and Food

2007-06-01

Novel copper(II) and silver(I) complexes incorporating benzimidazole and related nitrogen donor ligands: synthesis, biomimetic, anticancer and antifungal activities

Mark O'Connor
Technological University Dublin

Follow this and additional works at: <https://arrow.tudublin.ie/tourdoc>

 Part of the [Food Science Commons](#)

Recommended Citation

O'Connor, Mark, "Novel copper(II) and silver(I) complexes incorporating benzimidazole and related nitrogen donor ligands: synthesis, biomimetic, anticancer and antifungal activities" (2007). *Doctoral*. 6. <https://arrow.tudublin.ie/tourdoc/6>

This Theses, Ph.D is brought to you for free and open access by the Tourism and Food at ARROW@TU Dublin. It has been accepted for inclusion in Doctoral by an authorized administrator of ARROW@TU Dublin. For more information, please contact arrow.admin@tudublin.ie, aisling.coyne@tudublin.ie, vera.kilshaw@tudublin.ie.

**Novel Copper(II) and Silver(I) Complexes
incorporating Benzimidazole and related Nitrogen
Donor Ligands: Synthesis, Biomimetic,
Anticancer and Antifungal activities.**

011

A THESIS SUBMITTED TO DUBLIN INSTITUTE OF TECHNOLOGY IN
FULFILMENT OF THE REQUIREMENTS FOR THE DEGREE OF

DOCTOR OF PHILOSOPHY

Mark O' Connor B.Sc.

School of Food Science and Environmental Health,
Dublin Institute of Technology,
Marlborough St.,
Dublin 1.

June 2007

Research Supervisor: Prof. Michael Devereux
Head of School (Acting): Dr. Gary Henahan

Abstract

This project describes the synthesis and biomimetic/biological properties of sixty nine copper(II) and silver(I) complexes. The complexes were derived from reactions of four copper(II) carboxylate compounds along with copper(II) and silver(I) salts with various nitrogen donor ligands. Approximately sixty of the complexes are novel. X-ray crystal structures for five of the novel copper(II) complexes are reported.

$[\text{Cu}(\text{salH})_2(\text{H}_2\text{O})_2]$ (1), $[\text{Cu}_2(\text{asp})_4(\text{H}_2\text{O})_2] \cdot \text{H}_2\text{O}$ (2), $[\text{Cu}(\text{dipsH})_2(\text{H}_2\text{O})]$ (3) and $\{\text{Cu}(\text{msal})(\text{H}_2\text{O})\}_n$ (4) were generated when copper(II) hydroxide was reacted with the relevant carboxylic acid. Complexes (1) - (4) reacted with simple benzimidazoles to yield twelve complexes with three of them being structurally characterised. When (1) - (4) were reacted with the potential chelating ligands thiabendazole, 2-(2-pyridyl)benzimidazole, 1,10-phenanthroline and 2,2'-bipyridine twelve complexes resulted with one of them being structurally characterised.

Copper(II) acetate and the simple copper(II) salts, copper sulfate and copper chloride were each reacted with both the chelating and the simple benzimidazole ligands to yield twenty complexes with one being structurally elucidated by X-ray analysis.

Silver(I) salicylate ($[\text{Ag}_2(\text{salH})_2]$) was generated as described in the literature. All attempts to generate benzimidazole derivatives of $[\text{Ag}_2(\text{salH})_2]$ were unsuccessful. The silver(I) salts, silver nitrate, silver sulfate and silver acetate were reacted with both the chelating and the simple benzimidazole ligands to yield nineteen complexes.

None of the fifty copper(II) complexes generated during this study exhibited significant catalase activity but all did show SOD mimetic properties and selected complexes also exhibited anticancer activity against three human derived cancer cell lines. The antifungal activities of all of the complexes were also examined against the pathogen *Candida albicans*. At higher concentrations the majority of the copper(II) complexes exhibit very good activity but as the concentration is decreased their efficacy diminishes significantly. All of the silver(I) derivatives were extremely photo-stable and exhibited anti-mycotic activity far greater than the prescription drug Ketoconazole.

Declaration

I certify that this thesis which I now submit for examination for the award of Doctor of Philosophy, is entirely my own work and has not been taken from the work of others save and to the extent that such work has been cited and acknowledged within the text of my own work.

This thesis was prepared according to the regulations for postgraduate study by research of the Dublin Institute of Technology and has not been submitted in whole or in part for an award in any other Institute or University.

The work reported on in this this thesis conforms to the principles and requirements of the Institutes guidelines for ethics in research.

The Institute has permission to keep, to lend or to copy this thesis in whole or in part, on condition that any such use of the material of the thesis be duly acknowledged.

Signature Mark O'Carroll Date 20/8/07.

Acknowledgements

Firstly I would like to sincerely thank my supervisor Prof. Michael Devereux for his excellent guidance throughout these four years. Dr. Gary Henehan (Acting Head of School, Department of Food Science and Environmental Health, Dublin Institute of Technology, Cathal Brugha Street). A Strand I Research Grant from the Irish Technology Sector, funded through DIT is gratefully acknowledged.

I would like to thank Dr. Georgina Rosair for carrying out the X-ray crystallography work. I'd also like to thank Dr. Denise Egan and Dr. Fiona Lyng for undertaking the chemotherapeutic testing on a number of the compounds.

I'd like to thank all the academic and technical staff in DIT Cathal Brugha St., especially Noel. I'd like to thank Andrew and Aoife for four great years.

Finally, I'd like to thank my parents for their unfailing support throughout my college years.

Symbols and Abbreviations

$^{\circ}$	Degrees
Λ_M	molar conductivity ($S\text{ cm}^2\text{ mol}^{-1}$)
\AA	Angstrom (10^{-10}m)
ν	wavenumber (cm^{-1})
λ_{max}	max wavelength of maximum absorbance in nm
ϵ	molar extinction coefficient ($\text{dm}^3\text{ mol}^{-1}\text{ cm}^{-1}$)
$\mu_{\text{eff}}(\text{B.M.})$	effective magnetic moment (Bohr magneton)
μ_{so}	spin-only paramagnetism
$^{\circ}\text{C}$	degree Celsius
K	Kelvin
salH ₂	salicylic acid
dipsH ₂	3,5-diisopropylsalicylic acid
msalH ₂	3-methoxysalicylic acid
BZDH	benzimidazole
5-BZDHCOOH	5-benzimidazolecarboxylic acid
2-AmBZDH	2-aminobenzimidazole
2-CIBZDH	2-chloromethylbenzimidazole
2,5-Me ₂ BZDH	2,5-dimethylbenzimidazole
5,6-Me ₂ BZDH	5,6-dimethylbenzimidazole

6-NO ₂ BZDH	6-nitrobenzimidazole
2-PhBZDH	2-phenylbenzimidazole
2-PyBZDH	2-(2-pyridyl)-benzimidazole
TBZH	thiabendazole
2-MeOHBZDH	1H-benzimidazole-2-Methanol
phen	1,10-phenanthroline
bipy	2,2'-bipyridyl
EDTA	ethylenediaminetetraacetic acid
DMSO	dimethylsulphoxide
EtOH	ethanol
OAc	acetate
MeOH	methanol
Ph	phenyl
PPh ₃	triphenylphosphine
R	alkyl, aryl, aromatic substituent
DNA	deoxyribonucleic acid
HIV	Human Immunodeficiency Virus
MIC	minimum inhibitory concentration
IC	inhibitory concentration

PBS	phosphate buffered saline
SDA	sabouraud dextrose agar
SOD	superoxide dismutase
CAT	catalase
<i>ca.</i>	circa
h, min, s	hours, minutes, seconds
IR	infra-red
<i>sym, asym</i>	symmetric and asymmetric, respectively

TABLE OF CONTENTS:

INTRODUCTION	1
I.1 CHEMISTRY OF THE GROUP 11 METALS COPPER AND SILVER	2
I.1.1 General chemistry of the group 11 elements	2
I.1.2 Copper(I) chemistry	2
I.1.3 Copper(II) chemistry	4
I.1.4 General metabolic functions of copper	5
I.1.5 Silver(I) chemistry	6
I.1.6 Silver(II) chemistry	6
I.1.7 Biological applications of silver	7
I.2 ANTIFUNGAL AGENTS	8
I.2.1 Introduction to fungal infections	8
I.2.2 Candidiasis	9
I.2.3 Clinical needs for novel antifungal agents	10
I.2.4 METAL COMPLEXES AS ANTIFUNGAL AGENTS	15
I.2.4.1 Silver and zinc complexes of the sulfadrgugs	15
I.2.4.2 Imidazole and benzimidazole antifungals	16
I.2.4.3 Metal carboxylate antifungals	20
I.2.4.4 Metal phenanthroline antifungals	24
I.3 SUPEROXIDE DISMUTASE MIMICS (SODm)	25
I.3.1 Superoxide and its role in biological toxicity	25
I.3.2 Metal Complexes as SODm	27

1.3.2.1 Metal complexes exhibiting SOD-like activity	28
1.3.2.2 SOD activity of metal complexes of NSAIDs	35
I.4 METAL COMPLEXES AS ANTICANCER AGENTS	41
I.4.1 Introduction	41
I.4.2 Metal carboxylate anticancer compounds	42
I.4.3 Metal phenanthroline anticancer agents	44
I.4.4 Chemotherapeutic potential of Cu(II) benzimidazole derivatives	46
I.5 METAL CARBOXYLATE CHEMISTRY	47
I.5.1 Coordination modes of metal carboxylates	47
I.5.2 Infrared spectra of carboxylate complexes	51
I.5.3 THE CHEMISTRY OF SALICYLIC ACID	54
I.5.3.1 Introduction to salicylic acid	54
I.5.3.2 Medicinal applications of salicylic acid	54
I.5.3.3 Coordination modes of salicylic acid	56
I.5.3.4 Coordination complexes of salicylic acid	58
I.6 BENZIMIDAZOLES AND THEIR METAL COMPLEXES	75
I.6.1 Benzimidazole and their uses	75
I.6.2 Coordination complexes of Benzimidazole	78
RATIONALE	85
DISCUSSION	87
D.1 SYNTHESIS OF COPPER(II) SALICYLATE COMPLEXES	88
D.2 SYNTHESIS AND CHARACTERISATION OF COPPER(II) SALICYLATES INCORPORATING BENZIMIDAZOLE LIGANDS	93

D.2.1 The reactions of $[\text{Cu}(\text{salH})_2(\text{H}_2\text{O})_2]$ and $[\text{Cu}_2(\text{asp})_4(\text{H}_2\text{O})_2]\cdot\text{H}_2\text{O}$ with the simple benzimidazole ligands	93
D.2.2 Reaction of $[\text{Cu}(\text{salH})_2(\text{H}_2\text{O})_2]$ (1) and $[\text{Cu}_2(\text{asp})_4(\text{H}_2\text{O})_2]\cdot\text{H}_2\text{O}$ (2) with the chelating benzimidazoles thiabendazole (TBZH) and 2-(Pyridyl)Benzimidazole (2-PyBZDH)	107
D.2.3 The reactions of $[\text{Cu}(\text{dipsH})_2(\text{H}_2\text{O})]$ (3) with the simple benzimidazole ligands	111
D.2.4 Reaction of $[\text{Cu}(\text{dipsH})_2(\text{H}_2\text{O})]$ (3) with the chelating benzimidazoles thiabendazole (TBZH) and 2-(Pyridyl)Benzimidazole (2-PyBZDH)	124
D.2.5 Reaction of $\{\text{Cu}(\text{msal})(\text{H}_2\text{O})\}_n$ (4) with the simple benzimidazole ligands	128
D.2.6 Reaction of $\{\text{Cu}(\text{msal})(\text{H}_2\text{O})\}_n$ (4) with the chelating benzimidazoles thiabendazole (TBZH) and 2-(Pyridyl)Benzimidazole (2-PyBZDH)	131
D.3 SYNTHESIS AND CHARACTERISATION OF COPPER(II) SALICYLATES INCORPORATING THE N,N-DONOR LIGANDS 1,10-PHENANTHROLINE AND 2,2'-BIPYRIDINE	134
D.4 SYNTHESIS AND CHARACTERISATION OF COPPER(II) ACETATE AND SIMPLE COPPER(II) SALTS INCORPORATING BENZIMIDAZOLE LIGANDS	141
D.4.1 Reaction of $[\text{Cu}_2(\text{OAc})_4(\text{H}_2\text{O})_2]$ with the simple benzimidazole ligands	141
D.4.2 Reaction of $[\text{Cu}_2(\text{OAc})_4(\text{H}_2\text{O})_2]$ with the chelating benzimidazole ligands	149
D.4.3 Reaction of $\text{CuCl}_2\cdot 2\text{H}_2\text{O}$ with the simple benzimidazole ligands	154
D.4.4 Reaction of $\text{CuCl}_2\cdot 2\text{H}_2\text{O}$ with the chelating benzimidazole ligands	159
D.4.5 Reaction of $\text{CuSO}_4\cdot 5\text{H}_2\text{O}$ with the simple benzimidazole ligands	162
D.4.6 Reaction of $\text{CuSO}_4\cdot 5\text{H}_2\text{O}$ with the chelating benzimidazole ligands	167

D.5 SYNTHESIS OF SILVER SALTS CONTAINING BENZIMIDAZOLE LIGANDS	168
D.5.1 Attempted synthesis of silver salicylates with benzimidazole ligands	168
D.5.2 Reaction of AgNO ₃ with the simple and chelating benzimidazole ligands	169
D.5.3 Reaction of Ag ₂ SO ₄ with the simple and chelating benzimidazole ligands	175
D.5.4 Reaction of Ag(OAc) with the simple and chelating benzimidazole ligands	180
D.6 THE BIOMIMETIC ACTIVITY OF THE COPPER COMPLEXES (1) – (50)	187
D.6.1 Introduction	187
D.6.2 Catalase (CAT) mimetic activity of complexes (1) – (50)	191
D.6.3 The Superoxide Dismutase (SOD) activity of copper(II) salicylate and benzimidazole complexes	197
D.7 PRELIMINARY ANTICANCER ASSAYS OF SELECTED COMPLEXES	202
D.8 ANTIFUNGAL ACTIVITY OF COMPLEXES (1)-(69) AGAINST <i>CANDIDA ALBICANS</i>	207
EXPERIMENTAL	213
E.1 INSTRUMENTATION	214
E.2 CHEMICALS	216
E.3 SYNTHESIS OF COPPER(II) SALICYLATE COMPLEXES	217
E.3.1 [Cu(salH) ₂ (H ₂ O) ₂] (1)	217
E.3.2 [Cu ₂ (asp) ₄ (H ₂ O) ₂].H ₂ O (2)	217
E.3.3 [Cu(dipsH) ₂ (H ₂ O)] (3)	218
E.3.4 {Cu(msal)(H ₂ O)} _n (4)	218

E.4 SYNTHESIS OF COPPER(II) SALICYLATE COMPLEXES INCORPORATING BENZIMIDAZOLE LIGANDS	219
E.4.1 Synthesis of copper(II) salicylate complexes incorporating the simple benzimidazoles	219
E.4.1.1 [Cu(salH) ₂ (BZDH) ₂] (5)	219
E.4.1.2 [Cu(salH) ₂ (5,6-Me ₂ BZDH) ₂] (6)	220
E.4.1.3 [Cu(sal)(2,5-Me ₂ BZDH)(H ₂ O)] (7)	220
E.4.1.4 [Cu(sal)(6-NO ₂ BZDH)(H ₂ O)] (8)	220
E.4.1.5 [Cu(sal)(5-BZDHCOOH)(H ₂ O)] (9)	221
E.4.1.6 [Cu(salH) ₂ (2-AmBZDH)(H ₂ O) ₂] (10)	221
E.4.2 Synthesis of copper (II) salicylate complexes incorporating the chelating benzimidazoles	222
E.4.2.1 [Cu(sal)(TBZH)].H ₂ O (11)	222
E.4.2.2 [Cu(sal)(2-PyBZDH)].H ₂ O (12)	222
E.4.3 Synthesis of copper(II) 3,5-diisopropylsalicylate complexes incorporating the simple benzimidazoles	223
E.4.3.1 [Cu(dipsH) ₂ (BZDH) ₂] (13)	223
E.4.3.2 [Cu(dipsH) ₂ (2-MeOHBZDH) ₂].EtOH (14)	223
E.4.3.3 [Cu(dips)(2,5-Me ₂ BZDH)(H ₂ O)] (15)	224
E.4.3.4 [Cu(5-BZDCOO)(H ₂ O) ₂].EtOH (16)	224
E.4.3.5 [Cu(dips)(2-AmBZDH)(H ₂ O)] (17)	224
E.4.4 Synthesis of copper(II) 3,5-diisopropylsalicylate complexes incorporating the chelating benzimidazoles	225

E.4.4.1 [Cu(dips)(TBZH)] (18)	225
E.4.4.2 [Cu(2-PyBZD) ₂ (H ₂ O)] (19)	226
E.4.5 Synthesis of copper(II) 3-methoxysalicylate complexes incorporating the simple benzimidazoles	227
E.4.5.1 [Cu(msal)(BZDH)(H ₂ O)].2H ₂ O (20)	227
E.4.6 Synthesis of copper(II) 3-methoxysalicylate complexes incorporating the chelating benzimidazoles	227
E.4.6.1 [Cu(msal)(TBZH)].H ₂ O (21)	227
E.4.6.2 [Cu(msal)(2-PyBZDH)].H ₂ O (22)	228
E.5 Synthesis of copper (II) salicylate complexes incorporating the N,N-donor ligands 1,10-phenanthroline and 2,2-bipyridine	229
E.5.1 [Cu(sal)(phen)] (23)	229
E.5.2 [Cu(sal)(bipy)].EtOH.H ₂ O (24)	229
E.5.3 [Cu(dips)(phen)].H ₂ O (25)	230
E.5.4 [Cu(dips)(bipy)] (26)	230
E.5.5 [Cu(msal)(phen)].H ₂ O (27)	231
E.5.6 [Cu(msal)(bipy)].H ₂ O (28)	231
E.6 SYNTHESIS OF COPPER(II) ACETATE AND SIMPLE COPPER(II) SALTS INCORPORATING BENZIMIDAZOLE LIGANDS	232
E.6.1 Synthesis of copper(II) acetate salts of the simple benzimidazoles	232
E.6.1.1 [Cu(OAc) ₂ (2-AmBZDH) ₂] (29)	232
E.6.1.2 [Cu(OAc) ₂ (5,6-Me ₂ BZDH) ₂] (30)	232
E.6.1.3 [Cu(OAc) ₂ (5-BZDHCOOH) ₂] (31)	233

E.6.1.4 [Cu(OAc) ₂ (6-NO ₂ BZDH) ₂] (32)	233
E.6.1.5 [Cu(OAc) ₂ (2-PhBZDH) ₂] (33)	233
E.6.2 Synthesis of copper(II) acetate salts of the chelating benzimidazoles	234
E.6.2.1 {[Cu(TBZ) ₂ (H ₂ O)].EtOH} _n (34)	234
E.6.2.2 [Cu(OAc) ₂ (2-PyBZDH)] (35)	234
E.6.3 Synthesis of copper(II) chloride salts of the simple benzimidazoles	235
E.6.3.1 [Cu(BZDH) ₂ (H ₂ O)Cl]Cl (37)	235
E.6.3.2 [Cu(5-BZDHCOOH) ₂ (H ₂ O)Cl]Cl (38)	235
E.6.3.3 [Cu(2,5-Me ₂ BZDH) ₂ (H ₂ O)Cl]Cl (39)	236
E.6.3.4 [Cu(6-NO ₂ BZDH) ₂ (H ₂ O)Cl]Cl (40)	236
E.6.3.5 [Cu(2-PhBZDH) ₂ (H ₂ O)Cl]Cl (41)	236
E.6.3.6 [Cu(5,6-Me ₂ BZDH)(H ₂ O)Cl ₂] (42)	237
E.6.4 Synthesis of copper(II) chloride salts of the chelating benzimidazoles	237
E.6.4.1 [Cu(TBZH) ₂ Cl]Cl.2H ₂ O (43)	237
E.6.4.2 [Cu(2-PyBZDH) ₂ Cl]Cl (44)	238
E.6.5 Synthesis of copper(II) sulfate salts of the simple benzimidazoles	238
E.6.5.1 [Cu(BZDH)(H ₂ O)](SO ₄) (45)	238
E.6.5.2 [Cu(5-BZDHCOOH)(H ₂ O) ₂](SO ₄).2H ₂ O (46)	239
E.6.5.4 [Cu(2-AmBZDH) ₂ (H ₂ O) ₂](SO ₄).2H ₂ O (48)	239
E.6.5.5 [Cu(6-NO ₂ BZDH) ₂ (H ₂ O) ₂](SO ₄) (49)	240
E.6.6 Synthesis of copper(II) sulfate salts of the chelating benzimidazoles	240
E.6.6.1 [Cu(TBZH) ₂](SO ₄).EtOH (50)	240

E.7 SYNTHESIS OF SILVER(I) SALTS INCORPORATING BENZIMIDAZOLE	
LIGANDS	241
E.7.1 Synthesis of silver(I) nitrate salts of the simple and chelating benzimidazoles	241
E.7.1.1 [Ag(BZDH) ₂](NO ₃) (51)	241
E.7.1.2 [Ag(5-BZDHCOOH) ₂](NO ₃) (52)	241
E.7.1.3 [Ag(2-PhBZDH) ₂](NO ₃) (53)	242
E.7.1.4 [Ag(5,6-Me ₂ BZDH) ₂](NO ₃) (54)	242
E.7.1.5 [Ag(6-NO ₂ BZDH)](NO ₃) (55)	242
E.7.1.6 [Ag(2-CIBZDH)](NO ₃) (56)	242
E.7.1.7 [Ag(TBZH)](NO ₃) (57)	243
E.7.2 Synthesis of silver(I) sulfate salts of the simple and chelating benzimidazoles	244
E.7.2.1 [Ag ₂ (BZDH)](SO ₄) (58)	244
E.7.2.2 [Ag ₂ (2-AmBZDH)](SO ₄) (59)	244
E.7.2.3 [Ag ₂ (5-BZDHCOOH)](SO ₄) (60)	244
E.7.2.4 [Ag ₂ (5,6-Me ₂ BZDH)](SO ₄) (61)	245
E.7.2.5 [Ag ₂ (6-NO ₂ BZDH)](SO ₄) (62)	245
E.7.2.6 [Ag ₂ (2-PhBZDH)](SO ₄) (63)	245
E.7.2.7 [Ag ₂ (TBZH)](SO ₄) (64)	246
E.7.3 Synthesis of silver(I) acetate salts of the simple and chelating benzimidazoles	247
E.7.3.1 {Ag(BZD)} _n (65)	247
E.7.3.2 [Ag(5,6-Me ₂ BZDH)(OAc)] (66)	247
E.7.3.3 [Ag(5-BZDHCOOH)(OAc)] (67)	247

E.7.3.4 [Ag(2-AmBZDH) ₂ (OAc)] (68)	248
E.7.3.5 {Ag(TBZ)} _n (69)	248
E.8 HYDROGEN PEROXIDE DISPROPORTIONATION STUDIES	249
E.8.1 Hydrogen peroxide disproportionation by copper(II) complexes in the presence of added imidazole	249
E.9 SUPEROXIDE DISMUTASE MIMETIC STUDIES	249
E.9.1 The modified nbt xanthine – xanthine oxidase assay	249
E.10 ANTIMICROBIAL SUSCEPTIBILITY TESTING	251
E.10.1 Biological preparations	251
E.10.2 Preparation of complex solutions for antimicrobial susceptibility testing	251
E.10.3 Antimicrobial susceptibility testing method	252
CONCLUSION	253
REFERENCES	257
APPENDICES	267
PUBLICATIONS	285

FIGURES:

Figure 1: Structure of silver sulfadiazine	15
Figure 2: Structure of mafenide	15
Figure 3: General structure of the arylsulfonylureido ligand	16
Figure 4: X-ray crystal structure for $[\text{Zn}(\text{imppn})_2(\text{CH}_3\text{CO}_2)_2] \cdot 2\text{H}_2\text{O}$	18
Figure 5: X-ray crystal structure for $[\text{Ag}_2(\text{imppn})_4(\text{ClO}_4)_2]$	18
Figure 6: Bis-imidazole ligand symbols and structures	19
Figure 7: The X-ray crystal structure of $[\text{Ag}_2(2\text{-BIM})_2](\text{ClO}_4)_2$	19
Figure 8: X-ray crystal structure of $[\text{Zn}(2\text{-BIM})_2](\text{ClO}_4)_2$	20
Figure 9: X-ray crystal structure for $[\text{Co}(\text{phen})_3] \cdot \text{oda} \cdot 14\text{H}_2\text{O}$	21
Figure 10: X-ray crystal structure for $[\text{Co}(\text{phen})_3] \cdot \text{nda} \cdot 11.5\text{H}_2\text{O}$	21
Figure 11: X-ray crystal structure for $[\text{Cu}(\text{phen})_2(\text{norb})] \cdot 6.5\text{H}_2\text{O}$	22
Figure 12: The X-ray crystal structure of $\{\text{Mn}(\text{fum})(\text{bipy})(\text{H}_2\text{O})\}_n$	22
Figure 13: Structure of $[\text{Mn}(\text{phen})_2(\text{H}_2\text{O})_2](\text{fum}) \cdot 4\text{H}_2\text{O}$ with hydrogen bonding indicated	23
Figure 14: The structure of (a) 1,10 phenanthroline (phen) and (b) phendione	24
Figure 15: The structure and SOD activity for the manganese(III) salen complex C7	29
Figure 16: The structure and SOD activity for the manganese(III) salen complex C12	29
Figure 17: Structural formula for <i>N,N,N',N'</i> -tetrakis(2'-benzimidazolyl methyl)-1,2-ethanediamine (EDTB)	30
Figure 18: The X-ray crystal structure of the $[\text{Mn}(\text{EDTB})(\text{OAc})]^-$ cation in the complex $[\text{Mn}(\text{EDTB})(\text{OAc})] \cdot \text{OAc} \cdot \text{EtOH}$	30
Figure 19: The structure of (a) EDTA and (b) DTPA	31
Figure 20: The structure of $[\text{Cu}(2\text{-OxBZDH})\text{Cl}_2]$	32

Figure 21: The structure of [Cu(2-PyzBZDH)(DMF)Cl ₂]	32
Figure 22: The structure of [Cu(BZA)(TBZH) ₂].2BZA.TBZDH.2.H ₂ O	34
Figure 23: The arrangement of the neutral 2-PyBDZH, the anionic 2-PyBZD ⁻ and the BZA ⁻ ligands around one of the neutral Copper centres in [Cu(2-PyBZDH)(2-PyBZD)(BZA)]1.66EtOH	34
Figure 24: The structure of [Cu(BZA) ₂ (phen)(H ₂ O)]	35
Figure 25: The structures of (a) salicylic acid, (b) acetylsalicylic acid, (c) <i>p</i> -aminosalicylic acid and (d) 3,5-diisopropylsalicylic acid	36
Figure 26: The X-ray crystal structure of [Cu ₂ (Indo) ₄ DMF ₂].2DMF	38
Figure 27: The structure of indomethacin (IndoH)	38
Figure 28: X - ray crystal structure of [Cu ₂ (tolf) ₄ (DMF) ₂]	39
Figure 29: The structure of diclofenac	39
Figure 30: The structure of tenoxicam	40
Figure 31: The general structural formulae for coumarin-3-carboxylic acid (C-3-COOH) and its derivatives	42
Figure 32: The carboxylate functional group	47
Figure 33: Coordination modes of monocarboxylic acids	50
Figure 34: The structures of (a) salicylic acid and (b) salicin	54
Figure 35: The structure of acetylsalicylic acid (aspirin)	55
Figure 36: Some of the possible coordination modes of salicylic acid	56
Figure 37: X-ray crystal structure of [Cu(salH) ₂ (H ₂ O) ₂].2H ₂ O	58
Figure 38: The X-ray crystal structure of [Cu ₂ (salH) ₄ (EtOH)(H ₂ O)]	59
Figure 39: X-ray crystal structure of [Mn ₂ (salH) ₄ (H ₂ O) ₂]	60

Figure 40: X-ray crystal structure of $[\text{Cu}_2(\text{dipsH})_4(\text{DMF})_2]$	61
Figure 41: X-ray crystal structure $[\text{Cu}_3(\text{dns})_2(\text{dnsH})_2(\text{H}_2\text{O})_4].4\text{H}_2\text{O}$	62
Figure 42: X-ray crystal structure $[\text{Cu}(\text{meimH})_6].2\text{salH}$	63
Figure 43: X-ray crystal structure of $[\text{Cu}(\text{imH})_2(\text{salH})_2]$	64
Figure 44: X-ray crystal structure of $[\text{Cu}(\text{imH})_5].2\text{salH}_2$	64
Figure 45: X-ray crystal structure of $[\text{Cu}(\text{imH})_6].2\text{salH}_2$	65
Figure 46: X-ray structure of a $[\text{Cu}(\text{sal})(\text{bipy})].\text{EtOH}.\text{H}_2\text{O}$ unit	66
Figure 47: X-ray crystal structure of $[\text{Cu}_2(\text{salH})(\text{sal})(\text{bipy})_2].\text{ClO}_4$	67
Figure 48: The structure of $[\text{Mn}(\text{salH})_2(\text{bipy})].\text{H}_2\text{O}$	68
Figure 49: The structure of $[\text{Cu}(\text{salH})(\text{phen})_2].\text{salH}.\text{H}_2\text{O}$	69
Figure 50: The structure of $[\text{Cu}_2(\text{phen})_2(\text{sal})_2].2\text{H}_2\text{O}$	70
Figure 51: The coordination mode of salicylic acid in $[\text{Cu}_2(\text{phen})(\text{sal})(\text{salH})_2]_n$	70
Figure 52: The X-ray crystal structure of $[\text{Cu}_2(\text{phen})(\text{sal})(\text{salH})_2]$	71
Figure 53: The structure of $[\text{Cu}(\text{dipsH})_2(\text{phen})]$	72
Figure 54: The structure of $[\text{Ag}_2(\text{NH}_3)_2(\text{salH})_2]$	73
Figure 55: The X-ray crystal structure of $[\text{Ag}_2(\text{imH})_4](\text{salH})_2$	74
Figure 56: The structure of benzimidazole with numbering system	75
Figure 57: The structure of albendazole	76
Figure 58: The structure of fenbendazole	76
Figure 59: The structure of mebendazole	76
Figure 60: The structure of praziquantel	76
Figure 61: A benzimidazole phthalate (2:1) salt containing a $2,4\text{-PyBZDH}_2^-$ cation combined with a neutral 4-PyBZDH and a terphH anion	78

Figure 62: The X-ray crystal structure of $[\text{Zn}(\text{BZDH})_2\text{Br}_2]$	79
Figure 63: The proposed polymeric structure for $\{\text{Cu}(\text{BZD})_2\}_n$	80
Figure 64: The X-ray crystal structure of $[\text{Yb}(2\text{-PyBZD})_4](2\text{-PyBZDH}_2)$	80
Figure 65: The X-ray crystal structure of $[\text{Cu}(\text{TBZH})_2\text{NO}_3]\cdot\text{NO}_3\cdot\text{H}_2\text{O}$	81
Figure 66: The structure of the cation in $[\text{Cu}(\text{TBZH})_2\text{Cl}]\text{Cl}\cdot\text{H}_2\text{O}\cdot\text{EtOH}$	82
Figure 67: X-ray crystal structure of $[\text{Ag}_3(\text{bzd})_3(\text{PPh}_3)_5]$	83
Figure 68: X-ray crystal structure of $[\text{Ag}_2(3\text{-PyBZDH})_2]\cdot(\text{ClO}_4)_2$	83
Figure 69: The X-ray crystal structure of $[\text{Ag}(4\text{-PyBZDH})(\text{H}_2\text{O})]\cdot\text{ClO}_4$	84
Figure 70: The X-ray crystal structure of $[\text{Cu}_2(\text{asp})_4(\text{DMF})_2]$	90
Figure 71: A possible structure for $\{\text{Cu}(\text{msal})(\text{H}_2\text{O})\}_n$	92
Figure 72: Structure of benzimidazole and its derivatives	94
Figure 73: The X-ray crystal structure of $[\text{Cu}(\text{salH})_2(\text{BZDH})_2]$ (5)	100
Figure 74: Packing diagram for $[\text{Cu}(\text{salH})_2(\text{BZDH})_2]$ (5)	101
Figure 75: Possible structural motif for complexes (7) – (9)	104
Figure 76: Possible structural motif for complex (10)	106
Figure 77: Possible structural motif for complexes (11) and (12)	111
Figure 78: The X-Ray crystal structure of $[\text{Cu}(\text{dipsH})_2(\text{BZDH})_2]$ (13)	115
Figure 79: Packing diagram for $[\text{Cu}(\text{dipsH})_2(\text{BZDH})_2]$ (13)	116
Figure 80: The X-Ray crystal structure of $[\text{Cu}(\text{dipsH})_2(2\text{-MeOHBZDH})_2]\cdot\text{EtOH}$ (14)	117
Figure 81: Packing diagram for $[\text{Cu}(\text{dipsH})_2(2\text{-MeOHBZDH})_2]\cdot\text{EtOH}$ (14)	118
Figure 82: Possible structural motif for complex (16)	123
Figure 83: Possible structural motif for (19)	127
Figure 84: The X-Ray crystal structure of $[\text{Cu}(\text{msal})(\text{phen})]\cdot\text{H}_2\text{O}$ (27)	136

Figure 85: Packing diagram for [Cu(msal)(phen)].H ₂ O (27)	137
Figure 86: The X-Ray crystal structure of [Cu(OAc) ₂ (5,6-Me ₂ BZDH) ₂] (30)	143
Figure 87: Packing diagram for [Cu(OAc) ₂ (5,6-Me ₂ BZDH) ₂] (30)	144
Figure 88: Possible structural motif for (34)	152
Figure 89: Possible structural motif for (35)	153
Figure 90: Possible structural motif for complexes (37) – (41)	157
Figure 91: Possible structural motif for complex (42)	158
Figure 92: The structure of part of the the polymeric complex {Ag ₂ (2-PhBZDH) ₂ (Isoph)} _n {IsophH ₂ = isophthalic acid}	168
Figure 93: Possible structural motif for complexes (51) – (54)	173
Figure 94: Possible structural motif for complexes (54) – (57)	174
Figure 95: Possible structural motif for complex (65)	184
Figure 96: Possible structural motif for complex (69)	185
Figure 97: Possible structural motif for complexes (66) and (67)	185
Figure 98: Possible structural motif for complex (68)	186
Figure 99: The X-ray crystal structures of (a) [Cu ₂ (phga) ₄ (bipy) ₂] (phgaH = phenylglyoxylic acid) and (b) [Cu(<i>N</i> -baa) ₂ (phen)] (<i>N</i> -bbaH = <i>N</i> -benzoylanthranilic acid) : efficient copper carboxylate catalase mimetics.	189
Figure 100: Schematic drawing of the active site of bovine Cu/ZnSOD	190
Figure 101: Apparatus designed to measure the volume of oxygen disproportionated in the catalytic reactions.	215

TABLES:

Table 1: Human fungal infections	8
Table 2: Antifungal compounds in clinical use along with their typical structures and properties ⁸	13
Table 3: The O ₂ ^{•-} destroying activities for metal ions and their EDTA and DTPA complexes ^a	31
Table 4: The SOD activity of 2-substituted benzimidazole chloride complexes of copper(II)	32
Table 5: The SOD activity of copper(II) benzoate complexes	33
Table 6: The SOD activity of Cu-NSAID complexes as determined by Weser <i>et al</i> ¹⁹	37
Table 7: The chemotherapeutic potential for a range of Ag(I) carboxylate containing complexes along with cisplatin and Ag(I) perchlorate	43
Table 8: The chemotherapeutic potential for phen, phendione and their metal complexes along with the metal salts	44
Table 9: The chemotherapeutic potential for TBZH and its copper complexes	46
Table 10: Infra-red spectral data (ν_{OCO}) for coordinated acetate ligands.	53
Table 11: Characteristic IR bands (cm^{-1} , KBr discs) of the complexes (5) – (9) along with their free ligands	98
Table 12: Selected bond lengths [\AA] and angles [$^{\circ}$] around the copper centres in [Cu(salH) ₂ (BZDH) ₂] (5)	102
Table 13: Hydrogen bonds for [Cu(salH) ₂ (BZDH) ₂] (5) [\AA and $^{\circ}$]	102
Table 14: Characteristic IR bands (cm^{-1} , KBr discs) of the complex (10)	105

Table 15: Characteristic IR bands (cm^{-1} , KBr discs) of the complexes (11) and (12) and their free ligands	109
Table 16: Characteristic IR bands (cm^{-1} , KBr discs) of the complexes (13) - (17) and their free ligands	114
Table 17: Selected bond lengths [\AA] and angles [$^{\circ}$] around the copper centres in [Cu(dipsH) ₂ (BZDH) ₂] (13) and [Cu(dipsH) ₂ (2-MeOHBZDH) ₂].EtOH (14)	119
Table 18: Hydrogen bonds for [Cu(dipsH) ₂ (bzdH) ₂] (13) [\AA and $^{\circ}$]	120
Table 19: Hydrogen bonds for [Cu(dipsH) ₂ (2-MeOHBZDH) ₂].EtOH (14) [\AA and $^{\circ}$]	120
Table 20: Characteristic amine bands (cm^{-1} , KBr discs) for complex (17) and its containing free 2-AmbZDH	122
Table 21: Characteristic IR bands (cm^{-1} , KBr discs) of the complexes (18) and (19) and their free ligands	125
Table 22: Characteristic IR bands (cm^{-1} , KBr discs) for complex (20) and its free BZDH ligand	129
Table 23: Characteristic IR bands (cm^{-1} , KBr discs) of the complexes (21) and (22) and their free ligands	132
Table 24: Selected bond lengths [\AA] and angles [$^{\circ}$] around the copper centres in [Cu(msal)(phen)].H ₂ O (27)	138
Table 25: Hydrogen bonds for [Cu(msal)(phen)].H ₂ O (27) [\AA and $^{\circ}$].	138
Table 26: Selected bond lengths [\AA] and angles [$^{\circ}$] around the copper centre in [Cu(OAc) ₂ (5,6-Me ₂ BZDH) ₂] (30)	145
Table 27: Hydrogen bonds for [Cu(OAc) ₂ (5,6-Me ₂ BZDH) ₂] (30) [\AA and $^{\circ}$].	145

Table 28: Characteristic IR bands (cm^{-1} , KBr discs) of the complexes (29) - (33) and their free ligands	146
Table 29: Characteristic IR bands (cm^{-1} , KBr discs) of the complexes (34) and (35) and their free ligands	150
Table 30: Characteristic IR bands (cm^{-1} , KBr discs) of the complexes (37) - (42) and their free ligands	156
Table 31: Characteristic IR bands (cm^{-1} , KBr discs) of the complexes (43) and (44) and their free ligands	160
Table 32: Characteristic IR bands (cm^{-1} , KBr discs) of the complexes (45) - (49) and their free ligands	164
Table 33: Characteristic amine bands (cm^{-1} , KBr discs) for complex (48) and the containing free 2-AmbZDH ligand	165
Table 34: Characteristic IR bands (cm^{-1} , KBr discs) of the complexes (51) – (57) and their free ligands	172
Table 35: Characteristic IR bands (cm^{-1} , KBr discs) of the complexes (58) – (64) and their free ligands	178
Table 36: Characteristic IR bands (cm^{-1} , KBr discs) of the complexes (65) – (69) and their free ligands	183
Table 37: Characteristic amine bands (cm^{-1} , KBr discs) for complex (68) and its containing free 2-AmbZDH	186
Table 38: Time course of O_2 evolution in H_2O_2 disproportionation for the Copper(II) salicylate complexes and $\{[\text{Mn}_2(\text{oda})(\text{phen})_4(\text{H}_2\text{O})_2][\text{Mn}_2(\text{oda})_3(\text{phen})_4]\}$ ($\text{odaH}_2 =$ octanedioic acid) (with added imidazole) at S.T.P.	192

Table 39: Time course of O ₂ evolution in H ₂ O ₂ disproportionation the for Copper(II) salicylate complexes (with added imidazole) at S.T.P.	193
Table 40: Time course of O ₂ evolution in H ₂ O ₂ disproportionation for the copper(II) acetate, chloride and sulfate benzimidazole complexes (with added imidazole) at S.T.P.	194
Table 41: Molecules of H ₂ O ₂ disproportionated by copper(II) salicylate complexes and {[Mn ₂ (oda)(phen) ₄ (H ₂ O) ₂][Mn ₂ (oda) ₃ (phen) ₄]} (odaH ₂ = octanedioic acid) (in the presence of added imidazole) at S.T.P. conditions	195
Table 42: Molecules of H ₂ O ₂ disproportionated by the copper(II) diisopropylsalicylate complexes (in the presence of added imidazole) at S.T.P. conditions	195
Table 43: Molecules of H ₂ O ₂ disproportionated by the copper(II) 3-methoxysalicylate complexes (in the presence of added imidazole) at S.T.P. conditions	196
Table 44: Molecules of H ₂ O ₂ disproportionated by the copper(II) acetate complexes in the presence of added imidazole) at S.T.P. conditions	196
Table 45: Molecules of H ₂ O ₂ disproportionated by the copper(II) chloride and sulfate complexes in the presence of added imidazole) at S.T.P. conditions	196
Table 46: SOD activities of copper(II) salicylate complexes	199
Table 47: SOD activity of copper(II) 3,5-diisopropylsalicylate complexes	200
Table 48: SOD activity of copper(II) 3-methoxysalicylate complexes	200
Table 49: SOD activities of [Cu ₂ (OAc) ₄ (H ₂ O) ₂] and copper(II) acetate complexes (29) – (36)	200
Table 50: SOD activities of the copper(II) chloride and sulphate complexes (37) – (50)	201

Table 51: The anti-cancer activity of the free ligands, selected complexes, cisplatin and CuSO ₄ against human hepatic (<i>Hep-G2</i>), renal (<i>A-498</i>) and lung (<i>A-549</i>) cancer cell lines expressed as IC ₅₀ (μM)*	203
Table 52: Anti- <i>Candida</i> activity (as % cell growth) of Ketoconazole and the free aromatic acid and benzimidazole ligands	208
Table 53: Anti- <i>Candida</i> activity for copper(II) salicylate containing complexes	209
Table 54: Anti- <i>Candida</i> activity for copper(II) benzimidazole containing complexes	210
Table 55: Anti- <i>Candida</i> activity for silver(I) benzimidazole containing complexes	212
Table 56: Assay volumes used in the determination of O ₂ ^{•-} dismutase activity	250

INTRODUCTION

1.1 CHEMISTRY OF THE GROUP 11 METALS COPPER AND SILVER

1.1.1 General chemistry of the group 11 elements¹

The group 11 metals copper (Cu), silver (Ag) and gold (Au) have been known since ancient times and were almost certainly the first three metals known to man. They are widely distributed in nature as the native metal and in numerous sulfide ores. Silver also occurs as horn silver (AgCl). The metals in the group have the highest electrical and thermal conductivities known. Like the group 1 metals they have one electron in their outer orbital but differ in that the penultimate shell contains ten d electrons. The poor screening by the d electrons makes the atoms of the group much smaller in size, and their ionisation energies are consequently higher. Since the electrons of the d shell are also involved in metallic bonding, the heat of sublimation and the melting points of the group 11 elements are also much higher than those of the alkalis. These factors are responsible for the more noble character of the group, and the effect is to make their compounds more covalent and give them higher lattice energies. In spite of the similarity in electronic structures and ionisation potentials there is only moderate similarity in the chemistry of copper and the heavier elements silver and gold. The elements in the group show variable valancies with the most common oxidation states being Cu(II), Ag(I) and Au(III).

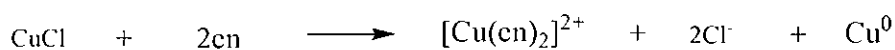
1.1.2 Copper(I) chemistry

Copper(I) complexes are diamagnetic and usually colourless except where colour results from either the anion or from charge-transfer bands. The diamagnetism is due to the fully

spin-paired outer electronic configuration of $[\text{Ar}] 3d^{10} 4s^0$. Because of the existence of the following Cu^+ disproportionation:



equilibrium can readily be displaced in either direction, thus Cu^{2+} can react with anions that do not give covalent bonds or bridging groups (e.g. ClO_4^- , SO_4^{2-}) to produce Cu^+ compounds and Cu^+ can react with complexing agents that have greater affinity for +2 state and produce Cu^{2+} (as below where en = ethylenediamine).



The occurrence of the Cu^+ ion in aqueous solution is rare, and most copper(I) compounds (e.g. CuCl , CuCN) are insoluble in water or are stable only in the form of complexes. This instability towards water is partly due to the greater lattice and solvation energies and higher formation constants for Cu(II) complexes, leaving Cu(I) complexes unstable. Copper(I) complexes are usually quite air- and moisture-sensitive, and are thus easily oxidised to copper(II). The stability of copper(I) relative to copper(II) is greatly enhanced in solvents which have a π -acceptor/donor character (e.g. acetonitrile). This is due to the effective solvation of the Cu^+ ion by the π -donor character of CH_3CN groups.¹ Copper (I) halide and other complexes are usually obtained by:

- (a) Direct interaction of ligands with copper(I) halide
- (b) Reduction of the corresponding copper(II) compounds
- (c) Reduction of Cu^{2+} in the presence of, or by the ligand.

The stoichiometries of Cu(I) compounds do not give an indication to the coordination environment, which can be very complicated, being mononuclear, binuclear with halide

bridges, polynuclear and the copper atom, two-, three-, or four-coordinate, or of infinite chains.

1.1.3 Copper(II) chemistry

The copper(II) oxidation state is by far the most common for copper as most Cu(I) compounds are readily oxidised to Cu(II) and further oxidation to Cu(III) is more difficult. Copper(II) complexes have an outer electronic configuration of $[\text{Ar}] 3d^9 4s^0$, are paramagnetic, and are mostly blue or green in colour due to the presence of an absorption band in the 600-900 nm region of the spectrum. Exceptions can occur due to the presence of charge transfer bands, causing the Cu(II) compounds to appear brown or red in colour. The coordination numbers for copper(II) complexes are usually four, five, and six, with tetrahedral, square planar, trigonal bipyramidal and octahedral structures commonly found. The shapes of the complexes are nearly always distorted due to the Jahn-Teller bond angle compression or the unequal occupation of the e_g orbitals when the d^9 -ion is subjected to an octahedral field. This gives the familiar coordination geometry of '2+4' distorted octahedral.¹

Electronic spectra of simple copper(II) complexes contain broad absorption bands in the region 625-900 nm. Because of the distortion of the octahedral geometry the crystal field is split, and thus the electronic bands are very difficult to assign unambiguously.¹

The theoretical spin-only value for copper(II) is $\mu_{so} = 1.73$ B.M.. With ligand contributions and mixing of the excited state T term into the ground state term E $[\mu_{eff} = \mu_{so}(1-2\lambda/10Dq)]$

and the high λ value (850 cm^{-1}), μ_{eff} 's of between 1.75 - 2.20 B.M. are obtained experimentally.

1.1.4 General metabolic functions of copper

Copper was first shown to be an essential biological element in the 1920s when anemia was found to result from Cu deficient diets in animals and addition of Cu salts corrected this affliction.² It is now recognised as an essential trace element for many biological functions. Copper functions primarily as a cofactor and is required for structural and catalytic properties of a variety of important enzymes, including cytochrome *c* oxidase, tyrosinase, *p*-hydroxyphenyl pyruvate hydrolase, dopamine beta hydroxylase, lysyl oxidase, and Cu-Zn superoxide dismutase (Cu/Zn SOD). These enzymes are involved in an array of biological processes required for growth, development and maintenance. Copper intake varies greatly depending on food choices and diet customs, while absorption of copper in the human body depends on a variety of factors including chemical form and presence of other dietary components. About 30-50 % of ingested copper, mostly Cu^{2-} , is absorbed in the small intestine, and very small amounts are absorbed in the stomach.³ The amount of copper ingested in food and water is relatively low, and most humans and animals are able to control excess amounts of Cu in the body by either decreased absorption or increased excretion. Acute and chronic copper toxicity are therefore rare in occurrence. Chronic copper toxicity primarily affects the liver, because it is the first site of deposition after it enters the blood. Toxicity is typically manifested by the development of liver cirrhosis

with episodes of hemolysis and damage to renal tubules, the brain, and other organs. Symptoms can progress to coma, hepatic necrosis, vascular collapse, and death.⁴ Chronic copper toxicity has been documented in dialysis patients receiving dialysis via copper tubing⁵, in workers using pesticides containing copper⁴, and in infants maintained for long periods on intravenous total parental nutrition.⁶

1.1.5 Silver(I) chemistry

Ag(I) is by far the best known oxidation state of silver, with the electron configuration [Kr] 4d¹⁰. Many simple ionic compounds are known containing Ag(I). The salts are generally insoluble in water, the exceptions being AgNO₃, AgF and AgClO₄. The most common coordination number of Ag(I) is two, but complexes of coordination number three, four and six are also found, with linear, trigonal planar, square planar and octahedral structures commonly found. Ag(I) has a relatively low affinity for oxygen donors, although compounds and complexes containing carboxylate ions, DMSO, DMF and crown ethers are known.⁷ Unlike Cu(I) and Au(I), Ag(I) does not disproportionate in water and is stable in both solid and solution.¹

1.1.6 Silver(II) chemistry⁷

The Ag(II) ion has the electron configuration [Kr] 4d⁹. Numerous complexes of Ag(II) are known, and are usually prepared by oxidising a solution of Ag(I) containing the complexing ligand with potassium persulfate. These complexes are usually square planar and paramagnetic. With neutral ligands cationic species such as [Ag(pyridine)₄]²⁺, [Ag(bipyridine)₂]²⁺ and [Ag(*ortho*-phenanthroline)₂]²⁺ form crystalline salts. The magnetic

moments of Ag(II) complexes range from $\mu_{\text{eff}} = 1.75$ to 2.2 B.M., consistent with a d^9 configuration. Ag(II) is so strongly oxidising that it reduces water, thus it only appears when stabilised in complexes or as insoluble compounds.

1.1.7 Biological applications of silver

Elemental silver and silver salts have been used for decades as antimicrobial agents in curative and preventative healthcare. Fungi and bacteria have been exposed to sub-inhibitory levels of Ag(I) for four billion years and no widespread resistance has developed to date. Silver and its simple salts have found important applications in the treatment of chronic ulcers, extensive burns and difficult to heal wounds. Ag(I) is the active ingredient in these simple systems and is well known as an excellent antimicrobial with high efficacy against gram positive and gram negative bacteria as well as a wide array of fungal microbes, but low toxicity against non target organisms.

Silver salts and compounds that release silver ions have also found applications in materials used in medical devices such as intravascular catheters where they prevent the growth of pathogens that cause catheter-related bloodstream infections which account for a significant proportion of nosocomial infections in intensive care units. More recently wound dressings containing fabrics impregnated with silver (FIS's - a new silver technology), which have antimicrobial efficacy, have been developed with the potential to provide a protective barrier against infection in severe burn wounds. Such FIS's owe their efficacy to the inclusion of discrete silver complexes which have the ability to release silver ions in a slow controlled manner.

I.2 ANTIFUNGAL AGENTS

I.2.1 Introduction to fungal infections

Fungal infections have recently emerged as a growing threat to human health especially in patients with weakened or compromised immune systems.⁸ Infections are often associated with complex disease entities, for example candidiasis in AIDS patients, aspergillosis in bone marrow or organ transplant patients.

Fungal diseases are classified by the fungal pathogen responsible for the infection and those most commonly found are listed in Table 1.

Table 1: Human fungal infections

Fungal Disease	Fungal Strain	Initial Infectious Area(s)
Candidiasis	<i>Candida albicans</i>	Mucosal Esophageal Vulvo-vaginal Dermal
Cryptococcosis	<i>Cryptococcus neoformans</i>	Meningeal
Aspergillosis	<i>Aspergillus</i>	Open wounds and cavities
Blastomycosis	<i>Blastomyces dermatitidis</i>	Respiratory
Coccidioidomycosis	<i>Coccidioides immitis</i>	Respiratory
Histoplasmosis	<i>Histoplasma capsulatum</i>	Respiratory

I.2.2 Candidiasis

Candida associated infections can range from superficial infections involving the oral cavity, vagina or skin to severe life-threatening infections involving many organs.^{9,10,11} Infections involving AIDS patients are almost exclusively mucosal as systemic invasion is a rare and late event. Before the era of antiretroviral therapy, oropharyngeal candidiasis was reported to occur in 50 % to 75 % of patients infected with HIV.⁸

The bulk of disease, especially initial episodes, is associated with the infection of *Candida albicans*. Recurrent disease is caused by the same strain of *Candida* in approximately 50 % of the cases; other cases are caused by different strains of *C. albicans* or new species. *Candida* strains, notably *glabrata* and *parapsilosis*, tend to cause infection in patients of advanced disease who have had extensive exposure to antifungal agents, especially the azoles.⁸

Most patients with oropharyngeal candidiasis are symptomatic and complain of some oral discomfort.¹² The classic presentation is of creamy-white plaques on an erythematous base, the pseudomembranous form or thrush. Patients with esophageal candidiasis develop ulcers and erosions on the esophagus and experience odynophagia or dysphagia. The combination of oral and esophageal candidiasis is symptomatic of patients with AIDS.

1.2.3 Clinical needs for novel antifungal agents

Classically, antifungal agents fall into one of two categories; those that effect membrane function by binding to ergosterol, and those that prevent synthesis of lanosterol, the precursor to ergosterol. The two most common examples from these groups are amphotericin B, which is a member of the polyene class, and ketoconazole, which is a member of the azole class.

Polyene antifungal agents have an atypical mode of action against fungal pathogens, instead of inhibiting an enzyme they bind to ergosterol, the principal sterol in the fungal membrane, thereby perturbing membrane function to the point of inducing leakage of cellular contents.¹³ For many years amphotericin B has been the only antifungal polyene that could be administered systemically to treat visceral infections. Its broad spectrum of activity against fungal species coupled with its unique mode of action should suggest that it is an ideal antifungal agent. This, however, is not the case as amphotericin B's mode of action exhibits poor selective conformational differences between ergosterol and cholesterol, the major sterol in mammalian cells, which indicate that it has potential toxicity to mammalian cells. This explanation would account for the nephrotoxicity that results when this particular agent is exposed to mammalian cells.

The azoles represent the largest class of antifungal agents in clinical use. They mainly inhibit the formation of lanosterol, which is a precursor to ergosterol, the major fungal sterol.¹³ With ergosterol depleted and replaced with unusual sterols, the normal permeability and fluidity of the fungal membrane is altered causing secondary

consequences for membrane-bound enzymes involved in cell wall synthesis. The principle molecular target of the azoles is a cytochrome P450-Erg11p which catalyses the oxidative removal of the 14 α -methyl group of lanosterol. The protein contains an iron protoporphyrin moiety located at the active site, and the antifungal azoles bind to the iron atom *via* a nitrogen atom in the imidazole ring. The remainder of the azole molecule binds to the apoprotein in a manner dependant on the individual azole structure. The exact conformation of the active site differs between fungal species and mammalian cytochrome P450, affording selectivity to the azole antifungal drugs.

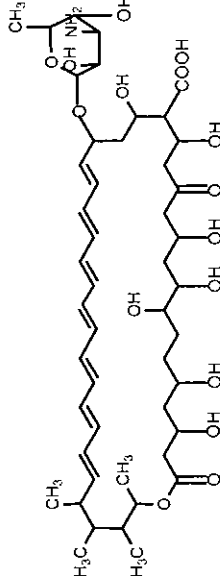
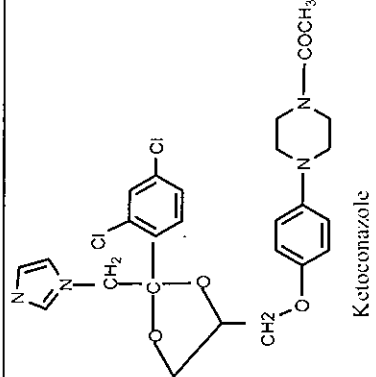
Resistance to azoles can occur by mutations that modify the target molecule or by overexpression of membrane efflux pumps that export antifungals from the cell.¹⁰ Combinations of both resistance mechanisms have even been detected in some *Candida albicans* isolates. Table 2 depicts the antifungal agents that are currently in clinical use or are about to be released onto the market. Clinical needs for novel antifungal agents have altered in recent times with the rise and fall of AIDS-related mycoses.⁸ The advent of highly active antiretroviral therapy (HAART) has enormously diminished the incidence of disseminated *Candida* infection. However, this decreasing trend in *Candida* infections is becoming overshadowed by the worrying increase in aspergillosis caused by the fungal pathogen *Aspergillus fumigatus*.

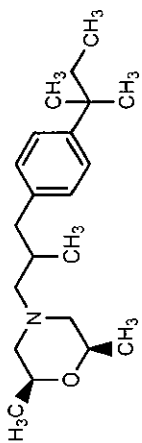
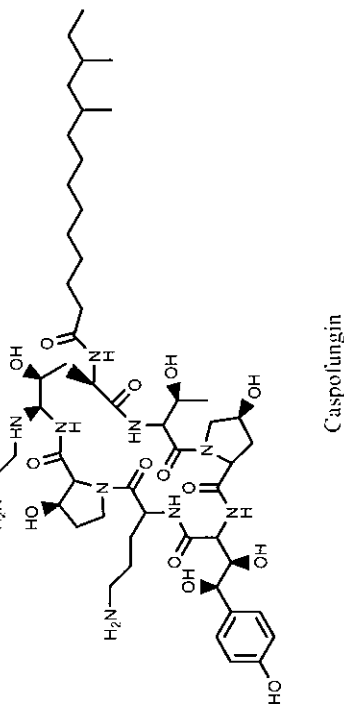
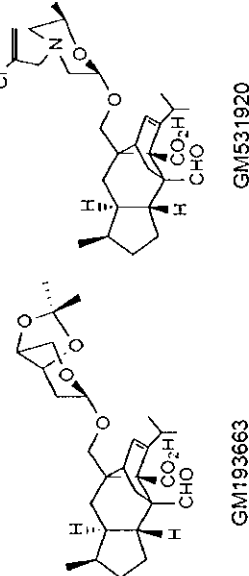
Due to this variety in fungal infection types it is necessary that antifungal agents meet two main criteria; (i) they must exhibit broad-spectrum activity and, (ii) they must exploit sufficient differences between mammalian and fungal cells, thereby displaying high

selectivity. It is evident that the majority of antifungal agents exploit selective differences in cell wall synthesis and composition between mammalian and fungal cell walls (Table 2).

The need for novel antifungals and in particular those that can display broad spectrum activity and alternative modes of action compared with those documented (Table 2) are required to meet the growing trend of diverse fungal infections and resistance. This need is highlighted from the reality that the antifungal discovery process based on screening compounds against molecular targets, which dates back before the genomics era, has so far not resulted in a single new agent emerging into the clinic or development process. Metal complexes may represent a novel class of antifungal agent in both their ability to act as fungi-toxic species and in their selective targeting of fungal cellular organelles.

Table 2: Antifungal compounds in clinical use along with their typical structures and properties⁸

Class	Specific Example	Structural Example	Molecular Target	Side Effects ¹⁴
Polycene	Amphotericin B Nystatin		Ergosterol function within fungal cellular wall.	Blindness Pulmonary toxicity
Azole	Ketoconazole Voriconazole Fluconazole Ravuconazole	<p>Amphotericin B</p>  <p>Ketoconazole</p>	Bind to the haem groups in cytochrome P450, thus causing fungal cell perturbation.	Nausea Vomiting Diarrhea Abdominal pain

Morpholines	<p>Amorolfine</p> <p>Terbinafine</p>  <p>Amorolfine is a morpholine derivative with a methyl group on the nitrogen and a 4-(2,4-dimethylphenyl)ethyl group on the 2-position. Terbinafine is a morpholine derivative with a methyl group on the nitrogen and a 4-(2,4-dimethylphenyl)ethyl group on the 2-position, and a methyl group on the 3-position.</p>	<p>Inhibit sterol Δ^{14} reductase and $\Delta^7 - \Delta^8$ isomerase.</p>	<p>Burning sensation, dryness of skin, scaling, itching</p>
Echinocandins	<p>Anidulafungin</p> <p>Caspofungin</p> <p>Micalofungin</p>  <p>Anidulafungin, Caspofungin, and Micalofungin are tricyclic echinocandins. They feature a central bicyclic core with a hydroxyl group and a methyl group, and a side chain containing a hydroxyl group, a methyl group, and a long alkyl chain.</p>	<p>Target protein complexes responsible for synthesis of cell wall polysaccharides.</p>	<p>Side effects unreported as yet</p>
Sordarins	<p>GM193663</p> <p>GM531920</p>  <p>GM193663 and GM531920 are sordarins. They are complex polycyclic structures with multiple hydroxyl groups, a methyl group, and a side chain containing a hydroxyl group, a methyl group, and a long alkyl chain.</p>	<p>Inhibit protein synthesis by blocking the function of fungal translational Elongation Factor</p>	<p>Side effects unreported as yet</p>

1.2.4 METAL COMPLEXES AS ANTIFUNGAL AGENTS

1.2.4.1 Silver and zinc complexes of the sulfadruugs¹⁵

Silver sulfadiazine (Figure 1) is known to possess significant antibacterial and antifungal properties. Due to these useful properties it is used alone or in combination with mafenide (Figure 2), cerium nitrate or chlorohexidine as a topical treatment for open wounds and burns. Complexes containing silver and zinc sulfonamides have been used over the past twenty years to successfully treat serious infections of this nature and offer a real alternative to the resistance problems suffered by the state-of-the-art antifungal agents. It is believed (but not yet fully understood) that the metal ions interfere with cell growth by (i) inhibition of transport functions in the cell wall (respiration), (ii) inhibition of cell division (interaction with DNA) and (iii) interruption of cell metabolism (changing enzyme structures).¹⁶ This multimodal efficacy, which occurs at very low concentrations, is unique to silver ion antimicrobials and reduces the possibility of developing resistant organisms.

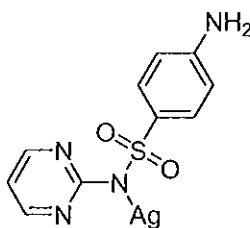


Figure 1: Structure of silver sulfadiazine

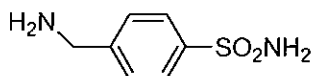


Figure 2: Structure of mafenide

Recently Mastrolorenzo *et al.*¹⁵ have synthesised an array of complexes incorporating arylsulfonylureido derivatives (Figure 3). These Ag(I) and Zn(II) complexes were tested as antifungals using the fungal strains *Aspergillus flavus*, *Aspergillus niger* and *Candida albicans*. MIC₁₀₀ values were reported in the region of 1.5 – 5 µg/ml for the tested compounds, values which compare favorably to those of ketoconazole.

Mode of action studies carried out on these complexes revealed that fungal cell death was achieved by the inhibition of phosphomannose isomerase, a key enzyme in the synthesis of fungal cell walls. Significantly no reduction in ergosterol levels were detected indicating that these complexes possess a unique mode of action over the state-of-the-art drugs.

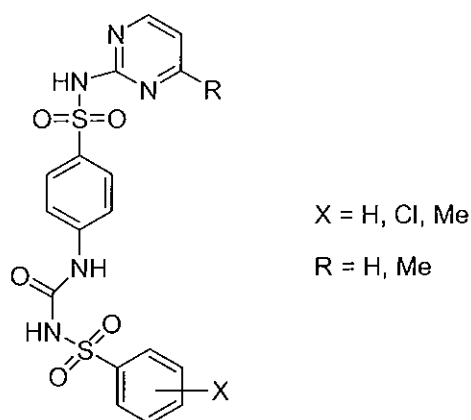


Figure 3: General structure of the arylsulfonylureido ligand

1.2.4.2 Imidazole and benzimidazole antifungals

The compound 2-(4-thiazolyl)benzimidazole (thiabendazole, TBZH) (Figure 72), was first reported as an antihelmintic agent¹⁷ and only later were its antifungal properties and potential for controlling fungal diseases recognised.¹⁸ Its fungistatic mode of action is generally attributed to the inhibition of oxygen consumption as it was found that TBZH

completely inhibits certain systems within fungal mitochondria function.¹⁹ Metal coordination complexes of thiabendazole were first synthesised as a means to improve its poor solubility. Kowala *et al.*, however, showed that TBZH complexes containing anions of halide, acetate and sulfate were also poorly soluble in water.²⁰

Copper derivatives of TBZH were shown by Devereux *et al.*²¹, to possess significant antifungal activity against *C. albicans*. Significantly, the most active of these complexes [Cu(TBZH)(O₂C-CH₂CH₂-CO₂)] and [Cu(TBZH)₂Cl].Cl.H₂O.EtOH (Figure 66) were found to have MIC₈₀ values at a concentration of 10 µg/ml whereas the free ligand TBZH was inactive at this concentration.

In 2003 this group synthesised and observed the antimicrobial activity of (Z)-3-(1H-imidazol-1-yl)-2-phenylpropenenitrile (imppn) and its complexes with Zn(II) and Ag(I)²² (Figure 4 and Figure 5). Although the imppn ligand contains an imidazole moiety identical to that found in the prescription drug ketoconazole, it did not display any significant antimycotic behaviour. This was also found to be the case for the metal complexes of imppn, where the presence of the metal ions did not enhance the biological activity in any way.

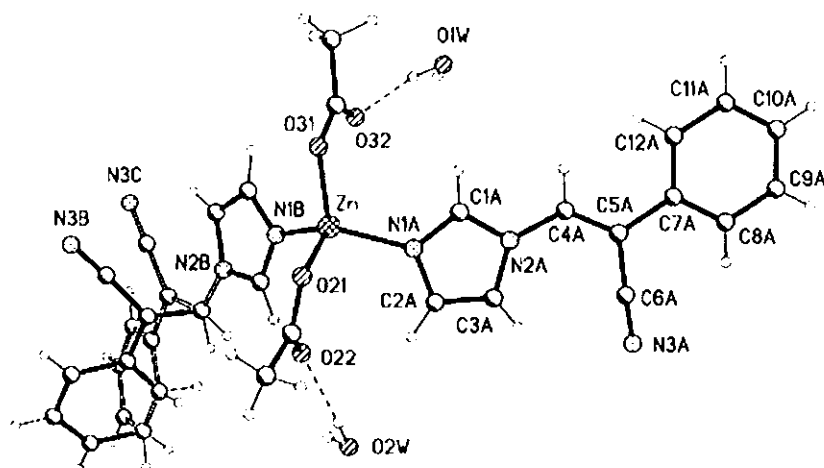


Figure 4: X-ray crystal structure for $[\text{Zn}(\text{imppn})_2(\text{CH}_3\text{CO}_2)_2] \cdot 2\text{H}_2\text{O}$

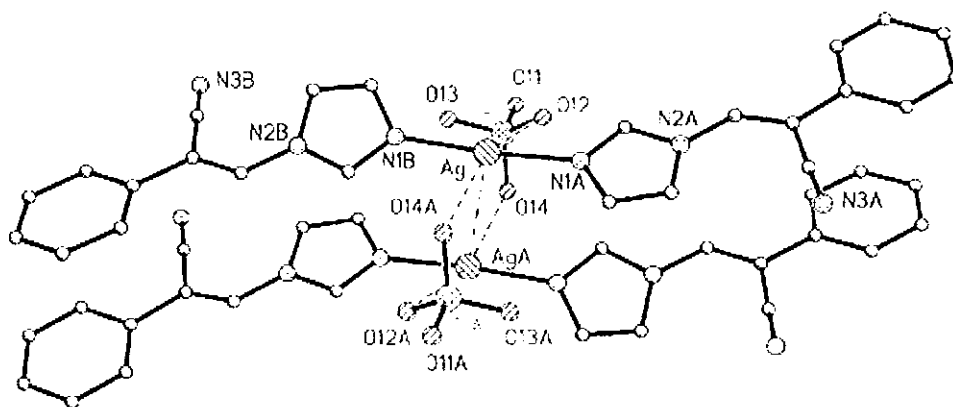


Figure 5: X-ray crystal structure for $[\text{Ag}_2(\text{imppn})_4(\text{ClO}_4)_2]$

The anti-*Candida* activity of metal complexes containing bis-imidazole type ligands (Figure 6) were studied by this laboratory and reported in 2004.^{23,24} These bis-imidazole ligands were reacted at room temperature with metal perchlorates to yield complexes of general formula $[\text{M}(\text{L})_2]\text{ClO}_4$ (Figure 7 and Figure 8), where $\text{M} = \text{Cu}(\text{II}), \text{Mn}(\text{II}), \text{Zn}(\text{II})$ and $\text{Ag}(\text{I})$; $\text{L} = 2\text{-BIM}$ or its derivatives. Of the complexes synthesised many displayed

considerable *in vitro* anti-*Candida* activity when tested as DMSO/water solutions. Overall the compounds exhibited IC_{100} values between 5 – 10 $\mu\text{g/ml}$ while the free ligands displayed no significant activity under identical conditions.

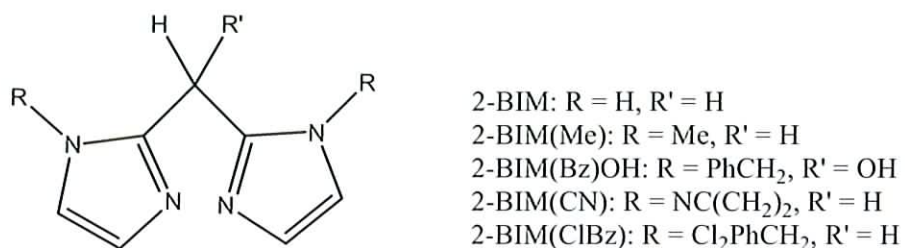


Figure 6: Bis-imidazole ligand symbols and structures

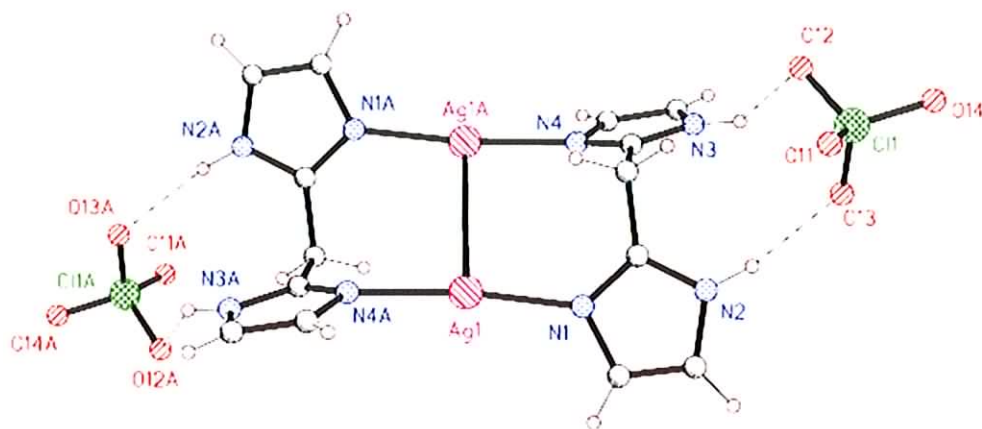


Figure 7: The X-ray crystal structure of $[\text{Ag}_2(2\text{-BIM})_2](\text{ClO}_4)_2$

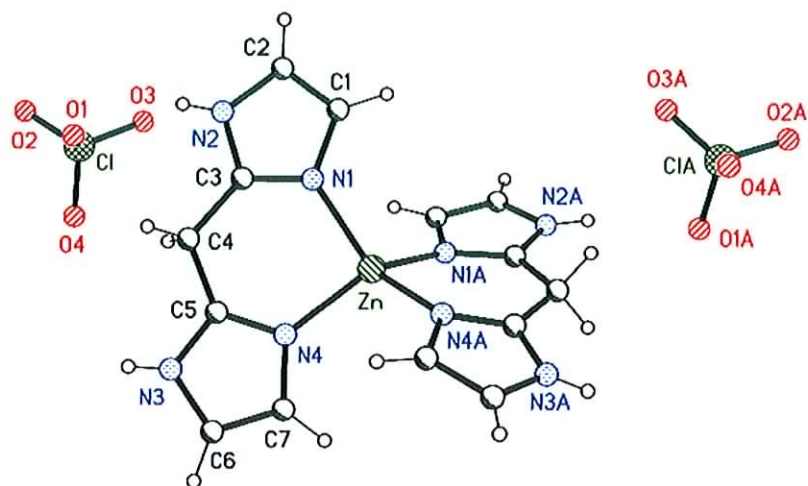


Figure 8: X-ray crystal structure of $[\text{Zn}(\text{2-BIM})_2](\text{ClO}_4)_2$

1.2.4.3 Metal carboxylate antifungals

In 1999 this research group reported the fungitoxic activity for a range of Co(II), Mn(II) and Cu(II) species containing the carboxylate ligands; octanedioic acid (oda), nonanedioic acid (nda), salicylic acid (salH_2) and *cis*-5-norborene-endo-2,3-dicarboxylic acid (norb) along with 1,10 phenanthroline (phen)²⁵ (Figure 9 - Figure 11). Of the complexes tested against *C. albicans* the cobalt(II) complexes (Figure 9 and Figure 10) displayed IC_{60} values at 20 $\mu\text{g/ml}$, the Mn(II) complexes incorporating phen and either norb or salH_2 carboxylates displayed significant antimycotic activity with 90 % cell death at 20 $\mu\text{g/ml}$.

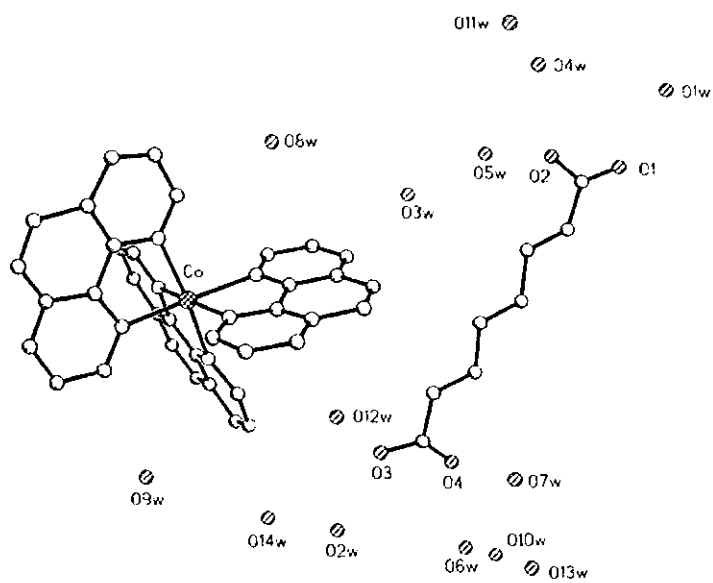


Figure 9: X-ray crystal structure for $[\text{Co}(\text{phen})_3]\cdot\text{oda}\cdot 14\text{H}_2\text{O}$

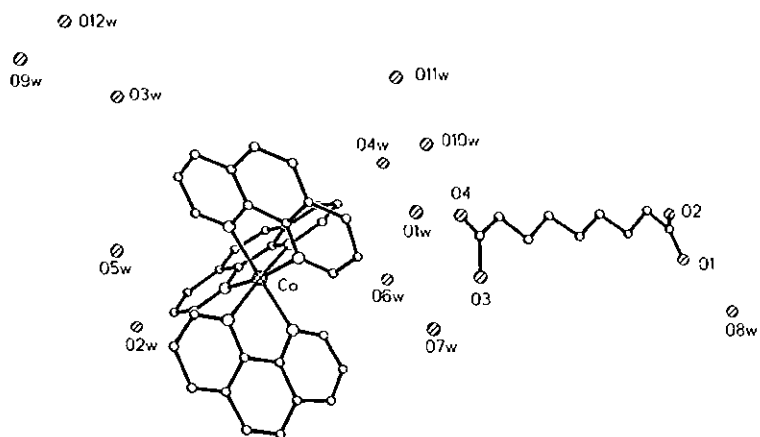


Figure 10: X-ray crystal structure for $[\text{Co}(\text{phen})_3]\cdot\text{nda}\cdot 11.5\text{H}_2\text{O}$

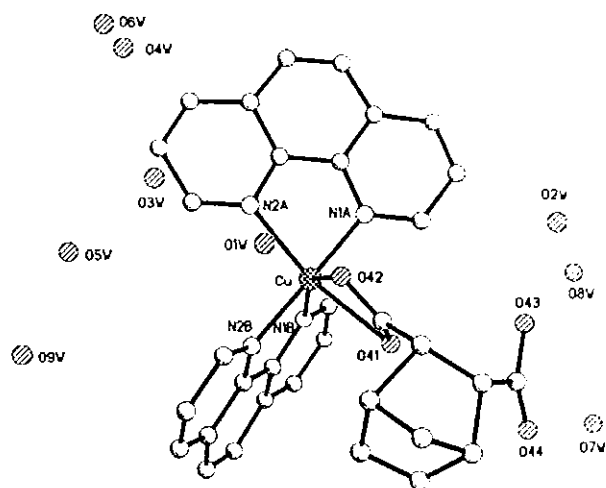


Figure 11: X-ray crystal structure for $[\text{Cu}(\text{phen})_2(\text{norb})].6.5\text{H}_2\text{O}$

Fungitoxicity investigations of Mn(II) fumarate complexes incorporating phen and bipy were reported by this group in 2000²⁶, (Figure 12 and Figure 13). Of the complexes tested two $[\text{Mn}(\text{fum})(\text{phen})]$ and $[\text{Mn}(\text{phen})_2(\text{H}_2\text{O})_2](\text{fum}).4\text{H}_2\text{O}$ (Figure 13) showed significant activity with 70 % of cells killed at 10 $\mu\text{g}/\text{ml}$.

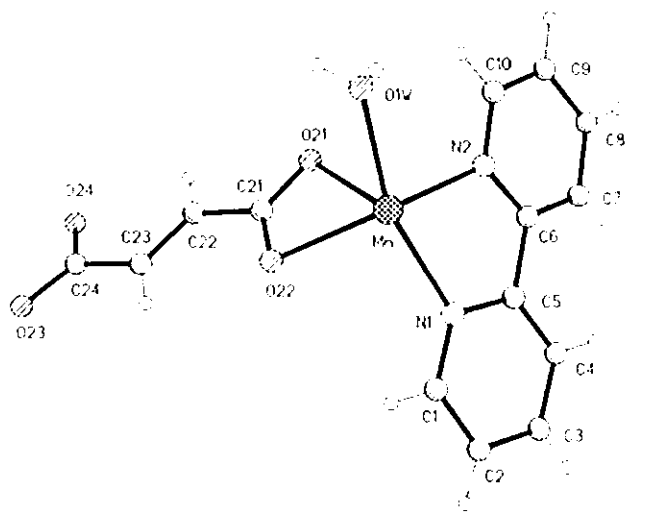


Figure 12: The X-ray crystal structure of $\{\text{Mn}(\text{fum})(\text{bipy})(\text{H}_2\text{O})\}_n$

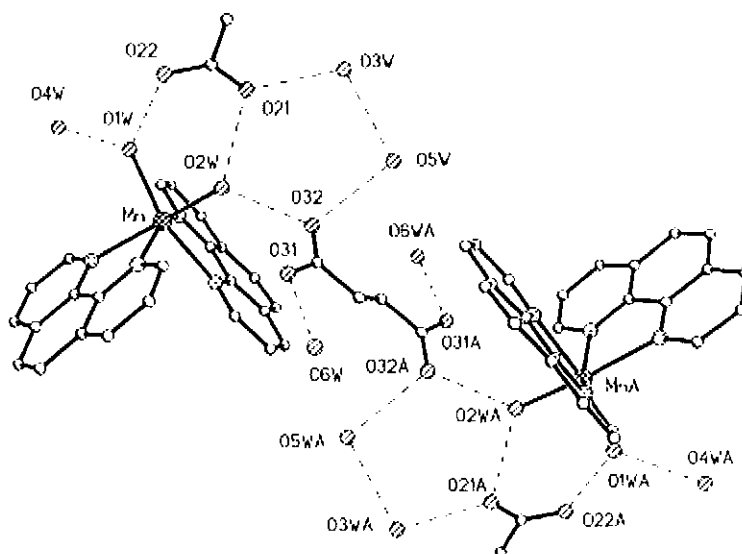


Figure 13: Structure of $[\text{Mn}(\text{phen})_2(\text{H}_2\text{O})_2](\text{fum}).4\text{H}_2\text{O}$ with hydrogen bonding indicated

Investigations into the anticancer and antifungal properties of $\text{Ag}(\text{I})$ complexes containing ammonia and salicylic acid, were recently carried out in this laboratory.²⁷ The antifungal activities of the complexes $[\text{Ag}_2(\text{salH})_2]$ and $[\text{Ag}_2(\text{salH})_2(\text{NH}_3)_2]$ (Figure 54) were far greater than those of the free silver salt and salH_2 . Significantly $[\text{Ag}_2(\text{salH})_2(\text{NH}_3)_2]$ was sixty times more potent than AgNO_3 , a well known silver based clinically applied antimicrobial agent.

1.2.4.4 Metal phenanthroline antifungals

The chelating ligand 1,10-phenanthroline (phen) (Figure 14) and certain types of its derivatives such as the compound 1,10-phenanthroline-5,6-dione (phendione) (Figure 14) represent a novel class of antifungal agents. Metal free phen has shown antifungal activity at concentrations of between 2 – 5 $\mu\text{g/ml}$ ²⁸ and this activity has been further improved by varying its structure (e.g. phendione).^{29,30} Metal complexes incorporating both phen and carboxylic acids were discussed earlier (1.2.4.3) and in general, complexes which contain phen, exhibit significant antifungal activity and in some cases improved activity over the free phen ligand itself.

Due to these important observations this group carried out mode of action studies and showed that phen and its metal complexes induced apoptosis when exposed to fungal and mammalian cells.²⁸ Exposure of *Candida albicans* to $[\text{Mn}(\text{phen})_2(\text{mal})].2\text{H}_2\text{O}$ or $[\text{Ag}_2(\text{phen})_3(\text{mal})].2\text{H}_2\text{O}$ resulted in DNA degradation whereas exposure to phen or $[\text{Cu}(\text{phen})_2(\text{mal})].2\text{H}_2\text{O}$ did not.²⁸ All drugs were found to induce extensive changes to the internal structure of yeast cells including retraction of the cytoplasm, nuclear fragmentation and disruption of the mitochondria.

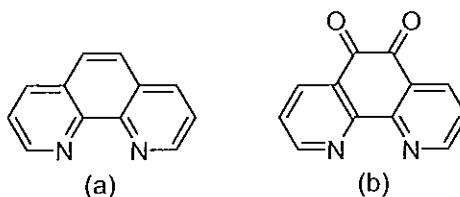


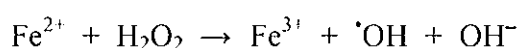
Figure 14: The structure of (a) 1,10 phenanthroline (phen) and (b) phendione

I.3 SUPEROXIDE DISMUTASE MIMICS (SODm)

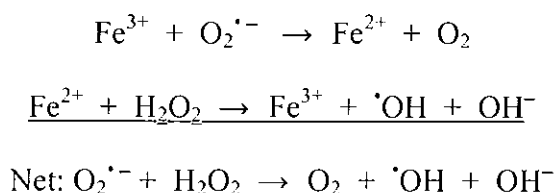
I.3.1 Superoxide and its role in biological toxicity

The superoxide anion, ($O_2^{\cdot-}$) generated in biological systems by the one electron reduction of O_2 has been implicated as the cause of many inflammatory processes, reperfusion injury and degenerative processes.³¹ For example McCord has implicated it in the promotion of arthritis due to its ability to degrade hyaluronic acid.³²

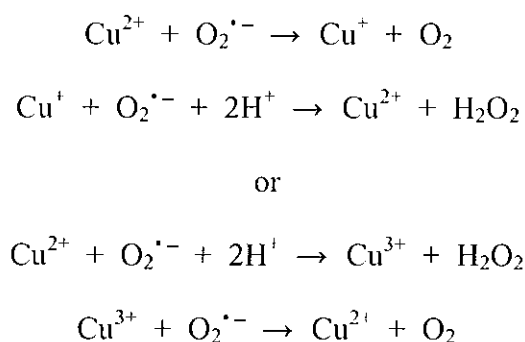
Superoxide reacts *in vivo* to produce toxic reactive oxygen and nitrogen species (RONS). Examples of these reactive species include nitric oxide (NO^{\cdot}), peroxynitrite ($ONOO^-$) and the perhydroxyl radical (HO_2^{\cdot}). At low concentrations RONS can play a beneficial biological role in the defense of infectious agents, in the function of cellular signaling pathways, and in the induction of a mitogenic response. At higher concentrations, however, RONS can cause oxidative damage to DNA, proteins and lipids. Normally a “redox balance” is established *in vivo* by enzymes capable of dismutating superoxide such as superoxide dismutase (SOD), discovered by McCord and Fridovich in 1969³³, which converts superoxide into hydrogen peroxide (H_2O_2) and oxygen (O_2). However, overproduction of $O_2^{\cdot-}$ combined with low concentrations of SOD can lead to RONS mediated oxidative stress. Superoxide can also release “free iron” from iron-containing proteins such as aconitase.³⁴ Released Fe^{2+} can participate in the Fenton reaction, generating highly reactive hydroxyl radicals. The majority of *in vivo* production of hydroxyl radicals occurs, according to Fenton chemistry.³⁵



The superoxide radical also participates in the metal catalysed Haber-Weiss reaction where the transition metal (Cu or Fe) is reduced and subsequently re-oxidised by H₂O₂, yielding such deleterious entities as [•]OH or FeH₂O₂, Fe(IV) and FeO²⁺, or the equivalent Cu compounds (CuH₂O₂⁺, Cu(III) or CuO²⁺).³⁶



Hydrogen peroxide is formed wherever O₂^{•-} is generated by the rapid spontaneous conversion of O₂^{•-} to H₂O₂ by SOD. The mechanism of the catalysis of superoxide dismutation by SOD is suggested to proceed by the alternation of oxidation states of the metal centre. For example Cu(II) may oscillate between Cu(II) and Cu(I) or between Cu(II) and Cu(III). These oscillations allow the following reactions to occur:



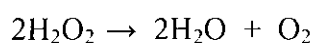
With the overall process being:



Unlike its precursor O₂^{•-}, hydrogen peroxide can cross cell membranes and is thought to produce more potent oxidants, such as [•]OH via the Haber-Weiss (or Fenton) reaction.

The biological existence of $\cdot\text{OH}$ is of major significance as it can lead to DNA oxidative damage, and thus cancer.

The hydrogen peroxide formed by superoxide dismutase is scavenged by catalase, a heme protein that catalyses the dismutation of H_2O_2 into water and molecular oxygen thus minimising the damaging effects of H_2O_2 .



1.3.2 Metal Complexes as SODm

The use of SOD as a pharmaceutical has been proposed for the treatment of a number of diseases including, hyperoxia, reperfusion injury, AIDS, ulcerative colitis as well as inflammation and inflammation-associated diseases, such as rheumatoid arthritis and osteoarthritis.³⁷ Recently there has been considerable interest in the development and screening of metal complexes as potential SOD mimics. Some of the advantages of using metal complexes as SOD mimics compared with the isolation of the SOD enzyme itself for therapeutic purposes are:

- i. **Molecular weight:** metal complexes typically have a lower molecular weight than the SOD enzyme by a factor of at least 50, thus permitting the complexes to gain access to certain intracellular spaces, whereas the cells are generally impermeable to the enzyme.
- ii. **Reactivity:** SOD mimics can only catalyse the dismutation of superoxide and should not react with hydrogen peroxide or peroxynitrite. The Cu/Zn SOD enzyme reacts with both hydrogen peroxide and with peroxynitrite, inactivating

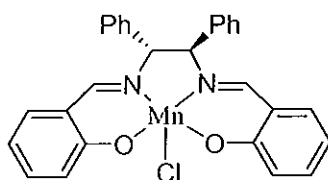
the enzyme.

- iii. Structure: The SOD enzyme structure is peptide-based and is thus readily degraded by proteases; therefore, it is not orally bioavailable. Metal complex SOD mimics could have an advantage over the enzyme here as it may be possible to develop an orally effect mimic.
- iv. Source: Metal SOD mimics can be prepared by total synthesis, whereas the enzymes are isolated from natural sources or prepared by recombinant DNA techniques. Consequently, the cost of manufacturing for the metallo-enzyme is far greater than for the transition metal mimics.

1.3.2.1 Metal complexes exhibiting SOD-like activity

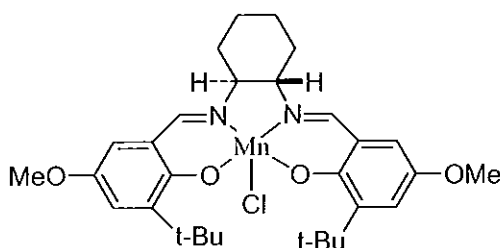
Unsurprisingly, as the catalytic role of SOD is based on the cyclic Cu(II)-Cu(I) redox reactions, it has been shown that many metal complexes also exhibit SOD activity with copper^{38,39} and manganese^{40,41,42,43} being of most interest. For instance CuSO₄ exhibits SOD activity with IC₅₀ values reported between 2 and 30 μM.^{33,44} These values compare to an IC₅₀ value of 0.04 μM for SOD.⁴⁵ The basic premise toward catalytic dismutation is that the metal must have the ability to oscillate between oxidation states thus affording the acceptance and donation of electrons in the formation of O₂ and H₂O₂ respectively.

In 1993 Baudry *et al.* reported the SOD-like activity of salen manganese(III) complexes using the NBT xanthine-xanthine oxidase assay.⁴⁰ Of the complexes tested two, termed C7 (Figure 15) and C12 (Figure 16), exhibited significant SOD activity. It was suggested that these salen-Mn(III) complexes mimic the four coordinated active site of Mn-SOD (found in human mitochondria), and this together with the lipophilic nature of the complexes enhances the SOD activity as well as exhibiting catalytic stability.



SOD activity : 0.818 $\mu\text{M} / \text{U}$

Figure 15: The structure and SOD activity for the manganese(III) salen complex C7



SOD activity : 0.32 mM / U

Figure 16: The structure and SOD activity for the manganese(III) salen complex C12

In 2001 Liao *et al.* synthesised a benzimidazole substituted ethanediamine compound EDTB (Figure 17) which upon reaction with manganese acetate produced the complex $[\text{Mn}(\text{EDTB})(\text{OAc})].\text{OAc}.\text{EtOH}$ (Figure 18) where manganese is in the +3 state.⁴¹ The complex produced SOD activity with $k_{\text{cat}} = 1.01 \times 10^7 \text{ M}^{-1} \text{ s}^{-1}$. This value compares favorably to a typical bovine SOD value of between $(2-3) \times 10^9 \text{ M}^{-1} \text{ s}^{-1}$, indicating that the complex is quite efficient in the dismutation of $\text{O}_2^{\cdot-}$.

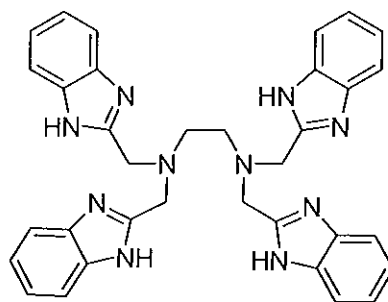


Figure 17: Structural formula for *N,N,N',N'*-tetrakis(2'-benzimidazolyl methyl)-1,2-ethanediamine (EDTB)

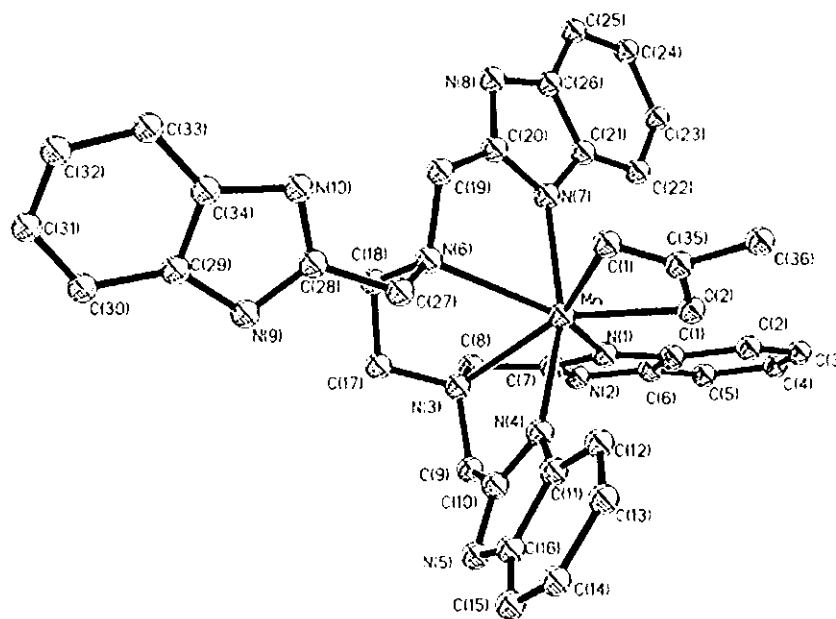


Figure 18: The X-ray crystal structure of the $[Mn(EDTB)(OAc)]^+$ cation in the complex $[Mn(EDTB)(OAc)] \cdot OAc \cdot EtOH$

Fe(III), Cu(II), and Mn(II) complexes of ethylenediaminetetraacetic acid (EDTA) (Figure 19) were shown by Naughton *et al.* to possess SOD activity (Table 3).⁴³ The SOD activity was reported for these complexes in comparison to the free metals and complexes of diethylenetriaminepentaacetic acid (DTPA) (Figure 19) (Table 3). A calibration plot, showing % Inhibition versus Units of SOD, was used to determine the percentage inhibition (68%) of 1 unit of SOD.

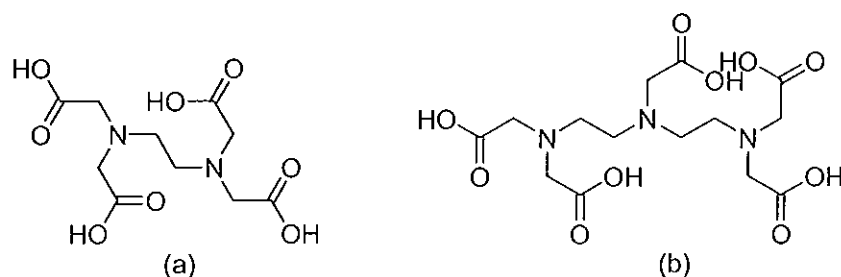


Figure 19: The structure of (a) EDTA and (b) DTPA

Table 3: The $O_2^{\cdot -}$ destroying activities for metal ions and their EDTA and DTPA complexes^a

	Aquated ion	EDTA complex	DTPA complex
Fe(III)	5.1	2.34	NA ^c
Cu(II)	0.29 ^b	3.55	NA
Mn(II)	0.77	1.38	NA

^a Results are given as concentrations [$\times 10^{-6}M$] with activities equivalent to 1U of bovine erythrocyte SOD (68% inhibition),^b Concentration is equivalent to 2U of SOD activity,

^c NA = no activity

Interestingly this study showed that DTPA should be used in preference to EDTA to remove or deactivate free catalytic metal ions as EDTA-metal complexes can exhibit and even enhance SOD destroying capabilities compared with the free metal ions.

Gdaniec *et al.*⁴⁶ have recently reported the SOD-like properties of a series of Cu(II) complexes of the 2-substituted benzimidazoles, 2-oxazolylbenzimidazole (2-OxBZDH), 2-pyrazinylbenzimidazole (2-PyzBZDH) and 2-(2-imidazol-2-yl)benzimidazole (2-ImBZDH). The complexes $[Cu(2-OxBZDH)Cl_2]$ (Figure 20), $[Cu(2-PyzBZDH)(DMF)Cl_2]$ (Figure 21) and $[Cu(2-ImBZDH)Cl_2]$ were shown to possess significant SOD-like properties in the NBT xanthine-xanthine oxidase assay (Table 4).

Table 4: The SOD activity of 2-substituted benzimidazole chloride complexes of copper(II)

Compound	μM of complex producing a 50% inhibition in NBT reduction
[Cu(2-OxBZDH)Cl ₂]	0.21
[Cu(2-PyzBZDH)(DMF)Cl ₂]	0.34
[Cu(2-ImBZDH)Cl ₂]	0.09

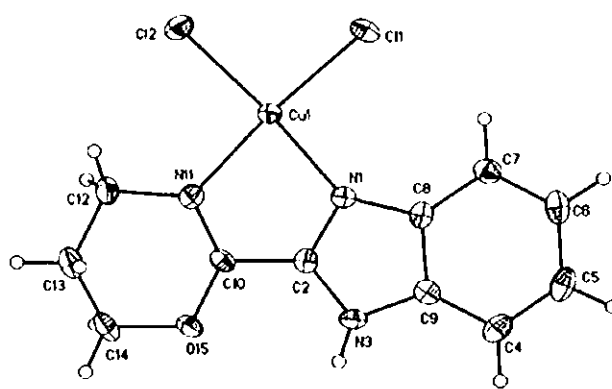


Figure 20: The structure of [Cu(2-OxBZDH)Cl₂]

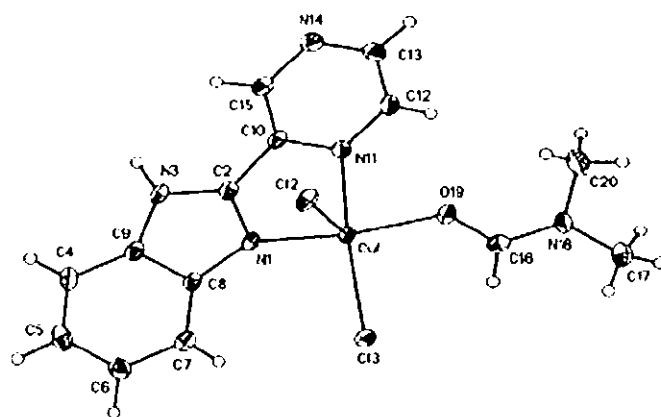


Figure 21: The structure of [Cu(2-PyzBZDH)(DMF)Cl₂]

This group has recently reported the SOD like properties of Cu(II) complexes of benzoic acid (BZAH) incorporating the chelating ligands 2-(4-thiazolyl)benzimidazole, 2-(2-pyridyl)benzimidazole and phen.⁴⁷ The complexes [Cu(BZA)₂](EtOH), [Cu(TBZH)₂(BZA)](BZA)0.5TBZH.H₂O (Figure 22), [Cu(2-PyBZDH)(2-PyBZD)(BZA)]1.66EtOH (Figure 23) and [Cu(BZA)₂(phen)(H₂O)] (Figure 24) were found to exhibit significant superoxide scavenging abilities in the NBT reduction assay with IC₅₀ values ranging from 0.83 μM to 2.83 μM. These compare to a value of 1.31 μM found for that of [Cu₂(indo)₄(H₂O)₂] which is considered to be an excellent SOD mimic. (Table 5)

Table 5: The SOD activity of copper(II) benzoate complexes

Complex	Concentration (μM) Equivalent to 1U SOD
[Cu(BZA) ₂](EtOH)	0.90
[Cu(TBZH) ₂ (BZA)](BZA)0.5TBZH.H ₂ O	0.83
[Cu(2-PyBZDH)(2-PyBZD)(BZA)]	0.95
[Cu(BZA) ₂ (phen)(H ₂ O)]	2.83

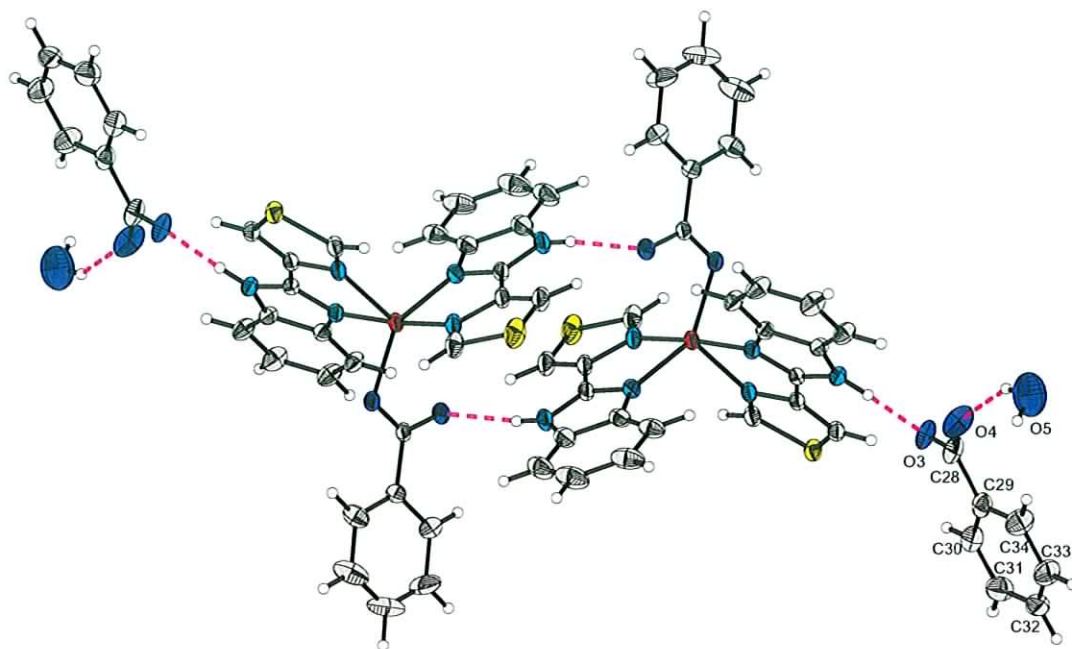


Figure 22: The structure of $[\text{Cu}(\text{BZA})(\text{TBZH})_2]_2 \cdot 2\text{BZA} \cdot \text{TBZDH} \cdot 2\text{H}_2\text{O}$

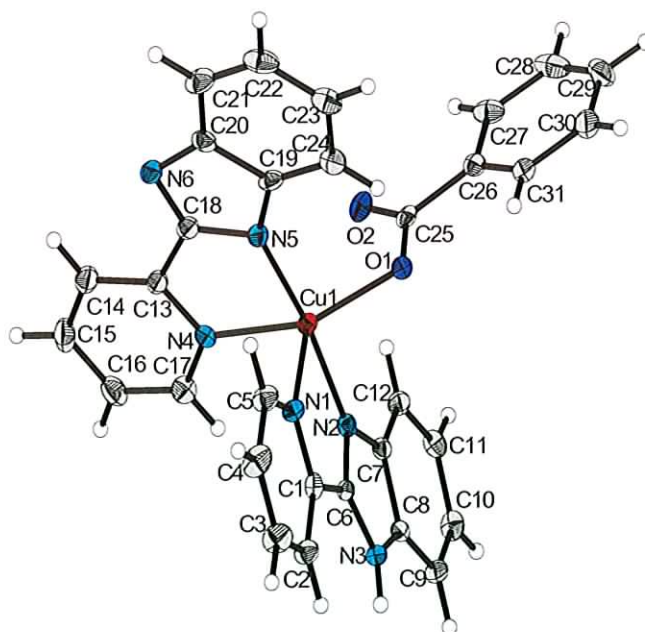


Figure 23: The arrangement of the neutral 2-PyBDZH, the anionic 2-PyBZD⁻ and the BZA⁻ ligands around one of the neutral Copper centres in $[\text{Cu}(2\text{-PyBZDH})(2\text{-PyBZD})(\text{BZA})]1.66\text{EtOH}$

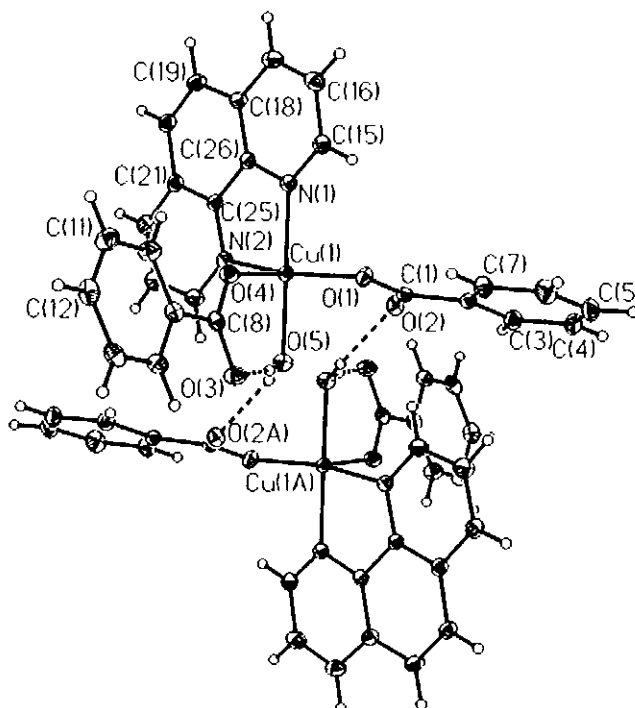


Figure 24: The structure of $[\text{Cu}(\text{BZA})_2(\text{phen})(\text{H}_2\text{O})]$

I.3.2.2 SOD activity of metal complexes of NSAIDs

A number of studies have been published on the SOD mimetic activity of metal NSAID complexes. They have been found to exhibit significant activity.

An EPR spectroscopic study carried out by Young and Lippard on the reactions of $\text{O}_2^{\bullet-}$ with $[\text{Cu}(\text{salH})_2]^{48}$ (where $\text{salH}_2 = \text{salicylic acid}$) observed that as the $\text{O}_2^{\bullet-}$ concentration increased there was a reduction in the Cu(II) signal due to the production of Cu(I). It was also noted that there was a significant difference in the reactions of anhydrous $[\text{Cu}(\text{salH})_2]$ and $[\text{Cu}(\text{salH})_2(\text{H}_2\text{O})_2]$ in dry DMSO. The reaction of $\text{O}_2^{\bullet-}$ with $[\text{Cu}(\text{salH})_2]$ produced only 15% Cu(II) salicylate. The analogous reaction of $[\text{Cu}(\text{salH})_2(\text{H}_2\text{O})_2]$ resulted in an increase of Cu(II) to 65%, which was attributed to the

reoxidation of Cu(I) to Cu(II). The difference was attributed to the presence of the water ligand in $[\text{Cu}(\text{salH})_2(\text{H}_2\text{O})_2]$ which is necessary for the cycling of Cu(I) to Cu(II).

In a study by Weser *et al.*⁴⁹ the SOD activities of the Cu(II) salicylate complexes $[\text{Cu}(\text{salH})_2]$, $[\text{Cu}(\text{aspH})_2]$, $[\text{Cu}(\text{asalH})_2]$ and $[\text{Cu}(\text{dipsH})_2]$ were found to decrease in the order of $[\text{Cu}(\text{salH})_2] > [\text{Cu}(\text{aspH})_2] > [\text{Cu}(\text{asalH})_2] > [\text{Cu}(\text{dipsH})_2]$. (aspH = acetylsalicylic acid, asalH = *p*-aminosalicylic acid and dipsH = 3,5-diisopropylsalicylic acid, Figure 25). All four complexes exhibited SOD activity with IC_{50} values ranging from 1 to 73 μM (Table 6). The study was carried out using a variety of assays including the NBT reduction assay using KO_2 as a source of $\text{O}_2^{\cdot-}$ and the inhibition of cytochrome c reduction using xanthine - xanthine oxidase as the source of $\text{O}_2^{\cdot-}$. Whilst all of the complexes exhibited SOD activity, the order of activity was not preserved across the different assays.

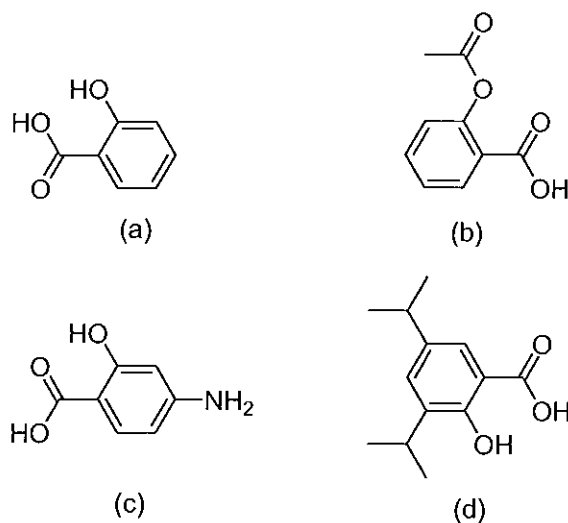


Figure 25: The structures of (a) salicylic acid, (b) acetylsalicylic acid, (c) *p*-aminosalicylic acid and (d) 3,5-diisopropylsalicylic acid

Table 6: The SOD activity of Cu-NSAID complexes as determined by Weser *et al*¹⁹

Compound	μM of complex producing a 50% inhibition in NBT reduction
SOD	0.04
SOD	0.06
[Cu(salH) ₂]	16
[Cu(salH) ₂]	1.3
[Cu(aspH) ₂]	23
[Cu(aspH) ₂]	2.15
[Cu(asalH) ₂]	28
[Cu(asalH) ₂]	3
[Cu(dipsH) ₂]	73
[Cu(dipsH) ₂]	2.85

Abuhijleh and Woods⁵⁰ have reported that the complex [Cu(meimH₆)](salH)₂ (where meimH = N-methylimidazole) (Figure 42) is a potent SOD mimic. An IC₅₀ value of 0.17 μM was determined using the indirect xanthine - xanthine oxidase system. The high SOD like activity of the complex was attributed to the coordination of four imidazole nitrogen atoms to the Cu(II) atom in the equatorial plane similar to the coordination site of Cu(II) in the native Cu/Zn SOD (Figure 100).

The SOD activity of the copper complex of the well known NSAID indomethacin (indoH) (Figure 27), [Cu₂(indo)₄(DMSO)₂] was first reported by Weser *et al* using pulse radiolysis (its DMF coordinated analogue is shown in Figure 26) . Second order rate constants of 6×10^9 and $1.1 \times 10^9 \text{ M}^{-1} \text{ s}^{-1}$ were obtained in aqueous and aqueous/aprotic solutions respectively. These values compared with $1.8 \times 10^5 \text{ M}^{-1} \text{ s}^{-1}$ for spontaneous superoxide dismutation, $2.6 \times 10^6 \text{ M}^{-1} \text{ s}^{-1}$ for indoH and $2.6 \times 10^9 \text{ M}^{-1} \text{ s}^{-1}$ for SOD, indicating [Cu₂(indo)₄(DMSO)₂] is a potent SOD mimic. Weser later determined IC₅₀ values for [Cu₂(indo)₄(DMSO)₂] which were found to range from 25 μM in acetonitrile

to 2 μM in DMSO.⁵¹ Dillon and co-workers determined an IC_{50} value of 0.23 μM for the complex using the NBT assay with xanthine - xanthine oxidase.⁵²

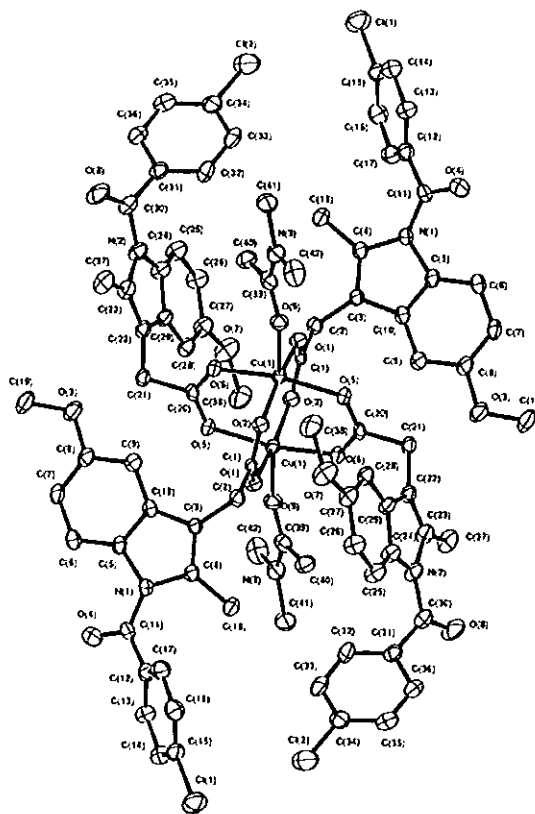


Figure 26: The X-ray crystal structure of $[\text{Cu}_2(\text{Indo})_4\text{DMF}_2] \cdot 2\text{DMF}$

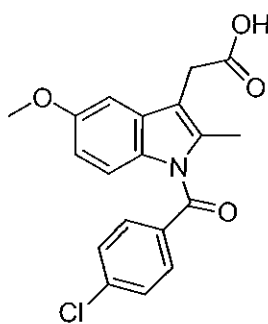


Figure 27: The structure of indomethacin (IndoH)

Demertzi *et al.*⁵³ have recently reported the structure and SOD like activity of a copper(II) complex of tolfenomic acid. The complex $[\text{Cu}_2(\text{tolf})_4(\text{DMF})_2]$ (Figure 28) is isostructural with $[\text{Cu}_2(\text{indo})_4(\text{DMSO})_2]$. Using the NBT reduction assay it was found to be a potent SOD mimic with an IC_{50} value of $1.97 \mu\text{M}$ reported. They also reported the activity of the copper complex $[\text{Cu}(\text{dicl})_2(\text{H}_2\text{O})]$ (where dicl = diclofenac, Figure 29) which was found to have an IC_{50} value of $2.17 \mu\text{M}$.

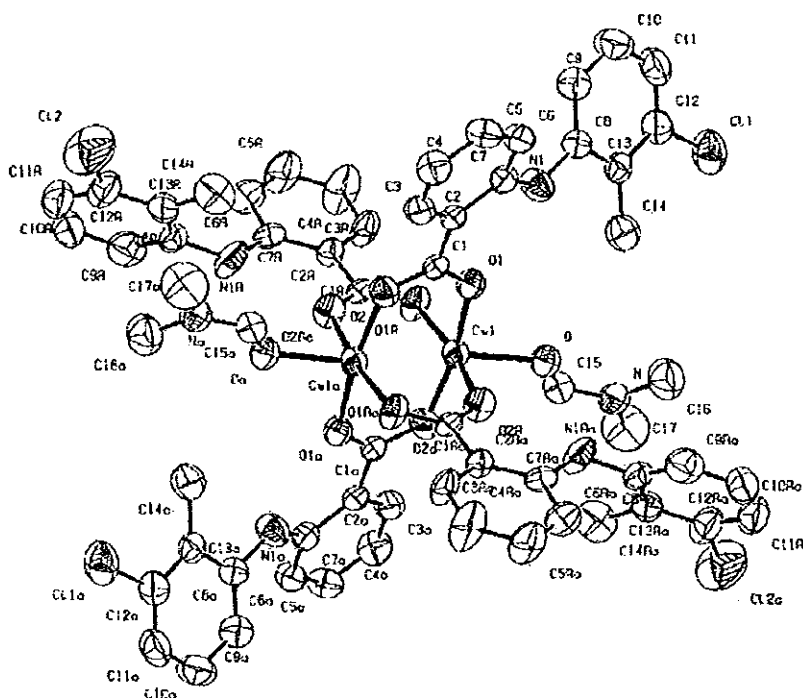


Figure 28: X - ray crystal structure of $[\text{Cu}_2(\text{tolf})_4(\text{DMF})_2]$

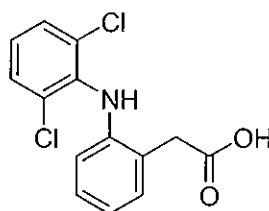


Figure 29: The structure of diclofenac

SOD activity has also been observed for other Cu-NSAIDs although IC_{50} values were not determined. Bury *et al.*⁵⁴ studied the SOD activity of a number of monomeric metal tenoxicam (Figure 30) complexes and showed that the Cu(II) complex exhibited the greatest activity followed by Mn(II), Co(II), Ni(II), Fe(III) and finally the free ligand. The salicylate iron complex was shown by Jay *et al.* to have $O_2^{\cdot -}$ scavenging properties.⁵⁵ The complex was shown to inhibit the reduction of NBT in a xanthine-xanthine oxidase system.

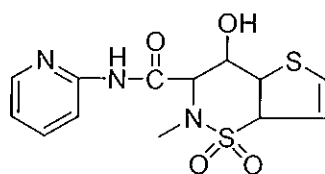


Figure 30: The structure of tenoxicam

I.4 METAL COMPLEXES AS ANTICANCER AGENTS

I.4.1 Introduction

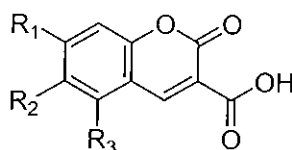
The importance of metal-based anticancer agents is undisputed as can be judged by the discovery and subsequent success of the platinum(II) complex, cisplatin. Since its discovery several synthesised derivatives have exhibited similar and, in some cases, improved activity in the treatment of a variety of solid tumors, especially testicular cancer. When combined with other drugs it has successfully been used to treat brain, ovarian, bladder and breast cancer.⁵⁶ Many other transition metal complexes have since been tested and have shown varying degrees of success against a variety of cancer cell lines.⁵⁷

One of the great biological ironies of metals is their ability to both treat and induce cancer.⁵⁸ Almost all metals are able to generate reactive oxygen species (ROS), this property explains a great part of both their carcinogenicity and their aptitude to treat cancer.

Often, in cancerous cells SOD activity is low while cellular metabolism is high. This situation can lead to raised levels of superoxide and therefore increased chances of tumor formation. SOD-like metallo-compounds can be used in the treatment of cancerous cells by converting $O_2^{\bullet-}$ into H_2O_2 , which itself is a regulator of cell death.⁵⁹

I.4.2 Metal carboxylate anticancer compounds

Recently this group has reported that Ag(I) carboxylate complexes of salicylic acid (salH_2) and Ag(I) complexes of coumarin-3-carboxylic acids (C-3-COOH)⁶⁰ (Figure 31), have exhibited significant anticancer activity against human carcinoma cell lines (Table 7) compared with their free ligands and in some cases cisplatin.



6-hydroxycoumarin-3-carboxylic acid (6-OH-C-3-COOH): $R_1 = \text{OH}$, $R_2, R_3 = \text{H}$
7-hydroxycoumarin-3-carboxylic acid (7-OH-C-3-COOH): $R_2 = \text{OH}$, $R_1, R_3 = \text{H}$
8-hydroxycoumarin-3-carboxylic acid (8-OH-C-3-COOH): $R_3 = \text{OH}$, $R_1, R_2 = \text{H}$
coumarin-3-carboxylic acid (C-3-COOH): $R_1, R_2, R_3 = \text{H}$

Figure 31: The general structural formulae for coumarin-3-carboxylic acid (C-3-COOH) and its derivatives.

The 6, 7 and 8-hydroxycoumarin-3-carboxylate containing complexes displayed significant anticancer activity against both cell lines with 6-OH-C-3-COO-Ag displaying the greatest ($\text{IC}_{50} = 2.7 \mu\text{M}$) against the human liver derived carcinoma (Hep-G₂) and 8-OH-C-3-COO-Ag being particularly potent ($\text{IC}_{50} = 17.0 \mu\text{M}$) against the human kidney derived carcinoma (A-498). Significantly the non-hydroxylated Ag(I) coumarin complex exhibited the weakest activity with IC_{50} values being in excess of $100 \mu\text{M}$ for both cell lines. It is interesting that these Ag(I) coumarin complexes did not intercalate DNA nor were they found to be mutagenic. These complexes did, however, cause a dose-dependant decrease in cellular DNA synthesis through an alternative mode of action, yet to be elucidated.

Table 7: The chemotherapeutic potential for a range of Ag(I) carboxylate containing complexes along with cisplatin and Ag(I) perchlorate.

Complex	Hep-G ₂ IC ₅₀ (μ M) \pm SEM	A-498 IC ₅₀ (μ M) \pm SEM
Cisplatin	15.0 \pm 2.6	14.0 \pm 2.3
AgClO ₄	7.6 \pm 0.7	44.4 \pm 2.3
<i>Coumarin-3-Carboxylates</i>		
C-3-COOH	>250	>250
6-OH-C-3-COOH	>250	>250
7-OH-C-3-COOH	>250	>250
8-OH-C-3-COOH	>250	>250
C-3-COO-Ag	170 \pm 3.5	110.0 \pm 1.6
6-OH-C-3-COO-Ag	2.7 \pm 2.8	30.0 \pm 2.4
7-OH-C-3-COO-Ag	7.5 \pm 0.5	35.5 \pm 1.9
8-OH-C-3-COO-Ag	5.5 \pm 2.0	17.0 \pm 2.2
<i>Salicylic acids</i>		
salH ₂	>250	>250
[Ag ₂ (salH) ₂]	20 \pm 1	18 \pm 2
[Ag ₂ (NH ₃) ₂ (salH) ₂]	9 \pm 0	32 \pm 7

Both [Ag(salH)₂] and [Ag₂(NH₃)₂(salH)₂] complexes showed no enhanced chemotherapeutic activity against Hep-G₂ compared with the simple Ag(I) perchlorate salt. However, both complexes did show an improvement compared with the metal salt against the A-498 carcinoma with dimeric [Ag₂(salH)₂] offering some bias toward inhibition. Although mode of action studies were not carried out on these complexes it was found previously that Ag(I) complexes interfere with mitochondrial function in fungal cells.⁶¹

I.4.3 Metal phenanthroline anticancer agents

The chemotherapeutic potential for 1,10-phenanthroline (phen) and a series of its coordinated analogues, where malonic acid acts as a coordinated counter ion⁶², is shown below in Table 8. Also shown in the same table are the chemotherapeutic potentials of Cu(II) and Ag(I) perchlorate complexes of phendione.⁶³ These results are shown in conjunction with the activity of cisplatin and simple metal salts.

Table 8: The chemotherapeutic potential for phen, phendione and their metal complexes along with the metal salts

Complex	Hep-G ₂ IC ₅₀ (μ M) \pm SEM	A-498 IC ₅₀ (μ M) \pm SEM
Cisplatin	15.0 \pm 2.6	14.0 \pm 2.3
Cu(ClO ₄) ₂ .6H ₂ O	>1000	> 1000
Mn(ClO ₄) ₂ .6H ₂ O	626.7 \pm 27.29	880.0 \pm 20.0
AgClO ₄	7.6 \pm 0.7	44.4 \pm 2.3
Phen	4.1 \pm 0.54	5.8 \pm 0.31
phendione	4.2 \pm 0.36	1.4 \pm 1.34
<i>phen malonate complexes</i>		
[Cu(phen) ₂ (mal)].2H ₂ O	0.8 \pm 0.02	3.8 \pm 0.41
[Mn(phen) ₂ (mal)].2H ₂ O	0.8 \pm 0.07	4.2 \pm 0.57
[Ag ₂ (phen) ₂ (mal)].2H ₂ O	4.7 \pm 0.26	4.0 \pm 0.32
<i>phendione complexes</i>		
[Cu(phendione) ₃](ClO ₄).4H ₂ O	0.88 \pm 0.06	0.78 \pm 0.09
[Ag(phendione) ₂](ClO ₄)	1.4 \pm 0.47	0.86 \pm 0.87

Phen, found to be active itself against Hep-G₂ (IC₅₀ = 4.1 μ M) and A-498 (IC₅₀ = 5.8 μ M) cell lines, once coordinated together with malonic acid displayed enhanced chemotherapeutic potential with IC₅₀'s ranging between 0.8 – 4.7 μ M for the liver derived carcinoma cell line (Hep-G₂) and between 3.8 – 4.0 μ M for the kidney derived cells (A-498).

Further studies were carried out on the phen-malonate complexes in order to elucidate the reduction in cancer cell viability. The effect these compounds had on DNA synthesis was also examined. Phen along with all its coordinated malonate analogues

were found to prevent DNA synthesis but were not found to intercalate. Additionally a standard Ames test proved that each of the complexes were non-mutagenic. Importantly this group of complexes showed IC_{50} cytotoxicity values of between 3 and 18 times greater than those obtained for cisplatin. It was therefore concluded that phen and these malonate metal complexes offer a possible alternative to cisplatin in the successful treatment and management of cancer.

Phendione was also found to be active itself with a similar cytotoxicity IC_{50} value to phen against Hep-G₂ (4.2 ± 0.36) carcinoma and a significantly improved value compared with phen against A-498 (1.4 ± 1.34) carcinoma. Coordination of phendione to Cu(II) and Ag(I) yields an improvement in cytotoxicity against both cell lines with Cu(II) being slightly more potent than its Ag(I) analogue (Hep-G₂ $IC_{50} = 0.88 \pm 0.06$, A-498 $IC_{50} = 0.78 \pm 0.09$). Although the Cu(II) and Mn(II) phen malonates exhibit almost identical IC_{50} values against Hep-G₂ as the $[Cu(\text{phendione})_3](ClO_4) \cdot 4H_2O$ complex, there is improvement in activity in both of the phendione Ag(I) and Cu(II) complexes compared to the phen malonate complexes against the A-498 kidney derived cell line, with the phendione complexes being approximately 5 times more active. The mechanism of action for these exciting and novel anticancer agents has yet to be determined but it has been demonstrated that, unlike doxorubicin, they do not intercalate DNA.

I.4.4 Chemotherapeutic potential of Cu(II) benzimidazole derivatives

Thiabendazole is a well known anthelmintic which is non-toxic to humans⁶⁴ and it has applications as a fungicide in agriculture.⁶⁵ Recently this group has published the anticancer activity for copper(II) complexes of TBZH. The chemotherapeutic potential for TBZH along with its copper containing complexes [Cu(TBZH)₂Cl]Cl.H₂O.EtOH and [Cu(TBZH)₂(NO₃)₂] is displayed in Table 9. The growth of the two human derived cancer cell lines CAL-27 (tongue) and SK-MEL-31 (skin) was inhibited by the coordinated metal complexes with IC₅₀ values ranging between 55.0 μM – 46.7 μM while thiabendazole itself was only found to exhibit mild cytotoxicity toward the cancer cells.

Table 9: The chemotherapeutic potential for TBZH and its copper complexes

Complex	CAL-27 IC ₅₀ (μM) ± SEM	SK-MEL-31 IC ₅₀ (μM) ± SEM
TBZH	676.7 ± 12.0	453.3 ± 66.0
[Cu(TBZH) ₂ Cl]Cl.H ₂ O.EtOH	55.0 ± 0.0	49.5 ± 7.7
[Cu(TBZH) ₂ (NO ₃) ₂]	54.0 ± 2.5	46.7 ± 5.0

Subsequent screening of the previously mentioned complexes [Cu(2-OxBZDH)Cl₂] (Figure 20), [Cu(2-PyzBZDH)(DMF)Cl₂] (Figure 21) and [Cu(2-ImBZDH)Cl₂]⁴⁶ which were found to be excellent SOD mimetics against bladder (5637), esophageal (KYSE-520) and cervical (SISO) human tumor cell lines revealed only modest cytotoxicity toward the cell lines compared with cisplatin.

1.5 METAL CARBOXYLATE CHEMISTRY

1.5.1 Coordination modes of metal carboxylates

Carboxylates serve as an important class of ligand in inorganic and bioinorganic chemistry. The versatility of the RCO_2^- ligand is attributed to the wide range of coordination modes that it can adopt. The coordination chemistry of monocarboxylic acids is well established, and a large number of carboxylate complexes have been structurally characterised.⁶⁶ In metal carboxylates the positively charged metal centres (M^{n+}) are found in combination with negatively charged carboxylate groups (RCO_2^-), and the bonding between the metals and the carboxylate group ranges from ionic to polar covalent. For a given type of compound (i.e. a given metal, oxidation state and structural type) a wide variety of physical and chemical properties can be conferred by varying the nature of the R group.

The carboxylate functional group has four lone pairs of electrons available for metal binding. These lone pairs subtend to an angle of 120° and are referred to as the *syn*- and *anti*-lone pairs (Figure 32). On the basis of stereoelectronic arguments it has been suggested that the *syn*-lone pairs are more basic than those in the *anti* position.⁶⁷

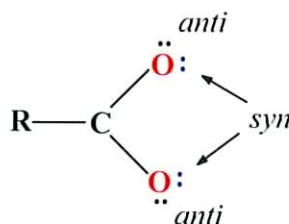


Figure 32: The carboxylate functional group

The various coordination modes of the RCO_2^- ligand are listed below:

(i) Ionic: The carboxylate salts of Na, K, Rb, and Cs have been shown to be ionic, with only coulombic interactions between the metal and the carboxylate ions (Figure 33(a)).

(ii) Monodentate: In lithium acetate the metal is coordinated to one of the carboxylate oxygens (Figure 33(b)).

(iii) Bidentate Chelating: Carboxylates may chelate either in a symmetrical mode (Figure 33(c)), with both metal-oxygen bonds being of equal length, or in the asymmetrical mode (Figure 33(d)) where one metal-oxygen bond is shorter than the other. In zinc(II) acetate dihydrate the bonding mode of the acetate is symmetrical bidentate chelating, while in the mixed-ligand complex $[\text{Zn}(\text{phen})_2(\text{O}_2\text{CCH}_3)][\text{ClO}_4]^{68}$ it is asymmetrical bidentate chelating. It has been found that the “bite angle” (i.e. the O-M-O angle) for a chelating carboxylate is *ca.* 60° which, being fairly small, distorts the octahedral geometry of many metal complexes.

(iv) Bridging: The planar carboxylate ion is ideally suited to the formation of complexes in which the carboxylate bridges two metal atoms (Figure 33(e-g)). The *syn-syn* mode is of particular interest since it is the type of bridging observed in the “lantern shaped” (paddlewheel) bimetallic carboxylates such as copper(II) acetate dihydrate. The *syn-syn* coordination mode is the only one which allows the ligand to bridge the short metal-metal

bonds found in these binuclear complexes. Several binuclear ruthenium complexes have carboxylate bridges in which the *anti-anti* mode of binding is found.⁶⁹

(v) Monodentate Terminal Bridging: This is one of the rarer binding modes (Figure 33(h)) and it has been suggested to be important biologically, and it is thought to act as an intermediate between other carboxylate bridging modes.⁶⁷ This coordination mode has been reported for the structurally characterised, H₂O₂ disproportionation catalyst [Mn₂(salH)₄(H₂O)₄]⁷⁰ (Figure 39).

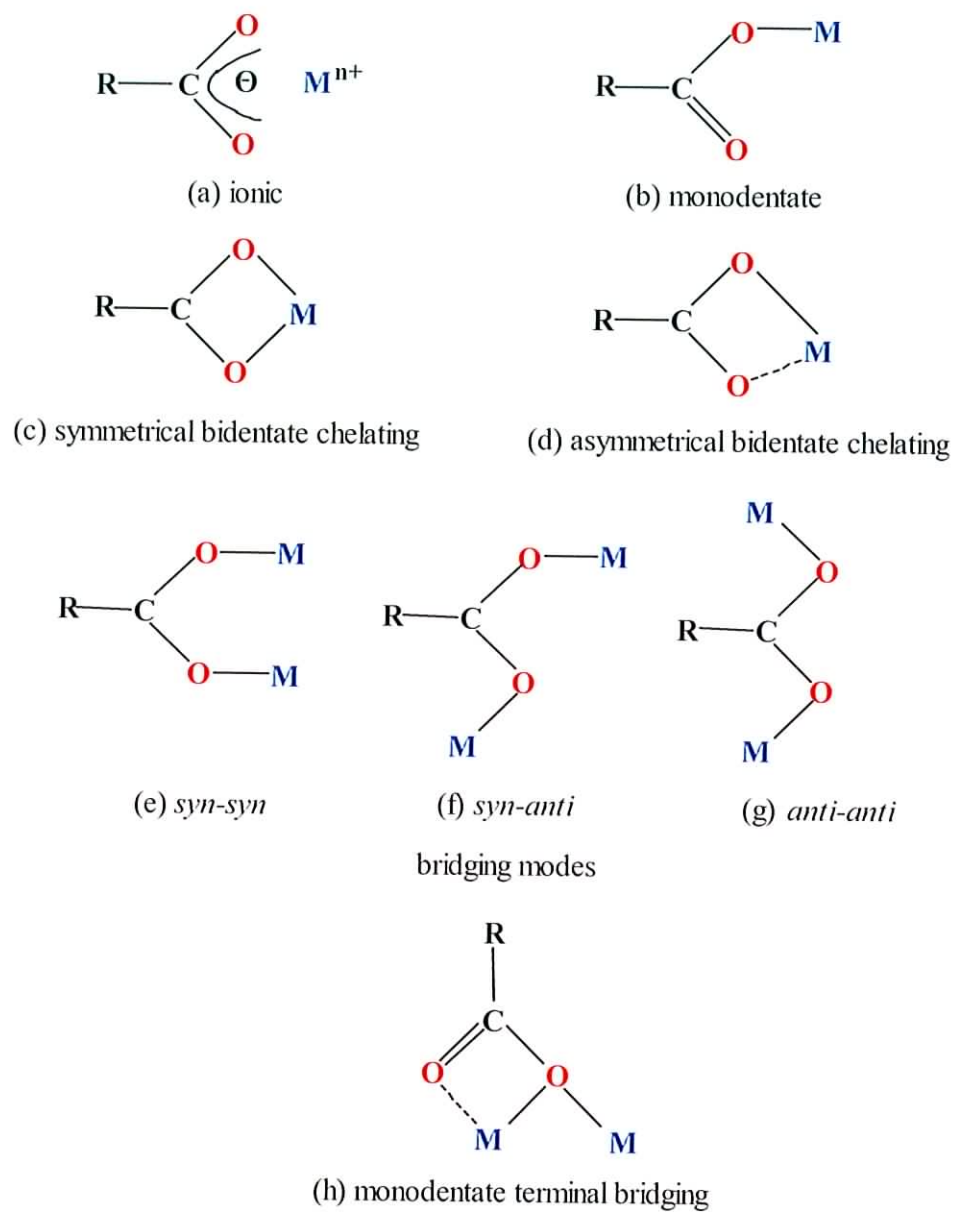


Figure 33: Coordination modes of monocarboxylic acids

1.5.2 Infrared spectra of carboxylate complexes^{71,72}

Upon complexation to a metal centre the $\nu_{\text{C=O}}$ absorption band of the $-\text{CO}_2\text{H}$ group in the free acid disappears, and two new bands relating to the antisymmetric ($\nu_{\text{asym}}(\text{COO})$) and symmetric ($\nu_{\text{sym}}(\text{COO})$) stretch appear around 1630-1585 and 1355-1330 cm^{-1} , respectively. The magnitude of separation between these two bands (Δ_{OCO} cm^{-1}) has been used as a diagnostic aid in the determination of the nature of the carboxylate coordination.

$$\Delta_{\text{OCO}} = (\nu_{\text{asym}}(\text{COO}) - \nu_{\text{sym}}(\text{COO})) \text{ cm}^{-1}$$

Deacon and Phillips⁷¹ compiled guidelines for diagnosing the type of carboxylate coordination based on a metal complex's infra-red spectrum. Their findings were based on spectral data obtained for eighty four complexed acetates and halogenoacetates, and are summarised below:

- (i) Ionic acetates, such as those of the alkali metals, have Δ_{OCO} values of *ca.* 165 cm^{-1} . For ionic trifluoroacetates the Δ_{OCO} value was *ca.* 235 cm^{-1} .
- (ii) Δ_{OCO} values < 105 cm^{-1} indicated symmetric chelating carboxylate coordination. Complexes in which the carboxylates bridge short metal-metal bonds may also show such low values.

(iii) Δ_{OCO} values substantially less than the ionic values (i.e. $< 150 \text{ cm}^{-1}$ for acetates) indicate the presence of chelating or bridging carboxylate. Unidentate carboxylates which are strongly hydrogen-bonded (“pseudo-bridging”) may also fall into this category.

(iv) For complexes with Δ_{OCO} values similar to those for ionic carboxylates the assignments were counted as untrustworthy. The authors found many examples of each type of coordination mode (except for symmetric chelating) in this category.

(v) Unidentate coordination was suggested for complexes where the Δ_{OCO} value was substantially greater than those for the ionic carboxylates (i.e. $> 200 \text{ cm}^{-1}$ for acetates). An explanation for this difference in energy may be that the bonding of one oxygen to a metal, with the other oxygen free, increases the energy of the antisymmetric stretching mode.

The above observations are summarised in Table 10.

For a variety of reasons there can be many contradictions in the ν_{OCO} proposed band assignments. For example anion exchange from the alkali halide infra-red discs can occur, and there can also be uncertainties in locating exactly the $\nu_{\text{sym}}(\text{COO})$ stretching band.

With alkoxy- and aryloxy-acetato ligands that contain both carboxylic acid and ether (RCOCR) moieties (e.g. (-)-menthoxyacetic acid, phenoxyacetic acid, and benzene-1,2-dioxyacetic acid) the ethereal oxygens are also potential donor atoms to metal centres. Coordination of the ethereal oxygens to a metal centre should lead to a shift of the ν_{COC}

infra-red stretching frequencies similar to that found for the carboxylate group. Surprisingly, the stretching frequencies of the ethereal $\nu_{\text{asym}}(\text{COO})$ and $\nu_{\text{sym}}(\text{COO})$ stretching bands of the alkoxy- and aryloxy-acetato ligands are somewhat insensitive with respect to coordination or non-coordination of the ether oxygen. Guinan *et al.*⁷³ reported that the ethereal bands appeared at similar positions to those in the free acids in the complex $[\text{Cu}(\text{menth})_2(\text{H}_2\text{O})_2]$ (menthH = (-)-menthoxyacetic acid). However, Brzyska and co-workers⁷⁴ noted a slight shift to lower frequencies of the ν_{OCO} in the infra-red spectra of rare earth complexes of benzene-1,2-dioxyacetic acid.

Table 10: Infra-red spectral data (ν_{OCO}) for coordinated acetate ligands.

$\Delta_{\text{OCO}}(\text{CH}_3\text{CO}_2^-)$ (cm^{-1})	Coordination mode
< 105	symmetric chelating or short bridging
< 150	chelating or bridging
<i>ca.</i> 165	untrustworthy assignments
> 200	Unidentate

1.5.3 THE CHEMISTRY OF SALICYLIC ACID

1.5.3.1 Introduction to salicylic acid

Salicylic acid (2-hydroxybenzoic acid, Figure 34) was first purified from salicin (Figure 34) in 1838 and chemically synthesised in 1860. It is found ubiquitously in plants, where it plays a role in disease resistance.⁷⁵ Salicylic acid is readily soluble in hot water and most other common solvents but only slightly soluble in cold water. Salicylic acid sublimates at 211 °C and has a pKa of 2.98.

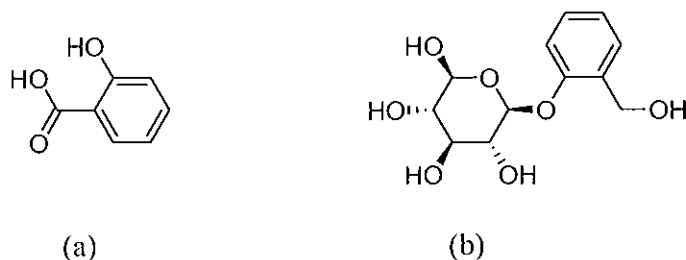


Figure 34: The structures of (a) salicylic acid and (b) salicin

1.5.3.2 Medicinal applications of salicylic acid

Salicylic acid and salicylates, obtained from natural sources, have long been used as medicaments. (Extracts of willow, a source of salicin, were used for the relief of pain and fever by the physician Hippocrates ~460BC). It has been used as an antiseptic, an antipyretic, and an antirheumatic. Aspirin (Figure 35) was introduced into medicine by Frederick Bayer & Company in 1889 as a more palatable form of salicylate. Soon after, other drugs having similar actions to aspirin were discovered and the group was termed the nonsteroidal anti-inflammatory drugs (NSAIDs).

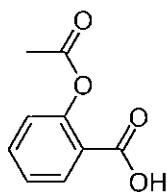


Figure 35: The structure of acetylsalicylic acid (aspirin)

Salicylic acid has applications in the treatment of dermatological complaints due to its keratolytic properties. It is applied externally, usually as a 1 to 5 % dusting-powder, lotion, or ointment for the treatment of chronic ulcers, dandruff, eczema, psoriasis, hyperhidrosis and parasitic skin diseases. It is also used in conjunction with many other agents, such as benzoic acid. Externally it produces slow and painless destruction of the epithelium and it is applied in the form of a paint in a collodion (10 to 17 %) or as a plaster (20 to 50 %) to destroy warts or corns.

Salicylate has been shown to have chemopreventative activity against colorectal and esophageal cancers.⁷⁶ It has also been shown that salicylate induces apoptosis in a number of leukemia cell lines.⁷⁷

Salicylic acid and its substituted derivatives have recently been shown to inhibit mycelial growth of *Eutypa lata* in solid as well as liquid culture medium in a concentration-dependant manner.⁷⁸ They found that salicylic acid causes considerable disturbances in many compartments of the fungal cell, particularly the mitochondria. Salicylic acid was found to directly affect cell respiration, redirecting electron flow from the cytochrome pathway into the cyanide-resistant alternative pathway. As a consequence, the cytochrome pathway is

not fully utilised. Salicylic acid also binds to a catalase protein which reduces the activity of the enzyme, promoting an accumulation of H_2O_2 , which is toxic for many cell functions.

1.5.3.3 Coordination modes of salicylic acid

In many cases the biological activity of salicylate is connected with the ability of the acid to bind to metal ions. The acid has three potential donor oxygens; the two carboxylate oxygens and the single phenolate oxygen. Some of the possible coordination modes of salicylic acid are shown in Figure 36.

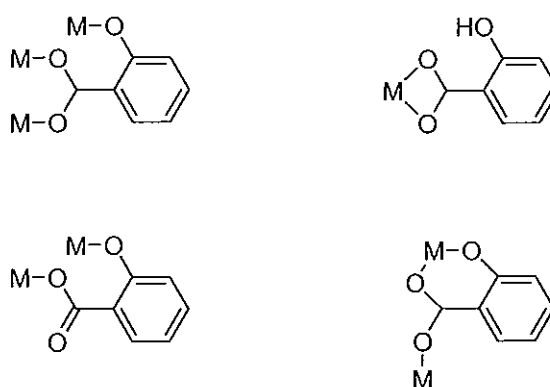


Figure 36: Some of the possible coordination modes of salicylic acid

It is well known that copper(II) complexes of inactive ligands and anti-inflammatory organic drugs are generally more active than the free ligands or organic drugs themselves.⁷⁹

It has been suggested that the biological activity of acetylsalicylic acid is due to its ability to form metal complexes⁸⁰, and that the active form of the drug is, in fact, a copper complex, formed *in vivo*.⁸¹ The laboratory synthesised copper(II) complex of aspirin $[\text{Cu}_2(\text{O}_2\text{CC}_6\text{H}_4\text{OCOCH}_3)_4]$ (Figure 70) has been found to be more effective than aspirin

itself as an anti-inflammatory agent. In addition, the copper complex also has antiulcer activity, which further distinguishes it from aspirin which itself is ulcerogenic.⁸²

Over seventy copper complexes have been studied as anti-inflammatory agents, and some of these are carboxylate complexes. Molecules such as anthranilic acid (2-aminobenzoic acid) and 3,5-diisopropylsalicylic acid were found to be inactive. However, the copper complexes of these acids were found to be potent anti-inflammatory agents.⁷⁹

1.5.3.4 Coordination complexes of salicylic acid

In 1959, Hanic and Michalov⁸³ determined the crystal structure of the square planar copper(II) complex $[\text{Cu}(\text{salH})_2(\text{H}_2\text{O})_2] \cdot 2\text{H}_2\text{O}$ (Figure 37). The two *trans* salicylate ligands coordinate to the metal in a unidentate fashion via their carboxylate groups with the remaining two coordination sites taken by two water molecules.

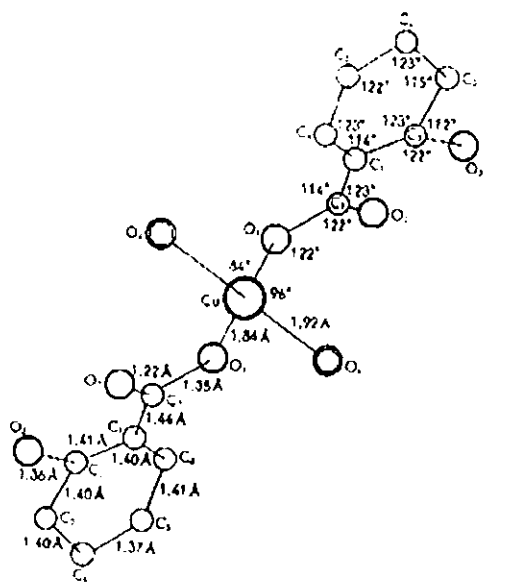


Figure 37: X-ray crystal structure of $[\text{Cu}(\text{salH})_2(\text{H}_2\text{O})_2] \cdot 2\text{H}_2\text{O}$

In his investigations on the complex $[\text{Cu}(\text{salH})_2] \cdot 4\text{H}_2\text{O}$, Ploquin⁸⁴ found a subnormal value for the magnetic moment, which points to considerable interaction between the Cu(II) atoms. However, Hanic and Michalov's description of the crystal structure did not indicate such an interaction between the Cu(II) atoms. Inoue *et al*⁸⁵ explained the apparent disagreement in these experimental findings through their preparation of two modifications of $[\text{Cu}(\text{salH})_2] \cdot 4\text{H}_2\text{O}$. The one that separated as turquoise blue needles had a magnetic moment of 1.92 B.M. and showed good agreement with the solved crystal structure. The

second form, which crystallised as blue-green plates, exhibited the anomalously low magnetic moment of 1.45 B.M., in accordance with Ploquin's result.

Yoneda *et al.*⁸⁶ structurally characterised the dinuclear complex $[\text{Cu}_2(\text{salH})_4(\text{EtOH})(\text{H}_2\text{O})]$ and its structure is shown in Figure 38. The complex adopts the classical "paddle – wheel" structure with two copper atoms bridged by four salicylate anions $[\text{Cu} - \text{Cu}: 2.621\text{\AA}]$. An interesting feature of the complex is the presence of two different ligands (a water and an EtOH molecule) at the apical positions.

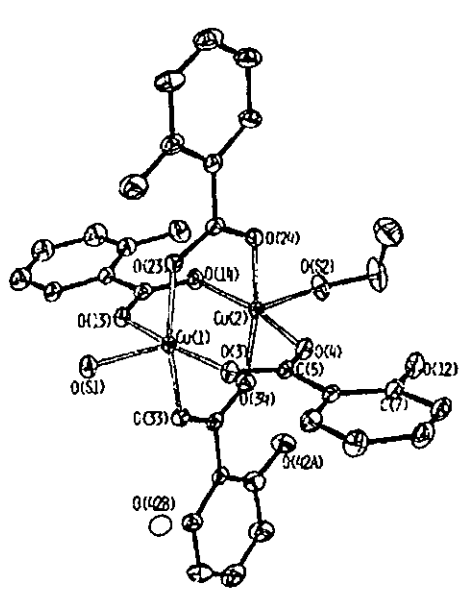


Figure 38: The X-ray crystal structure of $[\text{Cu}_2(\text{salH})_4(\text{EtOH})(\text{H}_2\text{O})]$

The manganese(II) salicylate complex $[\text{Mn}_2(\text{salH})_4(\text{H}_2\text{O})_4]$ (Figure 39) has also been structurally characterised.⁷⁰ The complex is comprised of two associated and pseudo seven-coordinate manganese(II) centres ($\text{Mn}-\text{Mn} = 3.719\text{\AA}$). Each manganese atom is asymmetrically chelated by two salicylate ligands, and perpendicular to the central plane

there are two coordinated water molecules. Association of the two metals occurs via the carboxylate oxygen atoms from a second pair of chelating salicylate ligands, effectively creating two asymmetric bridges between the manganese atoms. The stability of the complex is further enhanced by intra-molecular hydrogen bonding between the hydroxyl groups of the salicylate and one carboxylate oxygen of the same ligand.

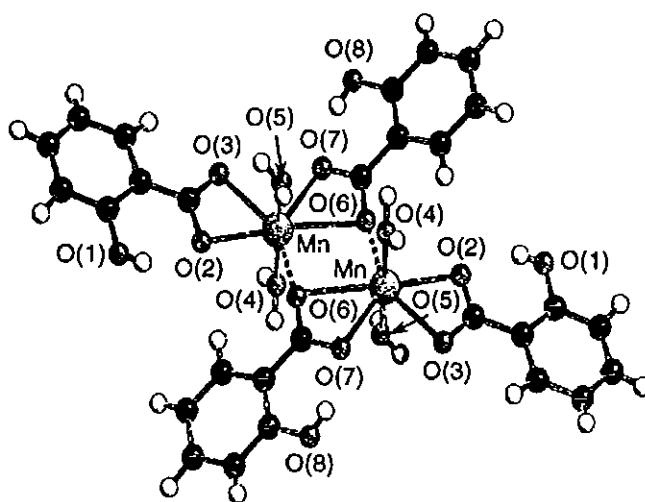


Figure 39: X-ray crystal structure of [Mn₂(salH)₄(H₂O)₂]

The complexes [Cu₂(dipsH)₄(DMF)₂] (Figure 40) and [Cu₂(dipsH)₄(Et₂O)₂] have been synthesised and characterised by Morgant *et al.*⁸⁷ The crystal structures of the two complexes are essentially the same except for the DMF or Et₂O accommodation. Both complexes are binuclear with the two copper atoms bridged by four 3,5-diisopropylsalicylic acid ligands [Cu-Cu: 2.613Å], giving the familiar “paddle-wheel” structure. The square pyramidal geometry about each Cu atom is completed by coordination to the DMF (or Et₂O) oxygen atom. As is typical of this type of dimer the two apical Cu-O bonds are significantly longer than the four Cu-carboxylate bonds. The axial Cu-O bond is also

longer in $[\text{Cu}_2(\text{dipsH})_4(\text{Et}_2\text{O})_2]$ (2.230 Å) than $[\text{Cu}_2(\text{dipsH})_4(\text{DMF})_2]$ (2.129 Å), which might be explained due to diethylether steric hindrance.

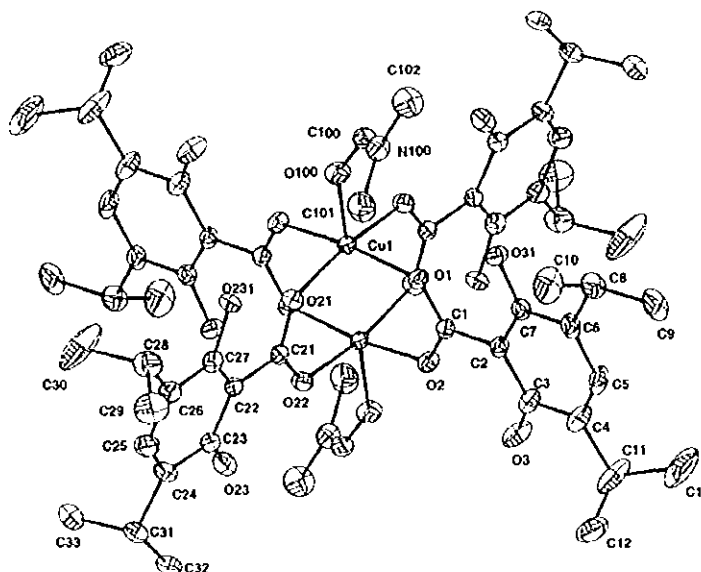


Figure 40: X-ray crystal structure of $[\text{Cu}_2(\text{dipsH})_4(\text{DMF})_2]$

In 2004 Valigura *et al.*⁸⁸ prepared and structurally characterised the trimeric complex $[\text{Cu}_3(\text{dns})_2(\text{dnsH})_2(\text{H}_2\text{O})_4] \cdot 4\text{H}_2\text{O}$ (where $\text{dnsH}_2 = 3,5\text{-dinitrosalicylic acid}$). An interesting feature of the complex is the presence of both monoanionic and dianionic salicylate, the first example of this in a substituted salicylate complex. The complex is centrosymmetrical with the Cu(1) atom being in the centre of symmetry. The two salicylate ligands are bonded to Cu(1) via one oxygen atom of the carboxylate group and the oxygen of the phenolato group, forming a six membered ring with square planar geometry. The second oxygen of the carboxylate group is bonded to the terminal Cu(2) atom forming the bridging *syn-anti* bonding mode. Each of the terminal Cu atoms exhibits square pyramidal geometry

formed by the carboxylate oxygen of the bridging salicylate and by two oxygens of the terminal chelating salicylate monoanion and by two oxygens of water molecules.

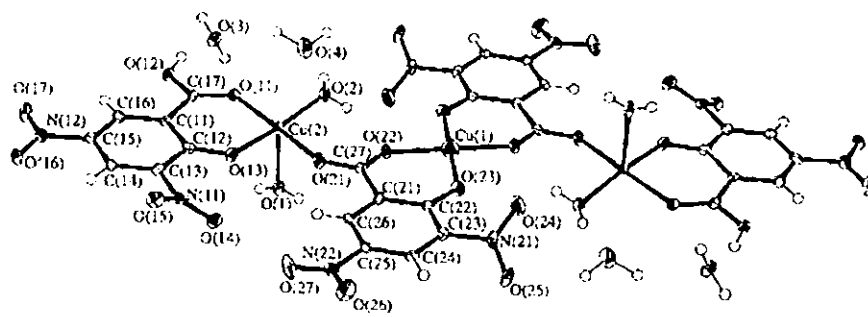


Figure 41: X-ray crystal structure $[\text{Cu}_3(\text{dns})_2(\text{dnsH})_2(\text{H}_2\text{O})_4] \cdot 4\text{H}_2\text{O}$

Abuhijleh and Woods⁸⁹ have prepared and characterised the complex $[\text{Cu}(\text{meimH})_6](\text{salH})_2$ (Figure 42) from the reaction of copper(II) aspirinate with N-methylimidazole. The complex consists of a hexakis (N-methylimidazole) copper (II) cation with two non-coordinated salicylate anions. The two apical N-methylimidazole ligands lie at a slightly larger distance (2.697 Å) from the copper centre than the equatorial ones (2.004 Å).

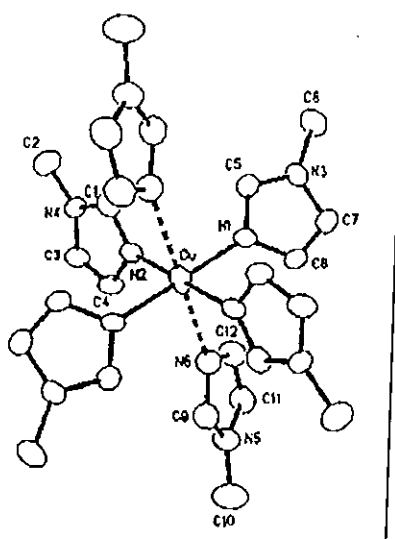


Figure 42: X-ray crystal structure $[\text{Cu}(\text{meimH})_6] \cdot 2\text{salH}$

They have also structurally characterised a series of mononuclear complexes of the type $[\text{Cu}(\text{imH})_n(\text{salH})_2]$ where $n = 2, 5$ or 6 .⁹⁰ (imH = imidazole) The complexes crystallise as a mixture from the reaction of copper(II) aspirinate with imidazole. $[\text{Cu}(\text{imH})_2(\text{salH})_2]$ (Figure 43) was shown to have a trans geometry in which the imidazole and salicylate ligands are both coordinated to the copper ion. The salicylate anions coordinate unidentally through a single carboxylate oxygen. The complexes $[\text{Cu}(\text{imH})_5] \cdot 2\text{salH}$ (Figure 44) and $[\text{Cu}(\text{imH})_6] \cdot 2\text{salH}$ (Figure 45) exhibit square pyramidal and octahedral geometry respectively. In $[\text{Cu}(\text{imH})_5] \cdot 2\text{salH}$ the five imidazole ligands are directly coordinated to the copper centre. The two salicylate groups are strictly counter-ions but are extensively hydrogen-bonded to the imidazole ligands. $[\text{Cu}(\text{imH})_6] \cdot 2\text{salH}$ is structurally similar to the previously mentioned $[\text{Cu}(\text{meimH})_6] \cdot 2\text{salH}$, however the Cu-N distances are shorter by 0.25 \AA . It is not clear whether this is due to electronic or steric differences.

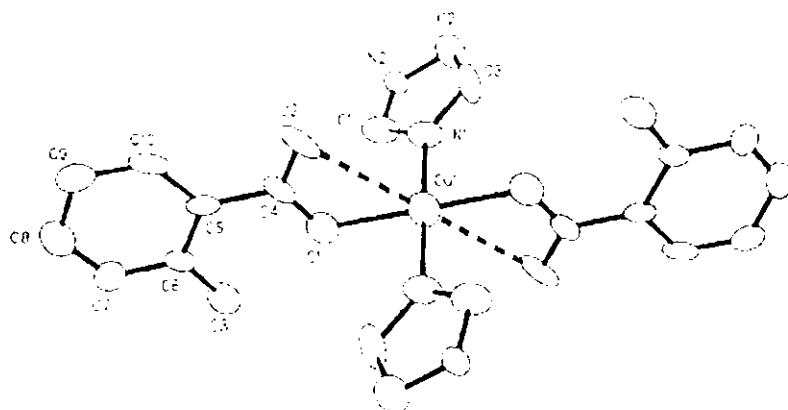


Figure 43: X-ray crystal structure of [Cu(imH)₂(salH)₂]

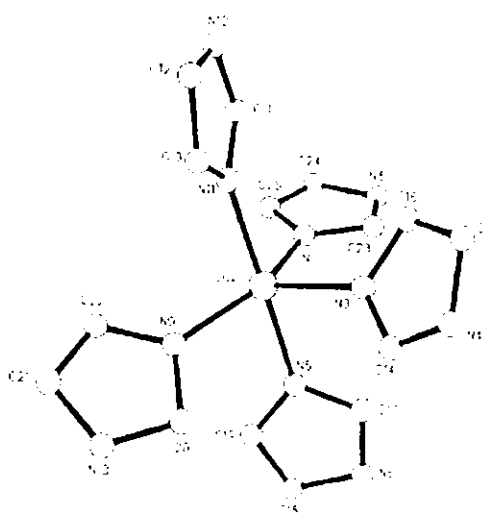


Figure 44: X-ray crystal structure of [Cu(imH)₅].2salH₂

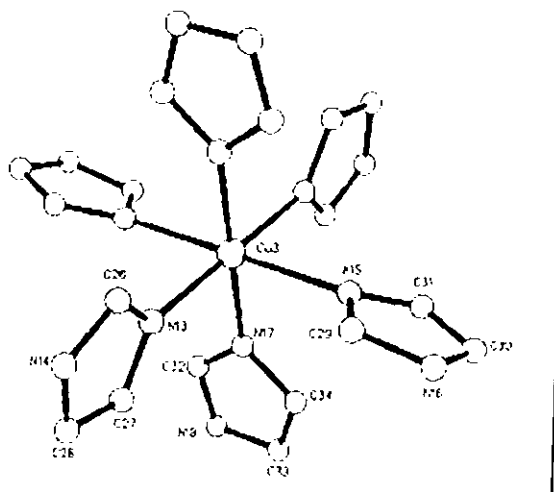


Figure 45: X-ray crystal structure of $[\text{Cu}(\text{imH})_6] \cdot 2\text{salH}_2$

The structure of the copper(II) salicylate complex incorporating bipy, $[\text{Cu}(\text{sal})(\text{bipy})] \cdot \text{EtOH} \cdot \text{H}_2\text{O}$ was reported by this group in 1999.⁹¹ Its structure is shown in Figure 46. The copper(II) ion is coordinated to the two nitrogen donors of the bipy ligand and chelated by the salicylate dianion via one carboxylate oxygen atom and the phenolate oxygen atom, giving the copper atom an approximate square planar geometry. The coordination sphere of the copper is completed by a long axial bond to the phenolate oxygen (Cu-O: 2.445 Å) of a second $[\text{Cu}(\text{sal})(\text{bipy})]$ unit. This axial interaction links the individual $[\text{Cu}(\text{sal})(\text{bipy})]$ units into $\{[\text{Cu}(\text{sal})(\text{bipy})] \cdot \text{EtOH} \cdot \text{H}_2\text{O}\}_2$ dimers.

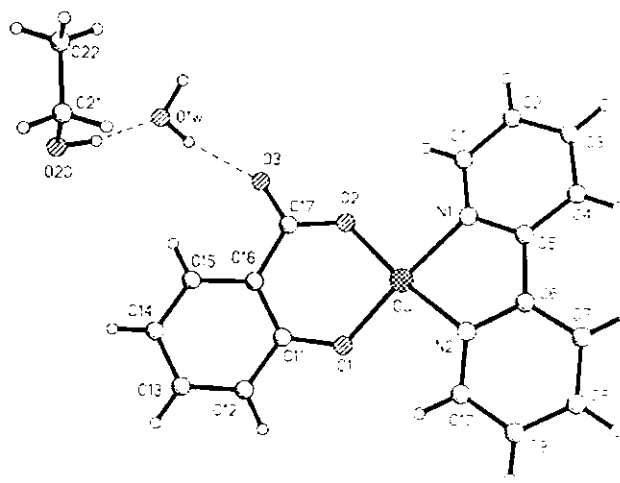


Figure 46: X-ray structure of a $[\text{Cu}(\text{sal})(\text{bipy})].\text{EtOH}.\text{H}_2\text{O}$ unit

Polanisami and co-workers⁹² have recently characterised the dimeric complex $[\text{Cu}_2(\text{salH})(\text{sal})(\text{bipy})_2].\text{ClO}_4$ (Figure 47). It consists of a discrete $[\text{Cu}_2(\text{salH})(\text{sal})(\text{bipy})_2]^-$ cation and an uncoordinated perchlorate anion. Interestingly the carboxylate proton of one of the salicylate ligands remains intact on the carboxylate group. Each copper ion is coordinated by two nitrogen atoms from the chelating bipy ligand, one carboxylate oxygen atom and one phenolate oxygen atom from the salicylate anion. The Cu-Cu distance of 3.265 Å rules out any magnetic interaction between the two metal centres.

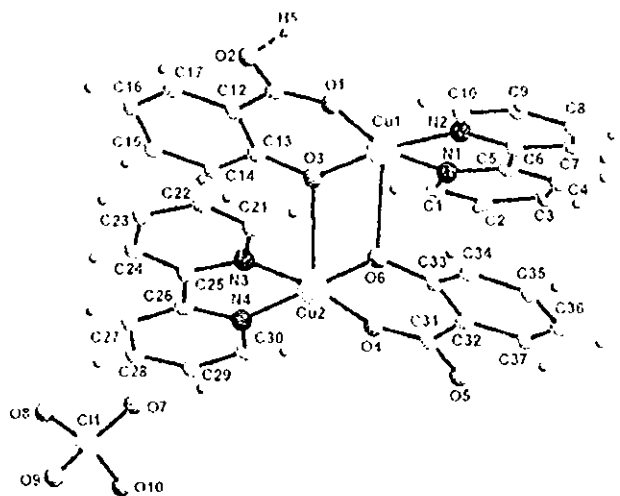


Figure 47: X-ray crystal structure of $[\text{Cu}_2(\text{salH})(\text{sal})(\text{bipy})_2]\cdot\text{ClO}_4$

Devereux *et al.*⁹³ have structurally characterised the polymeric manganese complex $[\text{Mn}(\text{salH})_2(\text{bipy})]\cdot\text{H}_2\text{O}$ (Figure 48). The Mn(II) ion is coordinated to both nitrogen atoms from a bipy ligand and to one carboxylate oxygen atom from each of the four salicylate ligands. Each salicylate carboxylate group coordinates to a pair of neighbouring manganese atoms in an asymmetric *syn-anti* bridging mode, leading to the formation of spiral chains.

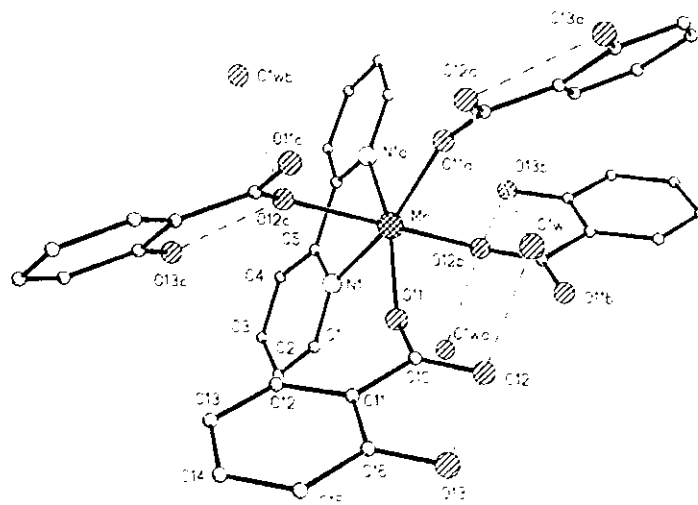


Figure 48: The structure of $[\text{Mn}(\text{salH})_2(\text{bipy})]\cdot\text{H}_2\text{O}$

In 2002 Lemoine *et al.*⁹⁴ reported the synthesis and crystal structures of two ternary Cu(II) complexes of salicylic acid and 1,10-phenanthroline. The monomeric complex $[\text{Cu}(\text{salH})(\text{phen})_2]\cdot\text{salH}\cdot\text{H}_2\text{O}$ (Figure 49) comprises a $[\text{Cu}(\text{salH})(\text{phen})_2]^+$ cation with another singly deprotonated salicylate acting as a counter-ion and a solvate water molecule. The Cu(II) ion exhibits a distorted octahedral geometry. The singly deprotonated salicylate group binds in an asymmetric chelating mode, with one tightly bound carboxylate oxygen ($\text{Cu}-\text{O} = 2.011 \text{ \AA}$) and a second more weakly bonded ($\text{Cu}-\text{O} = 2.719 \text{ \AA}$). The two phen ligands are bidentately coordinated through their nitrogen atoms to the copper centre.

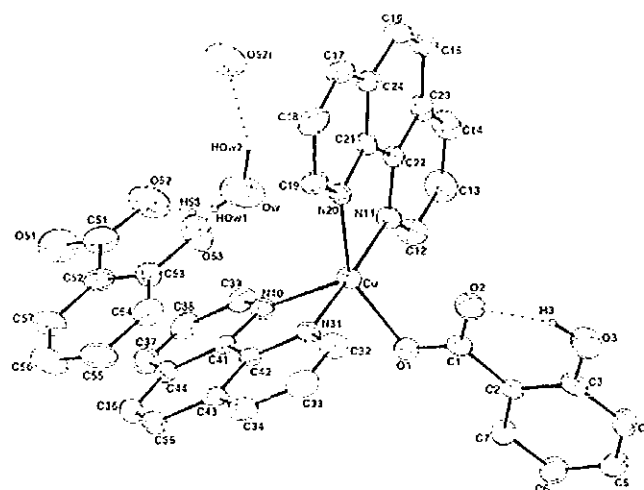


Figure 49: The structure of $[\text{Cu}(\text{salH})(\text{phen})_2] \cdot \text{salH} \cdot \text{H}_2\text{O}$

The second complex $[\text{Cu}_2(\text{phen})_2(\text{sal})_2] \cdot 2\text{H}_2\text{O}$ is structurally similar to the previously discussed complex $[\text{Cu}(\text{sal})(\text{bipy})] \cdot \text{EtOH} \cdot \text{H}_2\text{O}$ (Figure 46). The X-ray crystal structure of $[\text{Cu}_2(\text{phen})_2(\text{sal})_2] \cdot 2\text{H}_2\text{O}$ (Figure 50) showed it to consist of two $[\text{Cu}(\text{phen})(\text{sal})] \cdot \text{H}_2\text{O}$ units. Association of the two units occurs via a bond between the phenolate oxygen atom of one unit and the copper centre of the other. The metal centres are chelated by a phen ligand and a doubly deprotonated salicylate anion. One carboxylate oxygen from the doubly deprotonated salicylate ligand is directly bonded to the copper atom the other is involved in hydrogen bonding of a water molecule.

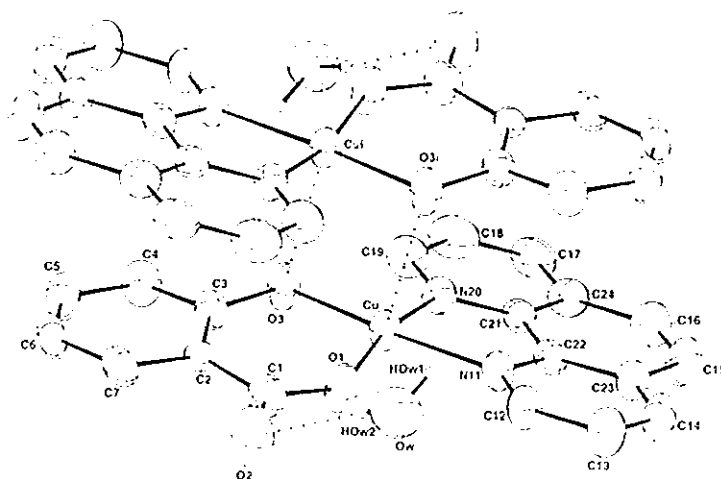


Figure 50: The structure of $[\text{Cu}_2(\text{phen})_2(\text{sal})_2] \cdot 2\text{H}_2\text{O}$

Also in 2002 Zhu and Cai⁹⁵ reported an unusual coordination mode of salicylic acid in the polymeric complex $[\text{Cu}_2(\text{phen})(\text{sal})(\text{salH})_2]_n$ (Figures 51 and 52). Each copper atom possesses a distorted octahedral geometry. All three oxygen atoms from the carboxylate and hydroxyl groups are bidently coordinated to copper ions.

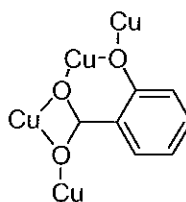


Figure 51: The coordination mode of salicylic acid in $[\text{Cu}_2(\text{phen})(\text{sal})(\text{salH})_2]_n$

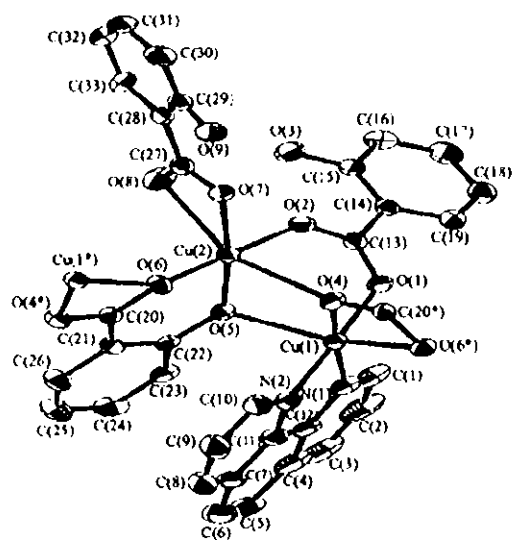


Figure 52: The X-ray crystal structure of $[\text{Cu}_2(\text{phen})(\text{sal})(\text{salH})_2]$

In 1993 Ranford and co-workers⁹⁶ synthesised copper(II), iron(III), cobalt(II), nickel(II), titanium(IV) and zinc(II) complexes of 3,5-diisopropylsalicylic acid and 1,10-phenanthroline. They structurally characterised the diisopropylsalicylatocopper(II) complex $[\text{Cu}(\text{dipsH})_2(\text{phen})]$ (Figure 53). The structure consists of monomeric units with an N_2O_4 donor set. Each salicylate ligand coordinates to the Cu(II) centre in an asymmetrical bidentate fashion with one short [1.951\AA] and one long [2.557\AA] Cu – O bond. The irregular octahedral geometry about the copper centre is completed by a chelating phen ligand.

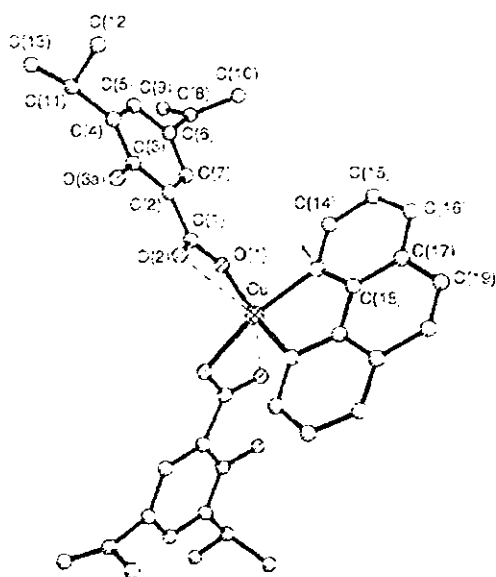


Figure 53: The structure of $[\text{Cu}(\text{dipsH})_2(\text{phen})]$

Recently the silver(I) complex $[\text{Ag}_2(\text{NH}_3)_2(\text{salH})_2]$ (Figure 54) has been characterised.⁹⁷ The two $[\text{Ag}(\text{NH}_3)(\text{salH})]$ units in the complex are linked by an Ag-Ag bonding interaction, supported by hydrogen-hydrogen bonding between the coordinated O atom of one unit and an ammonia hydrogen atom of the other. The salicylates coordinate in a monodentate fashion via their carboxylate groups.

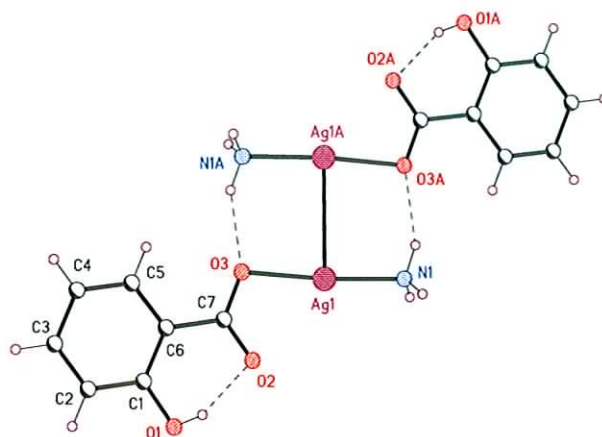


Figure 54: The structure of $[\text{Ag}_2(\text{NH}_3)_2(\text{salH})_2]$

The Ag(I) imidazole/salicylate complex $[\text{Ag}_2(\text{imH})_4](\text{salH})_2$ (Figure 55) has also recently been characterised by this group.⁹⁸ Two neutral imidazole ligands are bonded to the metal via their imine nitrogen atoms. There is a very weak Ag-Ag interaction (Ag-Ag = 3.178 Å). The binuclear complex is held together by hydrogen bonds involving the carboxylate oxygens of the salicylate groups and the hydrogen atom on the imidazole amine nitrogen atom.

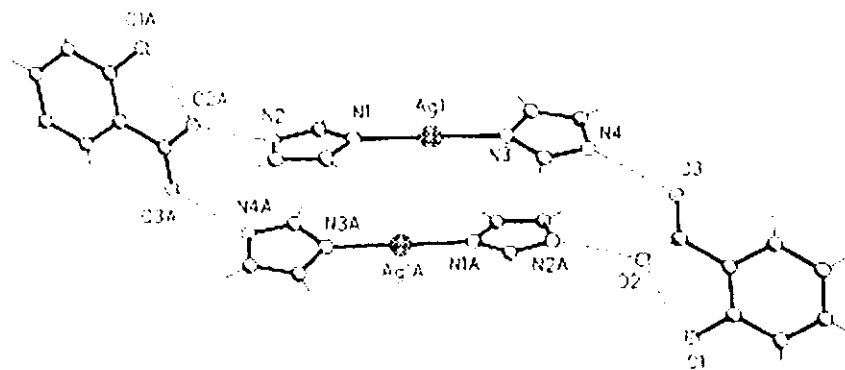


Figure 55: The X-ray crystal structure of $[\text{Ag}_2(\text{imH})_4](\text{salH})_2$

I.6 BENZIMIDAZOLES AND THEIR METAL COMPLEXES

I.6.1 Benzimidazole and their uses

Benzimidazole (BZDH) (Figure 56), a heterocyclic aromatic compound, contains fused benzene and imidazole rings. The imidazole nucleus and its derivatives are known to play crucial roles in the structures and functioning of a number of biologically important molecules, generally through the coordination to metal ions. 5,6-dimethylbenzimidazole supplies one of the five nitrogen atoms coordinated with vitamin B₁₂, and there is strong evidence that in proteins containing haem as a prosthetic group, e.g. haemoglobin, myoglobin, cytochrome C, imidazole nitrogen atoms in histidine residues of proteins are coordinated to the Fe metal centre.^{99,100} Thus the incorporation of benzimidazole into coordination complexes can yield useful compounds which can possess biomimetic behaviour.^{101,102,103,104}

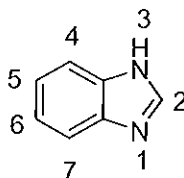


Figure 56: The structure of benzimidazole with numbering system

Benzimidazole and its derivatives are also well known for their parasitic and antiviral activities, and particularly well recognised is the compound albendazole (Figure 57), marketed as Albenza, Eskazole or Zentel, which is a drug indicated for the treatment of a variety of worm infestations.¹⁰⁵ Other well known antihelmintic agents are, thiabendazole, fenbendazole (sold under the brand name Pancur) (Figure 58), and mebendazole (Figure 59). Quite often these benzimidazoles are used in conjunction with the antiparasitic compound praziquantel (Figure 60) in the dual treatment of cystic

echinococcosis¹⁰⁵, an infection caused by tapeworm larvae which is potentially lethal to many animals and humans.¹⁰⁶

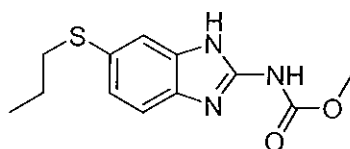


Figure 57: The structure of albendazole

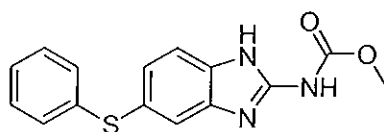


Figure 58: The structure of fenbendazole

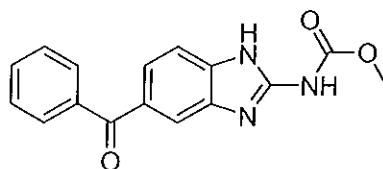


Figure 59: The structure of mebendazole

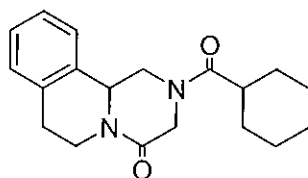


Figure 60: The structure of praziquantel.

The antiparasitic action of benzimidazole, studied by Sheth in 1975¹⁰⁷, is due to the inhibition of glucose uptake by the parasite without affecting blood glucose concentration levels. Benzimidazole compounds were also found to disrupt the microtubules by inhibition of the polymerisation of tubulin, with β -tubulin determined to be the drug target molecule. Microtubules serve as structural components within cells and are involved in many cellular processes including mitosis, particularly in cytokinesis. However, efficacy, low cost and oral administration have resulted in large scale use of benzimidazole-type chemotherapeutics in the treatment of intestinal nematode infections.

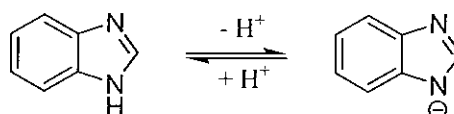
Due to these factors antihelminthic resistance toward BZDH and its derivatives has occurred^{108,109,110} and is thought to have been achieved where isolates reduce their binding affinity toward BZDH.^{108,111}

Another interesting benzimidazole-derived compound 2,5-dimethylbenzimidazole (2,5-Me₂BZDH) (Figure 72) was shown to possess the ability to inhibit influenza virus multiplication.¹¹² The compound was shown to be effective at a concentration of 2.5 mM in preventing the influenza B (Lee) virus and influenza A strain from multiplying over a period of 65 hours of incubation. The compound also demonstrated the ability to prevent significant multiplication even after a period of 1 h. Mode of action studies revealed that 2,5-Me₂BZDH acts as a virostatic agent rather than a virocidal and a direct mode of action could not be established.

I.6.2 Coordination complexes of Benzimidazole

Benzimidazole-type coordination compounds exhibit an array of biological activity with antifungal, anticancer, and SOD mimetic activity, having been mentioned throughout sections 1.2 - 1.4 already.

Benzimidazole can act as either a neutral or anionic ligand as the N1 position can deprotonate under certain conditions (Scheme 1). It has also been reported in the literature that certain benzimidazole derivatives, namely 2-(4-pyridyl)benzimidazole (2,4-PyBZDH), can behave as cations (Figure 61) when combined in a salt.¹¹³



Scheme 1: The deprotonation of benzimidazole

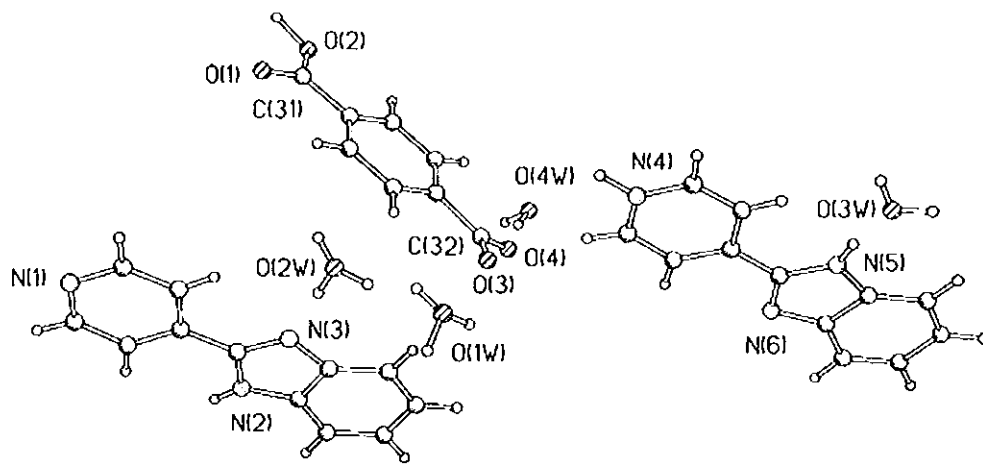


Figure 61: A benzimidazole phthalate (2:1) salt containing a 2,4-PyBZDH₂⁺ cation combined with a neutral 4-PyBZDH and a terphH anion

This flexibility, where benzimidazole-type ligands can act as neutral or charged species, has a direct influence on the types and coordination environments of their metal complexes. Figure 62 shows the X-ray structure of $[\text{Zn}(\text{BZDH})_2\text{Br}_2]$ where benzimidazole is neutral¹¹⁴, Figure 63 shows the $\{\text{Cu}(\text{BZD})_2\}_n$ polymer proposed by Goodgame *et al.* where both coordinated benzimidazoles act as an anionic species¹¹⁵ and Figure 64 depicts the interesting X-ray crystal structure of the 2-(2'-pyridyl)benzimidazole (2-PyBZDH) containing lanthanide complex, synthesised by Müller-Buschaum and Quitman in 2003¹¹⁶, $[\text{Yb}(2\text{-PyBZD})_4](2\text{-PyBZDH}_2)$. The ytterbium(III) atom in this complex is coordinated to four chelating anionic 2-PyBZD⁻ anions while a cationic 2-PyBZDH₂⁺ balances the overall charge.

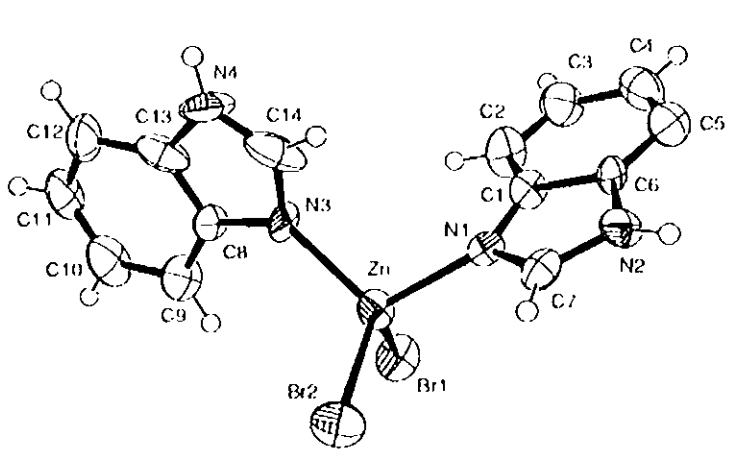


Figure 62: The X-ray crystal structure of $[\text{Zn}(\text{BZDH})_2\text{Br}_2]$

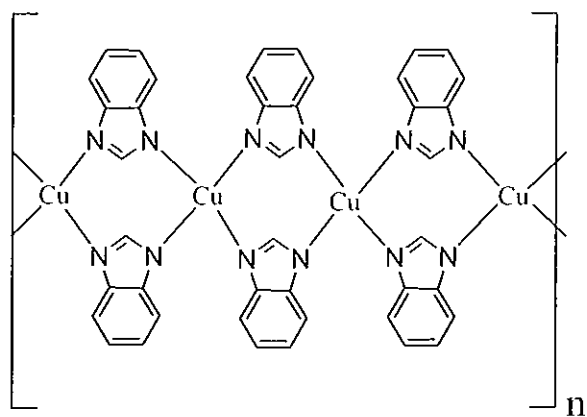


Figure 63: The proposed polymeric structure for $\{\text{Cu}(\text{BZD})_2\}_n$

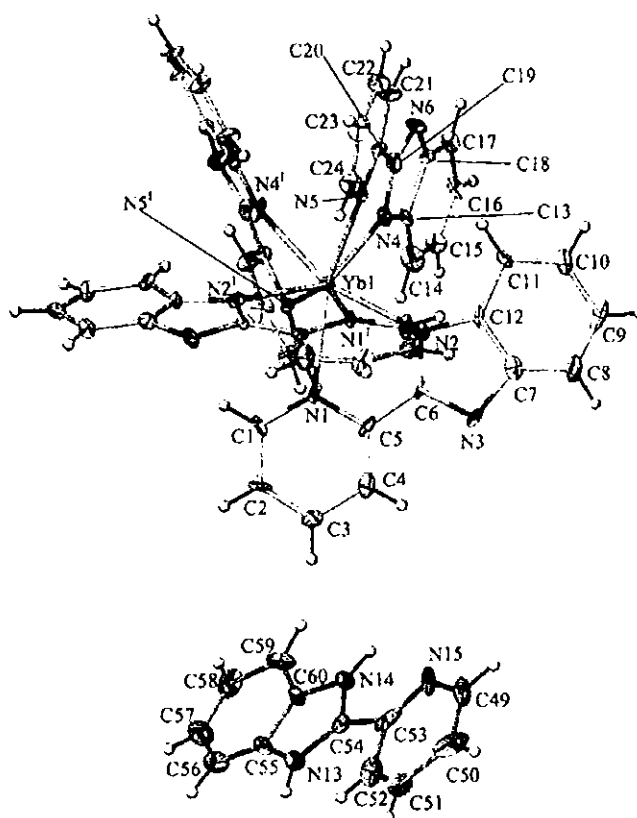


Figure 64: The X-ray crystal structure of $[\text{Yb}(\text{2-PyBZD})_4](\text{2-PyBZDH}_2)$

Grevy *et al.*¹¹⁷ have synthesised and characterised Li(I), Na(I), K(I), Pb(II), Co(II), Ni(II), Zn(II), Cd(II) and Hg(II) complexes of thiabendazole. The thiabendazole ligand was found to chelate through the imidazole and thiazole nitrogen atoms regardless of the nature of the metal ion. The crystal structure of the copper(II) complex $[\text{Cu}(\text{TBZH})_2\text{NO}_3]\cdot\text{NO}_3\cdot\text{H}_2\text{O}$ is shown in Figure 65. The copper centre is chelated by two thiabendazole ligands, one of the nitrate anions is coordinated in a bidentate mode to the metal ion completing the slightly distorted octahedral geometry. Another nitrate anion acts as an uncoordinated counter-ion.

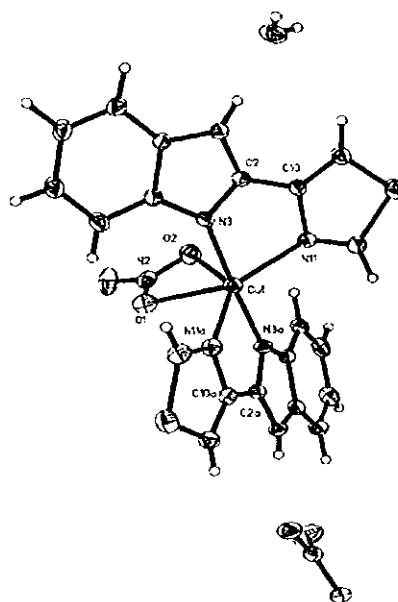


Figure 65: The X-ray crystal structure of $[\text{Cu}(\text{TBZH})_2\text{NO}_3]\cdot\text{NO}_3\cdot\text{H}_2\text{O}$

The complex $[\text{Cu}(\text{TBZH})_2\text{Cl}]\cdot\text{Cl}\cdot\text{H}_2\text{O}\cdot\text{EtOH}$ characterised by Devereux *et al.*¹¹⁸ exists where both uncoordinated and coordinated chloride anions act as counter charges to the cationic metal centre. This combined with the chelating nature of thiabendazole leaves an approximate tetrahedral arrangement about the copper ion.

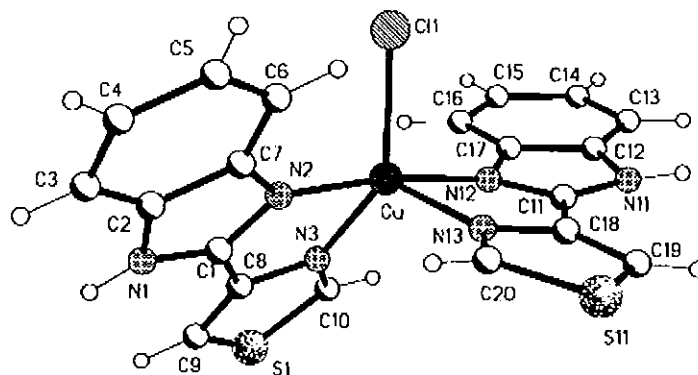


Figure 66: The structure of the cation in $[\text{Cu}(\text{TBZH})_2\text{Cl}]\text{Cl}\cdot\text{H}_2\text{O}\cdot\text{EtOH}$

Recently the structures of a number of Ag(I) complexes incorporating benzimidazole and substituted benzimidazoles have been reported.

The trinuclear complex $[\text{Ag}_3(\text{bzd})_3(\text{PPh}_3)_5]$ shown in Figure 67, characterised by Wu *et al.*¹¹⁹ is another example of a complex with an anionic benzimidazole ligand. Three Ag(I) cations are arranged in a triangular fashion, bridged by three anionic benzimidazole ligands. Two of the Ag(I) atoms are four coordinate with two PPh_3 groups coordinated and the third one is coordinated to one PPh_3 group.

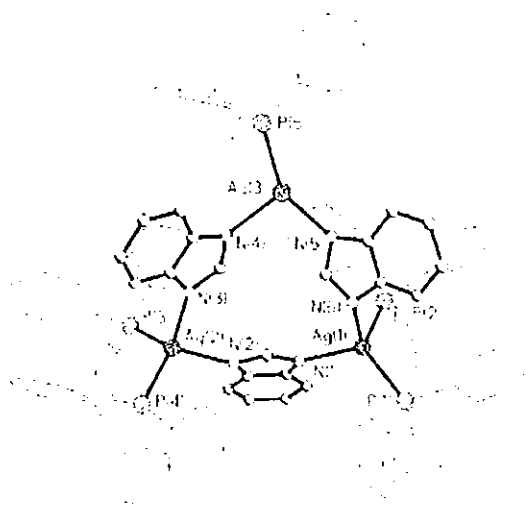


Figure 67: X-ray crystal structure of $[Ag_3(bzd)_3(PPh_3)_5]$

Su *et al.*¹²⁰ have structurally characterised the dimeric Ag(I) complex $[Ag_2(3-PyBZDH)_2](ClO_4)_2$ (Figure 68) (3-PyBZDH = 3-pyridylbenzimidazole). The Ag(I) cations are bridged by two 3-pyridylbenzimidazole ligands via the nitrogen atom from the pyridyl of one ligand and the imidazole nitrogen atom of the other. The perchlorate anions are weakly attached to the silver atoms (Ag-O = 2.747 Å).

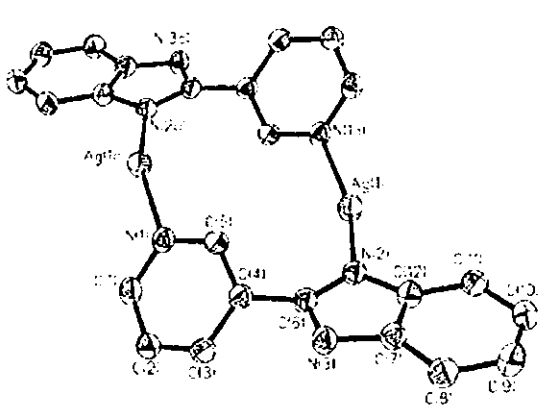


Figure 68: X-ray crystal structure of $[Ag_2(3-PyBZDH)_2](ClO_4)_2$

Also structurally characterised by Xia *et al.*¹²¹ are two polymeric Ag(I) complexes of the type $[\text{Ag}(4\text{-PyBZDH})(\text{H}_2\text{O})]\text{X}$ where $\text{X} = \text{NO}_3^-$ or ClO_4^- and 4-PyBZDH = 2-(4-pyridyl)benzimidazole (Figure 69). The Ag(I) in each complex is three coordinate with the third position taken up by a water molecule. In all three complexes the Ag(I) atoms are bridged by the benzimidazole ligands via the pyridine and benzimidazolyl nitrogen atoms leading to the formation of chains. The anions in the complexes act as uncoordinated counter-ions.

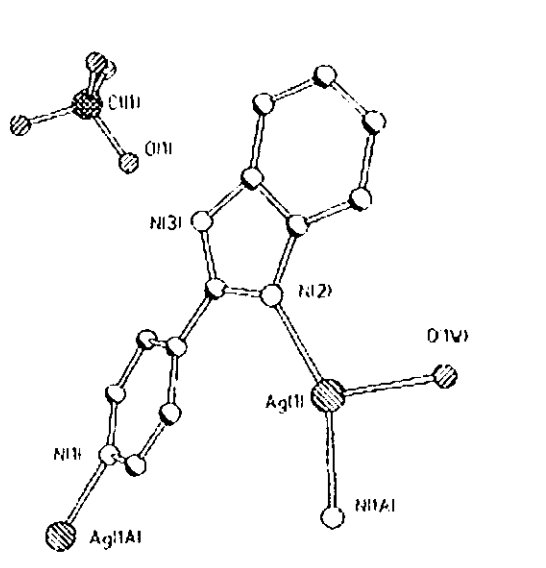


Figure 69: The X-ray crystal structure of $[\text{Ag}(4\text{-PyBZDH})(\text{H}_2\text{O})].\text{ClO}_4$

RATIONALE

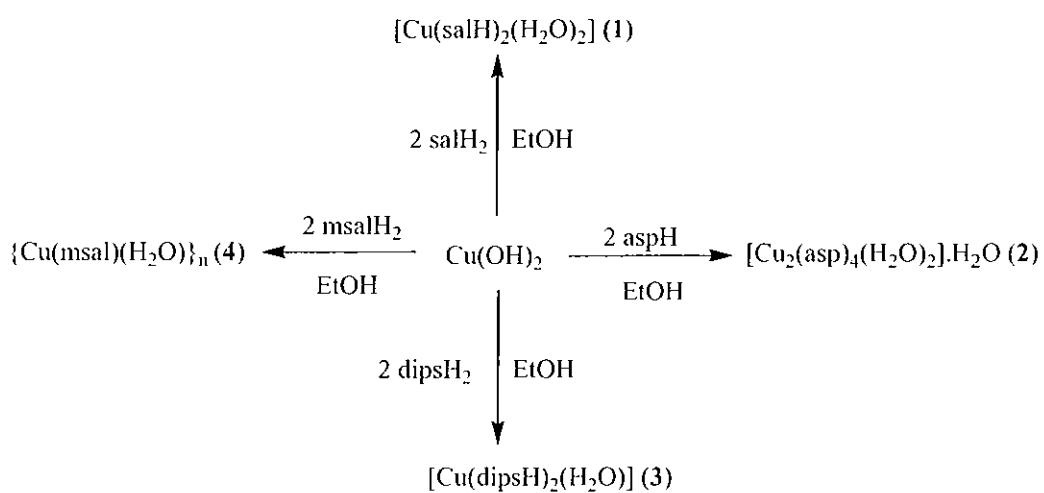
PROJECT RATIONALE

The present project aimed to investigate the biomimetic and biological properties of copper(II) and silver(I) complexes incorporating salicylate and benzimidazole ligands. The project extends the work being carried out by this group and its collaborators in the area of novel metal based anticancer and antimicrobial agents.

DISCUSSION

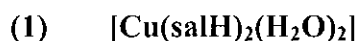
D.1 SYNTHESIS OF COPPER(II) SALICYLATE COMPLEXES

Synthetic routes to the salicylate complexes $[\text{Cu}(\text{salH})_2(\text{H}_2\text{O})_2]$ (**1**), $[\text{Cu}(\text{dipsH})_2(\text{H}_2\text{O})]$ (**3**) and $\{\text{Cu}(\text{msal})(\text{H}_2\text{O})\}_n$ (**4**) and the aspirinate complex $[\text{Cu}_2(\text{asp})_4(\text{H}_2\text{O})_2] \cdot \text{H}_2\text{O}$ (**2**) are shown in Scheme 2. The four complexes were generated by the reaction of $\text{Cu}(\text{OH})_2$ with the relevant carboxylic acid.



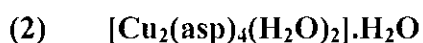
Scheme 2: Formation of copper(II) carboxylate complexes

Complexes (**1**) and (**4**) were obtained as brown powders, complex (**2**) as a blue powder and complex (**3**) as a green powder. They were formulated as shown below:



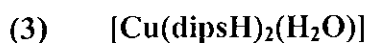
% Calc: C, 44.98; H, 3.78

% Found: C, 44.09; H, 3.39



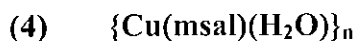
% Calc: C, 48.16; H, 3.82

% Found: C, 48.88; H 3.33



% Calc: C, 59.58; H, 6.92

% Found: C, 59.27; H 6.83



% Calc: C, 38.79; H, 3.26

% Found: C, 39.75; H 2.85

The physico-chemical properties of (1) are the same as for the previously discussed complex $[\text{Cu}(\text{salH})_2(\text{H}_2\text{O})_2]$ (Figure 37). The complex was shown to adopt a square planar geometry with the two salicylate ligands coordinated in a monodentate fashion via their carboxylate groups. The remaining coordination sites are taken up by two water molecules. The IR spectrum of (1) contains typical $\nu_{\text{asym}}(\text{OCO})$ $\{1603 \text{ cm}^{-1}\}$ and $\nu_{\text{sym}}(\text{OCO})$ $\{1410 \text{ cm}^{-1}\}$ bands. The calculated Δ_{OCO} value of 193 cm^{-1} is within the range expected for monodentate carboxylate ligands ($>200 \text{ cm}^{-1}$) but the relative reduction in the Δ_{OCO} values are typical where such carboxylate groups are involved in hydrogen bonding. The room temperature magnetic moment of 1.81 B.M. is consistent with a structure lacking Cu-Cu interactions. It is probable that (1) is identical to the compound that was published in 1959 for which a crystal structure was determined (Figure 37).

Complex (2) is likely a hydrated form of the structurally characterised dimeric complex $[\text{Cu}_2(\text{asp})_4]$. Its DMF coordinated analogue is shown in Figure 70.¹²²

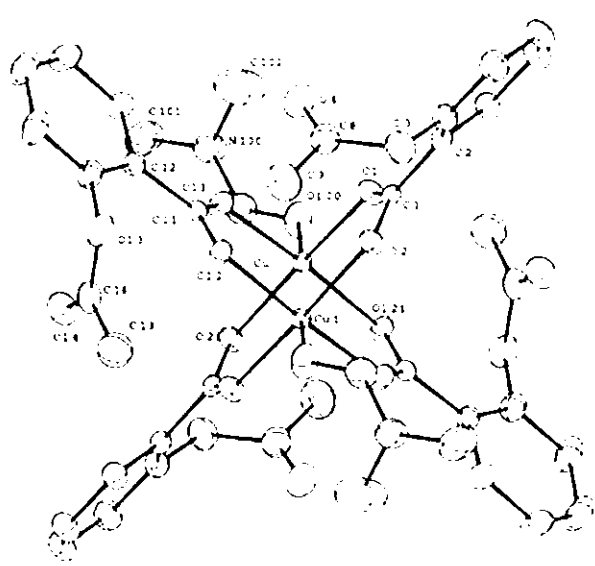


Figure 70: The X-ray crystal structure of $[\text{Cu}_2(\text{asp})_4(\text{DMF})_2]$

In the complex two copper centres are bridged by four carboxylate ligands giving the familiar paddle-wheel dimer structure. The copper centres are separated by a distance of 2.62 Å. The close inter-atomic distance in this type of dimer gives rise to subnormal magnetic moments in the region of 1.4 B.M.. The IR spectrum of (2) contains bands characteristic of acetylsalicylate anions. Bands present at 1726 cm^{-1} indicate the presence of the acetoxy carbonyl group. A band present at 816 cm^{-1} absent in the spectrum of acetylsalicylic acid is indicative of coordinated water.¹²³ A Δ_{OCO} value of 135 cm^{-1} is within the accepted range for the bridging bidentate carboxylate mode. The low magnetic moment value of 1.46 B.M. for (2) is in line with the proposed paddle-wheel type structure.

Complex (3) has a subnormal room temperature magnetic moment of 1.38 B.M.. In the IR spectrum the carboxylate bands are split $\{v_{\text{asym}}(\text{OCO}): 1628\text{ cm}^{-1}$ and 1592 cm^{-1} , $v_{\text{sym}}(\text{OCO}): 1468\text{ cm}^{-1}$ and $1390\text{ cm}^{-1}\}$ indicative of the presence of two different modes of coordination for the salicylate carboxylate groups. A manganese(II)

salicylate complex reported by Devereux *et al.*⁷⁰ which formulated as $[\text{Mn}_2(\text{salH})_4(\text{H}_2\text{O})_2]$ ($\text{salH}_2 = \text{salicylic acid}$) and whose structure is shown in Figure 39 exhibits similar physico-chemical properties to that of (3). It too has its asymmetric and symmetric OCO bands split in the IR spectrum. Furthermore the IR spectra of complex (3) and $[\text{Mn}_2(\text{salH})_4(\text{H}_2\text{O})_2]$ both exhibit bands in the region $840 - 820 \text{ cm}^{-1}$, which are not found in the spectrum of the respective carboxylic acids and which are characteristic of coordinated water molecules.

Complex (4) is peculiar in so far as it formulates as having just one 3-methoxysalicylate ligand per copper. The presence of the methoxy group is confirmed by the C-O-C band at 1061 cm^{-1} . This band has shifted from 1055 cm^{-1} in the spectrum of the free ligand and has lost significant intensity and therefore it is possible that the ethereal oxygen is involved in coordination to the copper centre. The complex also formulates as having one coordinated water supported by the typical band at 835 cm^{-1} in the IR spectrum. Significantly, the carboxylate bands in the IR spectrum are again split $\{\nu_{\text{asym}}(\text{OCO}): 1633 \text{ cm}^{-1}$ and 1606 cm^{-1} , $\nu_{\text{sym}}(\text{OCO}): 1472 \text{ cm}^{-1}$ and $1450 \text{ cm}^{-1}\}$ again suggesting that the complex contains two different modes of coordination for the 3-methoxysalicylate carboxylate groups. The room temperature magnetic moment for (4) is normal (1.65 B.M.) suggesting that no electronic interaction exists between the copper centres in the complex. The relative insolubility of (4) could suggest that it is polymeric in nature and a structure that fits its physico-chemical data is shown in Figure 71.

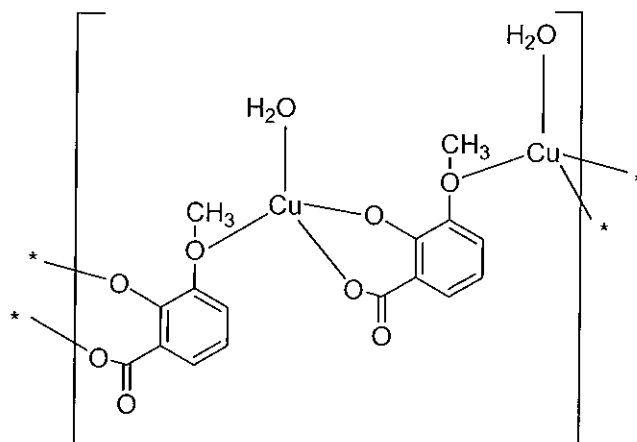


Figure 71: A possible structure for $\{\text{Cu}(\text{msal})(\text{H}_2\text{O})\}_n$

Complexes (1), (2) and (4) were found to be insoluble in common solvents but were soluble in DMSO. Complex (3) was soluble in ethanol and DMSO. Their molar conductivities recorded in DMSO show that complex (1) is essentially a non-electrolyte and therefore does not dissociate in this solvent. The molar conductivities of (2), (3) and (4) indicate that they dissociate slightly in DMSO. The UV spectra of (1) and (4) taken in DMSO solution as well as in the solid state as Nujol mulls show approximately similar shapes and positions of the absorption bands, indicating no appreciable change in the geometry of the complexes in solution. Complexes (2) and (3) exhibit shifts of the *d-d* transition bands in their DMSO solution spectra as compared to the solid state and therefore some change in the complexes is taking place in solution.

D.2 SYNTHESIS AND CHARACTERISATION OF COPPER(II) SALICYLATES INCORPORATING BENZIMIDAZOLE LIGANDS

D.2.1 The reactions of $[\text{Cu}(\text{salH})_2(\text{H}_2\text{O})_2]$ and $[\text{Cu}_2(\text{asp})_4(\text{H}_2\text{O})_2]\cdot\text{H}_2\text{O}$ with the simple benzimidazole ligands

$[\text{Cu}(\text{salH})_2(\text{H}_2\text{O})_2]$ (**1**) and $[\text{Cu}_2(\text{asp})_4(\text{H}_2\text{O})_2]\cdot\text{H}_2\text{O}$ (**2**) were each reacted with a range of potential benzimidazole ligands (see Figure 72) to yield the novel copper complexes (**5**) - (**10**) in accordance with the reactions shown in Schemes 3 and 4. The reactions of (**2**) demonstrate the relative facile hydrolysis of the coordinated acetylsalicylic acid ligand.

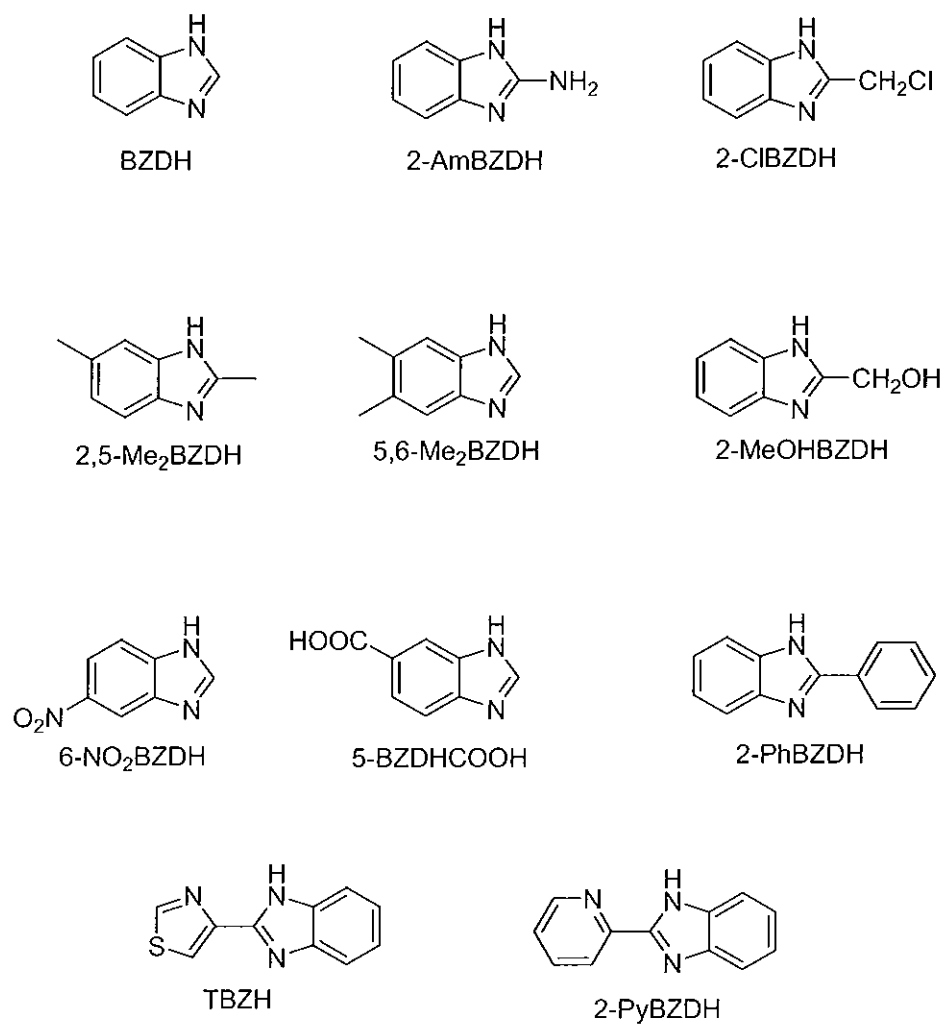
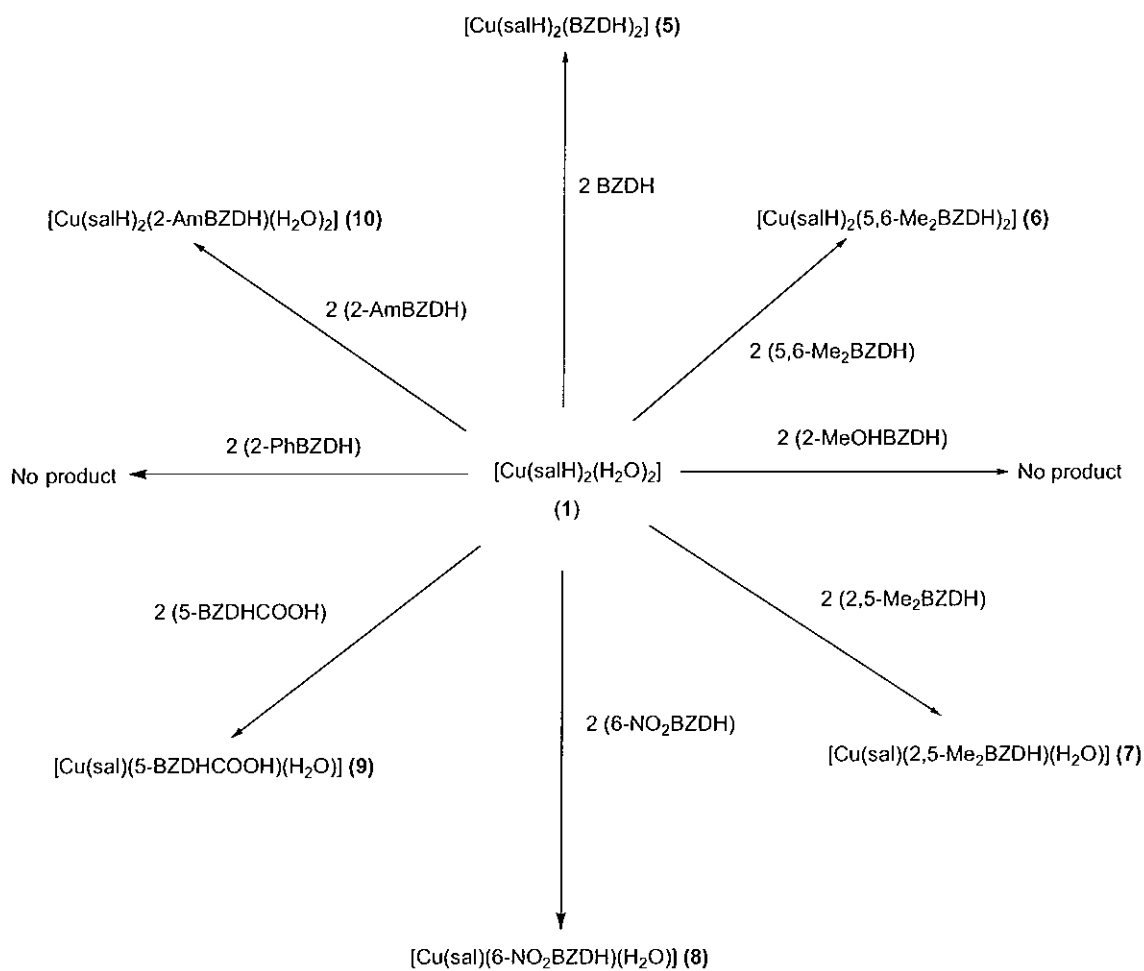
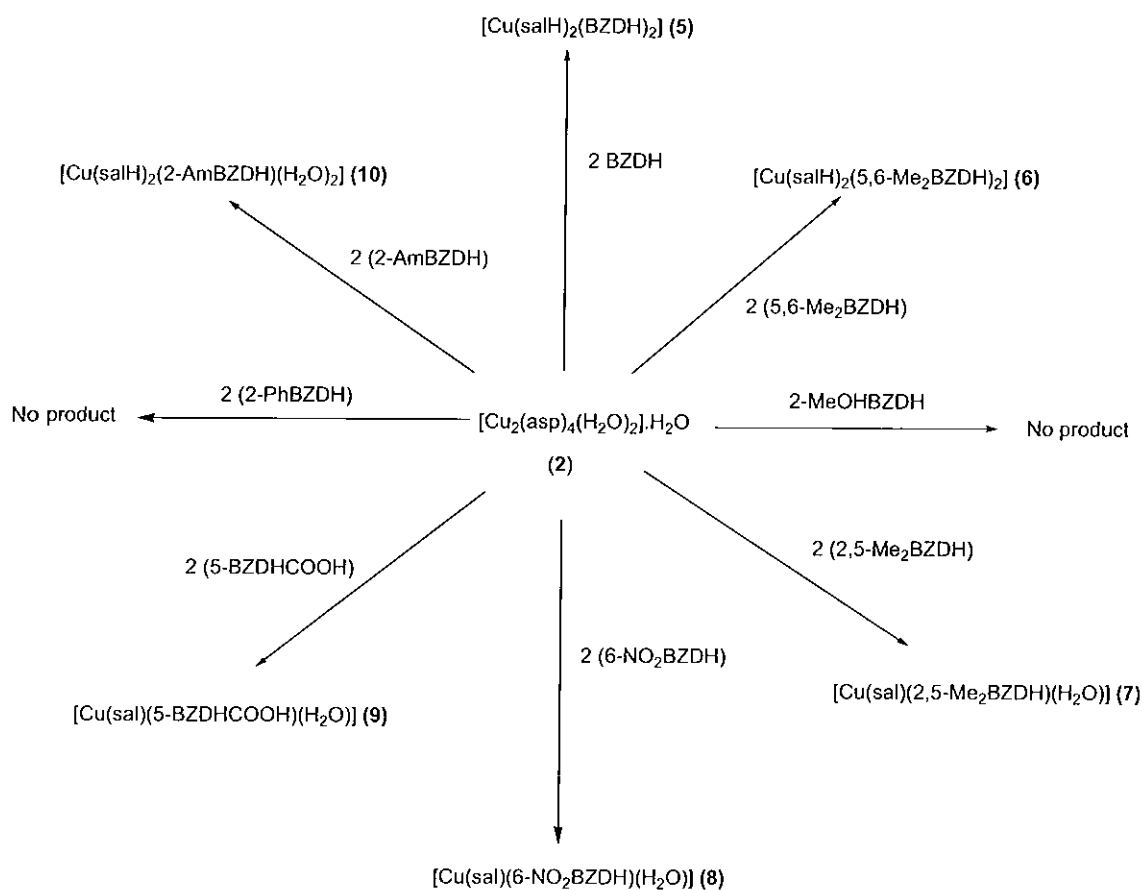


Figure 72: Structure of benzimidazole and its derivatives

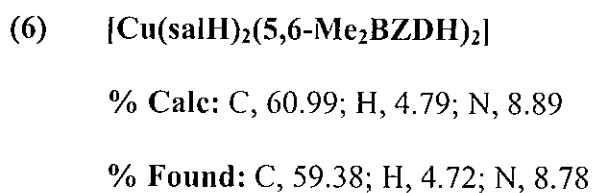
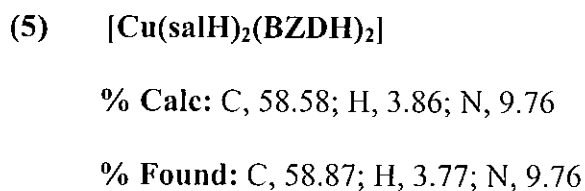


Scheme 3: Synthetic routes to complexes (5) - (10) starting with $[\text{Cu}(\text{salH})_2(\text{H}_2\text{O})_2] \text{ (1)}$



Scheme 4: Synthetic routes to complexes (5) - (10) starting with $[\text{Cu}_2(\text{asp})_4(\text{H}_2\text{O})_2] \cdot \text{H}_2\text{O}$ (2)

Complex (5) was obtained as blue crystals, complex (6) as a lilac powder and (7) – (10) were all isolated as green powders and the compounds were formulated as follows:



- (7) **[Cu(sal)(2,5-Me₂BZDH)(H₂O)]**
% **Calc:** C, 52.67; H, 4.43; N, 7.68
% **Found:** C, 55.27; H, 4.02; N, 7.92
- (8) **[Cu(sal)(6-NO₂BZDH)(H₂O)]**
% **Calc:** C, 44.16; H, 2.92; N, 11.03
% **Found:** C, 43.51; H, 2.71; N, 11.23
- (9) **[Cu(sal)(5-BZDHCOOH)(H₂O)]**
% **Calc:** C, 47.43; H, 3.18; N, 7.38
% **Found:** C, 46.77; H, 2.90; N, 7.48
- (10) **[Cu(salH)₂(2-AmbZDH)(H₂O)₂]**
% **Calc:** C, 49.75; H, 4.18; N, 8.29
% **Found:** C, 50.50; H, 3.75; N, 8.60

The IR spectra of the complexes (5) – (10) (see Appendix) were compared to those of the free ligands. The characteristic bands for the free ligands and some of the important IR spectral bands that provide evidence for the structure of the complexes are listed in Tables 11 and 14.

Table 11: Characteristic IR bands (cm^{-1} , KBr discs) of the complexes (5) – (9) along with their free ligands

	BZDH	(5)	5,6-Me ₂ BZDH	(6)	2,5-Me ₂ BZDH	(7)	6-NO ₂ BZDH	(8)	5-BZDHCOOH	(9)
Imidazole bands										
N-H (stretch)	3113	3112	3095	*	3044	3057	3103	*	3045	*
N-H (bending)	1135	1141	1158	1143	1145	1143	1132	1145	1134	1125
N-H (bending)	627	634	647	641	659	662	690	708	622	653
$\nu_{\text{C=N}}$	1587	1582	1584	1580	1553	1559	1591	1571	1588	1575
Carboxylate bands										
$\nu_{\text{asym}}(\text{OCO})$	-	1620	-	1563	-	1602	-	1617	-	1610
$\nu_{\text{sym}}(\text{OCO})$	-	1395	-	1398	-	1403	-	1402	-	1399
Δ_{OCO}	-	225	-	165	-	199	-	215	-	211
Metal-Ligand										
M-N	-	420	-	428	-	430	-	421	-	429
M-OH ₂	-	-	-	817	-	839	-	816	-	830

* Bands precluded by others in the infrared spectrum

Blue crystals of $[\text{Cu}(\text{salH})_2(\text{BZDH})_2]$ (**5**) suitable for X-ray analysis were obtained from the reaction solution upon standing for several days. The X-ray crystal structure of (**5**) is shown in Figure 73 and Figure 74. Selected bond lengths and angles are listed in Table 12. $[\text{Cu}(\text{salH})_2(\text{BZDH})_2]$ has a square planar Cu centre which contains two trans benzimidazole ligands and two salicylate ligands. The hydrogen bonding motif in the complex (see Figure 74 and Table 13) differs between the two carboxylate groups and so the Cu atom is not situated on an inversion centre. The ortho hydroxyl group makes hydrogen bonds to one carboxylate O atom, keeping the carboxylate co-planar with the phenyl ring in the case of the carboxylate containing O1, O2. However, for the other salicylate ligand the carboxylate is twisted by $18.33(6)^\circ$ with respect to the plane made by the phenyl ring and O6. In this case, the hydroxyl O makes intermolecular hydrogen bonds to a carboxyl O and a longer NH...O link. In contrast O3 makes just an intermolecular hydrogen bond to O2. The complex forms chains parallel to the shortest axis. These chains interdigitate such that the benzimidazoles form a stack and the distance between the imidazole centroids in these stacks alternates between $3.6622(7)$ and $3.8424(7)$ Å, albeit rather too long for significant π - π stacking interactions.

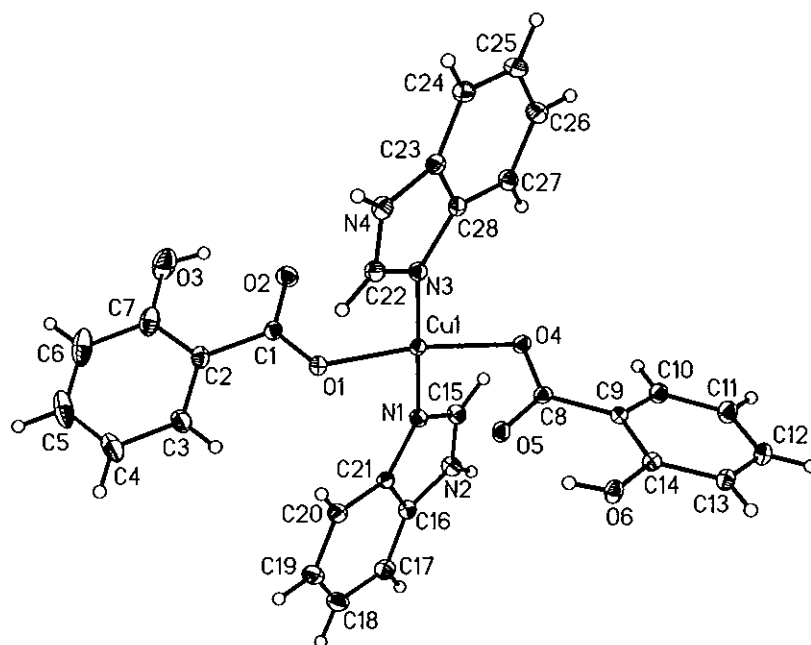


Figure 73: The X-ray crystal structure of $[\text{Cu}(\text{salH})_2(\text{BZDH})_2]$ (**5**)

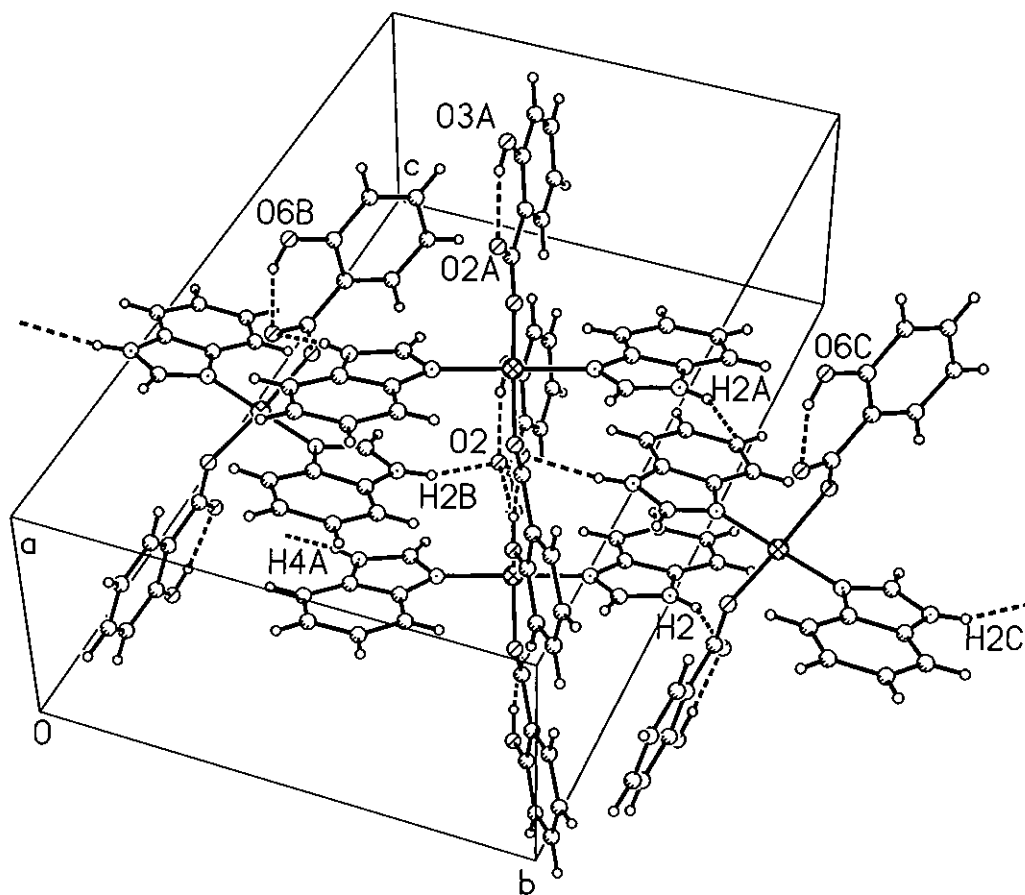


Figure 74: Packing diagram for [Cu(salH)₂(BZDH)₂] (5)

Table 12: Selected bond lengths [\AA] and angles [$^\circ$] around the copper centres in $[\text{Cu}(\text{salH})_2(\text{BZDH})_2]$ (**5**)

Complex (5)	
Bond lengths \AA	
Cu-O(1)	1.9601(9)
Cu-O(4)	2.0115(9)
Cu-N(3)	1.9827(10)
Cu-N(1)	1.9951(10)
Bond angles $^\circ$	
N(1)-Cu(1)-N(3)	179.47(4)
O(1)-Cu(1)-O(4)	69.42(3)
O(1)-Cu(1)-N(1)	89.86(4)
O(1)-Cu(1)-N(3)	90.52(4)
O(4)-Cu(1)-N(1)	87.90(4)
O(4)-Cu(1)-N(3)	91.65(4)

Table 13: Hydrogen bonds for $[\text{Cu}(\text{salH})_2(\text{BZDH})_2]$ (**5**) [\AA and $^\circ$].

D-H...A	d(D-H)	d(H...A)	d(D...A)	$\angle(\text{DHA})$
O(3)-H(3O)...O(2)	0.82	1.85	2.5681(15)	146.3
O(6)-H(6O)...O(5)	0.82	1.88	2.5974(13)	145.2
O(6)-H(6O)...O(2)#1	0.82	2.28	2.8682(13)	129.5
N(2)-H(2)...O(2)#2	0.86	2.04	2.8220(14)	150.9
N(4)-H(4A)...O(5)#3	0.86	2.11	2.9627(13)	168.7
N(4)-H(4A)...O(6)#3	0.86	2.85	3.4523(14)	128.8

Symmetry transformations used to generate equivalent atoms:
#1 $x-1, y, z$ #2 $-x+3/2, y+1/2, -z+1/2$ #3 $-x+1/2, y-1/2, -z+1/2$

Complex (6) formulates as having the same metal : benzimidazole : salicylate ratio of 1 : 2 : 2 as (5) and their IR spectra are very similar. The N-H stretching and bending bands in the spectra of the BZDH and 5,6-Me₂BZDH free ligands also appear (although shifted slightly) in the spectra of the two complexes indicative of the fact that the ligands are present in their neutral state. Furthermore, the band associated with the imidazolic $\nu_{C=N}$ in the free ligands has shifted in the spectra of (5) and (6) indicating that the benzimidazoles are bound to the metals through the nitrogen atom. For both complexes the $\nu_{\text{asym}}(\text{OCO})$ and $\nu_{\text{sym}}(\text{OCO})$ bands are not split. The Δ_{OCO} value of 225 cm^{-1} for (5) is in agreement with the crystal structure where the salicylate ligands are coordinated in a monodentate fashion. A Δ_{OCO} value of 165 cm^{-1} for (6) is below the value expected for a monodentate coordination mode but such reductions are typical where carboxylate groups are involved in hydrogen bonding. The room temperature magnetic moments of (5) and (6) are 1.83 B.M. and 2.05 B.M., respectively, which are consistent with structures lacking Cu-Cu interactions.

The molar conductivities of 13.2 $\text{S cm}^2 \text{mol}^{-1}$ (5) and 11.6 $\text{S cm}^2 \text{mol}^{-1}$ (6) indicate that the complexes dissociate slightly in DMSO. Both complexes exhibit significant shifts of the *d-d* transition bands {579 nm \rightarrow 738 nm (5) and 550 nm \rightarrow 722 nm (6)} in their DMSO solution spectra as compared to the solid state and therefore some change in the complexes is taking place in solution. Complex (6) is likely to have the same square planar structure as (5).

The complexes (7), (8) and (9) formulate as having the same metal : benzimidazole : salicylate ratio of 1 : 1 : 1. The N-H stretching and bending bands in the spectra of the free ligands also appear in the spectra of the complexes indicating that the ligands are

present in their neutral state. The IR spectra of the complexes contain typical ν_{asym} (OCO) and ν_{sym} (OCO) bands which are in similar positions and are not split. The calculated Δ_{OCO} values of 199, 215 and 211 cm^{-1} for (7), (8) and (9) respectively support the proposal that the carboxylate groups of the salicylate ligands are coordinated to the copper centres in a monodentate mode. New bands that do not appear in the spectra of the free ligands at 839 (7), 816 (8) and 830 cm^{-1} (9) have been attributed to the presence of coordinated water. Bands in the region below 500 cm^{-1} have been assigned to metal – nitrogen bonds.

The room temperature magnetic moments of 2.09 B.M. (7), 1.86 (8) and 1.63 B.M. (9) are consistent with structures lacking any significant Cu-Cu interactions. All three of the complexes are effectively insoluble in common solvents at room temperature, but they were found to be soluble in DMSO. The UV spectra of the complexes recorded in DMSO solution as well as in the solid state as Nujol mulls show approximately similar shapes and positioning of the absorption bands, indicating no appreciable change in their geometry in solution. The molar conductivities of (7) – (9) were found to be in the range 1.55 to 3.95 $\text{S cm}^2\text{mol}^{-1}$ indicating that the complexes do not dissociate in DMSO. A possible structure of (7) – (9) which fits their physico – chemical data is shown in Figure 75.

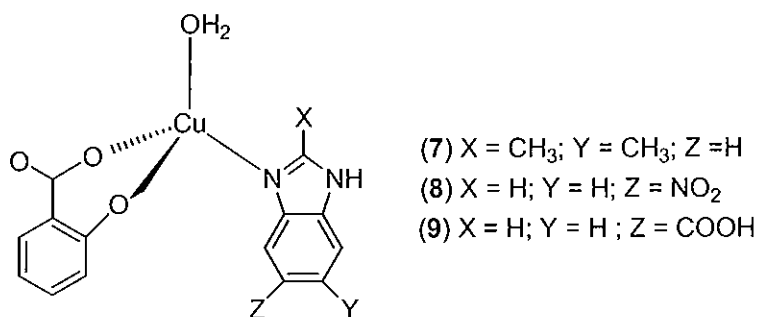


Figure 75: Possible structural motif for complexes (7) – (9)

Complex (10) formulates as having a metal : benzimidazole : salicylate ratio of 1 : 1 : 2. As well as the bands associated with a neutral 2-AmbZDH ligand the spectrum of (10) (see Appendix) contains bands that are characteristic of the salicylate anions with typical $\nu_{\text{asym}}(\text{OCO})$ and $\nu_{\text{sym}}(\text{OCO})$ values (Table 14).

Table 14: Characteristic IR bands (cm^{-1} , KBr discs) of the complex (10)

	2-AmbZDH	(10)
Imidazole bands		
N-H (stretch)	3054	*
N-H (bending)	1157	1158
N-H (bending)	623	652
$\nu_{\text{C=N}}$	1596	*
Amine bands		
N-H (stretch)	3381	3340
NH ₂ (assym deformation)	1632	1655
NH ₂ (sym deformation)	1269	1279
NH ₂ (rocking mode)	742, 728	755, 740
Carboxylate bands		
$\nu_{\text{asym}}(\text{OCO})$	-	1616
$\nu_{\text{sym}}(\text{OCO})$	-	1384
Δ_{OCO}	-	232
Metal-Ligand		
M-N	-	427
M-OH ₂	-	817

* Bands precluded by others in the infrared spectrum

The $\nu_{\text{asym}}(\text{OCO})$ peak for (10) is split and so two modes of interaction with the copper centre are likely for the two carboxylate groups. The bands characteristic of the amine group in 2-AmbZDH are also found in the spectrum of complex (10) (although shifted slightly) indicating that the amine nitrogen is unlikely to be involved in coordination to the metal. However the NH₂ group may be involved in some form of hydrogen

bonding. The spectrum of **(10)** also exhibits a band at 427 cm^{-1} which may be assigned to metal-nitrogen interactions. It is significant that this peak is not split (reflecting the fact that there is only one N-donor ligand present in the complex). Furthermore a peak at 817 cm^{-1} is characteristic of the presence of coordinated water molecules. The room temperature magnetic moment of complex **(10)** (1.86 B.M.) is in the expected range for simple copper(II) species (i.e. those lacking Cu-Cu interactions). A structure that fits for the physico-chemical data for **(10)** is shown in Figure 76.

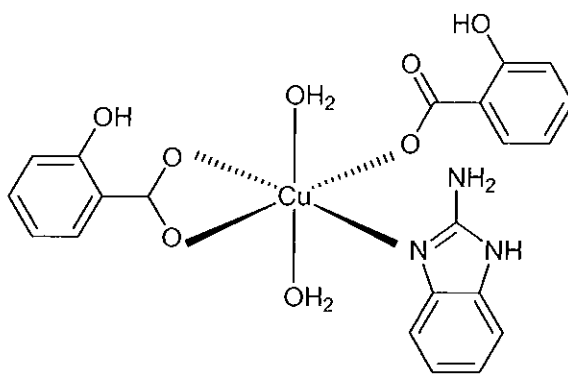
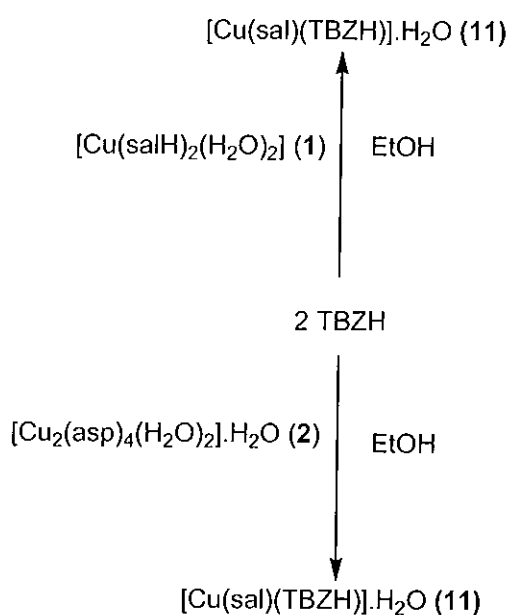


Figure 76: Possible structural motif for complex **(10)**

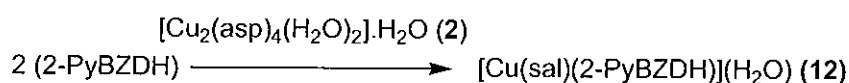
Complex **(10)** was found to be insoluble in all common solvents. On addition of **(10)** to DMSO an immediate purple precipitate was observed.

D.2.2 Reaction of $[\text{Cu}(\text{salH})_2(\text{H}_2\text{O})_2]$ (1) and $[\text{Cu}_2(\text{asp})_4(\text{H}_2\text{O})_2]\cdot\text{H}_2\text{O}$ (2) with the chelating benzimidazoles thiabendazole (TBZH) and 2-(Pyridyl)Benzimidazole (2-PyBZDH)

$[\text{Cu}(\text{salH})_2(\text{H}_2\text{O})_2]$ (1) and $[\text{Cu}_2(\text{asp})_4(\text{H}_2\text{O})_2]\cdot\text{H}_2\text{O}$ (2) both reacted with TBZH yielding the same product (11) (Scheme 5) but 2-PyBZDH only reacted with the copper asprinate (2) to yield the complex (12) (Scheme 6).

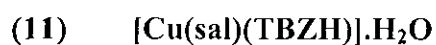


Scheme 5: Synthetic routes to complex (11)



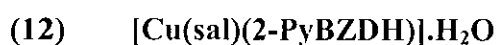
Scheme 6: Synthetic route to complex (12)

Complexes **(11)** and **(12)** were formed as green powders and formulated as shown below:



% Calc: C, 48.74; H, 3.13; N, 10.03

% Found: C, 48.50; H, 2.49; N, 10.00



% Calc: C, 55.41; H, 3.43; N, 10.20

% Found: C, 55.74; H, 3.15; N, 9.94

The IR spectra of the complexes **(11)** and **(12)** (see Appendix) were compared to those of the free ligands. The characteristic bands for the free TBZH and 2-PyBZDH ligands and the important IR spectral bands that provide evidence for the structure of the complexes are listed in Table 15.

Table 15: Characteristic IR bands (cm^{-1} , KBr discs) of the complexes (11) and (12) and their free ligands

	TBZH	(11)	2-PyBZDH	(12)
Imidazole bands				
N-H (stretch)	3096	3063	3057	3061
N-H (bending)	1096	1119	1094	1098
N-H (bending)	635	650	625	631
$\nu_{\text{C=N}}$	1579	1594	1568	1556
Thiazole bands				
$\nu_{\text{C=N}}$	1481	1484	-	-
C-S (stretch)	1231	1233	-	-
Pyridine bands				
$\nu_{\text{C=N}}$	-	-	1594	*
Pyridine ring stretching vibration	-	-	1315	1328
Carboxylate bands				
$\nu_{\text{asym}}(\text{OCO})$	-	1599	-	1600
$\nu_{\text{sym}}(\text{OCO})$	-	1452	-	1449
Δ_{OCO}	-	147	-	151
Metal-Ligand				
M-N	-	436	-	435
M-OH ₂	-	-	-	-

* Bands precluded by others in the infrared spectrum

The imidazolic $\nu_{\text{C=N}}$ and the thiazolic $\nu_{\text{C=N}}$ bands (1579 cm^{-1} and 1481 cm^{-1} , respectively) for the free ligand are shifted to 1594 cm^{-1} and 1484 cm^{-1} for (11) indicating that the ligand is chelating through the imidazolic and the thiazolic nitrogens. The C-S stretching band (at 1231 cm^{-1} for the free ligand) remains essentially unchanged supporting an uncoordinated mode for the sulfur atom of the thiazole ring.

The spectrum of (12) also has a strong imidazolic $\nu_{\text{C=N}}$ band at 1556 cm^{-1} which has shifted from that of the free 2-PyBZDH ligand (1568 cm^{-1}) indicating that the ligand is coordinated through one of the imidazolic nitrogens. Furthermore, a strong band at 1315 cm^{-1} (pyridine ring stretching vibration) in the spectrum of 2-PyBZDH is shifted

towards higher energy (1328 cm^{-1}) in the spectrum of **(12)** supporting the proposed coordinated nature of the pyridine nitrogen.

As well as the bands that have been assigned to the chelating benzimidazole ligands, the spectra of **(11)** and **(12)** also contain bands that are characteristic of salicylate anions. The calculated Δ_{OCO} values of both complexes are very close suggesting that the carboxylate groups in the two complexes have similar coordination modes. The absence of M-OH₂ bands suggest that the water molecules are unlikely to be directly coordinated to the metal centre. The fact that the complexes exhibit normal room temperature magnetic moments [2.18 B.M. (**(11)**), and 2.11 B.M. (**(12)**)] indicates that the copper centres are not associated electronically.

Both complexes are effectively insoluble in common solvents but were found to be soluble in DMSO. The molar conductivities of $5.2\text{ S cm}^2\text{ mol}^{-1}$ (**(11)**) and $4.45\text{ S cm}^2\text{ mol}^{-1}$ (**(12)**) of the complexes indicate that they are essentially non-electrolytes and thus do not dissociate in DMSO. The UV spectra of the complexes taken in DMSO solution as well as in the solid state as Nujol mull show approximately similar shapes and positions of the absorption bands, indicating no appreciable change in the geometry of the complexes in solution. It appears that the salicylate ligand in **(11)** and **(12)** is doubly deprotonated and a structure that fits their physico-chemical data is shown in Figure 77. Such a structure is well established for phenanthroline and bipyridine analogues of these complexes.⁹¹

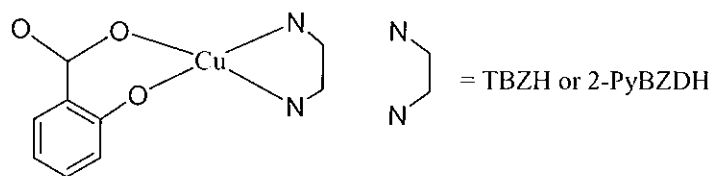
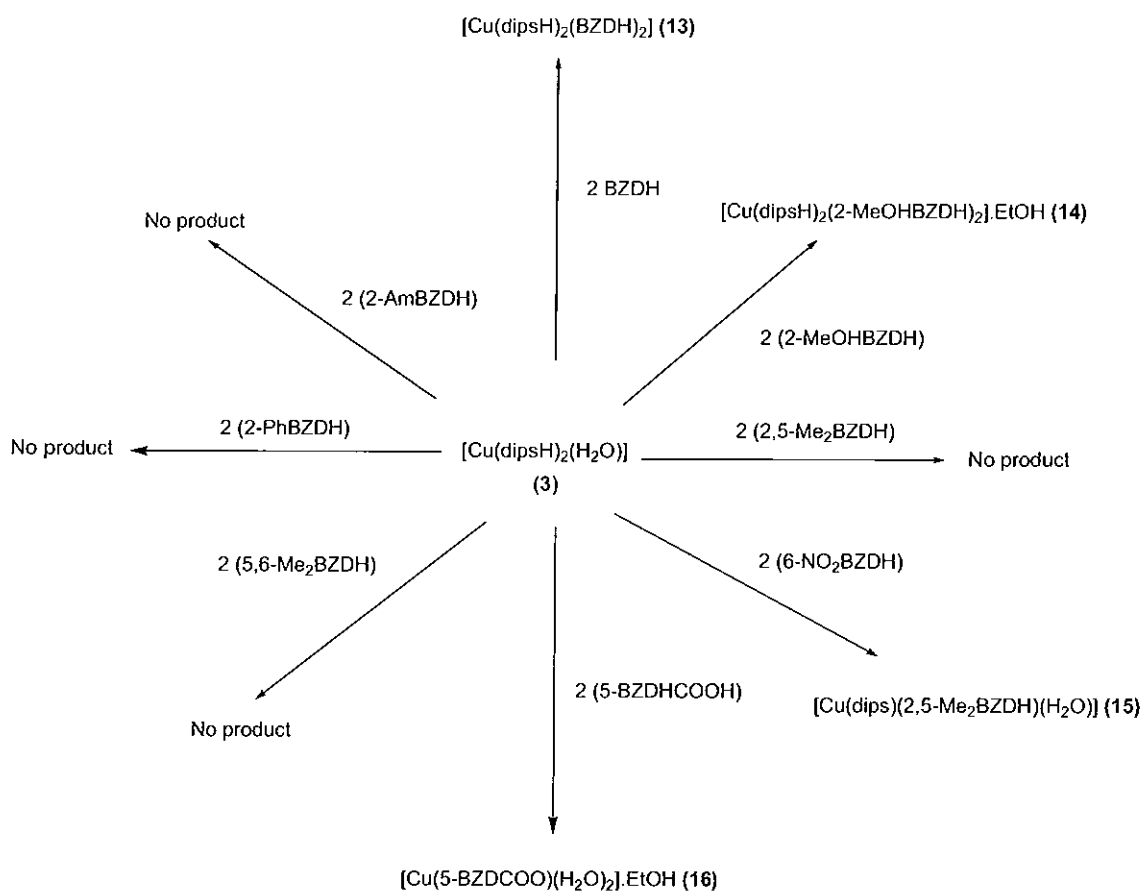


Figure 77: Possible structural motif for complexes (11) and (12)

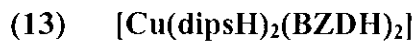
D.2.3 The reactions of $[\text{Cu}(\text{dipsH})_2(\text{H}_2\text{O})]$ (3) with the simple benzimidazole ligands

$[\text{Cu}(\text{dipsH})_2(\text{H}_2\text{O})]$ (3) was reacted with a range of benzimidazole ligands (see Figure 72) to yield the novel copper complexes (13) - (16) in accordance with the reactions shown in Scheme 7.



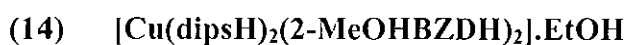
Scheme 7: Synthetic routes to complexes (13) – (16)

Complex (13) was obtained as purple crystals, (14) as blue crystals and (15) and (16) as green powders. They were formulated as shown below:



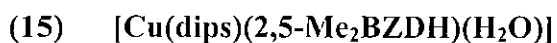
% Calc: C, 64.72; H, 6.25; N, 7.55

% Found: C, 64.36; H, 6.23; N, 7.33



% Calc: C, 62.14; H, 6.87; N, 6.59

% Found: C, 59.38; H, 5.96; N, 6.30



% Calc: C, 58.98; H, 6.30; N, 6.25

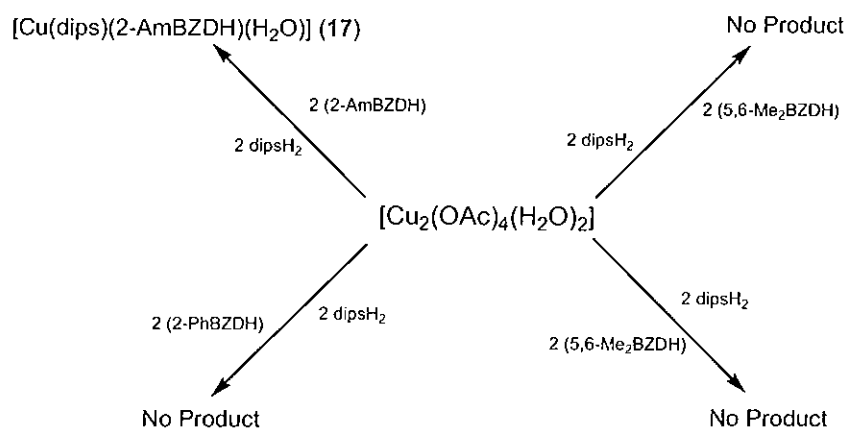
% Found: C, 61.09; H, 6.16; N, 6.25



% Calc: C, 44.34; H, 3.39; N, 9.41

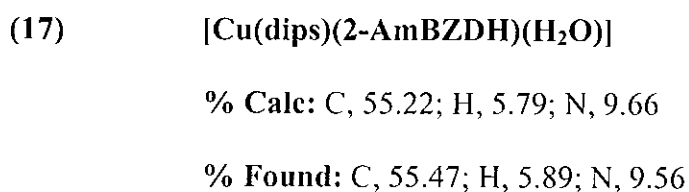
% Found: C, 44.44; H, 3.57; N, 8.18

The unsuccessful reactions from Scheme 7 were also attempted as one-pot reactions involving copper(II) acetate with 3,5-diisopropylsalicylic acid and the respective benzimidazole in accordance with Scheme 8. This only led to the synthesis of complex (17).



Scheme 8: Synthetic route to complex (17)

Complex (17) was obtained as a green powder and was formulated as shown below:



The IR spectra of the complexes (13) – (17) (see Appendix) were compared to those of the free ligands. The characteristic bands for the free ligands and some of the important IR spectral bands that provide evidence for the structure of the complexes are listed in Table 16.

Table 16: Characteristic IR bands (cm^{-1} , KBr discs) of the complexes (13) - (17) and their free ligands

	BZDH	(13)	2-MeOHBZDH	(14)	2,5-Me ₂ BZDH	(15)	5-BZDHC ₂ COOH	(16)	2-AmBZDH	(17)
Imidazole bands										
N-H (stretch)	3113	3138	*	3067	3044	*	3045	*	3054	*
N-H (bending)	1135	1141	1151	1151	1145	1149	1134	1127	1157	1149
N-H (bending)	627	632	623	640	659	635	622	628	623	636
$\nu_{\text{C=N}}$	1587	1590	1588	*	1553	1544	1588	1633	1596	1596
Carboxylate bands										
$\nu_{\text{asym}}(\text{OCO})$	-	1618	-	1552	-	1594	-	1607	-	1645
$\nu_{\text{sym}}(\text{OCO})$	-	1362	-	1388	-	1389	-	1399	-	1471
Δ_{OCO}	-	256	-	164	-	205	-	208	-	174
Metal-Ligand										
M-N	-	449	-	429	-	422	-	440	-	419
M-OH ₂	-	-	-	-	-	845	-	833	-	812

* Bands precluded by others in the infrared spectrum

Crystals of $[\text{Cu}(\text{dipsH})_2(\text{BZDH})_2]$ (**13**) (Figure 78) and $[\text{Cu}(\text{dipsH})_2(2\text{-MeOHBZDH})_2]\cdot\text{EtOH}$ (**14**) (Figure 80) suitable for X-ray structural analysis, were obtained from their respective mother liquors by slow evaporation and their structures were subsequently elucidated. The structures of the two complexes are depicted in Figures 78 – 81 and selected bond lengths and angles for them are listed in Table 17.

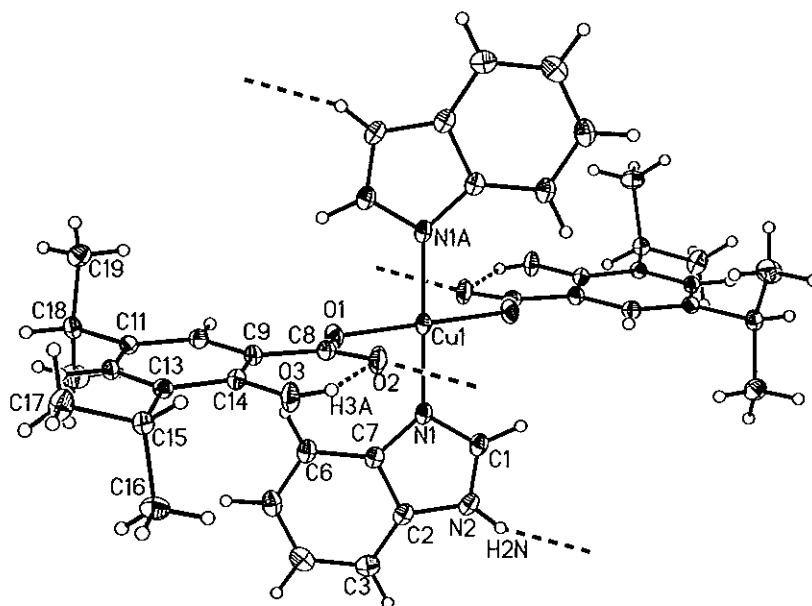


Figure 78: The X-Ray crystal structure of $[\text{Cu}(\text{dipsH})_2(\text{BZDH})_2]$ (**13**)

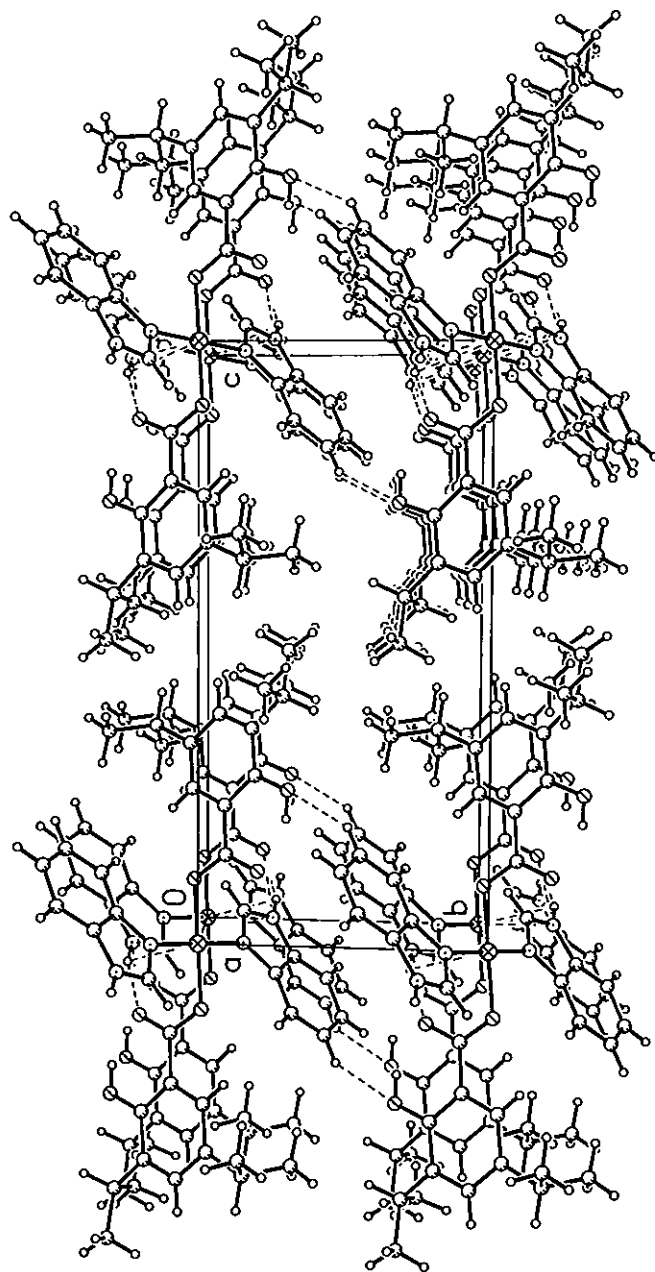


Figure 79: Packing diagram for $[\text{Cu}(\text{dipsH})_2(\text{BZDH})_2]$ (13)

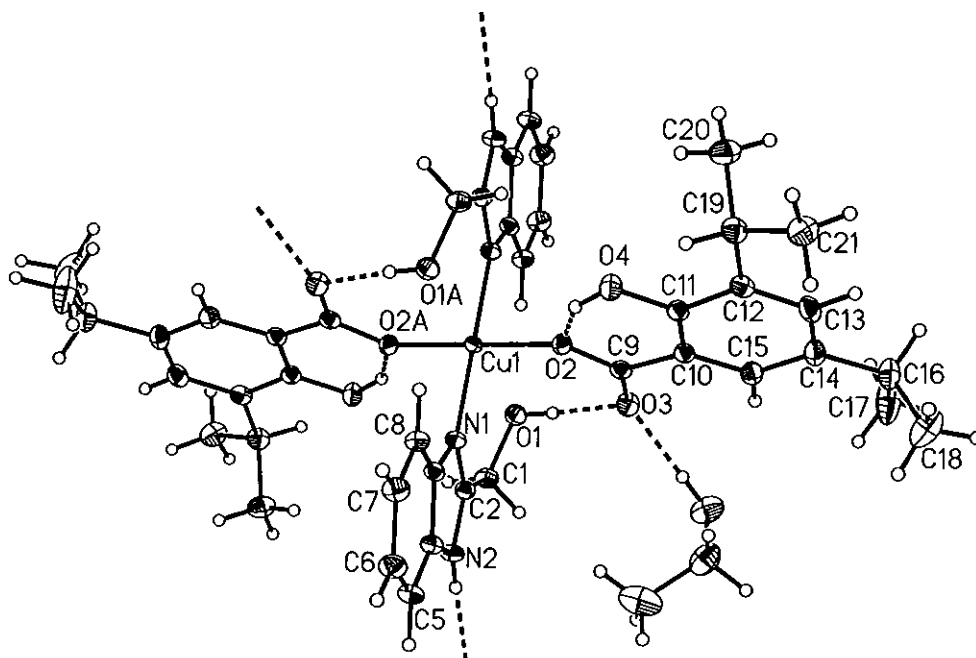


Figure 80: The X-Ray crystal structure of $[\text{Cu}(\text{dipsH})_2(2\text{-MeOHBZDH})_2]\cdot\text{EtOH}$ (**14**)

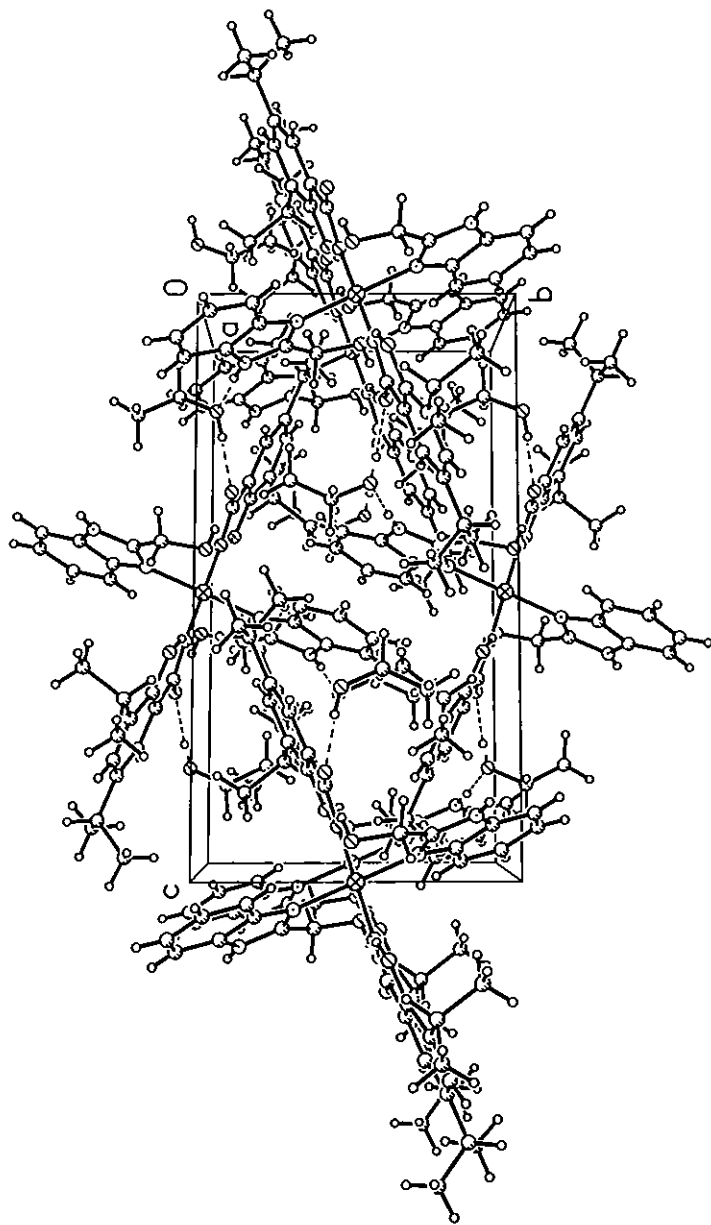


Figure 81: Packing diagram for [Cu(dipsH)₂(2-MeOHBZDH)₂].EtOH (**14**)

The two structures are very similar to that of [Cu(salH)₂(BZDH)₂] (**5**) (Figure 73). The structures of each of [Cu(dipsH)₂(BZDH)₂] (**13**) and [Cu(dipsH)₂(2-MeOHBZDH)₂].EtOH (**14**) comprise a copper centre with two coordinated oxygen atoms (one from each of the carboxylate groups of the two salicylate ligands) and two coordinated nitrogen atoms from the two benzimidazole ligands. The geometry of this CuO₂N₂ core is exactly square planar. For each structure there is significant intra- and intermolecular hydrogen bonding (Figures 79 and 81; Tables 18 and 19).

Table 17: Selected bond lengths [Å] and angles [°] around the copper centres in [Cu(dipsH)₂(BZDH)₂] (**13**) and [Cu(dipsH)₂(2-MeOHBZDH)₂].EtOH (**14**)

Complex (13)		Complex (14)	
Bond lengths Å			
Cu-O(1)	1.9278(10)	Cu(1)-O(2)	1.9795(11)
Cu-O(1)#1	1.9278(10)	Cu(1)-O(2)A	1.9795(11)
Cu-N(1)	1.9953(12)	Cu(1)-N(1)	1.9558(13)
Cu-N(1)#1	1.9953(12)	Cu(1)-N(1)#1	1.9558(13)
Bond angles °			
N(1)#1-Cu(1)-N(1)	180.00	N(1)#1-Cu(1)-N(1)	180.00(8)
O(1)-Cu(1)-O(1)#1	180.00(6)	O(2)-Cu(1)-O(2)#2	180.00
O(1)-Cu(1)-N(1)	91.54(5)	O(1)-Cu(1)-N(1)	89.39(5)
O(1)-Cu(1)-N(1)#1	88.46(5)	O(2)-Cu(1)-N(1)#1	90.61(5)
O(1)#1-Cu(1)-N(1)	88.46(5)	O(2)#2-Cu(1)-N(1)	89.39(5)
O(1)#1-Cu(1)-N(1)#1	91.54(5)	O(2)#2-Cu(1)-N(1)#1	89.39(5)

Table 18: Hydrogen bonds for [Cu(dipsH)₂(bzdH)₂] (**13**) [Å and °].

D–H...A	d(D–H)	d(H...A)	d(D...A)	<(DHA)
N(2)-H(2N)...O(2)#2	0.75(2)	2.03(2)	2.7361(16)	159(2)
O(3)-H(3A)...O(2)	0.84	1.83	2.5767(16)	146.7

Symmetry transformations used to generate equivalent atoms:

#1 -x,-y+2,-z #2 -x+1,-y+2,-z

Table 19: Hydrogen bonds for [Cu(dipsH)₂(2-MeOHBZDH)₂].EtOH (**14**) [Å and °].

D–H...A	d(D–H)	d(H...A)	d(D...A)	<(DHA)
N(2)-H(2N)...O(2)#2	0.850(14)	1.937(15)	2.7359(15)	156.0(17)
O(3)-H(3A)...O(2)	0.84	1.83	2.5735(14)	146.9

Symmetry transformations used to generate equivalent atoms:

#1 -x,-y+2,-z #2 -x+1,-y+2,-z

The IR spectra of complexes (**13**) and (**14**) (see Appendix) contain the typical bands indicative of benzimidazole ligands which have retained their imidazolic N-H functionality. As well as the bands that have been assigned to the benzimidazole ligands the spectra of (**13**) and (**14**) also contain bands that are characteristic of salicylate anions. The Δ_{OCO} value of 256 cm^{-1} for (**13**) is in agreement with the crystal structure of a monodentate coordination mode for the salicylate carboxylate groups. The Δ_{OCO} value of 164 cm^{-1} for (**14**) is lower than expected for monodentate coordination mode however, such relative reduction in the Δ_{OCO} values are typical where carboxylate groups are involved in extensive intra – or intermolecular hydrogen bonding as is observed in the structure. Bands below 500 cm^{-1} have been assigned to metal – nitrogen interactions.

The magnetic moments of 1.69 B.M. (**13**) and 1.79 B.M. (**14**) are consistent with structures lacking any significant interaction between the metal centres. The molar

conductivity of (13) ($18.65 \text{ S cm}^2 \text{ mol}^{-1}$) indicates that some dissociation is taking place in DMSO. The molar conductivity value of $5.15 \text{ S cm}^2 \text{ mol}^{-1}$ for complex (14) indicates that it is essentially a non-electrolyte. Both complexes exhibit significant shifts of the *d-d* transition bands { $563 \text{ nm} \rightarrow 733 \text{ nm}$ (13) and $575 \text{ nm} \rightarrow 740 \text{ nm}$ (14)} in their DMSO solution spectra as compared to the solid state and therefore some change in the complexes is taking place in solution. This phenomenon was also observed for the isostructural complexes $[\text{Cu}(\text{salH})_2(\text{BZDH})_2]$ (5) and $[\text{Cu}(\text{salH})_2(5,6\text{-Me}_2\text{BZDH})_2]$ (6).

The complexes (15) and (17) formulate as having the same metal : benzimidazole : salicylate ratio of 1 : 1 : 1. In the respective IR spectra the majority of the ligand absorption bands, some of them with changed intensity, appear again in the compounds. The N-H stretching band for all of the compounds has shifted slightly and all of the N-H bending characteristic bands have remained intact in the spectra of the complexes. The bands characteristic of the amine group in 2-AmBZDH are also found in the spectrum of complex (17) (although shifted slightly) (Table 20) indicating that the amine nitrogen is unlikely to be involved in coordination to the metal. However, the NH_2 group may be involved in some form of hydrogen bonding. Thus it appears that the benzimidazoles are present in complexes (15) and (17) as neutral ligands. Furthermore, the band associated with the imidazolic $\nu_{\text{C=N}}$ also remains in the spectra of both complexes. The calculated Δ_{OCO} values for both complexes are within the region indicative of a monodentate coordination mode for the salicylate carboxylate groups.

Table 20: Characteristic amine bands (cm^{-1} , KBr discs) for complex (17) and its free 2-AmBZDH ligand

	2-AmBZDH	(17)
Amine Bands		
N-H (stretch)	3381	*
NH ₂ (asym deformation)	1632	1620
NH ₂ (sym deformation)	1269	1276
NH ₂ (rocking modes)	742, 728	755, 742

* Bands precluded by others in the infrared spectrum

The room temperature magnetic moments of complexes (15) and (17) (2.31 and 2.06 B.M.) are in the expected region for simple copper(II) species (i.e. those lacking Cu-Cu interactions). The UV spectra of (15) taken in DMSO solution as well as in the solid state as a Nujol mull show approximately similar shapes and positions of the absorption bands, indicating no appreciable change in the geometry of the complex in solution. These complexes have very similar physico-chemical data to complexes (7) – (9) and it is believed they may be isostructural (see Figure 75).

Complex (16) is unique as it appears to have lost the dipsH₂ ligands altogether. The C=O band for the free 5-BZDHCOOH ligand, due to the carboxylic acid function, has disappeared in the IR spectrum for this complex and has been replaced by $\nu_{\text{asym}}(\text{OCO})$ and $\nu_{\text{sym}}(\text{OCO})$ bands which are not split (1607 cm^{-1} and 1399 cm^{-1} , respectively). The Δ_{OCO} value of 208 cm^{-1} for (16) indicates that the carboxylate ligands may be coordinated in a monodentate or monoatomic bridging fashion. The N-H stretching band in the spectrum of the 5-BZDHCOOH free ligand (a very strong band at 3207 cm^{-1}) has disappeared in the spectrum of (16) (Table 16) indicative of the fact that the benzimidazole moiety of the ligand is present in the anionic state. The copper : benzimidazole ratio appears to be 1 : 1, supporting the -2 charge of the benzimidazole ligand, and it is therefore unlikely that complex (16) is the same as $\{\text{Cu}(5-$

$\text{BZDHCOO})_2(\text{H}_2\text{O})\}_n$ which was previously generated in this laboratory.¹²⁴ The low magnetic moment (1.34 B.M.) for the complex indicates that electronic interactions exist between Cu centres in the structure and therefore it is likely that the anionic benzimidazole moiety of the ligand is bridging metal ions as is the case for BZD^- in $\{\text{Cu}(\text{BZD})_2\}_n$ (Figure 63). The molar conductivity of **(16)** ($5.68 \text{ S cm}^2 \text{ mol}^{-1}$) indicates that it is essentially a non-electrolyte in DMSO. The complex exhibits very little shifts of the $d-d$ transition bands in its DMSO solution spectrum as compared to the solid state and therefore no real change in the complex is taking place in solution. A structure that fits for the physico-chemical data of **(16)** is shown in Figure 82.

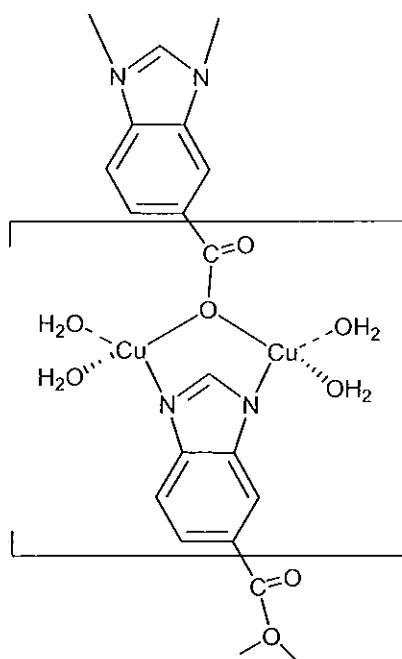
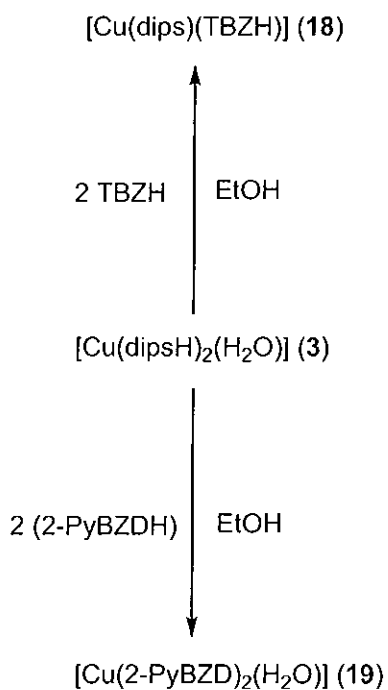


Figure 82: Possible structural motif for complex **(16)**

D.2.4 Reaction of [Cu(dipsH)₂(H₂O)] (3) with the chelating benzimidazoles thiabendazole (TBZH) and 2-(Pyridyl)Benzimidazole (2-PyBZDH)

TBZH and 2-PyBZDH successfully reacted with [Cu(dipsH)₂(H₂O)] (3) yielding complexes (18) and (19) in accordance with Scheme 9.



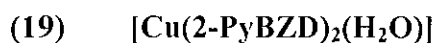
Scheme 9: Synthetic routes to complexes (18) and (19)

The complexes were formed as green powders and formulated as shown below:

(18) [Cu(dips)(TBZH)]

% Calc: C, 56.95; H, 4.78; N, 8.66

% Found: C, 56.81; H, 4.73; N, 8.43



% Calc: C, 61.33; H, 3.86; N, 17.88

% Found: C, 62.10; H, 3.74; N, 17.51

The IR spectra of the complexes (18) and (19) (see Appendix) were compared to those of the free ligands. The characteristic bands for the free TBZH and 2-PyBZDH ligands and the important IR spectral bands that provide evidence for the structure of the complexes are listed in Table 21.

Table 21: Characteristic IR bands (cm⁻¹, KBr discs) of the complexes (18) and (19) and their free ligands

	TBZH	(18)	2-PyBZDH	(19)
Imidazole bands				
N-H (stretch)	3096	3091	3057	-
N-H (bending)	1096	1113	1094	-
N-H (bending)	635	637	625	-
$\nu_{C=N}$	1579	1593	1568	1566
Thiazole bands				
$\nu_{C=N}$	1481	1482	-	-
C-S (stretch)	1231	1236	-	-
Pyridine bands				
$\nu_{C=N}$	-	-	1594	1604
Pyridine ring stretching vibration	-	-	1315	1329
Carboxylate bands				
$\nu_{asym}(OCO)$	-	1609	-	-
$\nu_{sym}(OCO)$	-	1443	-	-
Δ_{OCO}	-	166	-	-
Metal-Ligand				
M-N	-	573	-	574
M-OH ₂	-	-	-	819

In the IR spectra the imidazolic $\nu_{C=N}$ and the thiazolic $\nu_{C=N}$ bands (1579 cm^{-1} and 1481 cm^{-1} , respectively) for the free ligand are shifted to 1593 cm^{-1} and 1482 cm^{-1} for (18) indicating that the ligand is chelating through the imidazolic and the thiazolic nitrogens. The C-S stretching band (at 1231 cm^{-1} for the free ligand) remains essentially unchanged supporting an uncoordinated mode for the sulfur atom of the thiazole ring. Carboxylate bands due to the presence of salicylate anions are also present in the IR spectrum with typical $\nu_{\text{asym}}(\text{OCO})$ {1609 cm^{-1} } and $\nu_{\text{sym}}(\text{OCO})$ {1442 cm^{-1} } stretches. It is believed that (18) has a structure similar to analogous salicylate complexes (11) and (12) shown in Figure 77 above.

The IR spectrum of $\{\text{Cu}(2\text{-PyBZD})_2(\text{H}_2\text{O})\}_n$ (19) contains no bands indicative of the presence of salicylate ligands. However, the N-H stretching and bending peaks of 2-PyBZDH have essentially disappeared, suggesting the ligand is anionic in nature. The spectrum also has a strong imidazolic $\nu_{C=N}$ band at 1566 cm^{-1} which is shifted from that of the free ligand (1568 cm^{-1}) indicating that the ligands are also coordinated through one of their imidazolic nitrogens. The pyridyl $\nu_{C=N}$ bands at 1594 cm^{-1} and 1315 cm^{-1} are shifted to 1604 cm^{-1} and 1329 cm^{-1} , respectively, for the complex indicative of bonding through the pyridine nitrogen also. A new band at 819 cm^{-1} absent in the spectrum of 2-PyBZDH is indicative of coordinated water. The relative insolubility of (19) is indicative of a possible polymeric structure. The proposed structure for (19) which fits its physico-chemical data, is shown in Figure 83.

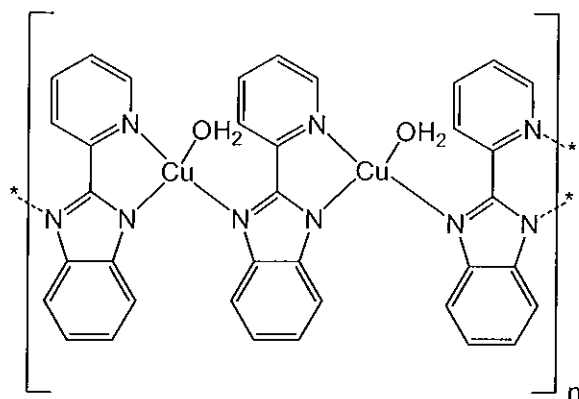
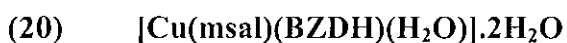


Figure 83: Possible structural motif for (19)

The room temperature magnetic moments of 1.98 B.M. (18), 1.92 B.M. (19) are consistent with the proposed structures which show no interaction between the metal centres. The UV spectrum of (18) recorded in DMSO solution as well as in the solid state as a Nujol mull shows approximately similar shapes and positions of the absorption bands, indicating no appreciable change in its geometry in solution. The molar conductivity value of $3.6 \text{ S cm}^2 \text{ mol}^{-1}$ for (18) indicates that the complex is non-electrolytic. Complex (19) is totally insoluble in all solvents supporting the proposed polymeric structure.

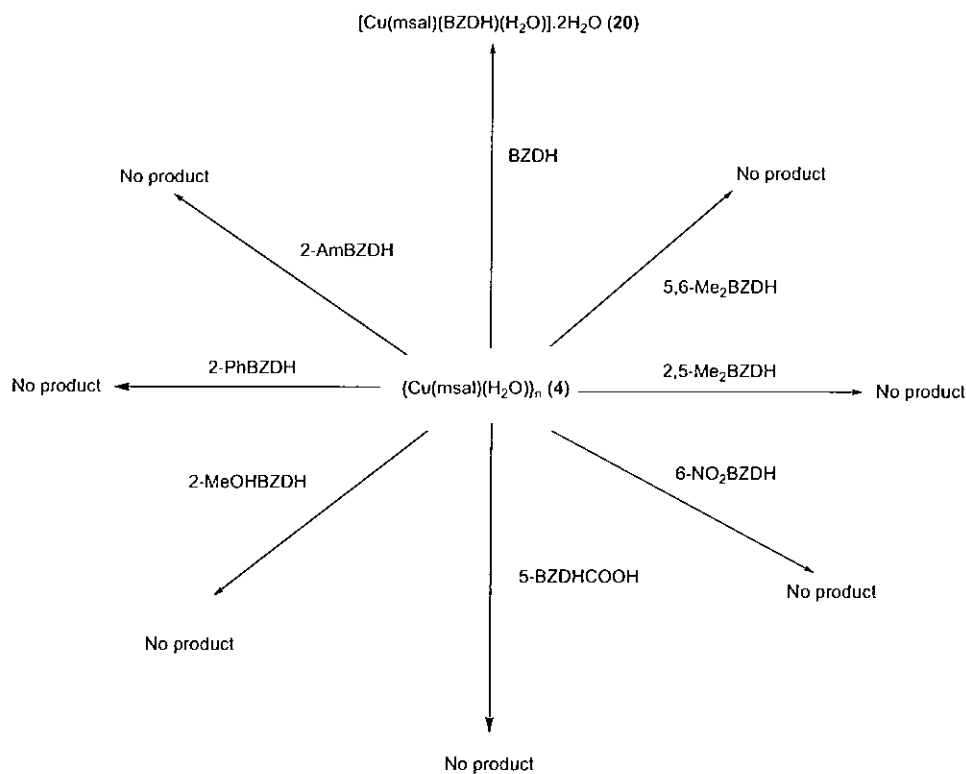
D.2.5 Reaction of $\{\text{Cu}(\text{msal})(\text{H}_2\text{O})\}_n$ (4) with the simple benzimidazole ligands

As can be seen from Scheme 10 the reactions of $\{\text{Cu}(\text{msal})(\text{H}_2\text{O})\}_n$ (4) with the benzimidazole ligands (Figure 72) were not very successful. BZDH was the only non-chelating benzimidazole to react with it yielding complex (20) which was obtained as a green powder. The complex was formulated as shown below:



% Calc: C, 44.83; H, 4.51; N, 6.97

% Found: C, 44.04; H, 3.25; N, 5.30



Scheme 10: Synthetic route to complex (20)

The above reactions (Scheme 10) were also attempted as one-pot reactions involving copper(II) acetate with 3-methoxysalicylic acid and the relevant benzimidazole. However, these reactions proved unsuccessful.

The IR spectrum of complex (20) (see Appendix) was compared to that of its free ligands. The characteristic bands for the free ligand and some of the important IR spectral bands that provide evidence for the structure of the complexes are listed in Table 22.

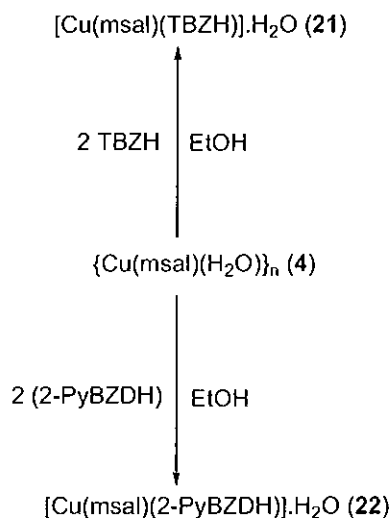
Table 22: Characteristic IR bands (cm^{-1} , KBr discs) for complex (20) and its free BZDH ligand

	BZDH	(20)
Imidazole bands		
N-H (stretch)	3113	3116
N-H (bending)	1135	1129
N-H (bending)	627	620
$\nu_{\text{C=N}}$	1587	1561
Carboxylate bands		
$\nu_{\text{asym}}(\text{OCO})$	-	1602
$\nu_{\text{sym}}(\text{OCO})$	-	1399
Δ_{OCO}	-	203
Metal-Ligand		
M-N	-	440
M-OH ₂	-	836

The N-H stretching and bending bands in the spectrum of the BZDH free ligand also appear (although shifted slightly) in the spectrum of the complex indicating that the ligand is present in its neutral state. The spectrum also contains typical $\nu_{\text{asym}}(\text{OCO})$ $\{1602 \text{ cm}^{-1}\}$ and $\nu_{\text{sym}}(\text{OCO})$ $\{1399 \text{ cm}^{-1}\}$ bands indicating the presence of carboxylate groups. The Δ_{OCO} value of 203 cm^{-1} is indicative of a monodentate coordination mode for the salicylate ligands. A new band absent in the spectrum of BZDH at 836 cm^{-1} has been assigned to a coordinated water molecule. The room temperature magnetic moment of 2.08 B.M. is consistent with a structure lacking any Cu-Cu interaction. A molar conductivity value of $1.45 \text{ S cm}^2 \text{ mol}^{-1}$ for complex (20) suggests that no dissociation of the complex is taking place in DMSO solution. It is believed that (20) has a similar structure to complexes (7) – (9) (Figure 75) for which its physico-chemical data fit.

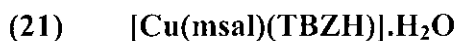
D.2.6 Reaction of $\{\text{Cu}(\text{msal})(\text{H}_2\text{O})\}_n$ (4) with the chelating benzimidazoles thiabendazole (TBZH) and 2-(Pyridyl)Benzimidazole (2-PyBZDH)

TBZH and 2-PyBZDH both reacted with $\{\text{Cu}(\text{msal})(\text{H}_2\text{O})\}_n$ (4) yielding the products (21) and (22) in accordance with Scheme 11.



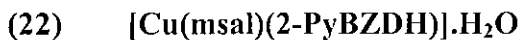
Scheme 11: Synthetic routes to complexes (21) and (22)

The complexes were formed as green powders and were formulated as shown below:



% Calc: C, 48.16; H, 3.37; N, 9.36

% Found: C, 47.21; H, 2.89; N, 10.35



% Calc: C, 54.24; H, 3.87; N, 9.49

% Found: C, 54.24; H, 3.94; N, 9.45

The IR spectra of the complexes (21) and (22) (see Appendix) were compared to those of the free ligands. The characteristic bands for the free ligands and the some of the important IR spectral bands that provide evidence for the structure of the complexes are listed in Table 23.

Table 23: Characteristic IR bands (cm^{-1} , KBr discs) of the complexes (21) and (22) and their free ligands

	TBZH	(21)	2-PyBZDH	(22)
Imidazole bands				
N-H (stretch)	3096	3095	3057	3064
N-H (bending)	1096	1087	1094	1085
N-H (bending)	635	630	625	632
$\nu_{\text{C}=\text{N}}$	1579	1567	1568	1564
Thiazole bands				
$\nu_{\text{C}=\text{N}}$	1481	1477	-	-
C-S (stretch)	1231	1233	-	-
Pyridine bands				
$\nu_{\text{C}=\text{N}}$	-	-	1594	1600
Pyridine ring stretching vibration	-	-	1315	1327
Carboxylate bands				
$\nu_{\text{asym}}(\text{OCO})$	-	1599	-	1529
$\nu_{\text{sym}}(\text{OCO})$	-	1442	-	1369
Δ_{OCO}	-	157	-	160
Metal-Ligand				
M-N	-	437	-	438
M-OH ₂	-	-	-	-

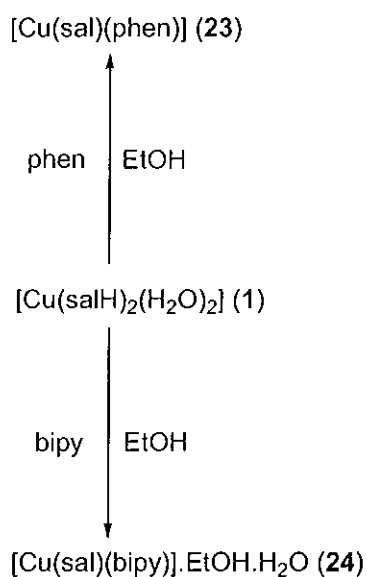
The imidazolic $\nu_{\text{C}=\text{N}}$ and the thiazolic $\nu_{\text{C}=\text{N}}$ bands (1579 cm^{-1} and 1481 cm^{-1} , respectively) for the free ligand are shifted to 1567 cm^{-1} and 1477 cm^{-1} for (21) indicating that the ligand is chelating through the imidazolic and the thiazolic nitrogens. The C-S stretching band (at 1231 cm^{-1} for the free ligand) remains essentially unchanged supporting an uncoordinated mode for the sulfur atom of the thiazole ring. The spectrum of (22) also has a strong imidazolic $\nu_{\text{C}=\text{N}}$ band at 1564 cm^{-1} which has shifted from that of the free ligand (1568 cm^{-1}) indicating that the ligand is coordinated

through one of the imidazolic nitrogens. Also the pyridyl $\nu_{C=N}$ band at 1594 cm^{-1} shifts to 1600 cm^{-1} indicative of bonding through the pyridine nitrogen. Furthermore, a strong band at 1315 cm^{-1} (pyridine ring stretching vibration) in the spectrum of 2-PyBZDH is shifted towards higher energy (1327 cm^{-1}) also supporting the proposed coordinated nature of the pyridine nitrogen. The similar Δ_{OCO} values $\{157\text{ cm}^{-1}$ (**21**) and 160 cm^{-1} (**22**) $\}$ suggest that the salicylate ligands in both complexes are coordinated in the same fashion. The presence of the methoxy group in (**21**) and (**22**) is confirmed by the C-O-C bands at 1060 cm^{-1} (**21**) and 1067 cm^{-1} (**22**) in their spectra. These bands have shifted from 1055 cm^{-1} in the spectrum of the free ligand suggesting that the methoxy ethereal oxygen may be either involved in coordination or hydrogen bonding in the complexes, although it is believed that the latter is the case. It is most probable that these two complexes are isostructural to their salicylic acid analogues (**11**) and (**12**) (Figure 77).

The room temperature magnetic moments for the two complexes are normal (1.85 and 1.97 B.M., respectively) supporting structures where the copper centres are not associated electronically. The UV spectra of (**21**) and (**22**) taken in DMSO solutions as well as in the solid state as Nujol mulls show approximately similar shapes and positions of the absorption bands, indicating no appreciable change in the geometry of the complexes in solution. The low molar conductivity values of both complexes ($6.05\text{ S cm}^2\text{ mol}^{-1}$ and $8.15\text{ S cm}^2\text{ mol}^{-1}$, respectively) indicate that no dissociation of the complexes is taking place in solution.

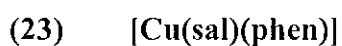
D.3 SYNTHESIS AND CHARACTERISATION OF COPPER(II) SALICYLATES INCORPORATING THE N,N-DONOR LIGANDS 1,10-PHENANTHROLINE AND 2,2'-BIPYRIDINE

[Cu(salH)₂(H₂O)₂] (1) was reacted with the chelating ligands 1,10-phenanthroline (phen) and 2,2'-bipyridine (bipy) in accordance with Scheme 12 to yield complexes (23) and (24). [Cu(dipsH)₂(H₂O)] (3) and {Cu(msal)(H₂O)}_n (4) were reacted with phen and bipy similarly to produce complexes (25) – (28).



Scheme 12: Synthetic routes to complexes (23) – (28)

While complexes (23) - (26) and (28) were obtained as green powders, (27) was isolated as green crystals which were suitable for X-ray analysis. The six compounds were formulated as shown below:



% Calc: C, 60.12; H, 3.23; N, 7.41

% Found: C, 58.97; H, 3.34; N, 7.08

- (24) **[Cu(sal)(bipy)].EtOH.H₂O**
% Calc: C, 54.91; H, 4.22; N, 6.99
% Found: C, 54.36; H, 4.80; N, 6.67
- (25) **[Cu(dips)(phen)].H₂O**
% Calc: C, 62.03; H, 5.83; N, 5.79
% Found: C, 62.48; H, 5.86; N, 5.87
- (26) **[Cu(dips)(bipy)]**
% Calc: C, 62.78; H, 5.50; N, 6.37
% Found: C, 62.26; H, 5.76; N, 6.33
- (27) **[Cu(msal)(phen)].H₂O**
% Calc: C, 56.14; H, 3.77; N, 6.83
% Found: C, 56.09; H, 3.41; N, 6.14
- (28) **[Cu(msal)(bipy)].H₂O**
% Calc: C, 53.53; H, 3.99; N, 6.94
% Found: C, 53.30; H, 3.52; N, 6.97

Crystals of (27) suitable for X-ray structural analysis were obtained when the reaction was carried out in DMSO and the mother liquor left to stand for several weeks. The structure of (27) is shown in Figures 84 and 85 and selected bond lengths and angles are listed in Table 24. (27) is essentially isostructural to the [Cu(sal)(bipy)] complex in [Cu(sal)(bipy)].EtOH.H₂O which was previously published by this group (Figure 46).

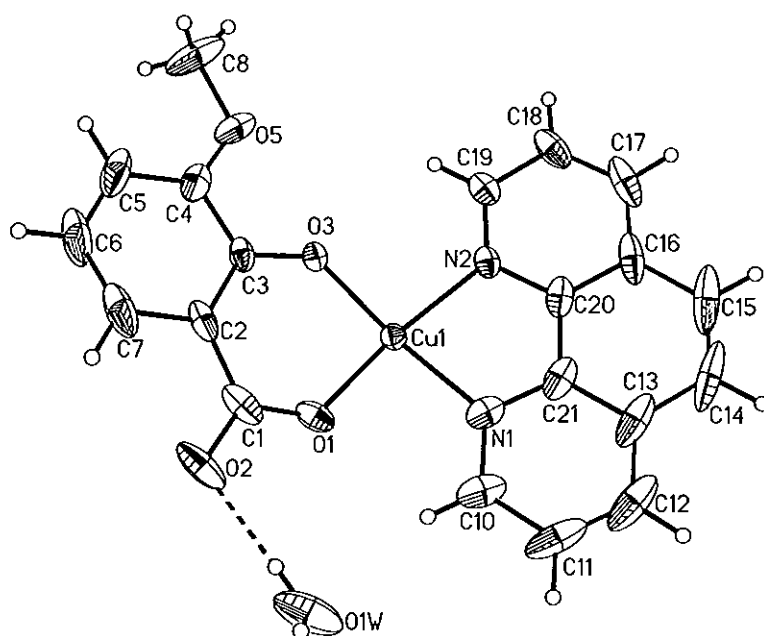


Figure 84: The X-Ray crystal structure of $[\text{Cu}(\text{msal})(\text{phen})]\cdot\text{H}_2\text{O}$ (**27**)

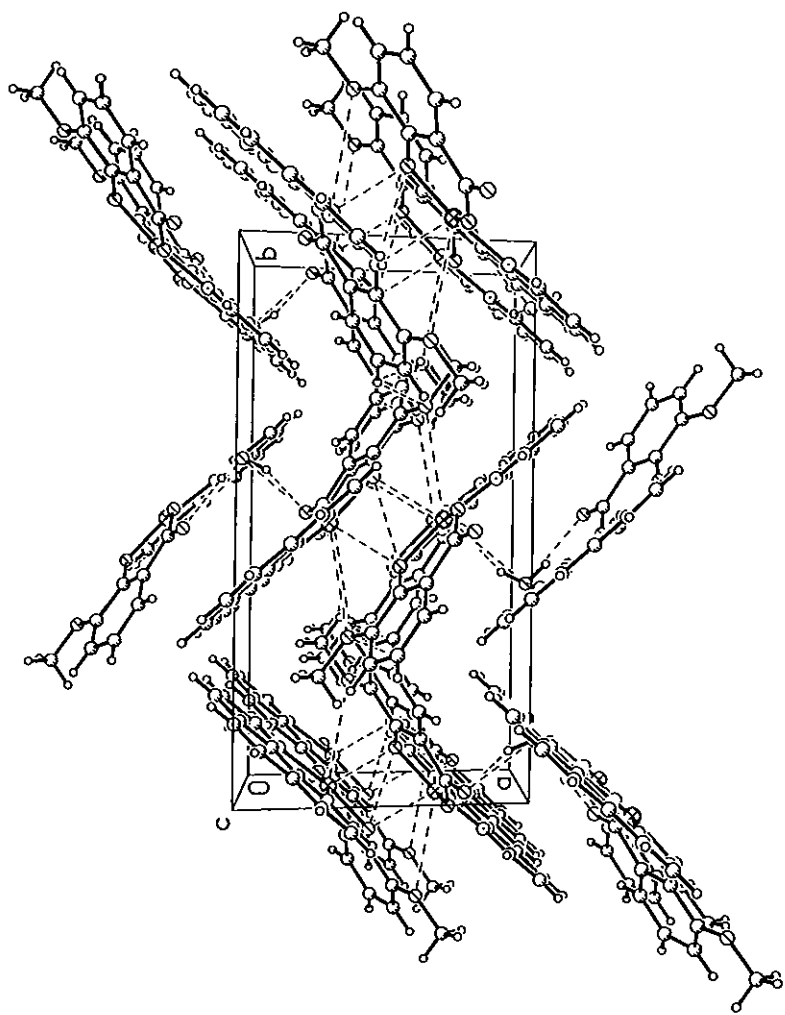


Figure 85: Packing diagram for [Cu(msal)(phen)]·H₂O (27)

Table 24: Selected bond lengths [Å] and angles [°] around the copper centres in [Cu(msal)(phen)].H₂O (**27**)

Complex (27)	
Bond lengths Å	
Cu(1)-O(1)	1.893(2)
Cu(1)-O(3)	1.900(2)
Cu(1)-N(1)	2.017(3)
Cu(1)-N(2)	2.009(12)
Bond angles °	
N(2)-Cu(1)-N(1)	81.43(12)
O(1)-Cu(1)-O(3)	93.94(10)
O(1)-Cu(1)-N(1)	89.51(12)
O(1)-Cu(1)-N(2)	169.08(11)
O(3)-Cu(1)-N(1)	170.82(10)
O(3)-Cu(1)-N(2)	94.15(10)

Table 25: Hydrogen bonds for [Cu(msal)(phen)].H₂O (**27**) [Å and °].

D-H...A	d(D-H)	d(H...A)	d(D...A)	<(DHA)
O(1W)-H(11W)...O(2)	0.891(19)	1.97(2)	2.856(6)	171(4)
O(1W)-H(11W)...O(1)	0.891(19)	2.69(4)	3.347(4)	131(4)
O(1W)-H(12W)...O(2)#1	0.89(2)	2.04(3)	2.891(4)	160(5)

In (**27**) the copper(II) ion is coordinated to the two nitrogen donors of the phen ligand and chelated by the salicylate dianion via one carboxylate oxygen atom and the phenolate oxygen atom, giving the copper atom an approximate square planar geometry. The two hydrogen atoms of the lattice water molecule are hydrogen bonded to the uncoordinated carboxylate oxygen of one molecule of (**27**) and the coordinated oxygen of another (Figures 84 - 85). These interactions are repeated throughout the

crystal lattice yielding a hydrogen bonded polymeric supra-molecular structure (Figure 85).

The IR spectra of (23), (25) and (27) (see Appendix) are very similar reflecting their structural similarity. The spectra contain absorption bands which are characteristic of the presence of chelating phen [846 cm^{-1} and 721 cm^{-1} (23), 845 cm^{-1} and 724 cm^{-1} (25) and 847 cm^{-1} and 722 cm^{-1} (27)].¹²⁵ As well as the bands that have been assigned to the chelating phen ligand the spectra of the three complexes also contain bands that are characteristic of salicylate anions with $\nu_{\text{asym}}(\text{OCO})$ {1599 cm^{-1} (23), 1612 cm^{-1} (25) and 1572 cm^{-1} (27)} and $\nu_{\text{sym}}(\text{OCO})$ {1384 cm^{-1} (23), 1454 cm^{-1} (25) and 1445 cm^{-1} (27)} bands. The normal room temperature magnetic moments of 2.11 B.M. (23), 2.05 B.M. (25) and 1.85 B.M. (27) are consistent with a structure lacking Cu-Cu interactions. The similarity in their UV spectra suggest that (23) and (25) adopt the same square planar geometry as [Cu(msal)(phen)].H₂O (27).

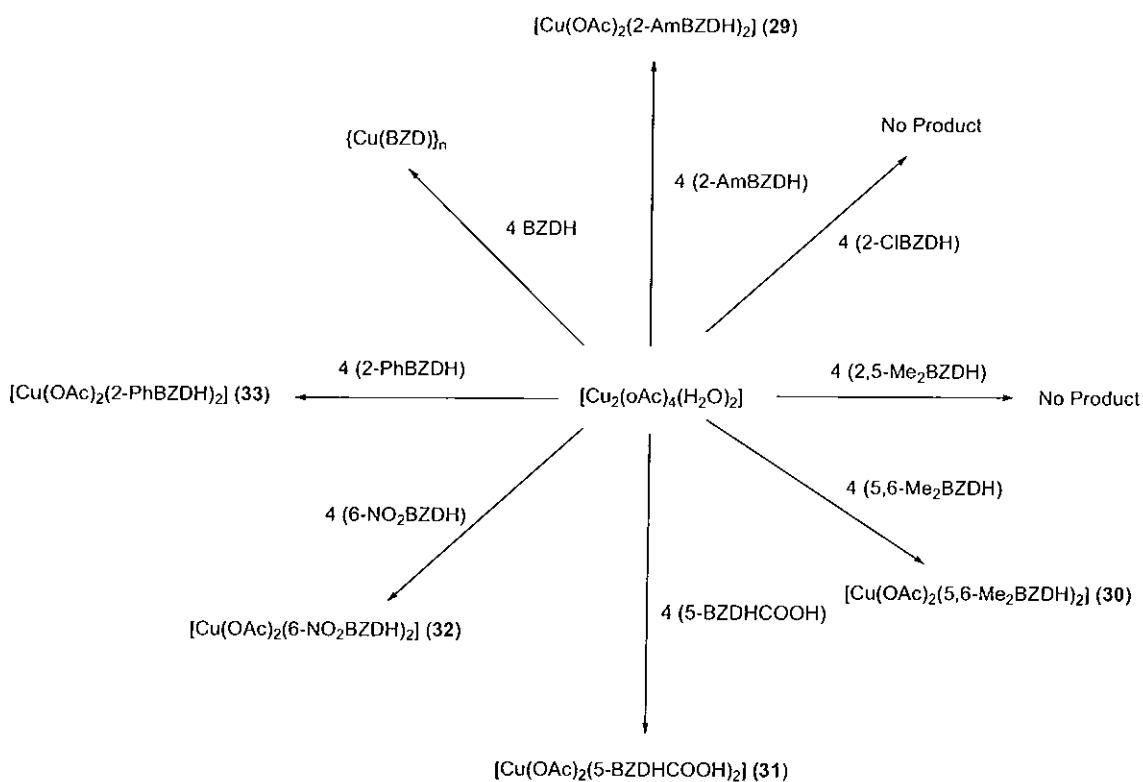
The IR spectra of (24) and (26) and (28) (see Appendix) are very similar reflecting their structural similarity and they are all similar to that of (27) and to the known complex [Cu(sal)(bipy)].EtOH.H₂O. The spectra contain absorption bands which are characteristic of the presence of chelating bipy [762 cm^{-1} and 731 cm^{-1} (24), 769 cm^{-1} and 733 cm^{-1} (26) and 760 cm^{-1} and 733 cm^{-1} (28)].⁷² Again, the spectra of the three complexes contain bands that are characteristic of salicylate anions with $\nu_{\text{asym}}(\text{OCO})$ {1601 cm^{-1} (24), 1614 cm^{-1} (26) and 1606 cm^{-1} (28)} and $\nu_{\text{sym}}(\text{OCO})$ {1451 cm^{-1} (24), 1456 cm^{-1} (26) and 1443 cm^{-1} (28)} and these bands appear in similar positions to those of (27) and [Cu(sal)(bipy)].EtOH.H₂O. The room temperature magnetic moments for the three complexes are normal (1.95, 1.90 and 2.29 B.M., respectively) supporting

structures where the copper centres are not associated electronically. The similarity in their UV spectra {which have similar λ_{max} values to that of $[\text{Cu}(\text{sal})(\text{bipy})]\cdot\text{EtOH}\cdot\text{H}_2\text{O}$ } suggest that (24), (26) and (28) adopt the same square planar geometry as the structurally characterised complex (27) and the previously characterised complex $[\text{Cu}(\text{sal})(\text{bipy})]\cdot\text{EtOH}\cdot\text{H}_2\text{O}$ (Figure 46).

D.4 SYNTHESIS AND CHARACTERISATION OF COPPER(II) ACETATE AND SIMPLE COPPER(II) SALTS INCORPORATING BENZIMIDAZOLE LIGANDS

D.4.1 Reaction of $[\text{Cu}_2(\text{OAc})_4(\text{H}_2\text{O})_2]$ with the simple benzimidazole ligands

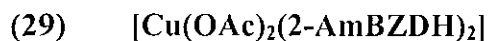
Copper(II) acetate was reacted with a range of simple benzimidazole ligands (Figure 72) in accordance with Scheme 13 to produce complexes (29) – (33).



Scheme 13: Synthetic routes to complexes (29) – (33)

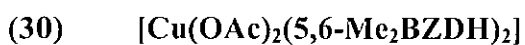
The reaction of $[\text{Cu}_2(\text{OAc})_4(\text{H}_2\text{O})_2]$ with BZDH produced the known red polymeric complex $\{\text{Cu}(\text{BZD})\}_n$ (Figure 63).¹²⁴ Blue crystals of (30) suitable for X-ray analysis were obtained from the reaction solution upon standing for several days. (29), (31) and

(32) were obtained as green powders and (33) as a purple powder. The complexes were formulated as below:



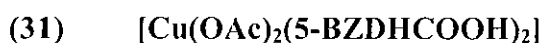
% Calc: C, 48.26; H, 4.50; N, 18.76

% Found: C, 48.25; H, 4.27; N, 18.86



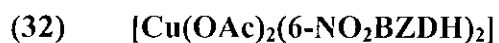
% Calc: C, 55.74; H, 5.52; N, 11.82

% Found: C, 55.66; H, 5.52; N, 11.78



% Calc: C, 47.48; H, 3.59; N, 11.07

% Found: C, 46.23; H, 3.20; N, 11.07



% Calc: C, 42.57; H, 3.18; N, 16.55

% Found: C, 42.95; H, 3.37; N, 16.23



% Calc: C, 63.20; H, 4.60; N, 9.83

% Found: C, 63.94; H, 4.67; N, 9.80

The structure of (30) is shown in Figures 86 and 87 and selected bond lengths and angles are listed in Table 26. Complex (30) has a square planar copper centre (Figure 86) which contains two trans benzimidazole and two acetate ligands. The copper atom is situated on an inversion centre. Neighbouring molecules are linked by significant π - π stacking interactions involving the benzimidazole ligands (Figure 87). There is significant hydrogen bonding involving the hydrogen of the NH of the benzimidazole rings and the uncoordinated oxygen of the carboxylate groups (Figure 87 and Table 27). Essentially complex (30) has a very similar structure to that of salicylate complex $[\text{Cu}(\text{salH})_2(\text{BZDH})_2]$ (5) (Figure 73).

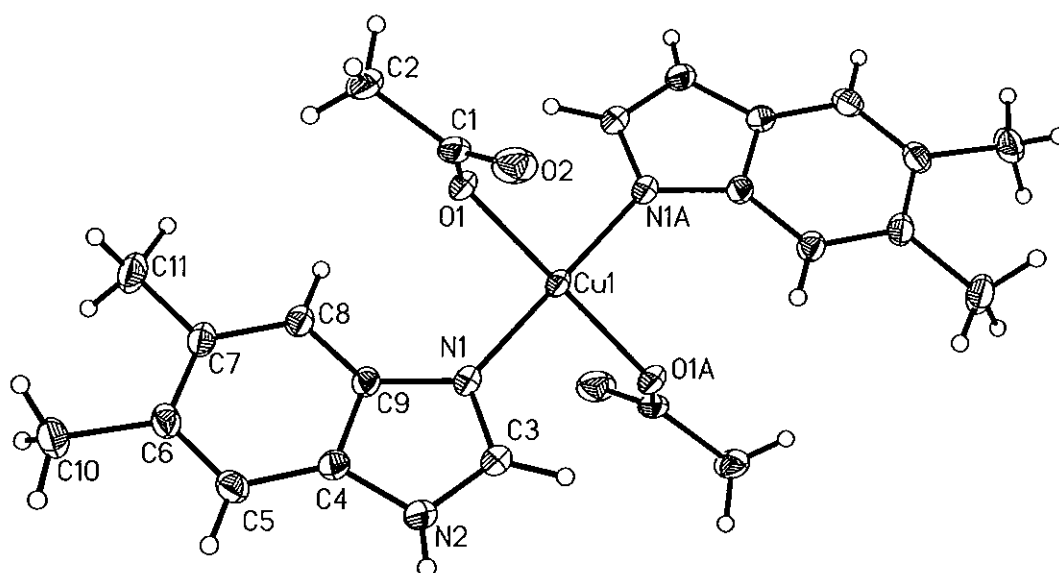


Figure 86: The X-Ray crystal structure of $[\text{Cu}(\text{OAc})_2(5,6\text{-Me}_2\text{BZDH})_2]$ (30)

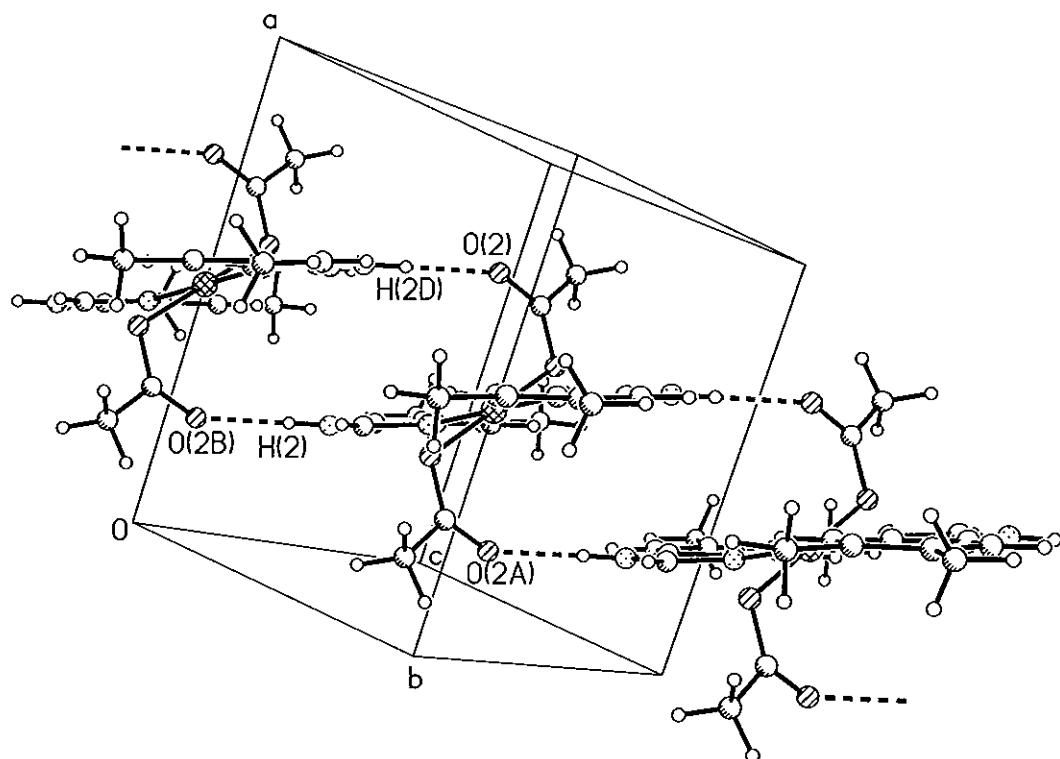


Figure 87: Packing diagram for [Cu(OAc)₂(5,6-Me₂BZDH)₂] (30)

Table 26: Selected bond lengths [Å] and angles [°] around the copper centre in [Cu(OAc)₂(5,6-Me₂BZDH)₂] (**30**)

Complex (30)	
Bond lengths Å	
Cu(1)-O(1)	1.9477(8)
Cu(1)-O(1a)	1.9477(8)
Cu(1)-N(1A)	1.9805(10)
Cu(1)-N(2)	2.009(12)
Bond angles °	
O(1)-Cu(1)-O(1A)	180.00(3)
O(1)-Cu(1)-N(1)	90.82(4)
O(1A)-Cu(1)-N(1)	89.18(4)
O(1)-Cu(1)-N(1A)	90.82(4)
O(1)-Cu(1)-O(1A)	180.00(3)

Table 27: Hydrogen bonds for [Cu(OAc)₂(5,6-Me₂BZDH)₂] (**30**) [Å and °].

D-H...A	d(D-H)	d(H...A)	d(D...A)	<(DHA)
N(2)-H(2)...O(2A)	0.81(2)	1.92(2)	2.7169(14)	168.3(19)

The suffix A denotes the symmetry operation: A: -x+1,-y+1,-z applied to generate equivalent atoms

The IR spectra of the complexes (**29**) - (**33**) (see Appendix) were compared to those of the free ligands. The characteristic bands for the free ligands and the some of the important IR spectral bands that provide evidence for the structure of the complexes are listed in Table 28.

Table 28: Characteristic IR bands (cm^{-1} , KBr discs) of the complexes (29) - (33) and their free ligands

	2-AmBZDH	(29)	5,6-Me ₂ BZDH	(30)	5-BZDHCOOH	(31)	6-NO ₂ BZDH	(32)	2-PhBZDH	(33)
Imidazole bands										
N-H (stretch)	3054	3064	3095	3102	3045	3049	3103	3116	3047	3067
N-H (bending)	1157	1136	1158	1159	1134	1141	1131	1130	1146	1150
N-H (bending)	623	622	647	647	622	672	690	708	621	634
$\nu_{\text{C-N}}$	1596	1585	1584		1588	*	1591	1586	1591	*
Amine bands										
N-H (stretch)	3381	3366	-	-	-	-	-	-	-	-
NH ₂ (assym deformation)	1632	1648	-	-	-	-	-	-	-	-
NH ₂ (sym deformation)	1269	1275	-	-	-	-	-	-	-	-
NH ₂ (rocking mode)	742, 728	745, *	-	-	-	-	-	-	-	-
Carboxylate bands										
$\nu_{\text{asym}}(\text{OCO})$	-	1609	-	1559	-	1591	-	1508	-	1570
$\nu_{\text{sym}}(\text{OCO})$	-	1471	-	1408	-	1409	-	1341	-	1399
Δ_{OCO}	-	138	-	151	-	182	-	167	-	171
Metal-Ligand										
M-N	-	507	-	486	-	460	-	429	-	436
M-OH ₂	-	-	-	-	-	-	-	-	-	-

* Bands precluded by others in the infrared spectrum

In the IR spectrum of $[\text{Cu}(\text{OAc})_2(5,6\text{-Me}_2\text{BZDH})_2]$ (**30**) the N-H stretching and bending bands in the spectrum of the 5,6-Me₂BZDH free ligand also appear (although shifted slightly) in the spectrum of the complex indicative of the fact that the ligand is present in its neutral state. Furthermore, the band associated with the imidazolic $\nu_{\text{C}=\text{N}}$ in the free ligand has shifted in the spectrum of (**30**) indicating that the benzimidazole ligand is bound to the metal through its nitrogen atom. The Δ_{OCO} value of 151 cm^{-1} is lower than expected for monodentate coordination mode however, such relative reduction in the Δ_{OCO} values are typical where carboxylate groups are involved in intra- or intermolecular hydrogen bonding as is the case here.

The complexes (**29**) and (**31**) – (**33**) formulate as having the same metal : benzimidazole : acetate ratio of 1 : 2 : 2 as (**30**) and their IR spectra are similar and it is likely they are all isostructural to (**30**). The N-H stretching and bending bands in the spectra of the free benzimidazole ligands also appear (although shifted slightly) in the spectra of the complexes indicative of the fact that the ligands are present in their neutral state. The bands characteristic of the amine group in 2-AmBZDH are also found in the spectrum of complex (**29**) (although shifted slightly) indicating that the amine nitrogen is unlikely to be involved in coordination to the metal. However the NH₂ group may be involved in some form of hydrogen bonding.

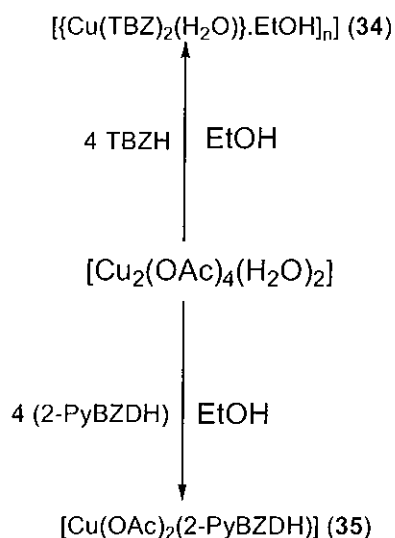
The IR spectra of the complexes contain typical $\nu_{\text{asym}}(\text{OCO})$ and $\nu_{\text{sym}}(\text{OCO})$ bands which are in similar positions and are not split. The calculated Δ_{OCO} value of the complexes (Table 28) are lower than expected for monodentate coordination mode however as seen in the spectrum of (**30**) such relative reduction in the Δ_{OCO} values are

typical where carboxylate groups are involved in intra- or intermolecular hydrogen bonding.

The molar conductivities of (30) – (33) were found to be in the range 0.9 to 10.38 S cm² mol⁻¹ indicating that they are essentially non-electrolytic in DMSO. Complex (30) exhibits significant shifts of its *d-d* transition bands {531 nm → 726 nm} in its DMSO solution spectrum as compared to the solid state and therefore some change in the complex is taking place in solution. The UV spectra of the complexes (29) and (31) - (33) recorded in DMSO solution as well as in the solid state as Nujol mulls show approximately similar shapes and positioning of the absorption bands, indicating no appreciable change in their geometry in solution. The room temperature magnetic moments of (29) – (33) (ranging from approximately 1.60 to 2.20 B.M.) are in the region consistent with a structure lacking Cu-Cu interactions.

D.4.2 Reaction of $[\text{Cu}_2(\text{OAc})_4(\text{H}_2\text{O})_2]$ with the chelating benzimidazole ligands

TBZH and 2-PyBZDH readily reacted with copper(II) acetate to yield complexes (34) and (35) (Scheme 14) as green powders.



Scheme 14: Synthetic routes to complexes (34) and (35)

The complexes were formulated as shown below:



% Calc: C, 50.03, H, 3.82, N, 15.91

% Found: C, 49.77; H, 2.97; N, 14.96



% Calc: C, 50.99; H, 4.01; N, 11.15

% Found: C, 48.78; H, 3.69; N, 11.91

The IR spectra of the complexes (34) and (35) (see Appendix) were compared to those of the free ligands. The characteristic bands for the free ligands and the some of the important IR spectral bands that provide evidence for the structure of the complexes are listed in Table 29.

Table 29: Characteristic IR bands (cm^{-1} , KBr discs) of the complexes (34) and (35) and their free ligands

	TBZH	(34)	2-PyBZDH	(35)
Imidazole bands				
N-H (stretch)	3096	-	3057	3074
N-H (bending)	1096	-	1094	1108
N-H (bending)	635	-	625	667
$\nu_{\text{C=N}}$	1579	1594	1568	1579
Thiazole bands				
$\nu_{\text{C=N}}$	1481	1474	-	-
C-S (stretch)	1231	1230	-	-
Pyridine bands				
$\nu_{\text{C=N}}$	-	-	1594	1560
Pyridine ring stretching vibration	-	-	1315	1378
Carboxylate bands				
$\nu_{\text{asym}}(\text{OCO})$	-	-	-	1606
$\nu_{\text{sym}}(\text{OCO})$	-	-	-	1458
Δ_{OCO}	-	-	-	148
Metal-Ligand				
M-N	-	437	-	438
M-OH ₂	-	829	-	-

The anionic nature of the TBZ⁻ in $\{[\text{Cu}(\text{TBZ})_2(\text{H}_2\text{O})]\cdot\text{EtOH}\}_n$ (**34**) is evident when its IR spectrum is compared to that of TBZH (Table 29). It can be seen that the N-H vibration band observed at 3096 cm^{-1} for the free ligand is absent from the spectrum of the complex. Also the bands associated with imidazolic N-H bending modes (of the free ligand) at 1096 cm^{-1} and 635 cm^{-1} are also absent in the spectrum of (**34**). The imidazolic $\nu_{\text{C}=\text{N}}$ and the thiazolic $\nu_{\text{C}=\text{N}}$ bands (1579 cm^{-1} and 1481 cm^{-1} , respectively) for the free ligand are shifted to 1594 cm^{-1} and 1474 cm^{-1} for (**34**) indicating that the ligand is chelating through the imidazolic and the thiazolic nitrogens. A small band at approximately 2970 cm^{-1} (aliphatic C-H stretching) in the spectrum of (**34**) supports the inclusion of an ethanol molecule in the formulation although it is thought that it is not coordinated to the metal centre but present as a molecule of crystallisation. Also, the C-S stretching band (at 1231 cm^{-1} for the free ligand) remains essentially unchanged supporting an uncoordinated mode for the sulfur atom of the thiazole ring. A new band in the spectrum of (**34**) at approximately 829 cm^{-1} is attributed to a water molecule bound to the metal centre.

The IR spectrum of complex (**35**) exhibits spectral features attributable to a neutral chelating 2-PyBZDH ligand. The pyridyl $\nu_{\text{C}=\text{N}}$ band at 1594 cm^{-1} shifts to 1560 cm^{-1} for the complex indicative of bonding through the pyridine nitrogen. Furthermore, a strong band at 1315 cm^{-1} (pyridine ring stretching vibration) in the spectrum of 2-PyBZDH is shifted towards higher energy (1378 cm^{-1}) also supporting the coordinated nature of the pyridine nitrogen. As well as the bands associated with the 2-PyBZDH ligand the spectrum of (**35**) also contains bands that are characteristic of acetate anions with typical $\nu_{\text{asym}}(\text{OCO})$ (1606 cm^{-1}) and $\nu_{\text{sym}}(\text{OCO})$ (1458 cm^{-1}) values. The calculated Δ_{OCO} value of 148 cm^{-1} is lower than the value expected for monodentate carboxylate

ligands ($>200\text{ cm}^{-1}$) but again this may be a result of hydrogen bonding involving the carboxylate groups.

The two complexes are effectively insoluble in common solvents but were found to be soluble in DMSO. The room temperature magnetic moments of complexes (34) and (35) (1.99 and 2.17 B.M. respectively) are in the expected region for simple copper(II) species (i.e. those lacking Cu-Cu interactions). The molar conductivity values indicate the complexes are non-electrolytic in DMSO. The UV spectra of the complexes recorded in DMSO solution as well as in the solid state as Nujol mulls show approximately similar shapes and positioning of the absorption bands, indicating no appreciable change in their geometry in solution. Possible structures that fit the physico-chemical data for (34) and (35) are shown in Figures 88 and 89.

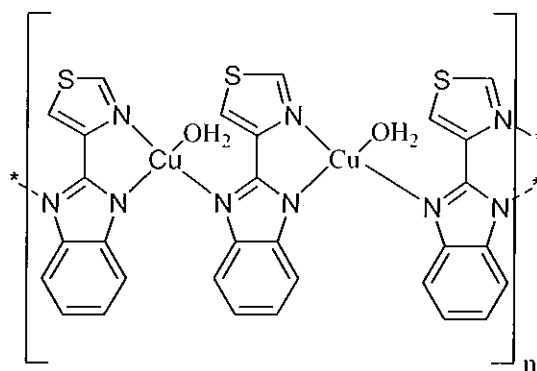


Figure 88: Possible structural motif for (34)

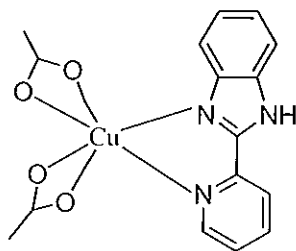
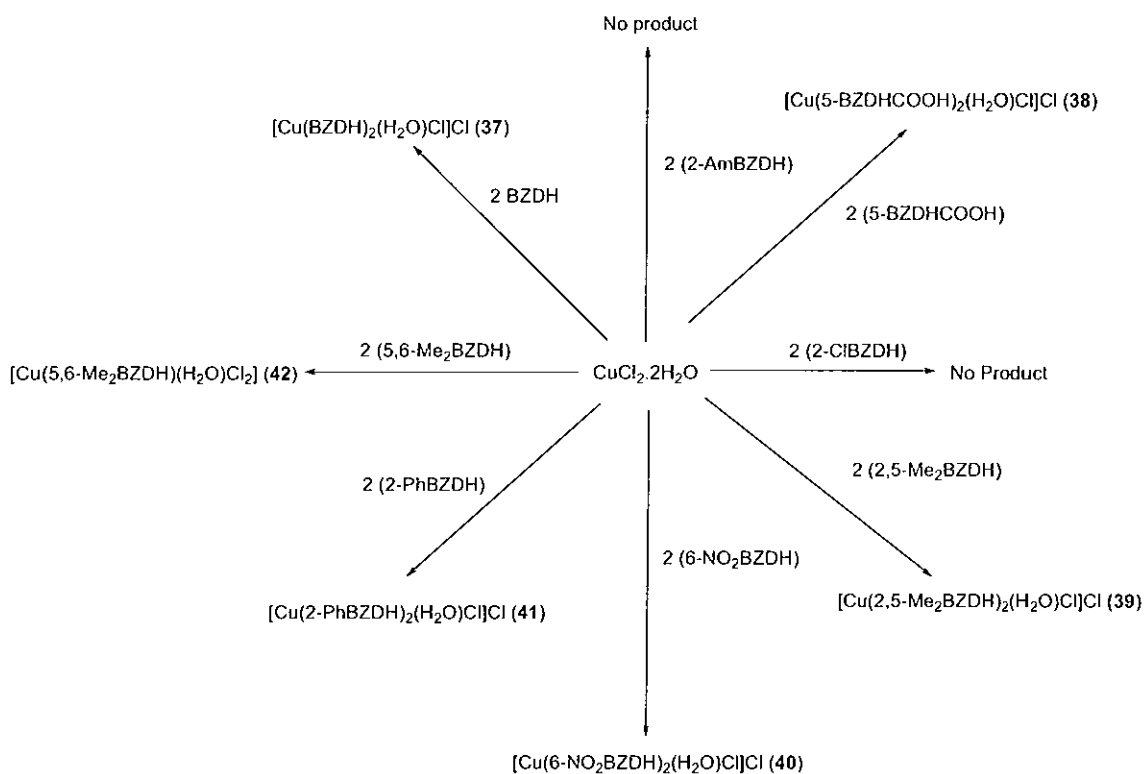


Figure 89: Possible structural motif for (35)

The known compound $[\text{Cu}(\text{OAc})_2(\text{phen})]$ (36) was generated using a previously published method.¹²⁴

D.4.3 Reaction of $\text{CuCl}_2 \cdot 2\text{H}_2\text{O}$ with the simple benzimidazole ligands

Copper(II) chloride was reacted with the benzimidazoles shown in Figure 72 resulting in the production of the six complexes (37) – (42) (Scheme 15).



Scheme 15: Synthetic routes to complexes (37) – (42).

Whilst complexes (37) – (40) were formed as green powders (41) and (42) were obtained as brown powders. The complexes were formulated as below:



% Calc: C, 43.26; H, 3.63; N, 14.41

% Found: C, 45.94; H, 3.39; N, 15.37

- (38) $[\text{Cu}(\text{5-BZDHCOOH})_2(\text{H}_2\text{O})\text{Cl}]\text{Cl}$
% Calc: C, 40.31; H, 2.96; N, 11.75
% Found: C, 42.57; H, 2.73; N, 11.96
- (39) $[\text{Cu}(\text{2,5-Me}_2\text{BZDH})_2(\text{H}_2\text{O})\text{Cl}]\text{Cl}$
% Calc: C, 48.60; H, 4.98; N, 12.59
% Found: C, 50.57; H, 4.70; N, 12.99
- (40) $[\text{Cu}(\text{6-NO}_2\text{BZDH})_2(\text{H}_2\text{O})\text{Cl}]\text{Cl}$
% Calc: C, 35.12; H, 2.53; N, 17.55
% Found: C, 36.38; H, 2.18; N, 17.91
- (41) $[\text{Cu}(\text{2-PhBZDH})_2(\text{H}_2\text{O})\text{Cl}]\text{Cl}$
% Calc: C, 57.73; H, 4.10; N, 10.36
% Found: C, 58.30; H, 4.42; N, 9.69
- (42) $[\text{Cu}(\text{5,6-Me}_2\text{BZDH})(\text{H}_2\text{O})\text{Cl}_2]$
% Calc: C, 36.19; H, 4.05; N, 9.38
% Found: C, 39.24; H, 3.67; N, 9.68

The IR spectra of the complexes (37) - (42) (see Appendix) were compared to those of the free ligands. The characteristic bands for the free ligands and the some of the important IR spectral bands that provide evidence for the structure of the complexes are listed in Table 30.

Table 30: Characteristic IR bands (cm^{-1} , KBr discs) of the complexes (37) - (42) and their free ligands

	BZDH	(37)	5-BZDHCO OH	(38)	2,5-Me ₂ BZDH	(39)	6-NO ₂ BZD H	(40)	2-PhBZDH	(41)	5,6-Me ₂ BZDH	(42)
Imidazole bands												
N-H (stretch)	3113	3112	3045	*	3044	3037	3103	3118	3047	3062	3095	3133
N-H (bending)	1135	1138	1134	1130	1145	1147	1131	1135	1146	1150	1158	1166
N-H (bending)	627	634	622	617	659	670	690	699	621	634	647	643
$\nu_{\text{C-N}}$	1587	1596	1588	1596	1553	1543	1591	1597	1591	1600	1584	1592
Metal-Ligand												
M-N	-	437	-	422	-	420	-	422	-	429	-	430
M-Cl	-	546	-	554	-	559	-	563	-	556	-	571
M-OH ₂	-	849	-	823	-	853	-	819	-	818	-	840

* Bands precluded by others in the infrared spectrum

The complexes (37) – (41) formulate as having the same metal : benzimidazole : chloride ratio of 1 : 2 : 2. In the respective IR spectra the majority of the ligand absorption bands, some of them with changed intensity appear again in the compounds. The N-H stretching band for all of the compounds has shifted slightly and all of the N-H bending (Table 30) characteristic bands have remained intact in the complexes indicative of the fact that the ligands are present in their neutral state. Furthermore, the band associated with the imidazolic $\nu_{C=N}$ in the free ligands has shifted in the spectra of the complexes indicating that the benzimidazoles are bound to the metals through the nitrogen atom. In the spectrum of complex (38) a strong carbonyl band at 1704 cm^{-1} is indicative of the non dissociated nature of the carboxylic acid function of the benzimidazole ligand. The presence of a new (weak) band in the range of $545 - 570\text{ cm}^{-1}$ in the spectra of all the complexes, which is not present in the spectra of the free ligands, indicates that one of the chloride anions is bound to the central metal.⁷² Bands in the region below 440 cm^{-1} have been tentatively assigned to metal – nitrogen interactions. All of the complexes have bands in the region of $800 - 850\text{ cm}^{-1}$ indicating that they have bound waters in their structures. A possible structure for (37) – (41) is shown in Figure 90.

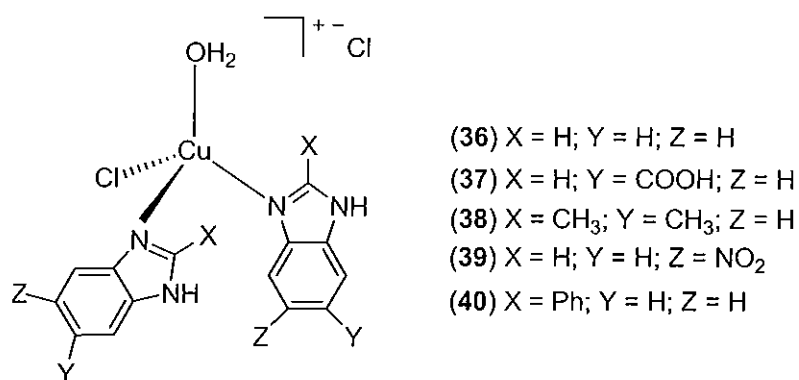


Figure 90: Possible structural motif for complexes (37) – (41)

Complex (42) formulates as having a metal : benzimidazole : chloride ratio of 1 : 1 : 2 with the main difference in its IR spectrum being the relative intensity of the bound chloride band at 570 cm^{-1} . This difference suggests that the structure of (42) may involve two bound chloride ligands as shown in Figure 91.

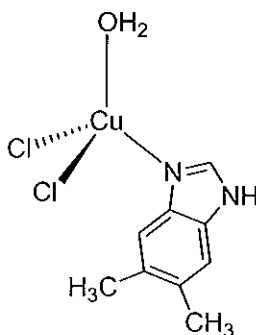
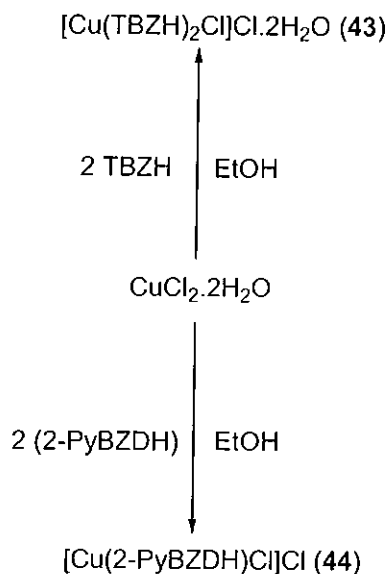


Figure 91: Possible structural motif for complex (42)

The room temperature magnetic moments of complexes (37) – (42) (ranging from 1.72 to 2.04 B.M.) are consistent with structures lacking significant Cu-Cu interactions. The molar conductivities of complexes (37) and (39) – (42) {ranging from 10.80 to 24.00 $\text{S cm}^2\text{ mol}^{-1}$ } indicate that some dissociation of these complexes is taking place in DMSO. Complex (38) dissociates significantly in this solvent {conductivity = 48.17 $\text{S cm}^2\text{ mol}^{-1}$ }. The UV spectra of the complexes (38) and (40) recorded in DMSO solution as well as in the solid state as Nujol mulls show changes in shape and structure indicating that the geometry of the complexes are changing in DMSO solution. The spectra remain unchanged for (37), (39), (41) and (42).

D.4.4 Reaction of $\text{CuCl}_2 \cdot 2\text{H}_2\text{O}$ with the chelating benzimidazole ligands

TBZH and 2-PyBZDH were reacted with copper(II) chloride to yield complexes (43) and (44) as shown in Scheme 16.



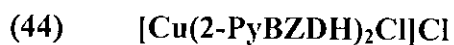
Scheme 16: Synthetic routes to complexes (43) and (44)

The complexes formed as green powders and were formulated as shown below:



% Calc: C, 41.92; H, 3.16; N, 14.66

% Found: C, 41.64; H, 3.03; N, 14.35



% Calc: C, 54.92; H, 3.46; N, 16.01

% Found: C, 54.80; H, 3.55; N, 15.83

The IR spectra of the complexes (43) and (44) (see Appendix) were compared to those of the free ligands. The characteristic bands for the free ligands and some of the important IR spectral bands that provide evidence for the structure of the complexes are listed in Table 31.

Table 31: Characteristic IR bands (cm^{-1} , KBr discs) of the complexes (43) and (44) and their free ligands

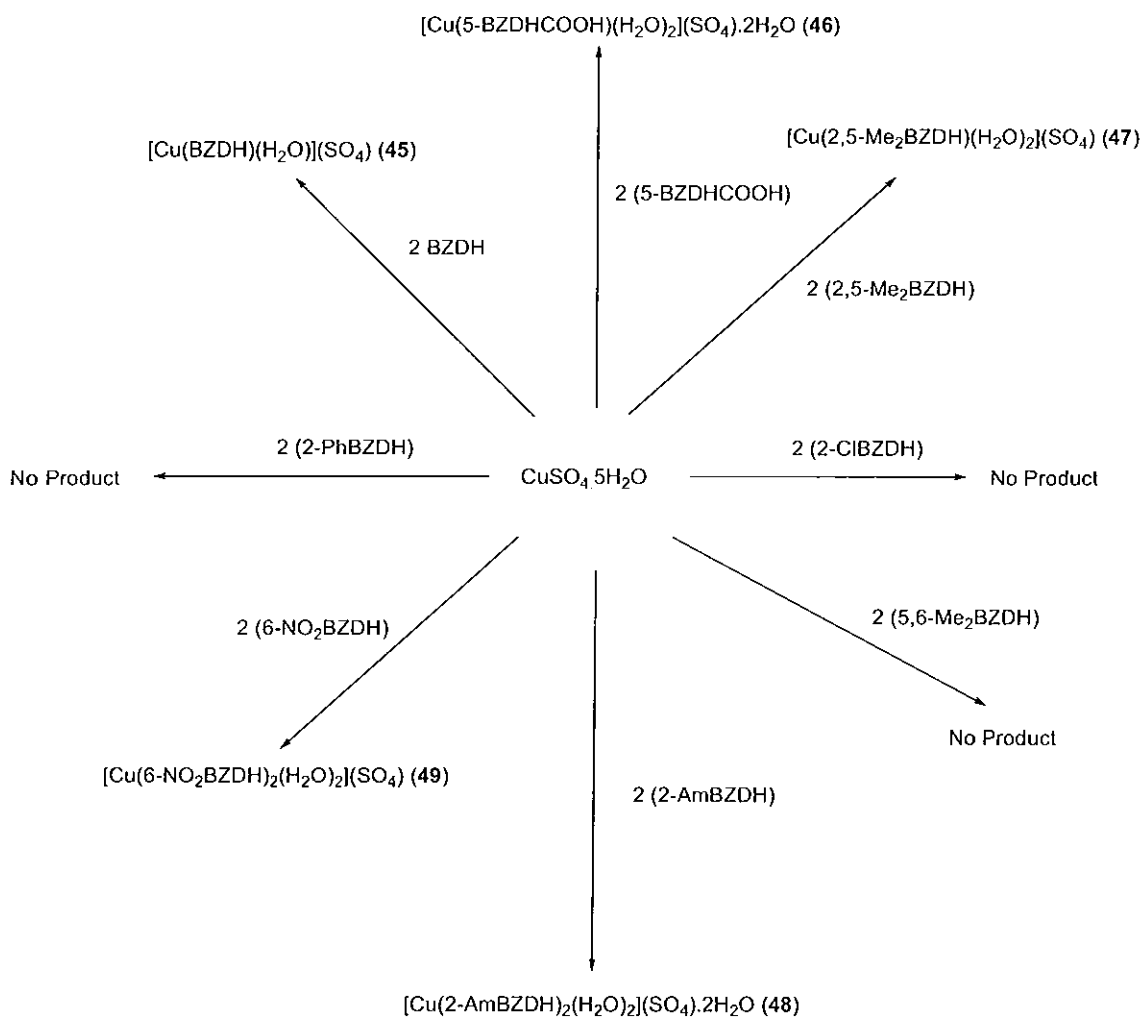
	TBZH	(43)	2-PyBZDH	(44)
Imidazole bands				
N-H (stretch)	3096	3090	3057	3023
N-H (bending)	1096	1117	1094	1094
N-H (bending)	635	635	625	633
$\nu_{\text{C}=\text{N}}$	1579	1596	1568	1571
Thiazole bands				
$\nu_{\text{C}=\text{N}}$	1481	1480	-	-
C-S (stretch)	1231	1232	-	-
Pyridine bands				
$\nu_{\text{C}=\text{N}}$	-	-	1594	1611
Pyridine ring stretching vibration	-	-	1315	1311
Metal-Ligand				
M-N	-	437	-	409
M-Cl	-	572	-	577
M-OH ₂	-	-	-	-

Complex (43) has an almost identical IR spectrum to a complex previously published by this group {formulated as $[\text{Cu}(\text{TBZH})_2\text{Cl}]\text{Cl}\cdot\text{H}_2\text{O}\cdot\text{EtOH}$ based on its crystal structure} and its structure is shown in Figure 66. Complex (43) is believed therefore to be the same but does not contain the ethanol molecule of crystallisation. It is likely that (44) is isostructural to (43).

The room temperature magnetic moments for the two complexes are normal (1.78 and 1.86 B.M., respectively) supporting structures where the copper centres are not associated electronically. The UV spectra of (43) and (44) taken in DMSO solutions as well as in the solid state as Nujol mulls show approximately similar shapes and positions of the absorption bands, indicating no appreciable change in the geometry of the complexes in solution. The molar conductivity values of both complexes (20.01 S cm² mol⁻¹ and 25.93 S cm² mol⁻¹, respectively) indicate that some dissociation of the complexes is taking place in solution.

D.4.5 Reaction of $\text{CuSO}_4 \cdot 5\text{H}_2\text{O}$ with the simple benzimidazole ligands

Copper(II) sulfate reacted with just five of the simple benzimidazole ligands yielding complexes (45) – (49) as shown in Scheme 17.



Scheme 17: Synthetic routes to complexes (45) – (49)

Complex (45) was obtained as a purple powder, complex (49) as a blue powder and complexes (46) – (48) as green powders. The complexes were formulated as shown below:

- (45) $[\text{Cu}(\text{BZDH})(\text{H}_2\text{O})](\text{SO}_4)$
%Calc: C, 30.27; H, 2.17; N, 10.09
% Found: C, 30.00; H, 2.12; N, 9.23
- (46) $[\text{Cu}(\text{5-BZDHCOOH})(\text{H}_2\text{O})_2](\text{SO}_4) \cdot 2\text{H}_2\text{O}$
%Calc: C, 24.46; H, 3.34; N, 7.13
% Found: C, 23.79; H, 3.38; N, 6.82
- (47) $[\text{Cu}(\text{2,5-Me}_2\text{BZDH})(\text{H}_2\text{O})_2](\text{SO}_4)$
%Calc: C, 31.62; H, 4.13; N, 8.20
% Found: C, 29.78; H, 3.87; N, 8.13
- (48) $[\text{Cu}(\text{2-AmbZDH})_2(\text{H}_2\text{O})_2](\text{SO}_4) \cdot 2\text{H}_2\text{O}$
% Calc: C, 33.77; H, 4.45; N, 16.88
% Found: C, 34.35; H, 3.95; N, 15.81
- (49) $[\text{Cu}(\text{6-NO}_2\text{BZDH})_2(\text{H}_2\text{O})_2](\text{SO}_4)$
%Calc: C, 32.22; H, 2.70; N, 16.10
% Found: C, 32.41; H, 2.80; N, 15.78

The IR spectra of the complexes (45) – (49) (see Appendix) were compared to those of the free ligands. The characteristic bands for the free ligands and some of the important IR spectral bands that provide evidence for the structure of the complexes are listed in Table 32.

Table 32: Characteristic IR bands (cm^{-1} , KBr discs) of the complexes (45) - (49) and their free ligands

	BZDH	(45)	5-BZDHCOOH	(46)	2,5-Me ₂ -BZDH	(47)	2-AmBZDH	(48)	6-NO ₂ BZDH	(49)
Imidazole bands										
N-H (stretch)	3113	3111	3045	*	3044	3059	3054	*	3103	3118
N-H (bending)	1135	*	1134	1133	1145	1137	1157	*	1131	1135
N-H (bending)	627	*	622	*	659	653	623	*	690	699
$\nu_{\text{C-N}}$	1587	1597	1588	1588	1553	1549	1596	1597	1591	1598
Metal-Ligand										
M-N	-	424	-	425	-	430	-	428	-	426
M-OH ₂	-	824	-	828	-	820	-	842	-	838
SO_4^{2-}	-	1115	-	1133	-	1068	-	1116	-	1122
	-	619	-	621	-	620	-	619	-	620

* Bands precluded by others in the infrared spectrum

In the respective IR spectra (Table 32) the majority of the ligand absorption bands, some of them with changed intensity appear again in the compounds. The N-H stretching band for all of the compounds has shifted slightly and all of the N-H bending characteristic bands have remained intact in the complexes indicative of the fact that the ligands are present in their neutral state. Furthermore, the band associated with the imidazolic $\nu_{C=N}$ in the free ligands has shifted in the spectra of the complexes indicating that the benzimidazoles are bound to the metals through the nitrogen atom. Bands in the region below 430 cm^{-1} have been tentatively assigned to metal-nitrogen interactions. The presence of the sulfate anion is characterised by the presence of a strong/broad band at $1068 - 1133\text{ cm}^{-1}$ in the spectra of the complexes. Further evidence of the sulfate anion is provided by the appearance of a new characteristic band at approximately 620 cm^{-1} in the spectra of all the complexes.⁷²

The bands characteristic of the amine group in 2-AmBZDH are also found in the spectrum of complex (48) (although shifted slightly) (Table 33) indicating that the amine nitrogen is unlikely to be involved in coordination to the metal. However the NH_2 group may be involved in some form of hydrogen bonding.

Table 33: Characteristic amine bands (cm^{-1} , KBr discs) for complex (48) and the containing free 2-AmBZDH ligand

	2-AmBZDH	(48)
Amine Bands		
N-H (stretch)	3381	*
NH_2 (asym deformation)	1632	1650
NH_2 (sym deformation)	1269	1275
NH_2 (rocking modes)	742, 728	755, 739

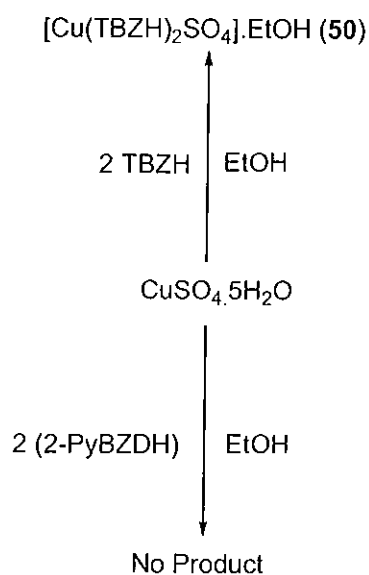
* Bands precluded by others in the infrared spectrum

The fact that the complexes exhibit normal room temperature magnetic moments indicates that the copper centres are not associated electronically. Complexes (45) – (47) formulate as having a copper : benzimidazole ratio of 1 : 1. Whereas the λ_{\max} value for (45) is 570 nm (46) and (47) exhibit bands at much higher values (673 and 701 nm, respectively) and therefore it is unlikely that they share the same geometry. Complex (45) exhibits a significant shift of its *d-d* transition bands {570 nm \rightarrow 781 nm} in its DMSO solution spectra as compared to the solid state and therefore some change in the complex is taking place in solution. This phenomenon is not observed for (46) and (47). All three complexes exhibit bands in their IR spectra in the region 800 to 850 cm^{-1} indicative of the presence of bound water molecules (see Table 32). Some dissociation of complex (47) is taking place in DMSO solution [$\Lambda_{\text{M}}(\text{DMSO})$: 23.05 $\text{S cm}^2 \text{mol}^{-1}$]. The other complexes are essentially non-electrolytic.

Complexes (48) and (49) formulate as having a copper : benzimidazole ratio of 1 : 2. They have very similar λ_{\max} values (694 and 681 nm, respectively) and therefore it is likely that they share the same geometry. Also bands at 842 cm^{-1} (48) and 838 cm^{-1} (49) in the respective IR spectra support the presence of bound water molecules in their formulations. Both complexes exhibit no significant shift of their *d-d* transition bands in their DMSO solution spectra as compared to the solid state and therefore no changes in the complexes are taking place in solution. No dissociation of complexes (48) and (49) is taking place in DMSO solution as indicated by their low conductivity values in that solvent [3.83 $\text{S cm}^2 \text{mol}^{-1}$ (48) and 12.85 $\text{S cm}^2 \text{mol}^{-1}$ (49)].

D.4.6 Reaction of $\text{CuSO}_4 \cdot 5\text{H}_2\text{O}$ with the chelating benzimidazole ligands

Copper(II) sulfate also reacted with the chelating benzimidazole ligand TBZH to give the known complex (50) but attempts to react it with 2-PyBZDH were unsuccessful (Scheme 18).



Scheme 18: The synthetic route to complex (50)

Complex (50) was obtained as a green powder and was formulated as shown below:



% Calc: C, 43.45; H, 3.31; N, 13.80

% Found: C, 43.19; H, 3.21; N, 13.40

The IR spectrum of complex (50) (see Appendix) was identical to that of the compound previously reported by this group.¹²⁴

D.5 SYNTHESIS OF SILVER SALTS CONTAINING BENZIMIDAZOLE LIGANDS

D.5.1 Attempted synthesis of silver salicylates with benzimidazole ligands

Silver salicylate $[\text{Ag}_2(\text{salH})_2]$ was generated using a method previously published.⁹⁷ $[\text{Ag}_2(\text{salH})_2]$ had been shown previously (in this laboratory) to react with selected imidazole ligands to generate a series of novel Ag(I)-containing imidazole complexes. In the present study all attempts to react $[\text{Ag}_2(\text{salH})_2]$ with either the simple benzimidazole or the chelating analogues were unsuccessful with the starting materials being recovered in all cases. The lack of reaction was a surprise as the benzimidazole ligands were found to react readily with silver salts (nitrates, sulfates and acetates – see below). Furthermore, silver complexes of aromatic carboxylates incorporating benzimidazole ligands are known but their synthesis involves the use of high pressure and temperature conditions.¹²¹ The structure of part of the the polymeric complex $\{\text{Ag}_2(4\text{-PyBZDH})_2(\text{Isoph})\}_n$ {IsophH₂ = isophthalic acid} is shown in Figure 92.¹²¹

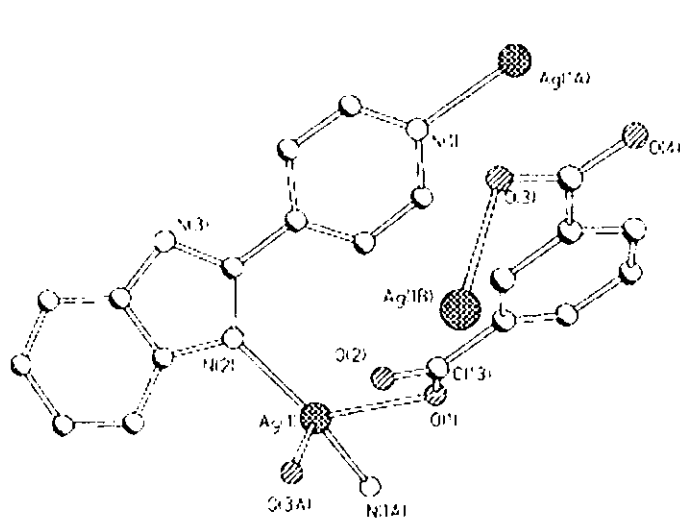
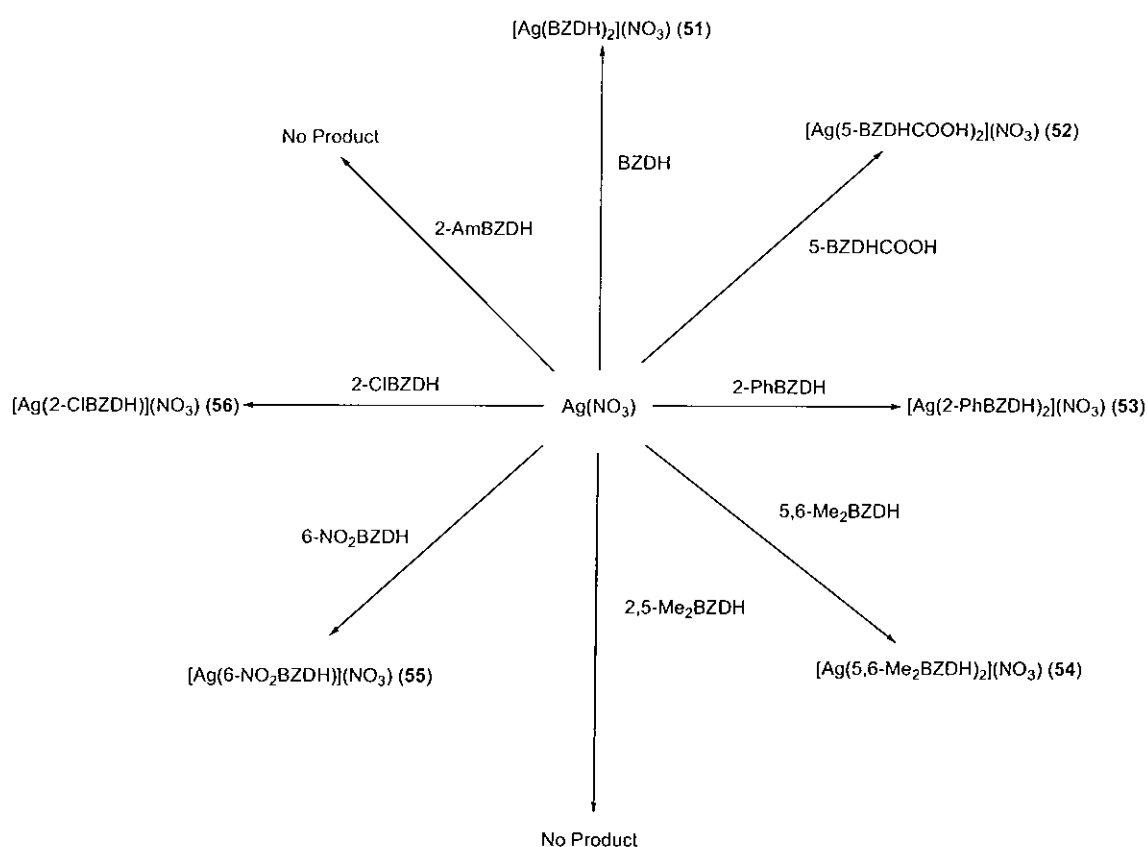


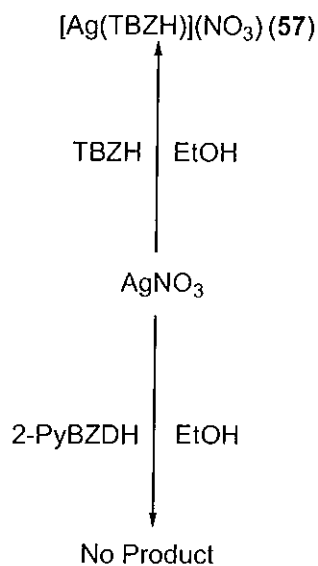
Figure 92: The structure of part of the the polymeric complex $\{\text{Ag}_2(2\text{-PhBZDH})_2(\text{Isoph})\}_n$ {IsophH₂ = isophthalic acid}

D.5.2 Reaction of AgNO₃ with the simple and chelating benzimidazole ligands

Silver nitrate was reacted with the simple benzimidazole ligands shown in Figure 72 resulting in the formation of the six new complexes (51) – (56) (Scheme 19). Also silver nitrate reacted easily with one equivalent of the chelating TBZH yielding the novel species (57) but it was unreactive towards 2-PyBZDH (Scheme 20).



Scheme 19: Synthetic routes to complexes (51) – (56)



Scheme 20: Synthetic route to complex (57)

Complexes (51), (53), (54) and (57) were formed as colourless powders, complexes (55) and (56) as yellow powders and complex (52) as a grey solid. The complexes were formulated as shown below:

- (51) $[\text{Ag}(\text{BZDH})_2](\text{NO}_3)$
 % Calc: C, 41.40; H, 2.98; N, 17.24
 % Found: C, 40.98; H, 2.90; N, 17.20
- (52) $[\text{Ag}(\text{5-BZDHCOOH})_2](\text{NO}_3)$
 % Calc: C, 37.52; H, 2.76; N, 13.67
 % Found: C, 36.97; H, 2.58; N, 13.62
- (53) $[\text{Ag}(\text{2-PhBZDH})_2](\text{NO}_3)$
 % Calc: C, 55.93; H, 3.61; N, 12.54
 % Found: C, 55.29; H, 3.70; N, 12.74

- (54) [Ag(5,6-Me₂BZDH)₂](NO₃)
% Calc: C, 46.77; H, 4.36; N, 15.15
% Found: C, 46.80; H, 4.26; N, 14.83
- (55) [Ag(6-NO₂BZDH)](NO₃)
% Calc: C, 25.25; H, 1.51; N, 16.82
% Found: C, 25.51; H, 1.62; N, 16.72
- (56) [Ag(2-ClBZDH)](NO₃)
% Calc: C, 28.56; H, 2.09; N, 12.49
% Found: C, 28.58; H, 2.01; N, 12.63
- (57) [Ag(TBZH)](NO₃)
% Calc: C, 32.36; H, 1.90; N, 15.10
% Found: C, 32.71; H, 2.02; N, 15.43

The IR spectra of the complexes (51) - (57) (see Appendix) were compared to those of the free ligands. The characteristic bands for the free ligands and some of the important IR spectral bands that provide evidence for the structure of the complexes are listed in Table 34.

Table 34: Characteristic IR bands (cm^{-1} , KBr discs) of the complexes (51) – (57) and their free ligands

	BZDH	(51)	5- BZDHCO OH	(52)	2-PhBZDH	(53)	5,6- Me ₂ BZD H	(54)	6- NO ₂ BZD H	(55)	2- CIBZDH	(56)	1BZH	(57)
Imidazole bands														
N-H (stretch)	3113	3114	3045	3054	3047	3050	3095	3146	3103	3101	3087	3099	3096	3095
N-H (bending)	1135	1135	1134	1117	1146	1147	1158	1159	1131	1124	1142	1147	1096	1095
N-H (bending)	627	628	622	608	621	633	647	641	690	706	641	642	635	635
$\nu_{\text{C-N}}$	1587	1588	1588	1589	1591	1597	1584	1591	1591	1607	1589	1596	1579	1578
Thiazole bands														
$\nu_{\text{C=N}}$	-	-	-	-	-	-	-	-	-	-	-	-	1481	1481
C-S (stretch)	-	-	-	-	-	-	-	-	-	-	-	-	1231	1230
Metal-Ligand														
M-N	-	420	-	417	-	432	-	427	-	420	-	438	-	433
M-OH ₂	-	-	-	-	-	-	-	-	-	-	-	-	-	-
NO ₃ ⁻ (uncoord)	-	1384	-	1384	-	1384	-	1384	-	1384	-	1384	-	1384

Complexes (51) – (54) formulate as having the same metal : benzimidazole : nitrate ratio of 1 : 2 : 1 and their IR spectra are similar reflecting their structural similarity. The N-H stretching and bending bands in the spectra of the free benzimidazole ligands also appear (although shifted slightly) in the spectra of the complexes indicative of the fact that the ligands are present in their neutral state. A new band common to all the spectra at 1384 cm^{-1} indicates the presence of an uncoordinated nitrate anion.⁷² A structure that fits for the physico – chemical properties of complexes (51) – (53) is shown in Figure 93. This linear arrangement is well known for silver salts containing two nitrogen donor ligands.⁷

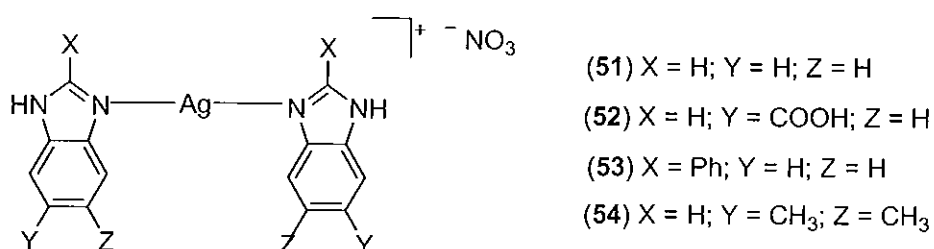


Figure 93: Possible structural motif for complexes (51) – (54)

The complexes (55) – (57) formulate as having the same metal : benzimidazole : nitrate ratio of 1 : 1 : 1. In the respective IR spectra (Table 34) the majority of the ligand absorption bands, some of them with changed intensity appear again in the compounds. The N-H stretching band for all of the compounds has shifted slightly and all of the N-H bending characteristic bands have remained intact in the complexes indicative of the fact that the ligands are present in their neutral state. Furthermore, the band associated with the imidazolic $\nu_{C=N}$ in the free ligands has shifted in the spectra of the complexes indicating that the benzimidazoles are bound to the metals through the nitrogen atom.

A new band absent in the spectra of the free ligands at 1384 cm^{-1} is indicative of the presence of a nitrate anion. A probable structure for the cations of compounds (55) – (57) is shown in Figure 94 and is similar to that of the known $[\text{Ag}(\text{Py})]^+$ complex.⁷ The TBZH ligand in complex (57) is most likely present as a chelating group.

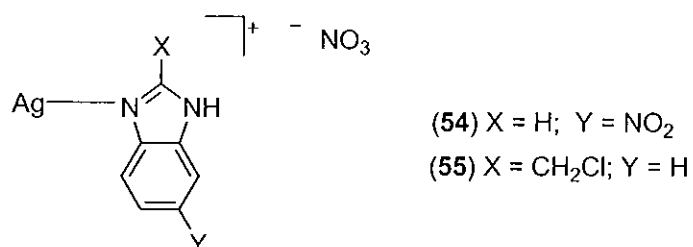
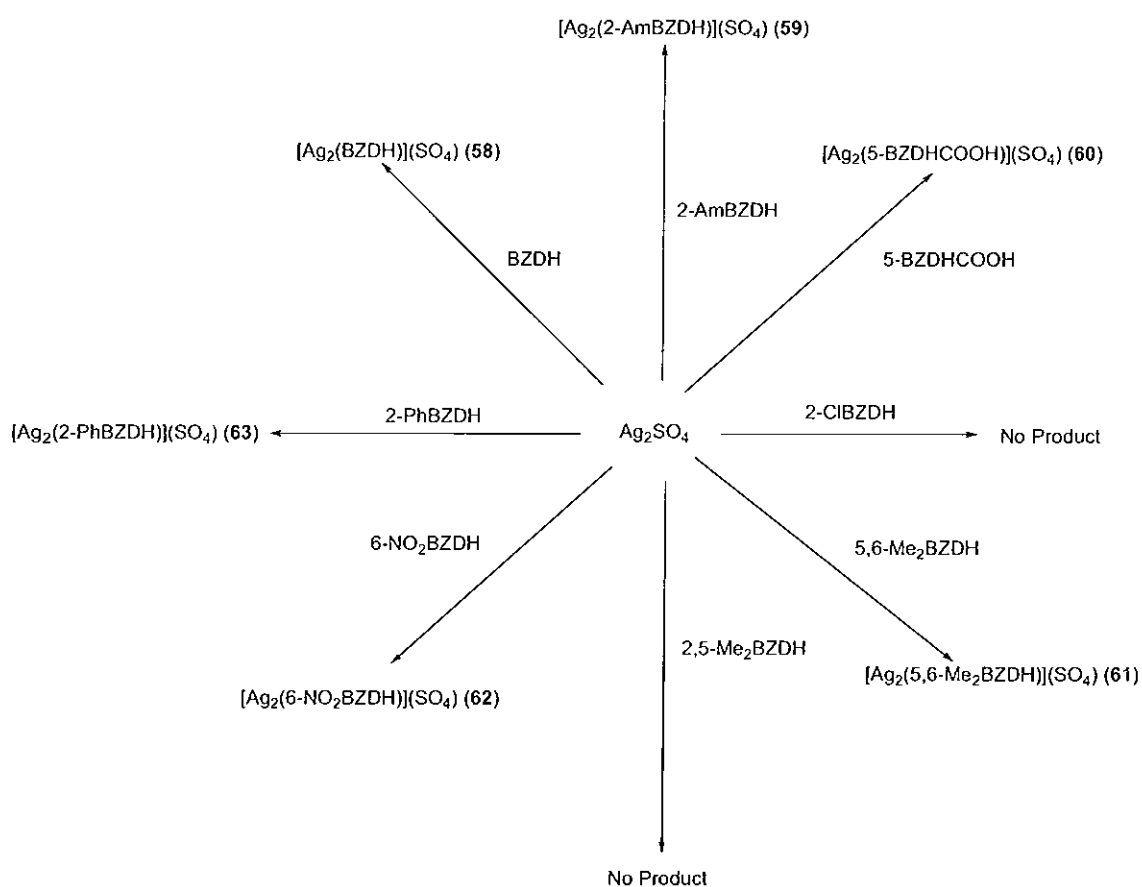


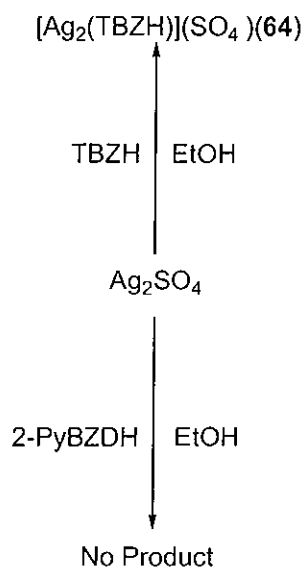
Figure 94: Possible structural motif for complexes (54) – (57)

D.5.3 Reaction of Ag_2SO_4 with the simple and chelating benzimidazole ligands

Silver sulfate reacted with the benzimidazole ligands yielding the six new salts (58) – (63) in accordance with the reactions shown in Scheme 21. Furthermore, whereas it reacted with the chelating ligand TBZH to give (64) it failed to react with 2-PyBZDH (Scheme 22).

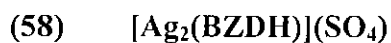


Scheme 21: Synthetic routes to complexes (58) – (63)



Scheme 22: Synthetic route to complex (64)

Complexes (58) – (64) were formed as colourless powders and were formulated as shown below:



% Calc: C, 19.56; H, 1.41; N, 6.52

% Found: C, 20.16; H, 1.47; N, 6.45



% Calc: C, 18.89; H, 1.59; N, 9.44

% Found: C, 19.42; H, 1.50; N, 9.53



% Calc: C, 20.27; H, 1.28; N, 5.91

% Found: C, 20.42; H, 1.48; N, 6.12

- (61) $[\text{Ag}_2(5,6\text{-Me}_2\text{BZDH})](\text{SO}_4)$
% Calc: C, 23.60; H, 2.20; N, 6.12
% Found: C, 22.89; H, 2.09; N, 5.80
- (62) $[\text{Ag}_2(6\text{-NO}_2\text{BZDH})](\text{SO}_4)$
% Calc: C, 17.70; H, 1.06; N, 8.94
% Found: C, 18.78; H, 1.06; N, 8.85
- (63) $[\text{Ag}_2(2\text{-PhBZDH})](\text{SO}_4)$
% Calc: C, 30.86; H, 1.99; N, 5.54
% Found: C, 31.17; H, 2.07; N, 5.68
- (64) $[\text{Ag}_2(\text{TBZH})](\text{SO}_4)$
% Calc: C, 23.41; H, 1.38; N, 8.19
% Found: C, 24.04; H, 1.40; N, 8.09

The IR spectra of the complexes (58) - (64) (see Appendix) were compared to those of the free ligands. The characteristic bands for the free ligands and some of the important IR spectral bands that provide evidence for the structure of the complexes are listed in Table 35.

Table 35: Characteristic IR bands (cm^{-1} , KBr discs) of the complexes (58) – (64) and their free ligands

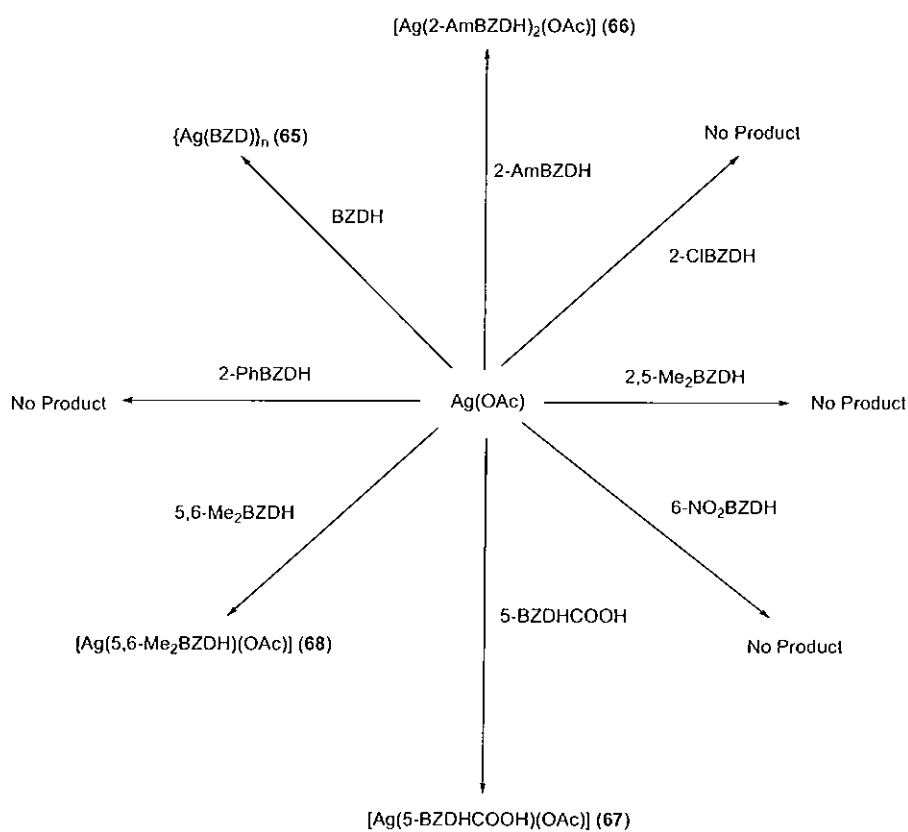
	BZDH	(58)	2- AmBZD H	(59)	5- BZDHC ₂ OH	(60)	5,6- Me ₂ BZDH	(61)	6- NO ₂ BZD H	(62)	2- PhBZDH	(63)	TBZH	(64)
Imidazole bands														
N-H (stretch)	3113	3137	3054	*	3045	3047	3095	3115	3103	3111	3047	3056	3096	3086
N-H (bending)	1135	*	1157	*	1134	*	1158	*	1131	*	1146	*	1096	*
N-H (bending)	627	*	623	*	622	*	647	*	690	693	621	*	635	*
$\nu_{\text{C-N}}$	1587	1598	1596	1591	1588	1589	1584	1593	1591	1600	1591	1595	1579	1578
Thiazole bands														
$\nu_{\text{C=N}}$	-	-	-	-	-	-	-	-	-	-	-	-	1481	1500
C-S (stretch)	-	-	-	-	-	-	-	-	-	-	-	-	1231	1232
Metal-Ligand														
M-N	-	417	-	503	-	417	-	424	-	427	-	431	-	435
M-OH ₂	-	-	-	-	-	-	-	-	-	-	-	-	-	-
SO ₄ ²⁻	-	1114	-	1119	-	1123	-	1119	-	1116	-	1071	-	1120
	-	618	-	618	-	617	-	616	-	617	-	609	-	616

* Bands precluded by others in the infrared spectrum

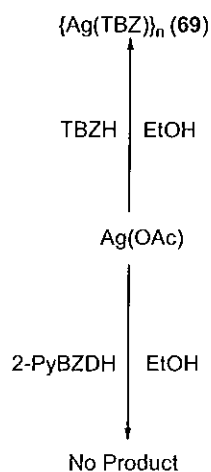
Complexes (58) – (64) formulate as having the same metal : benzimidazole : sulfate ratio of 2 : 1 : 1. The IR spectra of complexes (58) – (64) contain the typical bands indicative of benzimidazole ligands which have retained their imidazolic N-H functionality. As well as the bands that have been assigned to the neutral benzimidazole ligands the spectra of (58) – (63) also contain bands that are characteristic of sulfate anions (a strong/broad band at 1071 – 1123 cm^{-1} in the spectra of the complexes). Further evidence of the sulfate anion is provided by the appearance of a new characteristic band at approximately 620 cm^{-1} in the spectra of all the complexes. Although bands in the IR spectra of all six complexes can be assigned to metal-nitrogen interactions it is obvious that at least one of the silver ions must not bind to the benzimidazole ligands. It is not possible to predict a structure for this new class of complex based on the physico-chemical data available.

D.5.4 Reaction of Ag(OAc) with the simple and chelating benzimidazole ligands

Silver(I) acetate was reacted with the benzimidazoles shown in Figure 72 resulting in the production of the five complexes complexes (65) – (69) (Schemes 23 and 24).



Scheme 23: The synthetic routes to complexes (65) – (68)



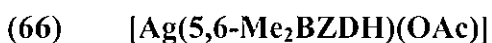
Scheme 24: The synthetic route to complex (69)

Complexes (65) – (68) were formed as colourless powders and complex (69) as a grey powder. They were formulated as shown below:



% Calc: C, 37.37; H, 2.24; N, 12.45

% Found: C, 37.89; H, 2.36; N, 12.63



% Calc: C, 42.20; H, 4.18; N, 8.95

% Found: C, 42.89; H, 4.03; N, 8.48



% Calc: C, 36.50; H, 2.76; N, 8.51

% Found: C, 36.53; H, 2.53; N, 8.00



% Calc: C, 44.36; H, 3.96; N, 19.40

% Found: C, 42.32; H, 3.22; N, 21.95



% Calc: C, 38.98; H, 1.96; N, 13.64

% Found: C, 38.28; H, 1.94; N, 13.06

The IR spectra of the complexes (65) - (69) (see Appendix) were compared to those of the free ligands. The characteristic bands for the free ligands and some of the important IR spectral bands that provide evidence for the structure of the complexes are listed in Table 36.

Table 36: Characteristic IR bands (cm^{-1} , KBr discs) of the complexes (65) – (69) and their free ligands

	BZDH	(65)	5,6-Me ₂ BZDH	(66)	5-BZDHCOOH	(67)	2-AmBZDH	(68)	TBZH	(69)
Imidazole bands										
N-H (stretch)	3113	*	3095	*	3045	*	3054	3073	3096	*
N-H (bending)	1135	*	1158	1164	1134	1134	1157	1147	1096	*
N-H (bending)	627	*	647	*	622	622	623	669	635	*
$\nu_{\text{C=N}}$	1587	1609	1584	*	1588	*	1596	1578	1579	1606
Thiazole bands										
$\nu_{\text{C=N}}$	-	-	-	-	-	-	-	-	1481	1472
C-S (stretch)	-	-	-	-	-	-	-	-	1231	1229
Carboxylate bands										
$\nu_{\text{asym}}(\text{OCO})$	-	-	-	1561	-	1555	-	1606	1481	-
$\nu_{\text{sym}}(\text{OCO})$	-	-	-	1412	-	1411	-	1458	1231	-
Δ_{OCO}	-	-	-	149	-	144	-	148	-	-
Metal-Ligand										
M-N	-	426	-	431	-	409	-	440	-	436

* Bands precluded by others in the infrared spectrum

The anionic nature of the BZD⁻ in {[Ag(BZD)]}_n (**65**) is evident when its IR spectrum is compared to that of BZDH. It can be seen that the N-H vibration band observed at 3113 cm⁻¹ for the free ligand is absent from the spectrum of the complex. Also the bands associated with imidazolic N-H bending modes (of the free ligand) at 1135 cm⁻¹ and 627 cm⁻¹ are also absent in the spectrum of (**65**). The imidazolic ν_{C=N} band at 1587 cm⁻¹ for the free ligand has shifted to 1609 cm⁻¹ for (**65**) indicating that the ligand is coordinating through the imidazolic nitrogen. A structure that fits for the physico – chemical properties of (**65**) is shown in Figure 95.

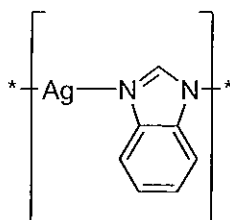


Figure 95: Possible structural motif for complex (**65**)

The anionic nature of the TBZ⁻ in {Ag(TBZ)}_n (**69**) is evident when its IR spectrum is compared to that of TBZH (Table 36). It can be seen that the N-H vibration band observed at 3096 cm⁻¹ for the free ligand is absent from the spectrum of the complex. Also the bands associated with imidazolic N-H bending modes (of the free ligand) at 1068 cm⁻¹ and 629 cm⁻¹ are also absent in the spectrum of (**69**). The thiazole ν_{C=N} bands in the spectrum of the complex appear shifted when compared to those of the free ligand (Table 36) and so it is likely that the thiazole nitrogen is also involved in coordination to the silver centre. A structure that fits for the physico – chemical data for (**69**) is shown in Figure 96.

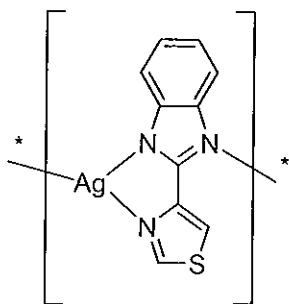


Figure 96: Possible structural motif for complex (69)

Complexes (66) and (67) formulate as having the same metal : benzimidazole : acetate ratio of 1 : 1 : 1. The IR spectrum of complexes (66) and (67) (see Appendix) contain the typical bands indicative of benzimidazole ligands which have retained their imidazolic N-H functionality (Table 36). As well as the bands that have been assigned to the benzimidazole ligands the spectra of (66) and (67) also contain bands that are characteristic of carboxylate anions. The similar Δ_{OCO} values of 149 cm^{-1} for (66) and 144 cm^{-1} for (67) suggest a similar coordination mode for the carboxylate groups (possibly chelating). The presence of the undissociated carboxylic functional group in the 5-BZDHCOOH ligand of (67) is supported by the presence of a strong C=O stretching band at 1664 cm^{-1} in its IR spectrum (found at 1667 cm^{-1} for the free ligand). A structure that fits for the physico – chemical properties of (66) and (67) is shown in Figure 97.

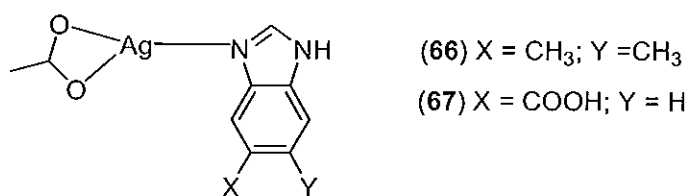


Figure 97: Possible structural motif for complexes (66) and (67)

Table 37: Characteristic amine bands (cm^{-1} , KBr discs) for complex (68) and its containing free 2-AmBZDH

	2-AmBZDH	(68)
Amine Bands		
N-H (stretch)	3381	3371
NH ₂ (asym deformation)	1632	*
NH ₂ (sym deformation)	1269	1281
NH ₂ (rocking modes)	742, 728	762, 738

* Bands precluded by others in the infrared spectrum

Complex (68) formulates as having a metal : benzimidazole : acetate ratio of 1 : 2 : 1. The bands characteristic of the amine group in 2-AmBZDH are also found in the spectrum of complex (68) (although shifted slightly) (Table 37) indicating that the amine nitrogen is unlikely to be involved in coordination to the metal. However the NH₂ group may be involved in some form of hydrogen bonding. The spectrum also contains bands characteristic of acetate anions with typical $\nu_{\text{asym}}(\text{OCO})$ (1606 cm^{-1}) and $\nu_{\text{sym}}(\text{OCO})$ (1458 cm^{-1}) values. The calculated Δ_{OCO} value of 148 cm^{-1} is lower than expected for monodentate coordination mode and some form of chelation may be taking place. A structure that fits for the physico – chemical data for (68) is shown in Figure 98.

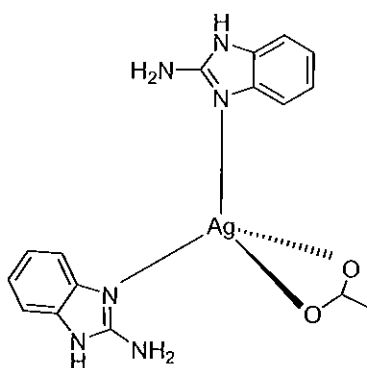


Figure 98: Possible structural motif for complex (68)

D.6 THE BIOMIMETIC ACTIVITY OF THE COPPER COMPLEXES (1) – (50)

D.6.1 Introduction

In normal mammalian cells reactive oxygen species (ROS) are produced through metabolic reactions resulting from aerobic respiration. Low levels of ROS are essential for proper cell function and a fine balance exists between the level of ROS produced during normal cellular metabolism and the amount of endogenous antioxidants (such as ROS scavengers and enzymes) present in the cells which protect tissues from oxidative damage. If this balance is disrupted a condition referred to as oxidative stress develops which is implicated in numerous patho-physiological processes such as rheumatoid arthritis, aging, inflammation and carcinogenesis.¹²⁶ Recently, it has been found that ROS such as the superoxide radical ($O_2^{\cdot-}$) or hydrogen peroxide (H_2O_2) are important regulators of cell death.¹²⁷ Particularly, H_2O_2 is implicated as a mediator of apoptosis in cells.¹²⁸ The cellular damage caused by H_2O_2 is likely produced in part through OH^{\cdot} radical production formed when H_2O_2 reacts with Fe^{2+} or Cu^{2+} .¹²⁹ Enzymatic antioxidants regulate the superoxide concentration by dismutation of $O_2^{\cdot-}$ to hydrogen peroxide {Superoxide dismutase (SOD) activity} which is then converted to water (peroxidase activity) or dismutated to water and dioxygen (catalase activity).

Many tumour cells have increased rates of metabolism compared with normal cells, which would typically lead to increased numbers of ROS.¹³⁰ Manganese SOD (MnSOD) is found in the matrix of mitochondria and has been shown to be depleted in most cancers when compared to normal tissue.¹³¹ The activity of cytoplasmic SOD (Cu/ZnSOD) has also been shown to vary in cancer cells.¹³¹ This suggests that a large amount of intracellular $O_2^{\cdot-}$ is found in such cancerous cells and that in the absence of significant SOD activity this $O_2^{\cdot-}$ can further metabolise to peroxynitrite ($OONO^{\cdot}$) and

the perhydroxyl radical (HO_2^\cdot) which play a role in the tumor formation.¹³² It has been demonstrated that returning MnSOD and Cu/ZnSOD enzyme activity to levels close to those found in non-malignant cells has resulted in conversion of the excess $\text{O}_2^{\cdot-}$ to H_2O_2 which leads to decreased tumour cell growth in a number of model systems.^{133,134,135}

The use of SOD enzymes as pharmaceutical agents is limited by cost and because of instability and low membrane permeability resulting from their high molecular weight. Low molecular weight copper SOD mimetic complexes can dismutate excess intracellular $\text{O}_2^{\cdot-}$ to H_2O_2 and O_2 , suggesting that they may increase the concentration of H_2O_2 in cancer cells thus inducing cell death by apoptosis. Furthermore, compared to manganese systems copper complexes are less likely to act as catalase mimics and catalytically disproportionate the H_2O_2 to water and molecular oxygen but rather react with it to form the desirable cytotoxic hydroxyl radical (Fenton chemistry). However a small number of mononuclear and dinuclear copper carboxylate complexes have recently been reported in the literature that show significant catalase mimetic functionality (Figure 99).^{136,137}

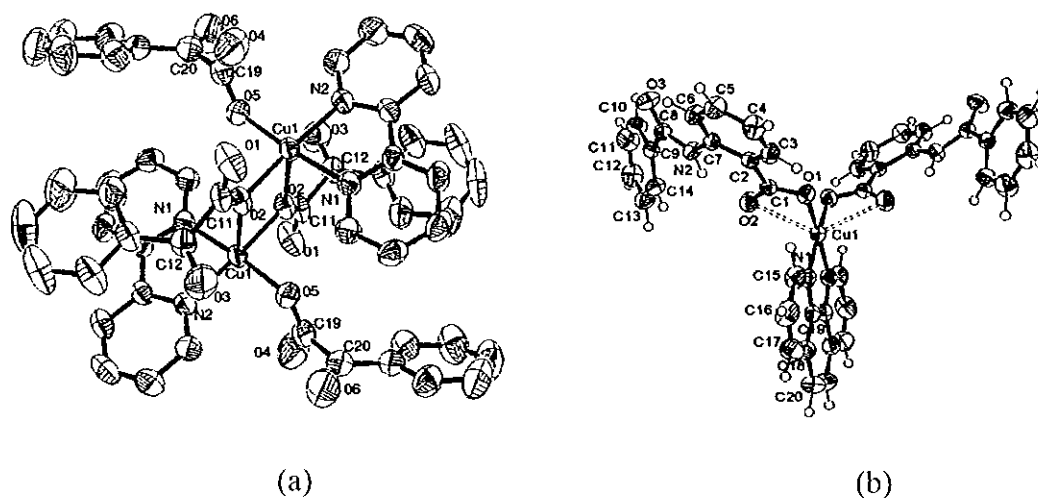


Figure 99: The X-ray crystal structures of (a) $[\text{Cu}_2(\text{phga})_4(\text{bipy})_2]$ ($\text{phgaH} =$ phenylglyoxylic acid)¹³⁶ and (b) $[\text{Cu}(\text{N-baa})_2(\text{phen})]$ ($\text{N-bbaH} =$ *N*-benzoylanthranilic acid)¹³⁷: efficient copper carboxylate catalase mimetics.

Recently in this laboratory other workers have been studying the anticancer activities of a range of simple copper complexes incorporating different types of nitrogen donor ligands.^{60,62,63,138,139} It has been found that the bis- or tris-chelate copper complexes incorporating 1,10-phenanthroline and 1,10-phenanthroline-5,6-dione (which possess N_4 or N_6 ligation) are potent anticancer agents *in-vitro* and that they appear to have a mechanism of action significantly different to that of the clinically used drug cisplatin.^{62,63} Furthermore, a number of these copper complexes are excellent SOD mimics^{139,140} and have been shown to induce apoptosis in cultured mammalian cells.¹⁴¹

A significant part of the rationale for the present study involves an effort to throw some light on the structure-activity-relationship of this class of simple copper complex. Therefore we have studied systems in which only one or two nitrogen atoms (either as monodentate or chelating ligands) are bound to the copper centre. At the active site of the native Cu/ZnSOD the copper is known to bind to four imidazole nitrogens from four histidine moieties (Figure 100). In this section we detail the catalase and SOD mimetic

activities of complexes (1) – (50) and discuss the anticancer activity of some selected complexes.

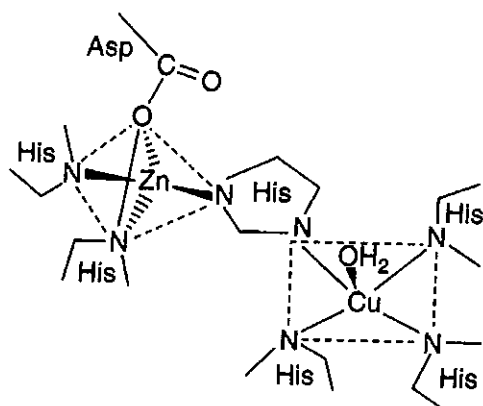


Figure 100: Schematic drawing of the active site of bovine Cu/ZnSOD

D.6.2 Catalase (CAT) mimetic activity of complexes (1) – (50)

The catalytic activity of complexes (1) – (50) towards the disproportionation of hydrogen peroxide was investigated by measuring the volume of evolved oxygen during the course of the reaction. In a typical experiment *ca.* 10 mg of the complex was mixed with 50 mg of imidazole and reacted with 35 % w/w H₂O₂ at 25 °C. The oxygen produced in the reaction was measured volumetrically over time. None of the fifty complexes exhibited catalytic activity on their own. Workers in this laboratory have previously shown that the catalase mimetic activity of manganese complexes is significantly improved in the presence of the base imidazole^{142,143,144} a phenomenon also observed by others.¹⁴⁵ Consequently we examined the catalase mimetic properties of complexes (1) – (50) in the presence of this base. The results from these reactions are summarised in Tables 38 - 45. The catalytic activity of the complexes is relatively poor when compared to the double salt {[Mn₂(oda)(phen)₄(H₂O)₂][Mn₂(oda)₃(phen)₄]} (odaH₂ = octanedioic acid) which had been shown to be the best manganese catalase mimic previously produced in this laboratory.^{142,146} Tables 38 - 40 show the rate of evolution of oxygen from the respective reactions for the complexes over the first 30 minutes. Examination of Tables 41 - 45 shows that over the first minute of reaction complex (23) (Table 41) appears to be the most efficient catalyst with 1012 molecules of peroxide disproportionated by one molecule of the complex. (44) (Table 45) appears to be the least efficient catalyst over the first minute with one molecule of the compound knocking down just 70 molecules of the peroxide. It should be noted that imidazole itself causes only a very slight disproportionation of the peroxide (Table 38).

Table 38: Time course of O₂ evolution (cm³) in H₂O₂ disproportionation for the Copper(II) salicylate complexes and {[Mn₂(oda)(phen)₄(H₂O)₂][Mn₂(oda)₃(phen)₄]} (odaH₂ = octanedioic acid) (with added imidazole) at S.T.P.

Time (min)	Imidazole	[Cu(OAc) ₄ (H ₂ O) ₂]	$\frac{[\text{Mn(oda)(phen)}_4(\text{H}_2\text{O})_2]}{[\text{Mn(oda)}_3(\text{phen})_4]}$	(1)	(2)	(5)	(6)	(7)	(8)	(9)	(10)	(11)	(12)	(23)	(24)
1	18	123	106	106	73	41	76	51	86	32	45	42	32	187	51
2	22	136	117	117	78	72	105	73	98	51	59	76	51	277	93
3	26	-	119	119	78	88	119	85	105	70	69	118	70	301	144
4	27	-	-	-	-	98	126	92	107	83	74	189	83	306	186
5	30	-	-	-	-	104	129	95	109	99	78	191	99	308	239
6	33	-	-	-	-	108	131	97	-	124	79	192	124	-	259
7	45	-	-	-	-	112	132	99	-	202	-	-	202	-	273
8	52	-	-	-	-	114	-	-	-	263	-	-	263	-	282
9	55	-	-	-	-	115	-	-	-	279	-	-	279	-	286
10	59	-	-	-	-	116	-	-	-	287	-	-	287	-	289
15	-	-	-	-	-	121	-	-	-	294	-	-	292	-	290
20	-	-	-	-	-	122	-	-	-	-	-	-	293	-	-

Table 39: Time course of O₂ evolution (cm³) in H₂O₂ disproportionation the for Copper(II) salicylate complexes (with added imidazole) at S.T.P.

Time (min)	(3)	(13)	(14)	(15)	(16)	(17)	(18)	(19)	(25)	(26)	(4)	(20)	(21)	(22)	(27)	(28)
1	57	93	65	18	29	24	18	40	20	12	111	110	61	19	134	83
2	74	102	85	23	49	57	24	96	49	24	155	149	91	25	300	241
3	83	104	91	42	72	63	30	150	59	39	175	157	157	35	327	273
4	87	105	92	51	90	78	38	183	76	54	183	160	206	46	334	283
5	90	-	94	63	106	85	47	210	94	67	189	161	215	59	340	284
6	-	-	-	72	125	89	57	211	135	82	191	162	217	74	342	284
7	-	-	-	80	142	92	68	-	178	110	195	-	220	90	344	-
8	-	-	-	86	148	95	79	-	180	200	196	-	221	109	344	-
9	-	-	-	90	149	98	90	-	-	213	197	-	222	133	-	-
10	-	-	-	95	150	-	104	-	-	222	-	-	-	192	-	-
15	-	-	-	100	-	-	146	-	-	237	-	-	-	226	-	-
20	-	-	-	101	-	-	-	-	-	242	-	-	-	227	-	-
25	-	-	-	-	-	-	-	-	-	245	-	-	-	-	-	-
30	-	-	-	-	-	-	-	-	-	-	-	-	-	-	-	-

Table 40: Time course of O₂ evolution (cm³) in H₂O₂ disproportionation for the copper(II) acetate, chloride and sulfate benzimidazole complexes (with added imidazole) at S.T.P.

Time (min)	(29)	(30)	(31)	(32)	(33)	(35)	(36)	(37)	(38)	(39)	(40)	(41)	(42)	(43)	(44)	(45)	(46)	(47)	(48)	(49)	(50)
1	46	93	92	132	19	131	87	101	71	64	75	72	215	36	15	143	77	80	80	64	93
2	55	102	114	136	25	208	145	218	94	97	91	89	248	50	18	154	89	108	105	78	102
3	61	104	123	138	33	216	271	248	121	113	101	98	251	63	25	155	95	125	121	85	104
4	66	105	128	138	39	218	297	257	151	125	103	103	253	76	28	156	99	136	137	91	105
5	70	-	132	-	44	219	305	261	183	128	104	107	254	86	41	157	101	145	142	93	-
6	74	-	133	-	50	220	312	264	185	132	105	108	-	95	49	157	103	150	148	95	-
7	78	-	137	-	56	-	317	266	190	-	105	-	-	104	59	-	104	155	153	96	-
8	80	-	138	-	61	-	319	267	194	-	-	-	-	113	72	-	-	156	157	97	-
9	82	-	-	-	65	-	-	268	196	-	-	-	-	124	83	-	-	159	160	-	-
10	83	-	-	-	68	-	-	-	198	-	-	-	-	135	93	-	-	162	163	-	-
15	-	-	-	-	80	-	-	-	203	-	-	-	-	175	154	-	-	179	169	-	-
20	-	-	-	-	-	-	-	-	206	-	-	-	-	176	251	-	-	180	170	-	-
25	-	-	-	-	-	-	-	-	207	-	-	-	-	-	262	-	-	-	-	-	-
30	-	-	-	-	-	-	-	-	-	-	-	-	-	-	263	-	-	-	-	-	-

Table 41: Molecules of H₂O₂ disproportionated by copper(II) salicylate complexes and {[Mn₂(oda)(phen)₄(H₂O)₂][Mn₂(oda)₃(phen)₄]} (odaH₂ = octanedioic acid) (in the presence of added imidazole) at S.T.P. conditions.

Complex	Total No. of molecules of H ₂ O ₂ disproportionated by one molecule of complex	No. of molecules of H ₂ O ₂ disproportionated during first min by one molecule of the complex
(1)	409	364
(2)	636	600
(5)	640	216
(6)	738	426
(7)	304	158
(8)	376	292
(9)	800	540
(10)	350	200
(11)	716	159
(12)	1084	117
(23)	1308	1012
(24)	1084	192
{[Mn(oda)(phen) ₄ (H ₂ O) ₂] [Mn(oda) ₃ (phen) ₄]}	24570	19500

Table 42: Molecules of H₂O₂ disproportionated by the copper(II) diisopropylsalicylate complexes (in the presence of added imidazole) at S.T.P. conditions.

Complex	Total No. of molecules of H ₂ O ₂ disproportionated by one molecule of complex	No. of molecules of H ₂ O ₂ disproportionated during first min by one molecule of the complex
(3)	422	268
(13)	626	554
(14)	364	252
(15)	410	74
(16)	372	72
(17)	382	94
(18)	620	76
(19)	942	178
(25)	952	46
(26)	730	82

Table 43: Molecules of H₂O₂ disproportionated by the copper(II) 3-methoxysalicylate complexes (in the presence of added imidazole) at S.T.P. conditions.

Complex	Total No. of molecules of H ₂ O ₂ disproportionated by one molecule of complex	No. of molecules of H ₂ O ₂ disproportionated during first min by one molecule of the complex
(4)	400	228
(20)	762	516
(21)	900	248
(22)	882	74
(27)	1250	498
(28)	1000	286

Table 44: Molecules of H₂O₂ disproportionated by the copper(II) acetate complexes in the presence of added imidazole) at S.T.P. conditions.

Complex	Total No. of molecules of H ₂ O ₂ disproportionated by one molecule of complex	No. of molecules of H ₂ O ₂ disproportionated during first min by one molecule of the complex
[Cu ₂ (OAc) ₄ (H ₂ O) ₂]	486	440
(29)	370	200
(30)	468	420
(31)	354	234
(32)	616	590
(33)	397	94
(35)	702	418
(36)	1017	278

Table 45: Molecules of H₂O₂ disproportionated by the copper(II) chloride and sulfate complexes in the presence of added imidazole) at S.T.P. conditions.

Complex	Total No. of molecules of H ₂ O ₂ disproportionated by one molecule of complex	No. of molecules of H ₂ O ₂ disproportionated during first min by one molecule of the complex
(37)	444	167
(38)	840	145
(39)	536	264
(40)	426	304
(41)	536	179
(42)	612	534
(43)	924	190
(44)	1264	70
(45)	390	354
(46)	368	276
(47)	554	248
(48)	448	210
(49)	456	306
(50)	520	462

D.6.3 The Superoxide Dismutase (SOD) activity of copper(II) salicylate and benzimidazole complexes

The SOD mimetic activities of almost all of the complexes (1) – (50) {with the exception of (10), (17) and (19) which were either insoluble in DMSO or reacted with the solvent} were examined with an indirect method in which the xanthine/xanthine-oxidase system served as the source for superoxide radicals.¹⁴⁷ The activities of the complexes were compared to that of $[\text{Cu}_2(\text{indo})_4(\text{H}_2\text{O})_2]$ {indoH = indomethacin [1-(4-chlorobenzoyl)-5-methoxy-2-methyl-1H-indole-3-acetic acid]} (Figure 26) which is considered to be an excellent SOD mimetic¹⁴⁸ and which is used therapeutically as an oral anti-inflammatory drug in veterinary medicine.^{149,150} The results are given in Tables 46 - 50 as concentrations equivalent to one unit of SOD activity (IC_{50} values).

Whereas free Cu^{2+} ions {using CuSO_4 (Table 50)} exhibit relatively low SOD activity significant activities were seen for all of the other compounds tested with one unit of SOD activity arising from the range of 0.56 to 2.77 μM aqueous solutions. Interestingly the complexes all have activities comparable with that (1.31 μM in this study) of $[\text{Cu}_2(\text{indo})_4\text{L}_2]$ (L = DMSO or DMF) for which the IC_{50} values vary significantly in the literature and appear to be solvent dependent (the reported value in DMSO is 2 μM).¹⁴⁸ The complexes all have activity significantly less than native Cu/ZnSOD (0.04 μM)¹⁴⁸ however they are potent SOD mimics considering the very low molecular weight of the complexes when compared to that of the enzyme (MW = 31200 amu).

The monomeric copper(II) salicylates (Table 46) exhibit SOD mimetic behaviour where the activity increases upon inclusion of the nitrogen bases in the inner sphere of the complexes and where the bis-benzimidazole complexes $[\text{Cu}(\text{salH})_2(\text{BZDH})_2]$ (5) and

[Cu(salH)₂(5,6-Me₂BZDH)₂] (**6**) are the most active. For the 3,5-diisopropylsalicylate complexes (Table 47) the mono-benzimidazole complexes [Cu(dips)(2,5-Me₂BZDH)(H₂O)] (**15**) and [Cu(dips)(TBZH)] (**19**) are the most active and it is interesting to note that in these two complexes the salicylate ligands are doubly deprotonated and believed to chelate to the metal centres. The activity of the 3-methoxysalicylates (Table 48) appears to be significantly lower with the most active compound being the mono-benzimidazole complex [Cu(msal)(TBZH)].H₂O (**21**) in which the salicylate is again believed to chelate to the copper centre. The activities of all of the salicylate complexes fall in the lower end of the range (0.17 – 29 μM) previously reported for copper(II) salicylate derivatives, a number of which are used therapeutically as anti-inflammatory agents in human and veterinary medicine.^{89,149}

It is interesting that the SOD activity of the copper(II) acetate complexes (Table 49) decreases for the benzimidazole and phenanthroline derivatives where it appears that the inclusion of the nitrogen donor ligands reduce the SOD activity. Whereas (**29**) – (**33**), (**35**) and (**36**) are all monomeric complexes [Cu₂(OAc)₄(H₂O)₂] is dimeric and has a similar “paddle wheel” structure to that of [Cu₂(indo)₄(DMF)₂].¹⁵¹ The copper(II) complexes [Cu₂(valp)₄(H₂O)₂] and [Cu(valp)₂(phen)] [valpH = valproic acid {(CH₃CH₂CH₂)₂CHCOOH}] were recently reported and are iso-structural to [Cu₂(OAc)₄(H₂O)₂] and (**36**), respectively.¹⁵² Their SOD mimetic activities were much lower relative to [Cu₂(OAc)₄(H₂O)₂] and (**36**) (10.4 and 4.5 μM) with the phen derivative being the superior catalyst. Clearly there is no correlation between solid state nuclearity (monomeric versus dimeric structures) and SOD mimetic activity but the type of carboxylate present appears to be important.

When the salicylate and acetate ligands are replaced by either chloride or sulfate anions the SOD activity of the benzimidazole complexes essentially increases (Table 50). Overall the sulfate complexes are superior to their chloride analogues. This may be related to the fact that the chloride complexes {(37) – (44)} all appear to have coordinated chloride in their inner spheres and it may be that the uncoordinated sulfate ions dissociate more easily to provide access to sites on the Cu(II) for O₂^{•-} bonding during catalysis.

Table 46: SOD activities of copper(II) salicylate complexes

Compound	Complex	Concentration (μM) Equivalent to 1U SOD (IC ₅₀)
(1)	[Cu(salH) ₂ (H ₂ O) ₂]	1.23
(2)	[Cu ₂ (asp) ₄ (H ₂ O) ₂].H ₂ O	0.84
(5)	[Cu(salH) ₂ (BZDH) ₂]	0.74
(6)	[Cu(salH) ₂ (5,6-Me ₂ BZDH) ₂]	0.66
(7)	[Cu(sal)(2,5-Me ₂ BZDH)(H ₂ O)]	2.77
(8)	[Cu(sal)(6-NO ₂ BZDH)(H ₂ O)]	1.14
(9)	[Cu(sal)(5-BZDHCOOH)(H ₂ O)]	0.89
(11)	[Cu(sal)(TBZH)].H ₂ O	1.08
(12)	[Cu(sal)(2-PyBZDH)].H ₂ O	0.94
(23)	[Cu(sal)(phen)]	1.01
(26)	[Cu(sal)(bipy)].EtOH.H ₂ O	1.42

Table 47: SOD activity of copper(II) 3,5-diisopropylsalicylate complexes

Compound	Complex	Concentration (μM) Equivalent to 1U SOD (IC_{50})
(3)	[Cu(dipsH) ₂ (H ₂ O)]	1.16
(13)	[Cu(dipsH) ₂ (BZDH) ₂]	0.94
(14)	[Cu(dipsH) ₂ (2-MeOHBZDH) ₂].EtOH	1.29
(15)	[Cu(dips)(2,5-Me ₂ BZDH)(H ₂ O)]	0.72
(16)	[Cu(5-BZDCOO)(H ₂ O) ₂].EtOH	1.24
(18)	[Cu(dips)(TBZH)]	0.77
(24)	[Cu(dips)(phen)].H ₂ O	1.23
(27)	[Cu(dips)(bipy)]	1.09

Table 48: SOD activity of copper(II) 3-methoxysalicylate complexes

Compound	Complex	Concentration (μM) Equivalent to 1U SOD (IC_{50})
(4)	{Cu(msal)(H ₂ O)} _n	1.42
(20)	[Cu(msal)(BZDH)(H ₂ O)].2H ₂ O	1.46
(21)	[Cu(msal)(TBZH)].H ₂ O	1.10
(22)	[Cu(msal)(2-PyBZDH)].H ₂ O	1.35
(25)	[Cu(msal)(phen)].H ₂ O	2.72
(28)	[Cu(msal)(bipy)].H ₂ O	1.89

Table 49: SOD activities of [Cu₂(OAc)₄(H₂O)₂] and copper(II) acetate complexes (29) – (36)

Compound	Complex	Concentration (μM) Equivalent to 1U SOD (IC_{50})
	[Cu ₂ (OAc) ₄ (H ₂ O) ₂]	0.63
(29)	[Cu(OAc) ₂ (2-AmBZDH) ₂]	1.25
(30)	[Cu(OAc) ₂ (5,6-Me ₂ BZDH) ₂]	0.91
(31)	[Cu(OAc) ₂ (5-BZDHCOOH) ₂]	1.01
(32)	[Cu(OAc) ₂ (6-NO ₂ BZDH) ₂]	1.07
(33)	[Cu(OAc) ₂ (2-PhBZDH) ₂]	1.37
(35)	[Cu(OAc) ₂ (2-PyBZDH)]	1.04
(36)	[Cu(OAc) ₂ (phen)]	1.18

Table 50: SOD activities of copper(II) sulfate and the copper(II) chloride and sulfate complexes (37) – (50)

Compound	Complex	Concentration (μM) Equivalent to 1U SOD (IC50)
(37)	[Cu(BZDH) ₂ (H ₂ O)Cl]Cl	0.81
(38)	[Cu(5-BZDHCOOH) ₂ (H ₂ O)Cl]Cl	0.98
(39)	[Cu(2,5-Me ₂ BZDH) ₂ (H ₂ O)Cl]Cl	0.89
(40)	[Cu(6-NO ₂ BZDH) ₂ (H ₂ O)Cl]Cl	1.24
(41)	[Cu(2-PhBZDH) ₂ (H ₂ O)Cl]Cl	0.65
(42)	[Cu(5,6-Me ₂ BZDH)(H ₂ O)Cl]Cl	0.78
(43)	[Cu(TBZH) ₂ Cl]Cl	0.99
(44)	[Cu(2-PyBZDH) ₂ Cl]Cl	0.94
(45)	[Cu(BZDH)(H ₂ O)](SO ₄)	0.57
(46)	[Cu(5-BZDHCOOH)(H ₂ O) ₂](SO ₄).2H ₂ O	0.56
(47)	[Cu(2,5-Me ₂ BZDH)(H ₂ O) ₂](SO ₄)	0.62
(48)	[Cu(2-AmBZDH) ₂ (H ₂ O) ₂](SO ₄).2H ₂ O	0.63
(49)	[Cu(6-NO ₂ BZDH) ₂ (H ₂ O) ₂](SO ₄)	0.60
(50)	[Cu(TBZH) ₂ (SO ₄)].EtOH	0.71
	CuSO ₄ .5H ₂ O ¹⁵³	30.00

D.7 PRELIMINARY ANTICANCER ASSAYS OF SELECTED COMPLEXES

Recently several reports have appeared in the literature describing the anti-cancer activity of copper(II) derivatives of several classes of nitrogen donors including purine¹⁵⁴, thiosemicarbazone¹⁵⁵, imidazole¹⁵⁶, benzohydroxamic acid¹⁵⁷ and amino acid¹⁵⁸ ligands. Some mixed chelate copper-based drugs have exhibited greater antineoplastic potency than cisplatin in *in vitro* and *in vivo* studies.^{159,160} We have recently demonstrated the chemotherapeutic potential of 1,10-phenanthroline^{63,64} and their copper chelates against renal and hepatic cancer derived cell lines and demonstrated that they may have a mechanism of action which appears to be different to that of cisplatin. The complex [Cu(mal)(phen)₂] was shown to induce apoptosis in cultured mammalian cells¹⁶¹ and is known to mediate significant cellular oxidative stress, promote membrane lipid peroxidation and interfere with mitochondria respiratory activity in fungal cells.¹⁶² Similar copper chelates of phen were studied by other workers and also showed high antineoplastic activity by inhibiting respiration and ATP synthesis.¹⁶³ Furthermore, [Cu(phen)]²⁺ type complexes are known to bind to DNA both intercalatively and non-intercalatively and are known as potent oxidative nucleases but the exact structure of [Cu(phen)]²⁺ when bound to DNA has not been fully characterised.¹⁶⁴

To evaluate their cancer chemotherapeutic potential the ability of BZDH, 5,6-Me₂BZDH, CuSO₄ and the DMSO soluble copper complexes [Cu(salH)₂(H₂O)₂] (**1**), [Cu(salH)₂(BZDH)₂] (**5**), [Cu(sal)(phen)] (**23**) [Cu₂(OAc)₄(H₂O)₂], [Cu(OAc)₂(5,6-Me₂BZDH)₂] (**30**) and [Cu(OAc)₂(phen)] (**36**) to kill human derived cancer cells was investigated using the hepatocellular carcinoma (Hep-G₂), kidney adenocarcinoma (A-

498) and lung cancer (A-549) cell lines and was determined by calculation of IC₅₀ (the drug concentration causing a 50 % reduction in cellular viability). These experiments were carried out by Dr. Denise Egan (IT Tallaght) and Dr. Fiona Lyng (DIT). Cells were continuously exposed to test agent for 96 hr, and their effects on cellular viability was evaluated. It was intended that the results from these studies would allow the identification of those derivatives with cancer chemotherapeutic potential. Therefore, profiles of cell viability against complex concentration were established and used to calculate the IC₅₀ values for each derivative (Table 51). Comparison of IC₅₀ values, allowed the relative potency of each of the test compounds to be determined and ranked.

Table 51: The anti-cancer activity of the free ligands, selected complexes, cisplatin and CuSO₄ against human hepatic (*Hep-G₂*), renal (*A-498*) and lung (*A-549*) cancer cell lines expressed as IC₅₀ (μM)*

Test Compound	Toxicities (IC ₅₀ μM)		
	<i>Hep-G₂</i> Mean ± S.D.	<i>A-498</i> Mean ± S.D.	<i>A-549</i> Mean ± S.D.
salH ₂	>500	>500	>500
phen	4.1 ± 0.5	5.8 ± 0.3	2.94 ± 0.1
Phendione	2.8 ± 1.34	4.2 ± 0.36	Not tested
BZDH	>500	>500	>500
5,6-Me ₂ BZDH	>500	>500	>500
CuSO ₄	>500	>500	>500
[Cu ₂ (OAc) ₄ (H ₂ O) ₂]	320 ± 2.5	134 ± 2.2	>500
[Cu(salH) ₂ (H ₂ O) ₂] (1)	350 ± 2.8	142 ± 1.8	59.81 ± 13.7
[Cu(OAc) ₂ (phen)] (36)	1.8 ± 0.3	1.0 ± 0.2	1.19 ± 0.2
[Cu(salH) ₂ (BZDH) ₂] (5)	138 ± 2.5	65 ± 1.4	58.15 ±
[Cu(sal)(phen)] (23)	2.5 ± 0.5	1.6 ± 0.3	1.42 ± 0.3
[Cu(OAc) ₂ (5,6-Me ₂ BZDH) ₂] (30)	105 ± 2.6	58 ± 1.9	23.44 ± 4.9
[Cu(phen) ₂ (mal)].2H ₂ O	0.8 ± 0.02	3.8 ± 0.41	Not tested
[Cu(phendione) ₃ (ClO ₄)].4H ₂ O	0.4 ± 0.09	0.6 ± 0.06	Not tested
Cisplatin	15 ± 2.7	14 ± 1	11.0 ± 4.7

* IC₅₀ (μM), indicates the compound concentration that inhibits the proliferation rate of tumour cells by 50% as compared to the control untreated cells. The values are means ± S.D. of 9 independent experiments. The cytotoxic activity of Phen, [Cu(phen)₂(mal)].2H₂O (malH₂ = malic acid)⁶², Phendione and [Cu(phendione)₃(ClO₄)].4H₂O⁶³ are also included.

To allow comparison of the activity of the complexes with that of the most active copper phen and copper phendione complexes synthesised previously in this laboratory the anticancer activities (against the liver and kidney cell lines only) of $[\text{Cu}(\text{phen})_2(\text{mal})] \cdot 2\text{H}_2\text{O}$ and $[\text{Cu}(\text{phendione})_3(\text{ClO}_4)] \cdot 4\text{H}_2\text{O}$ and the metal-free phen and phendione ligands are also included in Table 51.

With the exception of phen all of the free ligands are essentially inactive. A number of the compounds screened displayed a concentration-dependent cytotoxic profile across the three cell lines studied here. The most sensitive cell line was the A-549 lung cancer with five of the compounds showing significant improvements in activity when compared to the uncoordinated free ligands. The overall order of the observed cytotoxicity was seen as $[\text{Cu}_2(\text{OAc})_2(\text{phen})]$ (**36**) > $[\text{Cu}(\text{sal})(\text{phen})]$ (**23**) > $[\text{Cu}(\text{OAc})_2(5,6\text{-Me}_2\text{BZDH})_2]$ (**30**) > $[\text{Cu}(\text{salH})_2(\text{BZDH})_2]$ (**5**) > $[\text{Cu}(\text{salH})_2(\text{H}_2\text{O})_2]$ (**1**) > $[\text{Cu}_2(\text{OAc})_4(\text{H}_2\text{O})_2]$. The results presented in Table 51 also illustrate that the CuSO_4 (free Cu^{2+}) was incapable of eliciting a cytotoxic response. The inclusion of the N,N-donor ligand 1,10-phenanthroline (phen) in the simple Cu(II) complexes of the acetic and salicylic acids significantly increased the potency of the system. However, it is also noteworthy that the metal free phenanthroline is itself significantly cytotoxic and that the best copper complex containing it $[\text{Cu}(\text{OAc})_2(\text{phen})]$ (**36**) is approximately 2, 5 and 3 times more potent for the respective cell lines. The complexes $[\text{Cu}(\text{OAc})_2(\text{phen})]$ (**36**) and $[\text{Cu}(\text{sal})(\text{phen})]$ (**23**) were capable of killing all three cancer derived cell lines at very low concentrations (IC_{50} values: 1.8, 1.0 and 1.55 μM and 2.5, 1.6 and 1.42 μM for the liver, kidney and lung cell lines, respectively). The activities of $[\text{Cu}(\text{OAc})_2(\text{phen})]$ (**36**) and $[\text{Cu}(\text{sal})(\text{phen})]$ (**23**) fall well within the accepted activity parameters adopted for *in-vitro* screening of potential chemotherapeutic drugs.¹⁶⁵

Furthermore, the IC₅₀ values for them are superior to those of the clinically used drug cisplatin.¹⁶⁶

Significantly, no correlation was found between the potencies of SOD mimic capabilities and cell growth inhibitory activity for the six complexes (indeed all six exhibit excellent SOD mimetic activity). However all of the complexes do show significant activity against the renal and lung cell lines. It is of course possible that the complexes act on the cancer cells through mechanisms other than (or in conjunction with) SOD activity. Indeed the bis-1,10-phenanthroline copper(II) complex cation [Cu(phen)₂]²⁺ is known as a potent nuclease agent which causes oxidative cleavage of DNA in the presence of reducing agents.¹⁶⁷

Significantly, (36) and (23) are relatively soluble compared to the other four complexes and they have cytotoxicity comparable with the copper(II) bis-phenanthroline complexes previously studied in this laboratory⁶³ but are one quarter as active as the copper(II) tris-phenanthroline-diones.⁶¹ The lack of correlation between the SOD and cytotoxicity IC₅₀ values supports the notion that mechanisms other than SOD mimicking may also be responsible for the anticancer properties of this type of copper complex. Indeed complexes (36) and (23) are structurally related to the novel anticancer agent casiopeina II {[Cu(1,4-dimethyl-1,10-phenanthroline)(glycine)]NO₃} which has been shown to have a very complex *in vivo* cytotoxicity.¹⁶⁸ It should be noted that compounds that have good SOD activity and do not display cytotoxicity might have potential use as a therapeutic agent for treatment of other disorders where SOD activity is pathologically reduced. Indeed [Cu(salH)₂(H₂O)₂] (1) is one such example and is available

commercially as a DMSO solution (Dermacusal[®]) for the topical treatment of arthritic joint pain in horses and dogs.

D.8 ANTIFUNGAL ACTIVITY OF COMPLEXES (1)-(69) AGAINST *CANDIDA ALBICANS*

Benzimidazoles are relatively poor anti-*Candida* agents. Previously this group has shown that upon coordination to a copper centre the biological activity of benzimidazoles was significantly improved when tested against the pathogen in RPMI medium. The benzimidazole complexes previously examined generally incorporated carboxylates as counterions which did not exhibit any antifungal activity in their own right (as free acids) and also did not improve the activity of their complexes. Part of the current study was seeking to establish if the inclusion of salicylate in the benzimidazole complexes would improve the anti *Candida* potential of this class of compound. However as the salicylate complexes were found to have very poor solubility we also examined the substituted salicylates 3,5-diisopropylsalicylic acid and 3-methoxysalicylic acid. Therefore all of the free ligands and copper complexes generated during this study were examined for their antifungal activity towards *Candida albicans* (Tables 52 - 54). Each copper(II) complex was screened for its ability to inhibit the growth of an isolate of *Candida albicans* at concentrations of 100 $\mu\text{g}/\text{cm}^3$, 50 $\mu\text{g}/\text{cm}^3$, 20 $\mu\text{g}/\text{cm}^3$, 10 $\mu\text{g}/\text{cm}^3$ and 5 $\mu\text{g}/\text{cm}^3$ of minimal medium. Furthermore, the antifungal activity of these complexes was compared to the activity of their starting materials and the prescription drug Ketoconazole. At a concentration of 100 $\mu\text{g}/\text{cm}^3$ all of the salicylate complexes exhibit excellent activity towards the pathogen. As the concentration of the drug is decreased their efficacy diminishes until finally at 10 $\mu\text{g}/\text{cm}^3$ most of them are either essentially inactive or very poor antimycotics.

The substituted salicylate complexes were found to be less active, with the activity decreasing in the order of salH₂ > dipsH₂ > msalH₂ (Table 53). The vast majority of the free ligands are essentially inactive with salicylic acid being the only one (other than phen) that shows significant activity at 50 µg/cm³ (Table 52). The potent activity of phen has been documented by this group earlier but one surprise is the relative inactivity of the phen derivatives (23), (24) and (25) (Table 53). The copper(II) benzimidazole complexes all display excellent activity at 100 µg/cm³. Again their efficacy decreases as the concentration is lowered until at 10 µg/cm³ all are inactive with the exception of the two sulfate complexes (44) and (49) (Table 54).

Table 52: Anti-*Candida* activity (as % cell growth) of Ketoconazole and the free aromatic acid and benzimidazole ligands

Test Compound	% Cell Growth (at concentrations of 100 - 5 µg/cm ³)				
	100	50	20	10	5
Ketoconazole	5	14	20	25	26
salH ₂	10	14	71	-	-
dipsH ₂	20	69	91	-	-
msalH ₂	27	73	-	-	-
BZDH	59	82	-	-	-
2-CIBZDH	19	34	76	-	-
5,6-Me ₂ BZDH	89	-	-	-	-
2-PhBZDH	-	-	-	-	-
6-NO ₂ BZDH	91	-	-	-	-
2,5-Me ₂ BZDH	-	-	-	-	-
5-BZDHCOOH	75	92	-	-	-
2-AmBZDH	58	84	91	-	-
2-MeOHBZDH	-	-	-	-	-
TBZH	-	-	-	-	-
2-PyBZDH	-	-	-	-	-
phen	4	3	11	22	14
bipy	47	74	91	-	-

Note: - indicates no activity or 100% cell growth

Table 53: Anti-*Candida* activity for copper(II) salicylate containing complexes

Test Compound	% Cell Growth (at concentrations of 100 - 5 $\mu\text{g}/\text{cm}^3$)				
	100	50	20	10	5
[Cu(salH) ₂ (H ₂ O) ₂] (1)	8	8	51	-	-
[Cu(salH) ₂ (BZDH) ₂] (5)	8	9	69	-	-
[Cu(salH) ₂ (5,6-Me ₂ BZDH) ₂] (6)	9	10	30	-	-
[Cu(sal)(2,5-Me ₂ BZDH)(H ₂ O)] (7)	9	9	67	-	-
[Cu(sal)(6-NO ₂ BZDH)(H ₂ O)] (8)	8	9	63	-	-
[Cu(sal)(5-BZDHCOOH)(H ₂ O)] (9)	8	11	48	-	-
[Cu(salH) ₂ (2-AmBZDH)(H ₂ O) ₂] (10)	7	9	39	-	-
[Cu(sal)(TBZH)].H ₂ O (11)	8	10	83	-	-
[Cu(sal)(2-PyBZDH)].H ₂ O (12)	9	12	76	-	-
[Cu(sal)(phen)] (23)	38	57	71	81	-
[Cu(sal)(bipy)].EtOH.H ₂ O (26)	12	29	86	-	-
[Cu(dipsH) ₂ (H ₂ O)] (3)	53	90	-	-	-
[Cu(dipsH) ₂ (BZDH) ₂] (13)	50	73	-	-	-
[Cu(dipsH) ₂ (2-MeOHBZDH) ₂].EtOH (14)	49	82	-	-	-
[Cu(dips)(2,5-Me ₂ BZDH)(H ₂ O)] (15)	68	84	-	-	-
[Cu(5-BZDCOO)(H ₂ O) ₂].EtOH (16)	62	87	-	-	-
[Cu(dips)(2-AmBZDH)(H ₂ O)] (17)	49	71	-	-	-
[Cu(dips)(TBZH)] (18)	75	86	-	-	-
[Cu(dips)(phen)].H ₂ O (24)	8	56	80	-	-
[Cu(dips)(bipy)].H ₂ O (27)	11	52	-	-	-
{Cu(msal)(H ₂ O)} _n (4)	64	-	-	-	-
[Cu(msal)(BZDH)(H ₂ O)].2H ₂ O (20)	62	-	-	-	-
[Cu(msal)(TBZH)].H ₂ O (21)	68	-	-	-	-
[Cu(msal)(2-PyBZDH)].H ₂ O (22)	70	-	-	-	-
[Cu(msal)(phen)].H ₂ O (25)	45	69	-	-	-
[Cu(msal)(bipy)].H ₂ O (28)	63	-	-	-	-

Note: - indicates no activity or 100% cell growth

Table 54: Anti-*Candida* activity for copper(II) benzimidazole containing complexes

Test Compound	% Cell Growth (at concentrations of 100 - 5 $\mu\text{g}/\text{cm}^3$)				
	100	50	20	10	5
CuCl₂.2H₂O	88	-	-	-	-
CuSO₄.5H₂O	81	-	-	-	-
[Cu(OAc) ₂ (2-AmbZDH) ₂] (29)	9	20	62	-	-
[Cu(OAc) ₂ (5,6-Me ₂ BZDH) ₂] (30)	8	24	78	-	-
[Cu(OAc) ₂ (5-BZDHCOOH) ₂] (31)	9	31	59	-	-
[Cu(OAc) ₂ (6-NO ₂ BZDH) ₂] (32)	9	34	75	-	-
[Cu(OAc) ₂ (2-PhBZDH) ₂] (33)	9	37	71	-	-
[Cu(OAc) ₂ (2-PyBZDH)] (35)	9	18	69	-	-
[Cu(BZDH) ₂ (H ₂ O)Cl]Cl (37)	10	14	71	-	-
[Cu(5-BZDHCOOH) ₂ (H ₂ O)Cl]Cl (38)	9	22	54	-	-
[Cu(2,5-Me ₂ BZDH) ₂ (H ₂ O)Cl]Cl (39)	9	20	86	-	-
[Cu(6-NO ₂ BZDH) ₂ (H ₂ O)Cl]Cl (40)	8	11	71	-	-
[Cu(2-PhBZDH) ₂ (H ₂ O)Cl]Cl (41)	8	18	48	-	-
[Cu(5,6-Me ₂ BZDH)(H ₂ O)Cl ₂] (42)	9	17	50	-	-
[Cu(TBZH) ₂ Cl]Cl(H ₂ O) ₂ (43)	9	24	62	-	-
[Cu(2-PyBZDH) ₂ Cl]Cl (44)	8	10	58	-	-
[Cu(BZDH)(H ₂ O)](SO ₄) (45)	9	10	34	54	-
[Cu(5-BZDHCOOH)(H ₂ O) ₂](SO ₄).2H ₂ O (46)	9	34	69	-	-
[Cu(2,5-Me ₂ BZDH)(H ₂ O) ₂](SO ₄) (47)	8	14	35	-	-
[Cu(2-AmbZDH) ₂ (H ₂ O) ₂](SO ₄).2H ₂ O (48)	6	32	76	-	-
[Cu(6-NO ₂ BZDH) ₂ (H ₂ O) ₂](SO ₄) (49)	7	22	58	-	-
[Cu(TBZH) ₂ (SO ₄).EtOH (50)	6	21	64	70	-

Note: - indicates no activity or 100% cell growth

In an effort to explore the use of benzimidazoles as suitable ligands for silver based antimicrobials it was decided to try to make silver salicylate and react it with all of the simple benzimidazoles. $[\text{Ag}_2(\text{salH})_2]$ was easily generated using a published method but it failed to react with any of the benzimidazole ligands. However silver nitrate, silver sulfate and silver acetate all reacted smoothly with most of the benzimidazole ligands to yield the novel complexes (51) – (69).

These Ag(I) benzimidazole complexes were found to be excellent antimycotic agents (Table 55) with complexes (52) and (58) – (69) showing complete growth inhibition of the *Candida* cells at a concentration of $0.5 \mu\text{g}/\text{cm}^3$. The prescription drug Ketoconazole requires a concentration of $100 \mu\text{g}/\text{cm}^3$ to achieve a similar inhibition (Table 52). These complexes are totally insoluble and were found to be very light stable remaining colourless indefinitely when left exposed to ambient light. If these complexes are not toxic then they may offer significant potential as silver-based antimicrobial agents.

Table 55: Anti-*Candida* activity for silver(I) benzimidazole containing complexes

Test Compound	% Cell Growth (at concentrations of 2 – 0.1 $\mu\text{g}/\text{cm}^3$)				
	2	1	0.5	0.2	0.1
AgNO ₃	0	0	0	90	-
Ag ₂ SO ₄	0	0	0	85	-
Ag(OAc)	0	0	0	81	-
[Ag(BZDH) ₂](NO ₃) (51)	0	0	46	90	-
[Ag(5-CarBZDH) ₂](NO ₃) (52)	0	0	0	65	-
[Ag(2-PhBZDH) ₂](NO ₃) (53)	28	59	-	-	-
[Ag(5,6-Me ₂ BZDH)](NO ₃) (54)	0	0	83	54	-
[Ag(6-NO ₂ BZDH)](NO ₃) (55)	0	58	-	-	-
[Ag(2-CIBZDH)](NO ₃) (56)	0	0	36	50	-
[Ag(TBZH)](NO ₃) (57)	0	47	92	94	-
[Ag ₂ (BZDH)](SO ₄) (58)	0	0	0	46	82
[Ag ₂ (2-AmBZDH)](SO ₄) (59)	0	0	0	34	91
[Ag ₂ (5-BZDHCOOH)](SO ₄) (60)	0	0	0	43	81
[Ag ₂ (5,6-Me ₂ BZDH)](SO ₄) (61)	0	0	0	71	90
[Ag ₂ (6-NO ₂ BZDH)](SO ₄) (62)	0	0	0	39	96
[Ag ₂ (2-PhBZDH)](SO ₄) (63)	0	0	0	31	83
[Ag ₂ (TBZH)](SO ₄) (64)	0	0	0	53	94
{Ag(BZD)} _n (65)	0	0	0	57	-
[Ag(5,6-Me ₂ BZDH)(OAc)] (66)	0	0	0	42	95
[Ag(5-BZDHCOOH)(OAc)] (67)	0	0	0	38	96
[Ag(2-AmBZDH) ₂ (OAc)] (68)	0	0	0	29	96
{Ag(TBZ)} _n (69)	0	0	0	44	91

Note: - indicates no activity or 100% cell growth

EXPERIMENTAL

E.1 INSTRUMENTATION

Infrared (IR) spectra were recorded in the region $4000 - 400 \text{ cm}^{-1}$ on a Nicolet FT-IR 5DXB infrared spectrometer. Solid samples were prepared in a KBr matrix.

Electronic spectra measurements and the SOD mimetic activity of complexes using the NBT assay were carried out using UV grade disposable cuvettes on a thermostatically controlled Analytikjena Specord 200 spectrophotometer.

Measurement of drug minimum inhibitory concentrations (MIC) against *Candida albicans* was carried out using an Anthos bt 3 plate reader.

Cytotoxicity studies were carried out by Dr. Denise Egan, ITT Dublin and Dr. Fiona Lyng, DIT using the MTT assay.

Room temperature magnetic susceptibility measurements were carried out using a Johnson Matthey Magnetic Susceptibility Balance. $\text{Hg}[(\text{Co}(\text{SCN})_4]$ was used as a reference standard.

Conductivity measurements were made at 25°C using an Orion 150 Aplus conductivity meter. Measurements were made at concentrations of 4.0 mmol.

The apparatus shown in Figure 101 was used in the catalytic experiments to measure the volume of oxygen evolved.

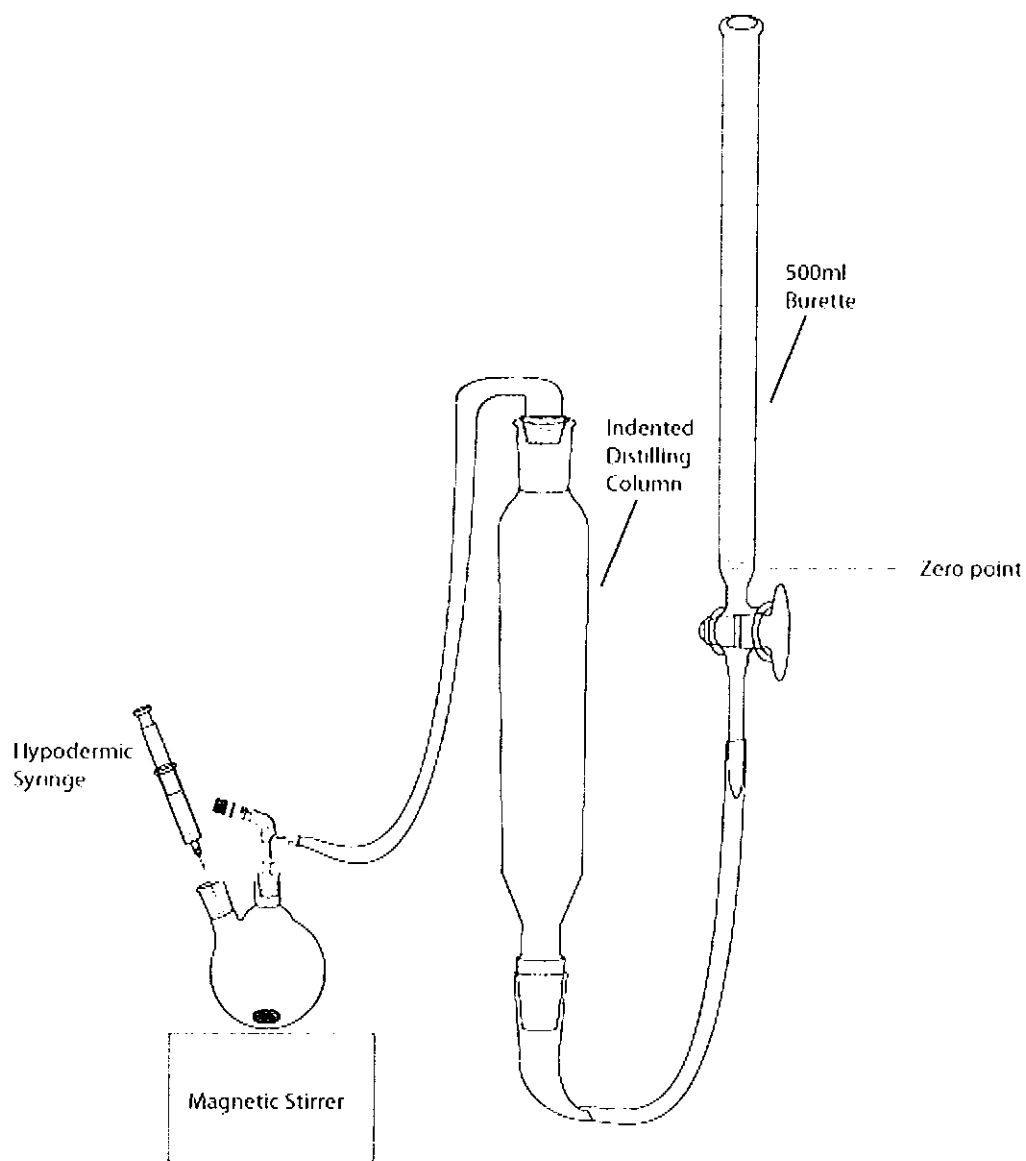


Figure 101: Apparatus designed to measure the volume of oxygen disproportionated in the catalytic reactions.

This apparatus was modified from a similar design by the late Prof. Michael T. Casey. It comprises a two necked round bottom flask, a magnetic stirrer, an indented distilling column and a 500 cm³ burette. A weighed amount of catalyst is placed in the round

bottomed flask, which is then connected to the distilling column *via* a vacuum takeoff adaptor. The distilling column, which is connected to an elevated 500 cm³ burette, is filled to a level equal to the zero point on the burette. Aqueous hydrogen peroxide is then introduced to the round bottom flask *via* the hypodermic syringe and the oxygen evolved between the catalyst and hydrogen peroxide is measured by the change in burette volume.

Elemental analyses were carried out by the Microanalytical Laboratory, University College Dublin, Ireland and the Microanalytical Laboratory, University College Cork, Ireland.

The X-ray crystallographic work was carried out by Dr. Georgina Rosair, Heriot Watt University, Edinburgh, UK.

E.2 CHEMICALS

All chemicals were purchased from commercial sources and generally were used without further purification.

E.3 SYNTHESIS OF COPPER(II) SALICYLATE COMPLEXES

In a typical synthesis the relevant carboxylic acid (19.98 mmol) was added to a suspension of $\text{Cu}(\text{OH})_2$ (0.97g, 9.94 mmol) in EtOH (100 cm^3) and the resulting suspension refluxed for 3 h. The product was filtered off, washed with water and ethanol, then air-dried.

E.3.1 $[\text{Cu}(\text{salH})_2(\text{H}_2\text{O})_2]$ (1)

Yield: 1.4173 g (40 %). % **Calc:** C, 44.98; H, 3.78. % **Found:** C, 44.09; H, 3.39. **IR (KBr):** 3438, 1603, 1568, 1529, 1485, 1455, 1410, 1303, 1232, 1149, 1099, 1037, 891, 838, 808, 775, 763, 711, 673, 621, 595, 512, 451, 428, 415, 406 cm^{-1} . **Solubility:** DMSO. μ_{eff} : 1.81 B.M. $\lambda_{\text{max}}(\text{Nujol}): \lambda_{\text{d-d}} = 742 \text{ nm}$ $\lambda_{\text{max}}(\text{DMSO}): \lambda_{\text{d-d}} = 754 \text{ nm}$, $\epsilon = 169.54 \text{ dm}^3 \text{ mol}^{-1} \text{ cm}^{-1}$. $\Lambda_{\text{M}}(\text{DMSO}): 4.2 \text{ S cm}^2 \text{ mol}^{-1}$.

E.3.2 $[\text{Cu}_2(\text{asp})_4(\text{H}_2\text{O})_2] \cdot \text{H}_2\text{O}$ (2)

Yield: 1.6316 g (36 %). % **Calc:** C, 48.16; H, 3.82. % **Found:** C, 48.88; H, 3.33. **IR (KBr):** 3433, 3083, 2984, 2938, 1759, 1726, 1618, 1572, 1514, 1483, 1417, 1450, 1417, 1404, 1372, 1242, 1219, 1198, 1163, 1146, 1096, 1035, 961, 934, 919, 879, 852, 816, 799, 757, 724, 708, 681, 657, 620, 602, 589, 552, 501, 433 cm^{-1} . **Solubility:** DMSO. μ_{eff} : 1.46 B.M. $\lambda_{\text{max}}(\text{Nujol}): \lambda_{\text{d-d}} = 659 \text{ nm}$ $\lambda_{\text{max}}(\text{DMSO}): \lambda_{\text{d-d}} = 755 \text{ nm}$, $\epsilon = 148.18 \text{ dm}^3 \text{ mol}^{-1} \text{ cm}^{-1}$. $\Lambda_{\text{M}}(\text{DMSO}): 10.85 \text{ S cm}^2 \text{ mol}^{-1}$.

E.3.3 [Cu(dipsH)₂(H₂O)] (3)

Yield: 2.8559 g (54 %). **% Calc:** C, 59.58; H, 6.92. **% Found:** C, 59.27; H, 6.83. **IR (KBr):** 3432, 2961, 2930, 2870, 1807, 1628, 1592, 1560, 1468, 1390, 1363, 1319, 1296, 1241, 1175, 1151, 1123, 1107, 1084, 1046, 944, 895, 877, 844, 808, 780, 741, 702, 639, 573, 536, 470 cm⁻¹. **Solubility:** DMSO, EtOH. μ_{eff} : 1.38 B.M. $\lambda_{\text{max}}(\text{Nujol})$: $\lambda_{\text{d-d}} = 703$ nm $\lambda_{\text{max}}(\text{DMSO})$: $\lambda_{\text{d-d}} = 766$ nm, $\epsilon = 113.26$ dm³ mol⁻¹ cm⁻¹. $\Lambda_{\text{M}}(\text{DMSO})$: 9.3 S cm² mol⁻¹.

E.3.4 {Cu(msal)(H₂O)}_n (4)

Yield: 2.0283 g (81 %). **% Calc:** C, 38.79; H, 3.26. **% Found:** C, 39.75; H, 2.85. **IR (KBr):** 3431, 2940, 2840, 1633, 1606, 1588, 1533, 1473, 1450, 1402, 1247, 1207, 1163, 1088, 1061, 934, 856, 835, 812, 779, 753, 696, 644, 465 cm⁻¹. **Solubility:** DMSO. μ_{eff} : 1.65 B.M. $\lambda_{\text{max}}(\text{Nujol})$: $\lambda_{\text{d-d}} = 764$ nm $\lambda_{\text{max}}(\text{DMSO})$: $\lambda_{\text{d-d}} = 766$ nm, $\epsilon = 122.61$ dm³ mol⁻¹ cm⁻¹ $\Lambda_{\text{M}}(\text{DMSO})$: 8.3 S cm² mol⁻¹.

E.4 SYNTHESIS OF COPPER(II) SALICYLATE COMPLEXES INCORPORATING BENZIMIDAZOLE LIGANDS

E.4.1 Synthesis of copper(II) salicylate complexes incorporating the simple benzimidazoles

Method (a): In a typical synthesis the relevant benzimidazole (2.68 mmol) was added to a suspension of $[\text{Cu}(\text{salH})_2(\text{H}_2\text{O})_2]$ (**1**) (0.5 g, 1.34 mmol) in EtOH (75 cm³) and the resulting mixture refluxed for 3 h. The product was filtered off, washed with water and ethanol, then air-dried.

Method (b): In a typical synthesis the relevant benzimidazole (1.12 mmol) was added to a suspension of $[\text{Cu}_2(\text{asp})_4(\text{H}_2\text{O})_2] \cdot \text{H}_2\text{O}$ (**2**) (0.5 g, 0.56 mmol) in EtOH (75 cm³) and the resulting mixture refluxed for 3 h. The product was filtered off, washed with water and ethanol, then air-dried.

E.4.1.1 $[\text{Cu}(\text{salH})_2(\text{BZDH})_2]$ (**5**)

Yield (a): 0.5079 g (66 %). % **Calc:** C, 58.58; H, 3.86; N, 9.76. % **Found:** C, 58.87; H, 3.77; N, 9.76. **IR (KBr):** 3238, 3145, 3112, 3064, 2990, 2916, 2839, 1760, 1741, 1619, 1595, 1582, 1568, 1509, 1497, 1479, 1454, 1395, 1355, 1323, 1305, 1272, 1224, 1195, 1141, 1113, 1086, 1031, 1010, 977, 971, 925, 864, 849, 832, 817, 777, 756, 733, 716, 705, 669, 634, 606, 560, 548, 536, 443, 420 cm⁻¹. **Solubility:** DMSO μ_{eff} : 1.83 B.M. $\lambda_{\text{max}}(\text{Nujol}): \lambda_{\text{d-d}} = 579 \text{ nm}$ $\lambda_{\text{max}}(\text{DMSO}): \lambda_{\text{d-d}} = 738 \text{ nm}$, $\epsilon = 84.15 \text{ dm}^3 \text{ mol}^{-1} \text{ cm}^{-1}$ $\Lambda_{\text{M}}(\text{DMSO}): 13.2 \text{ S cm}^2 \text{ mol}^{-1}$.

E.4.1.2 [Cu(salH)₂(5,6-Me₂BZDH)₂] (6)

Yield (a): 0.5147 g (61 %); **Yield (b):** 0.4453 g (63 %). **% Calc:** C, 60.99; H, 4.79; N, 8.89 **% Found:** C, 59.38; H, 4.72; N, 8.78. **IR (KBr):** 3427, 2971, 2943, 2359, 1624, 1595, 1580, 1563, 1504, 1478, 1454, 1398, 1385, 1331, 1309, 1270, 1253, 1209, 1143, 1086, 1030, 971, 948, 867, 851, 816, 752, 707, 689, 669, 641, 604, 537, 486, 450, 428 cm⁻¹.

Solubility: DMSO. μ_{eff} : 2.05 B.M. $\lambda_{\text{max}}(\text{Nujol})$: $\lambda_{\text{d-d}} = 550$ nm. $\lambda_{\text{max}}(\text{DMSO})$: $\lambda_{\text{d-d}} = 722$ nm, $\epsilon = 129.58$ dm³ mol⁻¹ cm⁻¹ $\Lambda_{\text{M}}(\text{DMSO})$: 11.6 S cm² mol⁻¹.

E.4.1.3 [Cu(sal)(2,5-Me₂BZDH)(H₂O)] (7)

Yield (a): 0.5003 g (75 %); **Yield (b):** 0.3418 g (88 %). **% Calc:** C, 55.41; H, 4.08; N, 8.1. **% Found:** C, 55.27; H, 4.02; N, 7.92. **IR (KBr):** 3427, 3124, 3057, 2921, 2797, 1603, 1559, 1504, 1462, 1404, 1323, 1254, 1232, 1143, 1099, 1054, 1034, 940, 896, 859, 839, 803, 759, 712, 676, 662, 639, 598, 586, 537, 452, 430 cm⁻¹. **Solubility:** DMSO.

μ_{eff} : 2.09 B.M. $\lambda_{\text{max}}(\text{Nujol})$: $\lambda_{\text{d-d}} = 725$ nm. $\lambda_{\text{max}}(\text{DMSO})$: $\lambda_{\text{d-d}} = 740$ nm, $\epsilon = 81.78$ dm³ mol⁻¹ cm⁻¹. $\Lambda_{\text{M}}(\text{DMSO})$: 1.55 S cm² mol⁻¹.

E.4.1.4 [Cu(sal)(6-NO₂BZDH)(H₂O)] (8)

Yield (a): 0.4175 g (82 %); **Yield (b):** 0.1187 g (70 %). **% Calc:** C, 43.36; H, 2.92; N, 7.21. **% Found:** C, 43.51; H, 2.71; N, 7.23. **IR (KBr):** 3432, 1759, 1726, 1617, 1571, 1514, 1484, 1451, 1402, 1344, 1304, 1242, 1197, 1163, 1146, 1096, 1070, 1035, 918, 885, 816, 798, 757, 739, 708, 680, 657, 589, 551, 505, 421 cm⁻¹.

Solubility: DMSO. μ_{eff} : 1.86 B.M. $\lambda_{\text{max}}(\text{Nujol})$: $\lambda_{\text{d-d}} = 629$ nm. $\lambda_{\text{max}}(\text{DMSO})$: $\lambda_{\text{d-d}} = 719$ nm, $\epsilon = 107.33$ dm³ mol⁻¹ cm⁻¹. $\Lambda_{\text{M}}(\text{DMSO})$: 1.75 S cm² mol⁻¹.

E.4.1.5 [Cu(sal)(5-BZDHCOOH)(H₂O)] (9)

Yield (a): 0.3592 g (71 %); **Yield (b):** 0.1681 g (48 %). **% Calc:** C, 47.43; H, 3.18; N, 7.38. **% Found:** C, 46.77; H, 2.99; N, 7.48. **IR (KBr):** 3366, 3213, 2928, 1749, 1635, 1610, 1575, 1488, 1450, 1399, 1292, 1240, 1199, 1160, 1125, 1095, 1013, 964, 920, 890, 830, 816, 792, 779, 756, 706, 681, 653, 597, 536, 474, 429 cm⁻¹. **Solubility:** DMSO. μ_{eff} : 1.62 B.M. $\lambda_{\text{max}}(\text{Nujol})$: $\lambda_{\text{d-d}} = 726$ nm. $\lambda_{\text{max}}(\text{DMSO})$: $\lambda_{\text{d-d}} = 729$ nm, $\epsilon = 130.95$ dm³ mol⁻¹ cm⁻¹. $\Lambda_{\text{M}}(\text{DMSO})$: 3.95 S cm² mol⁻¹.

E.4.1.6 [Cu(salH)₂(2-AmbZDH)(H₂O)₂] (10)

Yield (a): 0.5419 g (63 %); **Yield (b):** 0.4025 g (74 %). **% Calc:** C, 49.75; H, 4.18; N, 8.29. **% Found:** C, 50.5; H, 3.75; N, 8.60. **IR (KBr):** 3422, 3334, 2360, 2342, 1748, 1727, 1655, 1616, 1561, 1472, 1449, 1384, 1279, 1231, 1198, 1158, 1147, 1094, 1039, 1010, 948, 919, 876, 857, 817, 800, 755, 740, 719, 682, 652, 599, 545, 504, 463, 427 cm⁻¹. **Solubility:** insoluble. μ_{eff} : 1.86 B.M. $\lambda_{\text{max}}(\text{Nujol})$: $\lambda_{\text{d-d}} = 680$ nm.

E.4.2 Synthesis of copper (II) salicylate complexes incorporating the chelating benzimidazoles

E.4.2.1 [Cu(sal)(TBZH)].H₂O (11)

Yield (a): 0.6027 g (78 %); **Yield (b):** 0.3235 g (72 %). **% Calc:** C, 48.74; H, 3.13; N, 10.03. **% Found:** C, 48.59; H, 2.49; N, 10.00. **IR (KBr):** 3442, 3063, 29693, 2920, 2852, 2758, 2685, 2648, 2361, 1599, 1594, 1559, 1561, 1533, 1484, 1465, 1452, 1413, 1376, 1329, 1300, 1286, 1257, 1233, 1199, 1137, 1119, 1016, 999, 936, 832, 804, 749, 741, 704, 670, 650, 623, 585, 541, 484, 436, 417, 401 cm⁻¹. **Solubility:** DMSO. μ_{eff} : 2.18 B.M. $\lambda_{\text{max}}(\text{Nujol})$: $\lambda_{\text{d-d}} = 606$ nm. $\lambda_{\text{max}}(\text{DMSO})$: $\lambda_{\text{d-d}} = 686$ nm, $\epsilon = 90.05$ dm³ mol⁻¹ cm⁻¹. $\Lambda_{\text{M}}(\text{DMSO})$: 5.2 S cm² mol⁻¹.

E.4.2.2 [Cu(sal)(2-PyBZDH)].H₂O (12)

Yield (b): 0.1026 g (38 %). **% Calc:** C, 55.27; H, 3.63; N, 10.18. **% Found:** C, 55.74; H, 3.15; N, 9.94. **IR (KBr):** 3443, 3061, 2752, 2615, 1600, 1556, 1505, 1485, 1464, 1450, 1390, 1371, 1328, 1307, 1289, 1252, 1155, 1138, 1098, 1051, 1024, 1004, 980, 883, 856, 833, 822, 808, 787, 748, 707, 695, 667, 651, 631, 583, 536, 504, 435, 415 cm⁻¹. **Solubility:** DMSO. μ_{eff} : 2.11 B.M. $\lambda_{\text{max}}(\text{Nujol})$: $\lambda_{\text{d-d}} = 703$ nm. $\lambda_{\text{max}}(\text{DMSO})$: $\lambda_{\text{d-d}} = 674$ nm, $\epsilon = 101$ dm³ mol⁻¹ cm⁻¹. $\Lambda_{\text{M}}(\text{DMSO})$: 4.45 S cm² mol⁻¹.

E.4.3 Synthesis of copper(II) 3,5-diisopropylsalicylate complexes incorporating the simple benzimidazoles

In a typical synthesis the relevant benzimidazole (1.8 mmol) was added to a solution of [Cu(dipsH)₂(H₂O)] (3) (0.5 g, 0.9 mmol) in EtOH (75 cm³) and the resulting suspension refluxed for 3 h. The product was filtered off, washed with water and ethanol, then air-dried.

E.4.3.1 [Cu(dipsH)₂(BZDH)₂] (13)

Yield: 0.3627 g (55 %). **% Calc:** C, 64.72; H, 6.25; N, 7.55. **% Found:** C, 64.36; H, 6.23; N, 7.33. **IR (KBr):** 3427, 3139, 3031, 2959, 2926, 2867, 1807, 1618, 1590, 1550, 1500, 1466, 1458, 1487, 1405, 1362, 1315, 1303, 1267, 1245, 1176, 1154, 1141, 1126, 1112, 1085, 1070.1009, 965.943, 896, 8884, 845, 814, 774, 753, 746, 660, 640, 634, 620, 577, 549, 527, 503, 460, 449, 423 cm⁻¹. **Solubility:** DMSO. μ_{eff} : 1.69 B.M. $\lambda_{\text{max}}(\text{Nujol})$: $\lambda_{\text{d-d}} = 563$ nm. $\lambda_{\text{max}}(\text{DMSO})$: $\lambda_{\text{d-d}} = 733$ nm, $\epsilon = 81.95$ dm³ mol⁻¹ cm⁻¹. $\Lambda_{\text{M}}(\text{DMSO})$: 18.65 S cm² mol⁻¹.

E.4.3.2 [Cu(dipsH)₂(2-MeOHBZDH)₂].EtOH (14)

Yield: 0.3047 g (47 %). **% Calc:** C, 62.14; H, 6.87; N, 6.59. **% Found:** C, 59.38; H, 5.96; N, 6.30. **IR (KBr):** 3425, 3115, 3067, 2961, 2927, 2869, 1620, 1553, 1469, 1457, 1388, 1362, 1329, 1292, 1242, 1175, 1151, 1122, 1106, 1079, 1043, 1005, 920, 894, 812, 776, 744, 640, 575, 540, 492, 429 cm⁻¹. **Solubility:** DMSO. μ_{eff} : 1.79 B.M. $\lambda_{\text{max}}(\text{Nujol})$: $\lambda_{\text{d-d}} = 575$ nm. $\lambda_{\text{max}}(\text{DMSO})$: $\lambda_{\text{d-d}} = 740$ nm, $\epsilon = 44.18$ dm³ mol⁻¹ cm⁻¹. $\Lambda_{\text{M}}(\text{DMSO})$: 5.15 S cm² mol⁻¹.

E.4.3.3 [Cu(dips)(2,5-Me₂BZDH)(H₂O)] (15)

Yield: 0.2336 g (68 %). **% Calc:** C, 61.31; H, 6.31; N, 6.50. **% Found:** C, 61.09; H, 6.16; N, 6.25. **IR (KBr):** 3347, 2959, 2869, 2340, 1804, 1633, 1614, 1594, 1544, 1531, 1469, 1460, 1447, 1389, 1361, 1341, 1315, 1299, 1250, 1231, 1175, 1149, 1124, 1105, 1082, 1040, 942, 922, 893, 873, 845, 807, 781, 751, 635, 574, 487, 437, 422 cm⁻¹. **Solubility:** DMSO. μ_{eff} : 2.31 B.M. $\lambda_{\text{max}}(\text{Nujol})$: $\lambda_{\text{d-d}} = 752$ nm. $\lambda_{\text{max}}(\text{DMSO})$: $\lambda_{\text{d-d}} = 754$ nm, $\epsilon = 56.5$ dm³ mol⁻¹ cm⁻¹. $\Lambda_{\text{M}}(\text{DMSO})$: 7.03 S cm² mol⁻¹.

E.4.3.4 [Cu(5-BZDCOO)(H₂O)₂].EtOH (16)

Yield: 0.1975 g (82 %). **% Calc:** C, 44.34; H, 3.39; N, 9.41. **% Found:** C, 44.44; H, 3.57; N, 8.18. **IR (KBr):** 3208, 2961, 1633, 1609, 1492, 1399, 1296, 1242, 1198, 1127, 1047, 965, 939, 923, 833, 792, 778, 753, 685, 628, 598, 475, 440 cm⁻¹. **Solubility:** DMSO. μ_{eff} : 1.34 B.M. $\lambda_{\text{max}}(\text{Nujol})$: $\lambda_{\text{d-d}} = 720$ nm. $\lambda_{\text{max}}(\text{DMSO})$: $\lambda_{\text{d-d}} = 699$ nm, $\epsilon = 74.1$ dm³ mol⁻¹ cm⁻¹. $\Lambda_{\text{M}}(\text{DMSO})$: 5.68 S cm² mol⁻¹.

E.4.3.5 [Cu(dips)(2-AmbZDH)(H₂O)] (17)

To a solution [Cu₂(OAc)₄(H₂O)₂] (0.5 g, 1.25 mmol) in EtOH (75 cm³) was added 2-aminobenzimidazole (0.3325 g, 2.5 mmol) and 3,5-diisopropylsalicylic acid (0.55 g, 2.5 mmol) and the resulting green suspension refluxed for 3 h. On cooling to room temperature the green product was filtered off, washed with two portions of water and ethanol, and then air-dried.

Yield: 0.1572 g (33 %). **% Calc:** C, 55.10; H, 6.01; N, 9.64. **% Found:** C, 55.47; H, 5.89; N, 9.56. **IR (KBr):** 3624, 3416, 2956, 2867, 2360, 2341, 1645, 1620, 1596, 1574, 1557, 1519, 1471, 1444, 1385, 1361, 1312, 1290, 1276, 1241, 1221, 1176, 1149, 1125, 1011, 944, 921, 896, 878, 853, 812, 799, 769, 742, 668, 636, 541, 504, 451, 436, 419 cm^{-1} . **Solubility:** DMSO. μ_{eff} : 2.06 B.M. $\lambda_{\text{max}}(\text{Nujol})$: $\lambda_{\text{d-d}} = 614 \text{ nm}$. $\lambda_{\text{max}}(\text{DMSO})$: $\lambda_{\text{d-d}} = 711 \text{ nm}$, $\varepsilon = 88.4 \text{ dm}^3 \text{ mol}^{-1} \text{ cm}^{-1}$. $\Lambda_{\text{M}}(\text{DMSO})$: $4.5 \text{ S cm}^2 \text{ mol}^{-1}$.

E.4.4 Synthesis of copper(II) 3,5-diisopropylsalicylate complexes incorporating the chelating benzimidazoles

E.4.4.1 [Cu(dips)(TBZH)] (18)

Yield: 0.3138 g (86 %). **% Calc:** C, 56.95; H, 4.78; N, 8.66. **% Found:** C, 56.81; H, 4.73; N, 8.43. **IR (KBr):** 3433, 3091, 3057, 2956, 2922, 2864, 2747, 1627, 1609, 1593, 1524, 1482, 1460, 1443, 1383, 1360, 1330, 1305, 1280, 1236, 1201, 1173, 1149, 1113, 1051, 1016, 995, 936, 622, 906, 896, 873, 860, 832, 815, 799, 761, 747, 683, 653, 637, 573, 533, 488, 455, 422 cm^{-1} . **Solubility:** DMSO. μ_{eff} : 1.98 B.M. $\lambda_{\text{max}}(\text{Nujol})$: $\lambda_{\text{d-d}} = 611 \text{ nm}$. $\lambda_{\text{max}}(\text{DMSO})$: $\lambda_{\text{d-d}} = 692 \text{ nm}$, $\varepsilon = 83.73 \text{ dm}^3 \text{ mol}^{-1} \text{ cm}^{-1}$. $\Lambda_{\text{M}}(\text{DMSO})$: $3.6 \text{ S cm}^2 \text{ mol}^{-1}$.

E.4.4.2 [Cu(2-PyBZD)₂(H₂O)] (19)

Yield: 0.3541 g (84 %). **% Calc:** C, 52.26; H, 3.65; N, 15.24. **% Found:** C, 52.10; H, 3.40; N, 14.51. **IR (KBr):** 3432, 3053, 1604, 1566, 1513, 1475, 1456, 1445, 1428, 1384, 1329, 1303, 1275, 1232, 1145, 1120, 1092, 1047, 1006, 987, 918, 819, 794, 749, 739, 705, 645, 630, 619, 575, 513, 432, 416, 407cm⁻¹. **Solubility:** insoluble. μ_{eff} : 1.92 B.M. $\lambda_{\text{max}}(\text{Nujol})$: $\lambda_{\text{d-d}} = 681$ nm.

E.4.5 Synthesis of copper(II) 3-methoxysalicylate complexes incorporating the simple benzimidazoles

In a typical synthesis the relevant benzimidazole (2.6 mmol) was added to a suspension of $\{\text{Cu}(\text{msal})(\text{H}_2\text{O})\}_n$ (**4**) (0.5 g, 2 mmol) in EtOH (75 cm³) and the resulting mixture refluxed for 3 h. The product was filtered off, washed with water and ethanol, then air-dried.

E.4.5.1 $[\text{Cu}(\text{msal})(\text{BZDH})(\text{H}_2\text{O})] \cdot 2\text{H}_2\text{O}$ (**20**)

Yield: 0.5567 g (56 %). % Calc: C, 44.83; H, 4.51; N, 6.97. % Found: C, 44.04; H, 3.25; N, 5.36. IR (KBr): 3431, 3116, 2990, 2838, 2362, 2343, 1602, 1561, 1502, 1474, 1445, 1399, 1365, 1306, 1248, 1202, 1160, 1113, 1085, 1061, 1009, 974, 927, 887, 855, 836, 807, 777, 748, 648, 620, 441 cm⁻¹. Solubility: DMSO. μ_{eff} : 2.08 B.M. $\lambda_{\text{max}}(\text{Nujol})$: $\lambda_{\text{d-d}} = 725$ nm. $\lambda_{\text{max}}(\text{DMSO})$: $\lambda_{\text{d-d}} = 640$ nm, $\epsilon = 237.8 \text{ dm}^3 \text{ mol}^{-1} \text{ cm}^{-1}$. $\Lambda_{\text{M}}(\text{DMSO})$: $1.45 \text{ S cm}^2 \text{ mol}^{-1}$.

E.4.6 Synthesis of copper(II) 3-methoxysalicylate complexes incorporating the chelating benzimidazoles

E.4.6.1 $[\text{Cu}(\text{msal})(\text{TBZH})] \cdot \text{H}_2\text{O}$ (**21**)

Yield: 0.6722 g (75 %). % Calc: C, 48.05; H, 3.58; N, 9.34. % Found: C, 47.21; H, 2.89; N, 10.35. IR (KBr): 3442, 3095, 2833, 1686, 1653, 1628, 1599, 1567, 1526, 1477, 1442, 1403, 1328, 1301, 1283, 1233, 1204, 1151, 1119, 1087, 1060, 1013, 997, 939, 925, 875, 851, 835, 803, 748, 673, 651, 630, 575, 554, 486, 437, 422 cm⁻¹. Solubility: DMSO. μ_{eff} : 1.85 B.M. $\lambda_{\text{max}}(\text{Nujol})$: $\lambda_{\text{d-d}} = 647$ nm. $\lambda_{\text{max}}(\text{DMSO})$: $\lambda_{\text{d-d}} = 676$ nm, $\epsilon = 159.93 \text{ dm}^3 \text{ mol}^{-1} \text{ cm}^{-1}$. $\Lambda_{\text{M}}(\text{DMSO})$: $6.05 \text{ S cm}^2 \text{ mol}^{-1}$.

E.4.6.2 [Cu(msal)(2-PyBZDH)].H₂O (22)

Yield: 0.5589 g (63 %). **% Calc:** C, 54.11; H, 4.09; N, 9.47. **% Found:** C, 54.24; H, 3.94; N, 9.45. **IR (KBr):** 3433, 3064, 2980, 2928, 2831, 2747, 2705, 2623, 2361, 1600, 1564, 1529, 1476, 1460, 1445, 1369, 1341, 1328, 1311, 1292, 1230, 1198, 1158, 1118, 1085, 1068, 1051, 1023, 1007, 983, 906, 858, 820, 796, 749, 694, 678, 650, 632, 580, 562, 505, 438, 414 cm⁻¹. **Solubility:** DMSO. μ_{eff} : 1.97 B.M. $\lambda_{\text{max}}(\text{Nujol})$: $\lambda_{\text{d-d}} = 578$ nm. $\lambda_{\text{max}}(\text{DMSO})$: $\lambda_{\text{d-d}} = 665$ nm, $\varepsilon = 165.38$ dm³ mol⁻¹ cm⁻¹. $\Lambda_{\text{M}}(\text{DMSO})$: 8.15 S cm² mol⁻¹.

E.5 Synthesis of copper (II) salicylate complexes incorporating the N,N-donor ligands 1,10-phenanthroline and 2,2-bipyridine

The relevant chelating ligand (phen or bipy) (2.68 mmol) was added to a suspension of $[\text{Cu}(\text{salH})_2(\text{H}_2\text{O})_2]$ (**1**) (0.5 g, 1.34 mmol) in EtOH (50 cm³) and the resulting suspension refluxed for 3 h. The product was filtered off, washed with water and ethanol, then air-dried.

E.5.1 $[\text{Cu}(\text{sal})(\text{phen})]$ (**23**)

Yield: 0.73 g (72 %). **% Calc:** C, 60.1; H, 3.2; N, 7.4 **% Found:** C, 58.9; H, 3.3; N, 7.0. **IR (KBr):** 3416, 3089, 3059, 2360, 2342, 1629, 1599, 1574, 1543, 1519, 1492, 1461, 1450, 1429, 1360, 1342, 1320, 1243, 1223, 1136, 1107, 1032, 911, 884, 874, 847, 809, 772, 741, 721, 710, 667, 651.628, 585, 543, 432 cm⁻¹. **Solubility:** EtOH, MeOH and DMSO. μ_{eff} : 2.11 B.M. $\lambda_{\text{max}}(\text{Nujol})$: $\lambda_{\text{d-d}} = 586$ nm. $\lambda_{\text{max}}(\text{DMSO})$: $\lambda_{\text{d-d}} = 635$ nm, $\epsilon = 134.3$ dm³ mol⁻¹ cm⁻¹. $\Lambda_{\text{M}}(\text{DMSO})$: 1.8 S cm² mol⁻¹.

E.5.2 $[\text{Cu}(\text{sal})(\text{bipy})].\text{EtOH}.\text{H}_2\text{O}$ (**24**)

Yield: 0.336 g (67 %). **% Calc:** C, 54.91; H, 4.22; N, 6.99. **% Found:** C, 54.36; H, 4.8; N, 6.67 **IR (KBr):** 3424, 3110, 3059, 1601, 1563, 1533, 1511, 1464, 1451, 1397, 1363, 1321, 1253, 1140, 1104, 1057, 1033, 1021, 884, 864, 836, 810, 762, 731, 709, 667, 642, 587, 539, 436, 418 cm⁻¹. **Solubility:** DMSO. μ_{eff} : 1.95 B.M. $\lambda_{\text{max}}(\text{Nujol})$: $\lambda_{\text{d-d}} = 627$ nm. $\lambda_{\text{max}}(\text{DMSO})$: $\lambda_{\text{d-d}} = 624$ nm, $\epsilon = 75.19$ dm³ mol⁻¹ cm⁻¹. $\Lambda_{\text{M}}(\text{DMSO})$: 0.9 S cm² mol⁻¹.

The relevant chelating ligand (phen or bipy) (1.52 mmol) was added to a solution of [Cu(dipsH)₂(H₂O)] (3) (0.4 g, 0.76 mmol) in EtOH (50 cm³) and the resulting suspension refluxed for 3 h. The product was filtered off, washed with water and ethanol, then air-dried.

E.5.3 [Cu(dips)(phen)].H₂O (25)

Yield: 0.3148 g (86 %). **% Calc:** C, 62.03; H, 5.83; N, 5.80. **% Found:** C, 62.48; H, 5.86; N, 5.87. **IR (KBr):** 3431, 3075, 3055, 2952, 2864, 1807, 1628, 1612, 1575, 1548, 1516, 1491, 1467, 1454, 1427, 1369, 1344, 1312, 1284, 1241, 1223, 1174, 1148, 1107, 1047, 972, 944, 921, 893, 873, 845, 815, 802, 751, 737, 724, 685, 646, 634, 578, 542, 432, 421 cm⁻¹. **Solubility:** DMSO. μ_{eff} : 2.05 B.M. $\lambda_{\text{max}}(\text{Nujol})$: $\lambda_{\text{d-d}} = 631$ nm. $\lambda_{\text{max}}(\text{DMSO})$: $\lambda_{\text{d-d}} = 644$ nm, $\epsilon = 67.31$ dm³ mol⁻¹ cm⁻¹. $\Lambda_{\text{M}}(\text{DMSO})$: 0.78 S cm² mol⁻¹.

E.5.4 [Cu(dips)(bipy)] (26)

Yield: 0.3241 g (82 %). **% Calc:** C, 62.78; H, 5.50; N, 6.37. **% Found:** C, 62.26; H, 5.76; N, 6.33. **IR (KBr):** 3444, 3074, 3029, 2954, 2862, 2360, 2341, 1614, 1579, 1563, 1549, 1469, 1456, 1447, 1369, 1349, 1310, 1280, 1254, 1244, 1229, 1215, 1177, 1158, 1146, 1122, 1102, 1054, 1014, 1031, 1019, 944, 892, 878, 853, 814, 799, 770, 733, 685, 668, 658, 636, 569, 538, 442, 418 cm⁻¹. **Solubility:** DMSO. μ_{eff} : 1.90 B.M. $\lambda_{\text{max}}(\text{Nujol})$: $\lambda_{\text{d-d}} = 632$ nm. $\lambda_{\text{max}}(\text{DMSO})$: $\lambda_{\text{d-d}} = 629$ nm, $\epsilon = 58.23$ dm³ mol⁻¹ cm⁻¹. $\Lambda_{\text{M}}(\text{DMSO})$: 0.94 S cm² mol⁻¹.

The relevant chelating ligand (phen or bipy) (2.6 mmol) was added to a suspension of $\{\text{Cu}(\text{msal})(\text{H}_2\text{O})\}_n$ (**4**) (0.5 g, 2 mmol) in EtOH (50 cm³) and the resulting suspension refluxed for 3 h. The product was filtered off, washed with water and ethanol, then air-dried.

E.5.5 $[\text{Cu}(\text{msal})(\text{phen})]\cdot\text{H}_2\text{O}$ (**27**)

Yield: 0.5507 g (64 %). **% Calc:** C, 56.14; H, 3.77; N, 6.55 **% Found:** C, 56.09; H, 3.41; N, 6.14. **IR (KBr):** 3432, 3059, 2835, 1630, 1568, 1572, 1554, 1519, 1472, 1445, 1429, 1369, 1340, 1234, 1199, 1147, 1108, 1063, 923, 874, 847, 821, 800, 751, 736, 722, 674, 627, 566, 453, 432 cm⁻¹. **Solubility:** DMSO. μ_{eff} : 1.85 B.M. $\lambda_{\text{max}}(\text{Nujol})$: $\lambda_{\text{d-d}} = 602$ nm. $\lambda_{\text{max}}(\text{DMSO})$: $\lambda_{\text{d-d}} = 640$ nm, $\epsilon = 273.8$ dm³ mol⁻¹ cm⁻¹. $\Lambda_{\text{M}}(\text{DMSO})$: 1.45 S cm² mol⁻¹.

E.5.6 $[\text{Cu}(\text{msal})(\text{bipy})]\cdot\text{H}_2\text{O}$ (**28**)

Yield: 0.3577 g (47 %). **% Calc:** C, 53.53; H, 3.99; N, 6.94. **% Found:** C, 53.30; H, 3.52; N, 6.97. **IR (KBr):** 3440, 3109, 3052, 3032, 2992, 2829, 2361, 1606, 1598, 1588, 1555, 1496, 1472, 1443, 1332, 1322, 1249, 1231, 1194, 1171, 1160, 1122, 1076, 1058, 1031, 1019, 911, 853, 819, 794, 774, 760, 754, 733, 666, 639, 624, 584, 558, 478, 445, 427 cm⁻¹. **Solubility:** DMSO. μ_{eff} : 2.29 B.M. $\lambda_{\text{max}}(\text{Nujol})$: $\lambda_{\text{d-d}} = 627$ nm. $\lambda_{\text{max}}(\text{DMSO})$: $\lambda_{\text{d-d}} = 627$ nm, $\epsilon = 217.43$ dm³ mol⁻¹ cm⁻¹. $\Lambda_{\text{M}}(\text{DMSO})$: 1.35 S cm² mol⁻¹.

E.6 SYNTHESIS OF COPPER(II) ACETATE AND SIMPLE COPPER(II) SALTS INCORPORATING BENZIMIDAZOLE LIGANDS

E.6.1 Synthesis of copper(II) acetate salts of the simple benzimidazoles

In a typical synthesis the relevant benzimidazole (5 mmol) was added to a solution of $[\text{Cu}_2(\text{OAc})_4(\text{H}_2\text{O})_2]$ (0.5 g, 1.25 mmol) in EtOH (50 cm³) and the resulting suspension refluxed for 3 h. The product was filtered off, washed with water and ethanol, then air-dried.

E.6.1.1 $[\text{Cu}(\text{OAc})_2(2\text{-AmBZDH})_2]$ (29)

Yield: 0.4128 g (73 %). **%Calc:** C, 48.26; H, 4.50; N, 18.76. **% Found:** C, 48.25; H, 4.27; N, 18.86. **IR (KBr):** 3451, 3366, 3064, 2953, 2912, 2870, 1648, 1609, 1585, 1559, 1501, 1471, 1483, 1378, 1345, 1275, 1222, 1152, 1089, 1038, 1013, 916, 879, 745, 687, 649, 622, 551, 507 cm⁻¹. **Solubility:** insoluble. μ_{eff} : 1.95 B.M. $\lambda_{\text{max}}(\text{Nujol})$: $\lambda_{\text{d-d}} = 687$ nm.

E.6.1.2 $[\text{Cu}(\text{OAc})_2(5,6\text{-Me}_2\text{BZDH})_2]$ (30)

Yield: 0.2470 g (42 %). **% Calc:** C, 55.74; H, 5.52; N, 11.82. **% Found:** C, 55.66; H, 5.52; N, 11.78. **IR (KBr):** 3432, 3102, 3062, 2966, 2934, 2879, 2815, 2656, 1772, 1706, 1559, 1500, 1474, 1448, 1408, 1337, 1307, 1271, 1251, 1212, 1191, 1159, 1087, 1047, 1006, 968, 931, 882, 856, 841, 823, 784, 732, 675, 647, 618, 575, 486, 452, 435 cm⁻¹. **Solubility:** DMSO. μ_{eff} : 1.65 B.M. $\lambda_{\text{max}}(\text{Nujol})$: $\lambda_{\text{d-d}} = 531$ nm. $\lambda_{\text{max}}(\text{DMSO})$: $\lambda_{\text{d-d}} = 726$ nm, $\epsilon = 123.4$ dm³ mol⁻¹ cm⁻¹. $\Lambda_{\text{M}}(\text{DMSO})$: 0.9 S cm² mol⁻¹.

E.6.1.3 [Cu(OAc)₂(5-BZDHCOOH)₂] (31)

Yield: 0.4527g (71 %). **% Calc:** C, 47.48; H, 3.59; N, 11.07. **% Found:** C, 46.23; H, 3.20; N, 11.07. **IR (KBr):** 3423, 3049, 1911, 1775, 1644, 1591, 1488, 1467, 1409, 1394, 1317, 1300, 1195, 1141, 1084, 1030, 100, 941, 861, 814, 744, 698, 672, 569, 531, 460 cm⁻¹. **Solubility:** DMSO. μ_{eff} : 1.59 B.M. $\lambda_{\text{max}}(\text{Nujol})$: $\lambda_{\text{d-d}} = 651$ nm. $\lambda_{\text{max}}(\text{DMSO})$: $\lambda_{\text{d-d}} = 711$ nm, $\epsilon = 159.57 \text{ dm}^3 \text{ mol}^{-1} \text{ cm}^{-1}$. $\Lambda_{\text{M}}(\text{DMSO})$: $10.38 \text{ S cm}^2 \text{ mol}^{-1}$.

E.6.1.4 [Cu(OAc)₂(6-NO₂BZDH)₂] (32)

Yield: 0.5194 g (80 %). **% Calc:** C, 42.57; H, 3.18; N, 16.55. **% Found:** C, 42.95; H, 3.37; N, 16.23. **IR (KBr):** 3425, 3116, 2363, 1611, 1586, 1561, 1508, 1460, 1412, 1384, 1341, 1298, 1253, 1231, 1196, 1184, 1130, 1070, 1009, 949, 892, 824, 797, 763, 739, 710, 644, 618, 597, 547, 429 cm⁻¹. **Solubility:** DMSO. μ_{eff} : 2.20 B.M. $\lambda_{\text{max}}(\text{Nujol})$: $\lambda_{\text{d-d}} = 614$ nm. $\lambda_{\text{max}}(\text{DMSO})$: $\lambda_{\text{d-d}} = 678$ nm, $\epsilon = 140.55 \text{ dm}^3 \text{ mol}^{-1} \text{ cm}^{-1}$. $\Lambda_{\text{M}}(\text{DMSO})$: $1.08 \text{ S cm}^2 \text{ mol}^{-1}$.

E.6.1.5 [Cu(OAc)₂(2-PhBZDH)₂] (33)

Yield: 0.2537 g (35 %) **% Calc:** C, 63.20; H, 4.60; N, 9.83 **% Found:** C, 63.94; H, 4.67; N, 9.80 **IR (KBr):** 3432, 3130, 3067, 2980, 2915, 2867, 2804, 2763, 1570, 1497, 1482, 1463, 1424, 1399, 1335, 1325, 1288, 1133, 1013, 989, 923, 810, 763, 740, 698, 675, 634, 614, 571, 506, 488, 436 cm⁻¹ **Solubility:** DMSO. μ_{eff} : 1.74 B.M. $\lambda_{\text{max}}(\text{Nujol})$: $\lambda_{\text{d-d}} = 618$ nm. $\lambda_{\text{max}}(\text{DMSO})$: $\lambda_{\text{d-d}} = 678$ nm, $\epsilon = 127.53 \text{ dm}^3 \text{ mol}^{-1} \text{ cm}^{-1}$. $\Lambda_{\text{M}}(\text{DMSO})$: $2.81 \text{ S cm}^2 \text{ mol}^{-1}$.

E.6.2 Synthesis of copper(II) acetate salts of the chelating benzimidazoles

E.6.2.1 {[Cu(TBZ)₂(H₂O)].EtOH}_n (34)

Yield: 0.6528 g (69 %). **% Calc:** C, 50.03; H, 3.82; N, 15.91. **% Found:** C, 49.77; H, 2.97; N, 14.96. **IR (KBr):** 3378, 2974, 1919, 1594, 1551, 1474, 1406, 1378, 1325, 1295, 1273, 1230, 1197, 1146, 1112, 1067, 1015, 999, 923, 912, 874, 829, 743, 706, 686, 640, 562, 485, 437 cm⁻¹. **Solubility:** DMSO. μ_{eff} : 1.99 B.M. $\lambda_{\text{max}}(\text{Nujol})$: $\lambda_{\text{d-d}} = 683$ nm. $\lambda_{\text{max}}(\text{DMSO})$: $\lambda_{\text{d-d}} = 697$ nm, $\epsilon = 67.59$ dm³ mol⁻¹ cm⁻¹. $\Lambda_{\text{M}}(\text{DMSO})$: 1.81 cm² mol⁻¹.

E.6.2.2 [Cu(OAc)₂(2-PyBZDH)] (35)

Yield: 0.6528 g (69 %). **% Calc:** C, 50.99; H, 4.01; N, 11.15. **% Found:** C, 48.78; H, 3.69; N, 11.91. **IR (KBr):** 3456, 3372, 3074, 3016, 2361, 2343, 1606, 1579, 1560, 1495, 1458, 1378, 1280, 1256, 1223, 1147, 1108, 1002, 913, 861, 809, 738, 717, 701, 667, 535, 506, 438 cm⁻¹. **Solubility:** DMSO. μ_{eff} : 2.17 B.M. $\lambda_{\text{max}}(\text{Nujol})$: $\lambda_{\text{d-d}} = 621$ nm. $\lambda_{\text{max}}(\text{DMSO})$: $\lambda_{\text{d-d}} = 687$ nm, $\epsilon = 76.53$ dm³ mol⁻¹ cm⁻¹. $\Lambda_{\text{M}}(\text{DMSO})$: 0.93 cm² mol⁻¹.

E.6.3 Synthesis of copper(II) chloride salts of the simple benzimidazoles

In a typical synthesis the relevant benzimidazole (7.4 mmol) was added to a solution of $\text{CuCl}_2 \cdot 2\text{H}_2\text{O}$ (0.5 g, 3.7 mmol) in EtOH (50 cm^3) and the resulting suspension refluxed for 3 h. The product was filtered off, washed with water and ethanol, then air-dried.

E.6.3.1 $[\text{Cu}(\text{BZDH})_2(\text{H}_2\text{O})\text{Cl}]\text{Cl}$ (37)

Yield: 0.8719 g (62 %). **% Calc:** C, 43.26; H, 3.63; N, 14.51. **% Found:** C, 45.94; H, 3.39; N, 15.37. **IR (KBr):** 3432, 3198, 3144, 3112, 2980, 2909, 2836, 2559, 2361, 1776, 1623, 1596, 1491, 1463, 1421, 1364, 1303, 1272, 1248, 1198, 1138, 1110, 1009, 974, 929, 895, 884, 849, 777, 749, 634, 618, 549, 437, 425 cm^{-1} . **Solubility:** DMSO. μ_{eff} : 1.89 B.M. $\lambda_{\text{max}}(\text{Nujol}): \lambda_{\text{d-d}} = 709 \text{ nm}$. $\lambda_{\text{max}}(\text{DMSO}): \lambda_{\text{d-d}} = 874 \text{ nm}$, $\epsilon = 111.58 \text{ dm}^3 \text{ mol}^{-1} \text{ cm}^{-1}$. $\Lambda_{\text{M}}(\text{DMSO}): 17.35 \text{ S cm}^2 \text{ mol}^{-1}$.

E.6.3.2 $[\text{Cu}(5\text{-BZDHCOOH})_2(\text{H}_2\text{O})\text{Cl}]\text{Cl}$ (38)

Yield: 0.8529 g (48 %). **% Calc:** C, 40.31; H, 2.96; N, 11.75. **% Found:** C, 42.57; H, 2.73; N, 11.96. **IR(KBr):** 3433, 3207, 2706, 2653, 2598, 2547, 1924, 1770, 1704, 1627, 1596, 1504, 1466, 1425, 1414, 1364, 1312, 1245, 1130, 1195, 973, 955, 932, 896, 880, 823, 814, 777, 767, 750, 715, 684, 617, 591, 554, 448, 422 cm^{-1} . **Solubility:** DMSO. μ_{eff} : 2.04 B.M. $\lambda_{\text{max}}(\text{Nujol}): \lambda_{\text{d-d}} = 676 \text{ nm}$. $\lambda_{\text{max}}(\text{DMSO}): \lambda_{\text{d-d}} = 879 \text{ nm}$, $\epsilon = 137.52 \text{ dm}^3 \text{ mol}^{-1} \text{ cm}^{-1}$. $\Lambda_{\text{M}}(\text{DMSO}): 48.17 \text{ S cm}^2 \text{ mol}^{-1}$.

E.6.3.3 [Cu(2,5-Me₂BZDH)₂(H₂O)Cl]Cl (39)

Yield: 0.7695 g (49 %). **% Calc:** C, 48.60; H, 4.98; N, 12.59. **% Found:** C, 50.57; H, 4.70; N, 12.99. **IR (KBr):** 3440, 3268, 3037, 2918, 2861, 2498, 1850, 1633, 1602, 1543, 1471, 1409, 1309, 1290, 1251, 1229, 1147, 1057, 947, 873, 853, 754, 787, 670, 622, 552, 502, 446, 420, 411 cm⁻¹. **Solubility:** DMSO. μ_{eff} : 1.72 B.M. $\lambda_{\text{max}}(\text{Nujol})$: $\lambda_{\text{d-d}} = 726$ nm. $\lambda_{\text{max}}(\text{DMSO})$: $\lambda_{\text{d-d}} = 907$ nm, $\epsilon = 114.65$ dm³ mol⁻¹ cm⁻¹. $\Lambda_{\text{M}}(\text{DMSO})$: 17.9 S cm² mol⁻¹.

E.6.3.4 [Cu(6-NO₂BZDH)₂(H₂O)Cl]Cl (40)

Yield: 1.2616 g (74 %). **% Calc:** C, 35.12; H, 2.53; N, 17.55. **% Found:** C, 36.38; H, 2.18; N, 17.91. **IR (KBr):** 3398, 3153, 3118, 1798, 1628, 1597, 1538, 1496, 1472, 1452, 1406, 1380, 1337, 1303, 1256, 1189, 1135, 1117, 1070, 973, 894, 841, 819, 799, 755, 736, 699, 657, 600, 563, 542, 411, 422 cm⁻¹. **Solubility:** DMSO. μ_{eff} : 2.03 B.M. $\lambda_{\text{max}}(\text{Nujol})$: $\lambda_{\text{d-d}} = 689$ nm. $\lambda_{\text{max}}(\text{DMSO})$: $\lambda_{\text{d-d}} = 908$ nm, $\epsilon = 147.18$ dm³ mol⁻¹ cm⁻¹. $\Lambda_{\text{M}}(\text{DMSO})$: 24.0 S cm² mol⁻¹.

E.6.3.5 [Cu(2-PhBZDH)₂(H₂O)Cl]Cl (41)

Yield: 1.0883 g (85 %). **% Calc:** C, 57.73; H, 4.10; N, 10.36. **% Found:** C, 58.30; H, 4.42; N, 9.69. **IR (KBr):** 3442, 3150, 3062, 2973, 1625, 1600, 1541, 1483, 1464, 1451, 1417, 1321, 1286, 1229, 1150, 1129, 1075, 1043, 990, 921, 882, 818, 773, 760, 735, 695, 634, 556, 567, 756, 488, 429 cm⁻¹. **Solubility:** DMSO. μ_{eff} : 1.76 B.M. $\lambda_{\text{max}}(\text{Nujol})$: $\lambda_{\text{d-d}} = 909$ nm. $\lambda_{\text{max}}(\text{DMSO})$: $\lambda_{\text{d-d}} = 908$ nm, $\epsilon = 26.25$ dm³ mol⁻¹ cm⁻¹. $\Lambda_{\text{M}}(\text{DMSO})$: 22.1 S cm² mol⁻¹.

E.6.3.6 [Cu(5,6-Me₂BZDH)(H₂O)Cl₂] (42)

Yield: 0.2343 g (22 %). **% Calc:** C, 36.19; H, 4.05; N, 9.38 %. **Found:** C, 39.24; H, 3.67; N, 9.68. **IR (KBr):** 3383, 3133, 2971, 2941, 2861, 1622, 1592, 1505, 1474, 1440, 1392, 1334, 1310, 1267, 1251, 1204, 1166, 1146, 1085, 1006, 974, 857, 841, 681, 643, 571, 484, 447, 430 cm⁻¹. **Solubility:** DMSO. μ_{eff} : 1.85 B.M. $\lambda_{\text{max}}(\text{Nujol}): \lambda_{\text{d-d}} = 876$ nm. $\lambda_{\text{max}}(\text{DMSO}): \lambda_{\text{d-d}} = 847$ nm, $\varepsilon = 122.98$ dm³ mol⁻¹ cm⁻¹. $\Lambda_{\text{M}}(\text{DMSO}): 10.8$ S cm² mol⁻¹.

E.6.4 Synthesis of copper(II) chloride salts of the chelating benzimidazoles

E.6.4.1 [Cu(TBZH)₂Cl]Cl·2H₂O (43)

Yield: 1.2801g (60 %). **% Calc:** C, 41.92 H, 3.16; N, 14.66. **% Found:** C, 41.64; H, 3.03; N, 14.35. **IR (KBr):** 3470, 3188, 3090, 3074, 3043, 2830, 2755, 2687, 1626, 1596, 1480, 1464, 1429, 1286, 1232, 1207, 1182, 1146, 1117, 1014, 997, 936, 877, 761, 748, 730, 649, 635, 572, 486, 437 cm⁻¹. **Solubility:** DMSO μ_{eff} : 1.78 B.M. $\lambda_{\text{max}}(\text{Nujol}): \lambda_{\text{d-d}} = 716$ nm. $\lambda_{\text{max}}(\text{DMSO}): \lambda_{\text{d-d}} = 787$ nm, $\varepsilon = 131.2$ dm³ mol⁻¹ cm⁻¹. $\Lambda_{\text{M}}(\text{DMSO}): 20.01$ S cm² mol⁻¹.

E.6.4.2 [Cu(2-PyBZDH)₂Cl]Cl (44)

Yield: 1.2404 g (64 %). **% Calc:** C, 54.92; H, 3.46; N, 16.01. **% Found:** C, 54.80; H, 3.55; N, 15.83. **IR (KBr):** 3426, 3089, 3023, 2975, 2910, 2857, 2797, 2748, 2695, 2635, 2515, 1611, 1571, 1541, 1483, 1461, 1447, 1425, 1395, 1322, 1311, 1291, 1267, 1231, 1146, 1121, 1094, 1065, 1053, 1019, 987, 910, 851, 821, 796, 790, 771, 757, 742, 696, 685, 640, 633, 577, 561, 499, 429, 409 cm⁻¹. **Solubility:** DMSO. μ_{eff} : 1.86 B.M. $\lambda_{\text{max}}(\text{Nujol}): \lambda_{\text{d-d}} = 683 \text{ nm}$. $\lambda_{\text{max}}(\text{DMSO}): \lambda_{\text{d-d}} = 773 \text{ nm}$, $\epsilon = 160.73 \text{ dm}^3 \text{ mol}^{-1} \text{ cm}^{-1}$. $\Lambda_{\text{M}}(\text{DMSO}): 25.93 \text{ S cm}^2 \text{ mol}^{-1}$.

E.6.5 Synthesis of copper(II) sulfate salts of the simple benzimidazoles

In a typical synthesis the relevant benzimidazole (4 mmol) was added to a solution of CuSO₄·5H₂O (0.5 g, 2 mmol) in EtOH (50 cm³) and the resulting suspension refluxed for 3 h. The product was filtered off, washed with water and ethanol, then air-dried.

E.6.5.1 [Cu(BZDH)(H₂O)](SO₄) (45)

Yield: 0.3295 g (53 %). **% Calc:** C, 30.27; H, 2.17; N, 10.09. **% Found:** C, 30.00; H, 2.12; N, 9.23. **IR (KBr):** 3386, 3161, 3111, 2984, 2913, 2885, 2845, 1624, 1597, 1498, 1467, 1435, 1365, 1306, 1277, 1254, 1115, 1035, 1009, 973, 920, 884, 841, 824, 777, 744, 619, 438, 426 cm⁻¹. **Solubility:** DMSO. μ_{eff} : 1.81 B.M. $\lambda_{\text{max}}(\text{Nujol}): \lambda_{\text{d-d}} = 570 \text{ nm}$. $\lambda_{\text{max}}(\text{DMSO}): \lambda_{\text{d-d}} = 781 \text{ nm}$, $\epsilon = 143.53 \text{ dm}^3 \text{ mol}^{-1} \text{ cm}^{-1}$. $\Lambda_{\text{M}}(\text{DMSO}): 4.53 \text{ S cm}^2 \text{ mol}^{-1}$.

E.6.5.2 [Cu(5-BZDHCOOH)(H₂O)₂](SO₄).2H₂O (46)

Yield: 0.5873 g (74 %). **%Calc:** C, 24.46; H, 3.34; N, 7.13. **% Found:** C, 23.79; H, 3.38; N, 6.82. **IR (KBr):** 3207, 2456, 1910, 1776, 1667, 1624, 1588, 1487, 1456, 1412, 1385, 1363, 1308, 1290, 1241, 1133, 1104, 1019, 983, 954, 929, 890, 828, 809, 775, 754, 677, 621, 534, 479, 423, 407 cm⁻¹. **Solubility:** DMSO. μ_{eff} : 2.00 B.M. $\lambda_{\text{max}}(\text{Nujol})$: $\lambda_{\text{d-d}} = 673$ nm. $\lambda_{\text{max}}(\text{DMSO})$: $\lambda_{\text{d-d}} = 788$ nm, $\epsilon = 131.73 \text{ dm}^3 \text{ mol}^{-1} \text{ cm}^{-1}$. $\Lambda_{\text{M}}(\text{DMSO})$: $23.05 \text{ S cm}^2 \text{ mol}^{-1}$.

E.6.5.3 [Cu(2,5-Me₂BZDH)(H₂O)₂](SO₄) (47)

Yield: 0.4923 g (72 %). **%Calc:** C, 31.62; H, 4.13; N, 8.20. **% Found:** C, 29.78; H, 3.87; N, 8.13 **IR (KBr):** 3568, 3424, 3059, 1630, 1577, 1549, 1461, 1421, 1309, 1299, 1198, 1137, 1097, 1068, 992, 938, 878, 820, 804, 765, 677, 653, 635, 620, 481, 430 cm⁻¹. **Solubility:** DMSO. μ_{eff} : 1.88 B.M. $\lambda_{\text{max}}(\text{Nujol})$: $\lambda_{\text{d-d}} = 701$ nm. $\lambda_{\text{max}}(\text{DMSO})$: $\lambda_{\text{d-d}} = 792$ nm, $\epsilon = 155.1 \text{ dm}^3 \text{ mol}^{-1} \text{ cm}^{-1}$. $\Lambda_{\text{M}}(\text{DMSO})$: $3.23 \text{ S cm}^2 \text{ mol}^{-1}$.

E.6.5.4 [Cu(2-AmBZDH)₂(H₂O)₂](SO₄).2H₂O (48)

Yield: 0.8775 g (88 %). **% Calc:** C, 33.77; H, 4.45; N, 16.88. **% Found:** C, 34.35; H, 3.95; N, 15.81. **IR (KBr):** 3326, 3183, 2887, 2785, 1685, 1650, 1597, 1579, 1493, 1471, 1388, 1275, 1215, 1116 1011, 975, 912, 879, 842, 755, 739, 690, 619, 505, 428 cm⁻¹. **Solubility:** DMSO. μ_{eff} : 2.06 B.M. $\lambda_{\text{max}}(\text{Nujol})$: $\lambda_{\text{d-d}} = 624$ nm. $\lambda_{\text{max}}(\text{DMSO})$: $\lambda_{\text{d-d}} = 718$ nm, $\epsilon = 127.98 \text{ dm}^3 \text{ mol}^{-1} \text{ cm}^{-1}$. $\Lambda_{\text{M}}(\text{DMSO})$: $3.83 \text{ S cm}^2 \text{ mol}^{-1}$.

E.6.5.5 [Cu(6-NO₂BZDH)₂(H₂O)₂](SO₄) (49)

Yield: 0.8950 g (86 %). **%Calc:** C, 32.22; H, 2.70; N, 16.10. **% Found:** C, 32.41; H, 2.80; N, 15.78. **IR (KBr):** 3399, 3151, 3118, 2978, 2887, 1629, 1598, 1529, 1491, 1418, 1379, 1346, 1300, 1278, 1243, 1135, 1122, 1071, 1043, 980, 937, 895, 838, 797, 761, 737, 699, 620, 593, 539, 426 cm⁻¹. **Solubility:** DMSO. μ_{eff} : 1.81 B.M. $\lambda_{\text{max}}(\text{Nujol})$: $\lambda_{\text{d-d}} = 681$ nm. $\lambda_{\text{max}}(\text{DMSO})$: $\lambda_{\text{d-d}} = 778$ nm, $\varepsilon = 91.68 \text{ dm}^3 \text{ mol}^{-1} \text{ cm}^{-1}$. $\Lambda_{\text{M}}(\text{DMSO})$: 12.85 S cm² mol⁻¹.

E.6.6 Synthesis of copper(II) sulfate salts of the chelating benzimidazoles

E.6.6.1 [Cu(TBZH)₂](SO₄).EtOH (50)

Yield: 0.9842g (82 %). **% Calc:** C, 43.45; H, 3.31; N, 13.80. **% Found:** C, 43.19; H, 3.21; N, 13.40. **IR (KBr):** 3425, 3097, 3071, 2987, 2809, 2652, 2360, 2342, 1623, 1592, 1579, 1517, 1482, 1455, 1442, 1405, 1358, 1329, 1306, 1278, 1231, 1165, 1124, 1082, 1034, 1007, 991, 959, 935, 903, 874, 836, 770, 741, 669, 620, 600, 573, 537, 489, 434 cm⁻¹. **Solubility:** DMSO. μ_{eff} : 1.97 B.M.. $\lambda_{\text{max}}(\text{Nujol})$: $\lambda_{\text{d-d}} = 652$ nm. $\lambda_{\text{max}}(\text{DMSO})$: $\lambda_{\text{d-d}} = 726$ nm, $\varepsilon = 144.29 \text{ dm}^3 \text{ mol}^{-1} \text{ cm}^{-1}$. $\Lambda_{\text{M}}(\text{DMSO})$: 10.84 S cm² mol⁻¹.

E.7 SYNTHESIS OF SILVER(I) SALTS INCORPORATING BENZIMIDAZOLE LIGANDS

E.7.1 Synthesis of silver(I) nitrate salts of the simple and chelating benzimidazoles

In a typical synthesis a solution of AgNO_3 (0.45g, 2.5 mmol) in water (15 cm^3) was added to a suspension of the relevant benzimidazole (2.5 mmol) in EtOH (15 cm^3) and the resulting colourless suspension stirred for 3 h. The colourless product was filtered off, washed with water and ethanol, then air-dried.

E.7.1.1 $[\text{Ag}(\text{BZDH})_2](\text{NO}_3)$ (51)

Yield: 0.4823 g (48 %). **% Calc:** C, 41.40; H, 2.98; N, 17.24. **% Found:** C, 40.98; H, 2.9; N, 17.20. **IR (KBr):** 3441, 3148, 3114, 3096, 3061, 2969, 2864, 2801, 1898, 1772, 1623, 1599, 1588, 1494, 1478, 1459, 1438, 1410, 1384, 1365, 1303, 1274, 1247, 1203, 1135, 1107, 1005, 970, 959, 933, 887, 834, 825, 769, 752, 746, 728, 627, 608, 419 cm^{-1} .

Solubility: insoluble.

E.7.1.2 $[\text{Ag}(\text{5-BZDHCOOH})_2](\text{NO}_3)$ (52)

Yield: 0.5736 g (47 %). **% Calc:** C, 37.52; H, 2.76; N, 13.67. **% Found:** C, 36.97; H, 2.58; N, 13.62. **IR (KBr):** 3433, 3147, 3054, 2360, 2342, 1676, 1628, 1589, 1416, 1384, 1313, 1269, 1231, 1117, 1081, 1041, 966, 932, 884, 818, 773, 743, 718, 681, 668, 608, 591, 558, 417 cm^{-1} . **Solubility:** insoluble.

E.7.1.3 [Ag(2-PhBZDH)₂](NO₃) (53)

Yield: 0.5573 g (40 %). **% Calc:** C, 55.93; H, 3.61; N, 12.54. **% Found:** C, 55.29; H, 3.70; N, 12.74. **IR (KBr):** 3529, 3050, 2859, 2794, 1623, 1597, 1545, 1496, 1477, 1462, 1446, 1412, 1384, 1335, 1317, 1277, 1226, 1147, 1120, 1075, 1029, 1003, 982, 971, 925, 847, 827, 816, 776, 761, 745, 696, 633, 568, 477, 432 cm⁻¹. **Solubility:** insoluble.

E.7.1.4 [Ag(5,6-Me₂BZDH)₂](NO₃) (54)

Yield: 0.4602 g (58 %). **% Calc:** C, 46.77; H, 4.36; N, 15.15. **% Found:** C, 46.80; H, 4.26; N, 14.83. **IR (KBr):** 3446, 3146, 3027, 2963, 2925, 2858, 2762, 2645, 1635, 1591, 1477, 1447, 1384, 1306, 1265, 1237, 1159, 1130, 1082, 1024, 1000, 955, 864, 845, 781, 717, 641, 615, 568, 477, 442, 427 cm⁻¹. **Solubility:** insoluble.

E.7.1.5 [Ag(6-NO₂BZDH)](NO₃) (55)

Yield: 0.6198 g. (74 %) **% Calc:** C, 25.25; H, 1.51; N, 16.82. **% Found:** C, 25.51; H, 1.62; N, 16.72 **IR (KBr):** 3441, 3101, 2360, 1768, 1624, 1607, 1586, 1502, 1455, 1384, 1345, 1298, 1226, 1194, 1124, 1067, 946, 894, 882, 812, 795, 759, 735, 706, 634, 590, 546, 420 cm⁻¹. **Solubility:** insoluble.

E.7.1.6 [Ag(2-CIBZDH)](NO₃) (56)

Yield: 0.5063 g (60 %). **% Calc:** C, 28.56; H, 2.09; N, 12.49. **% Found:** C, 28.58; H, 2.01; N, 12.63. **IR (KBr):** 3435, 3099, 3028, 2894, 2765, 1767, 1623, 1596, 1538, 1464, 1449, 1403, 1384, 1334, 1280, 1223, 1147, 1049, 1001, 920, 850, 746, 705, 642, 628, 477, 438 cm⁻¹. **Solubility:** insoluble.

E.7.1.7 [Ag(TBZH)](NO₃) (57)

Yield: 0.6726 g (35 %). **% Calc:** C, 32.36; H, 1.90; N, 15.10. **% Found:** C, 32.71; H, 2.02; N, 15.43. **IR (KBr):** 3444, 3095, 3047, 2934, 2795, 2655, 1622, 1578, 1481, 1455, 1406, 1384, 1323, 1306, 1277, 1230, 1195, 1156, 1095, 1012, 987, 926, 903, 876, 824, 767, 739, 652, 635, 617, 570, 536, 489, 433 cm⁻¹. **Solubility:** insoluble.

E.7.2 Synthesis of silver(I) sulfate salts of the simple and chelating benzimidazoles

In a typical synthesis Ag_2SO_4 (0.2953g, 2.5 mmol) was added to a suspension of the relevant benzimidazole (2.5 mmol) in EtOH (20 cm^3) and the resulting suspension stirred for 3 h. The product was filtered off, washed with water and ethanol, then air-dried.

E.7.2.1 $[\text{Ag}_2(\text{BZDH})](\text{SO}_4)$ (58)

Yield: 0.8521 g (85 %). **% Calc:** C, 19.56; H, 1.41; N, 6.52. **% Found:** C, 20.16; H, 1.47; N, 6.45. **IR (KBr):** 3422, 3137, 3048, 2980, 2907, 2820, 1623, 1598, 1484, 1461, 1450, 1436, 1364, 1303, 1251, 1231, 1114, 1006, 974, 955, 884, 860, 776, 742, 727, 617, 426, 417 cm^{-1} . **Solubility:** insoluble.

E.7.2.2 $[\text{Ag}_2(2\text{-AmBZDH})](\text{SO}_4)$ (59)

Yield: 0.9967 g (90 %). **% Calc:** C, 18.89; H, 1.59; N, 9.44. **% Found:** C, 19.42; H, 1.50; N, 9.53. **IR (KBr):** 3384, 3194, 1647, 1591, 1561, 1489, 1468, 1385, 1323, 1276, 1215, 1119, 1072, 908, 734, 690, 618, 592, 503 cm^{-1} . **Solubility:** insoluble.

E.7.2.3 $[\text{Ag}_2(5\text{-BZDHCOOH})](\text{SO}_4)$ (60)

Yield: 0.3818 g (27 %). **% Calc:** C, 37.52; H, 2.76; N, 13.67. **% Found:** C, 37.42; H, 2.48; N, 13.62. **IR (KBr):** 3422, 3205, 3104, 3048, 2825, 1919, 1676, 1628, 1589, 1560, 1509, 1489, 1413, 1365, 1314, 1292, 1272, 1233, 1123, 1060, 966, 930, 890, 829, 772, 744, 682, 617, 591, 561, 534, 417 cm^{-1} . **Solubility:** insoluble.

E.7.2.4 [Ag₂(5,6-Me₂BZDH)](SO₄) (61)

Yield: 1.0679 g (94 %) % **Calc:** C, 23.60; H, 2.20; N, 6.12 % **Found:** C, 22.89; H, 2.09; N, 5.80 **IR (KBr):** 3424, 3115, 3023, 2964, 2935, 2859, 1636, 1593, 1489, 1474, 1446, 1410, 1386, 1339, 1311, 1269, 1239, 1119, 1066, 1001, 964, 842, 786, 616, 479, 444, 424 cm⁻¹ **Solubility:** insoluble.

E.7.2.5 [Ag₂(6-NO₂BZDH)](SO₄) (62)

Yield: 1.0419 g (88 %). % **Calc:** C, 17.70; H, 1.06; N, 8.94. % **Found:** C, 18.78; H, 1.06; N, 8.85. **IR (KBr):** 3385, 3111, 2968, 2820, 1626, 1600, 1522, 1474, 1420, 1404, 1380, 1347, 1299, 1273, 1235, 1116, 1066, 961, 884, 836, 824, 798, 760, 737, 693, 617, 590, 540, 427 cm⁻¹. **Solubility:** insoluble.

E.7.2.6 [Ag₂(2-PhBZDH)](SO₄) (63)

Yield: 0.9502 g (75 %). % **Calc:** C, 30.86; H, 1.99; N, 5.54. % **Found:** C, 32.17; H, 2.07; N, 5.68. **IR (KBr):** 3433, 3056, 3017, 2974, 2928, 2889, 2853, 2802, 2758, 2685, 2362, 1623, 1595, 1542, 1494, 1462, 1447, 1414, 1379, 1320, 1282, 1226, 1113, 1071, 1002, 969, 922, 902, 814, 773, 764, 742, 704, 691, 607, 561, 551, 483, 431 cm⁻¹. **Solubility:** insoluble.

E.7.2.7 [Ag₂(TBZH)](SO₄) (64)

Yield: 1.1611g (91 %). **% Calc:** C, 23.41; H, 1.38; N, 8.19. **% Found:** C, 24.04; H, 1.40; N, 8.09. **IR (KBr):** 3432, 3086, 2955, 2886, 2811, 2758, 2677, 2346, 1654, 1624, 1578, 1561, 1542, 1499, 1453, 1425, 1327, 1297, 1280, 1232, 1120, 1008, 992, 918, 903, 885, 832, 762, 742, 616, 550, 489, 435 cm⁻¹. **Solubility:** insoluble.

E.7.3 Synthesis of silver(I) acetate salts of the simple and chelating benzimidazoles

In a typical synthesis Ag(OAc) (0.4173g, 2.5 mmol) was added to a suspension of the relevant benzimidazole (2.5 mmol) in EtOH (20 cm³) and the resulting suspension stirred for 3 h. The product was filtered off, washed with water and ethanol, then air-dried.

E.7.3.1 {Ag(BZD)}_n (65)

Yield: 0.9891 g (90 %). **% Calc:** C, 37.37; H, 2.24; N, 12.45. **% Found:** C, 37.89; H, 2.33; N, 12.78. **IR (KBr):** 3457, 3072, 1751, 1636, 1609, 1463, 1453, 1384, 1364, 1300, 1239, 1204, 1145, 1113, 998, 910, 777, 742, 7345, 633, 554, 470, 426 cm⁻¹. **Solubility:** insoluble.

E.7.3.2 [Ag(5,6-Me₂BZDH)(OAc)] (66)

Yield: 0.4229 g (55 %). **% Calc:** C, 42.20; H, 4.18; N, 8.95. **% Found:** C, 42.89; H, 4.03; N, 8.48. **IR (KBr):** 3436, 3001, 1638, 1561, 1473, 1459, 1412, 1338, 1309, 1250, 1236, 1204, 1164, 1096, 991, 926, 849, 637, 488, 471, 431 cm⁻¹. **Solubility:** insoluble.

E.7.3.3 [Ag(5-BZDHCOOH)(OAc)] (67)

Yield: 0.6838 g (79 %). **% Calc:** C, 36.50; H, 2.76; N, 8.51. **% Found:** C, 36.53; H, 2.53; N, 8.00. **IR (KBr):** 3422, 3207, 2470, 1911, 1775, 1664, 1624, 1555, 1485, 1458, 1411, 1364, 1309, 1291, 1241, 1151, 1134, 1082, 1018, 955, 929, 890, 828, 776, 754, 738, 651, 622, 589, 534, 424, 409 cm⁻¹. **Solubility:** insoluble.

E.7.3.4 [Ag(2-AmbZDH)₂(OAc)] (68)

Yield: 0.3263 g (33 %). **% Calc:** C, 44.36; H, 3.96; N, 19.40. **% Found:** C, 42.32; H, 3.22; N, 21.95. **IR (KBr):** 3457, 3371, 3073, 3015, 2361, 2343, 1891, 1735, 1606, 1578, 1494, 1458, 1281, 1222, 1193, 1147, 1107, 1096, 1002, 912, 831, 738, 669, 584, 505, 438 cm⁻¹. **Solubility:** insoluble.

E.7.3.5 {Ag(TBZ)}_n (69)

Yield: 0.6726 g (45 %). **% Calc:** C, 38.98; H, 1.96; N, 13.64. **% Found:** C, 38.28; H, 1.94; N, 13.06. **IR (KBr):** 3444, 3095, 2934, 2795, 1622, 1606, 1578, 1481, 1472, 1455, 1406, 1384, 1306, 1277, 1230, 1195, 1095, 1012, 987, 903, 876, 824, 767, 739, 631, 617, 536, 489, 433 cm⁻¹. **Solubility:** insoluble.

E.8 HYDROGEN PEROXIDE DISPROPORTIONATION STUDIES

E.8.1 Hydrogen peroxide disproportionation by copper(II) complexes in the presence of added imidazole

Reactions were carried out at 25°C using the apparatus described in Figure 101. A weighed sample of the copper(II) complex (10 mg) and solid imidazole (50 mg) were added to the flask, aqueous H₂O₂ (35 % w/w, 10 cm³, 114 mmol) was then injected using a hypodermic syringe. The resulting mixture was stirred, and the O₂ evolved was measured as a function of time.

E.9 SUPEROXIDE DISMUTASE MIMETIC STUDIES

E.9.1 The modified nbt xanthine – xanthine oxidase assay

The O₂^{•-} dismutase activities of the metal complexes were assessed using a modified NBT assay with xanthine – xanthine oxidase used as the source of O₂^{•-}.

Nitro-blue-tetrazolium (NBT) was used as the detector molecule, and the reduction of NBT²⁻ to blue formazan (MF⁻) by O₂^{•-} was followed spectrophotometrically at 550 nm. Xanthine was used as the source of superoxide as it oxidizes aerobically in the presence of xanthine oxidase to form O₂^{•-} and urate.

The assay procedure was typically carried out as follows using double distilled water for all solutions:

Reaction mixtures contained 50 μM xanthine, 100 μM NBT, and 50 mM phosphate buffered saline (PBS) at pH 7.8 and at 25°C in a volume of 3 cm^3 . An amount of xanthine oxidase (in 20 μL) was added to give a change in absorbance at 550 nm of 0.025 / min, this corresponds to a flux of 1 μM $\text{O}_2^{\cdot-}$ / min. The concentration of the tested compound did not exceed 1 μM , therefore, a 0.1 mM concentration of tested solution was setup as shown in Table 56. Xanthine oxidase was added to start the $\text{O}_2^{\cdot-}$ flux and NBT reduction was measured in a thermostatically controlled UV-visible spectrophotometer (25°C) at 550 nm for 3 min. The tested compounds were checked to see if they reacted with NBT or caused an inhibition of xanthine oxidase. This was done by following the change of absorbance at 550 nm in the presence of 100 mM NBT and tested compound, and then by examining the conversion of xanthine to urate (in the absence of NBT) at 295 nm in the presence of tested compound.

Table 56: Assay volumes used in the determination of $\text{O}_2^{\cdot-}$ -dismutase activity

Tested compound (μl)	NBT reaction mixture (cm^3)	Water (μl)	Xanthine Oxidase (μl)
0	3	30	20
10	3	20	20
20	3	10	20
30	3	0	20

E.10 ANTIMICROBIAL SUSCEPTIBILITY TESTING

E.10.1 Biological preparations

Fungal Isolates: Isolates of *C. albicans* were obtained from Oxiod (ATCC 10231). Isolates were stored on Sabouraud dextrose agar (SDA) plates at 4°C and were subcultured monthly from the initial received.

Sterilisation was achieved by autoclaving at 121°C and 100 kPa for 15 min.

Cell density was measured using M^cFarland standards.

Sabouraud dextrose agar (SDA) was obtained from Difco (0109-17-1) and made up according to the manufacturers instructions.

Minimal Media: 2% glucose, 0.17% yeast nitrogen base without amino acids and 0.5% ammonium sulfate were dissolved in a Duran bottle with distilled water. The resulting solution was autoclaved and stored at 4°C.

E.10.2 Preparation of complex solutions for antimicrobial susceptibility testing

Tested complexes (0.1g) were ground to a fine powder and dissolved/suspended in 10 cm³ of pure DMSO. This solution was then added to 90 cm³ of water to yield a stock solution at a concentration of 1000 µg/cm³. Dilutions of the stock solution were prepared; 100 µg/cm³, 50 µg/cm³, 20 µg/cm³, 10 µg/cm³ and 5 µg/cm³.

E.10.3 Antimicrobial susceptibility testing method

Prior to testing yeast cells were grown for 24 h on SDA at 37°C. Cell suspensions were prepared in sterile PBS (5 cm³) to a density of 0.5 M^cFarland standard, yielding a final inoculum concentration of 3.5x10⁴ – 5.0x10⁵ cells cm⁻³. The prepared cell suspension (90 µl) was dispensed into microtitre plates and to this was added the test complex solution (10 µl) to yield working test complexes at concentrations of 100 µg/cm³, 50 µg/cm³, 20 µg/cm³, 10 µg/cm³, 5 µg/cm³ and 2.5 µg/cm³. Plates were then incubated for 24 h at 37°C with continuous shaking. Each complex was assessed in triplicate and three independent experiments were performed.

CONCLUSION

Copper(II) hydroxide reacted with salicylic acid (salH₂), acetylsalicylic acid (aspH), 3,5-diisopropylsalicylic acid (dipsH₂) and 3-methoxysalicylic acid (msalH₂) to yield [Cu(salH)₂(H₂O)₂] (1), [Cu₂(asp)₄(H₂O)₂]·H₂O (2), [Cu(dipsH)₂(H₂O)] (3) and the novel polymeric complex {Cu(msal)(H₂O)}_n (4) respectively.

When (1) and (2) were reacted with a series of simple benzimidazoles five new complexes were generated. The complex [Cu(salH)₂(BZDH)₂] (5) was characterised by X-ray crystallography which showed it to have a square planar geometry. The reactions of (1) and (2) with the chelating ligand thiabendazole resulted in the generation of (11). Complex (1) failed to react with 2-(2-pyridyl)benzimidazole however, (2) reacted with this ligand to produce complex (12).

Complex (3) reacted with the simple benzimidazoles to give four new species (13), (14), (15) and (16). Complexes (13) and (14) were characterised by X-ray crystallography and were shown to be isostructural to (5). The complex [Cu(5-BZDCOO)(H₂O)₂].EtOH (16) contained no salicylate anion however, it did contain the dianionic benzimidazole moiety 5-BZDCOO²⁻. Complex (17) was generated by a one pot reaction of 3,5-diisopropylsalicylic, copper(II) acetate and 2-aminobenzimidazole.

The reactions of {Cu(msal)(H₂O)}_n (4) with the benzimidazole ligands were not very successful a fact that may be related to the doubly deprotonated nature of the salicylate ligand. BZDH was the only non-chelating benzimidazole to react with it yielding complex (20). Attempts to carry out one pot reactions of 3-methoxysalicylic acid, with copper(II) acetate and the simple benzimidazole ligands were unsuccessful.

(4) reacted with the two chelating benzimidazoles TBZH and 2-PyBZDH to give two new complexes [Cu(msal)(TBZH)] (21) and [Cu(msal)(2-PyBZDH)] (22).

Complexes (1), (3) and (4) reacted with the chelating ligands 1,10-phenanthroline and 2,2'-bipyridine to generate the six complexes (23) – (28). Complex (27) was structurally characterised. Again the complex was found to adopt a square planar geometry.

Copper(II) acetate and the simple copper(II) salts, copper sulfate and copper chloride reacted with the benzimidazole ligands to yield the twenty one complexes (29) – (35) and (38) – (50). Complex (30) was characterised by X-ray crystallography and again was found to be isostructural to (5).

Attempts to react [Ag₂(salH)₂] with the benzimidazole ligands were unsuccessful. However, the benzimidazoles reacted readily with the silver(I) salts, silver nitrate, silver sulfate and silver acetate to yield 19 complexes. In the polymeric complexes (64) and (69) the benzimidazoles are present as anionic ligands.

All of the copper complexes generated during this study were examined for catalase mimetic activity. In the absence of added imidazole all of the complexes showed no activity and when the base was added the activity was very moderate.

All of the soluble copper(II) complexes were assessed for their ability to dismutate superoxide using the NBT assay. The complexes all showed excellent SOD mimetic activity with one unit of SOD activity arising from the range of 0.56 to 2.77 μM

aqueous solutions. Of the complexes tested the copper(II) sulfate complexes {(44) – (49)} were the most active.

Complexes (5), (23) and (30) exhibited anticancer activity comparable with that of cisplatin against three human derived cancer cell lines. These results suggest that it would be worthwhile screening all of the other SOD active complexes also.

The antifungal activity of complexes (1) – (69) was also examined against the pathogen *Candida albicans*. The copper(II) complexes were tested over a concentration range of 100 $\mu\text{g}/\text{cm}^3$ to 10 $\mu\text{g}/\text{cm}^3$. At the higher concentration the majority of the complexes exhibit very good activity towards the pathogen. As the concentration of the drug molecules is decreased their efficacy diminishes until finally at 10 $\mu\text{g}/\text{cm}^3$ most of them are either essentially inactive or exhibit moderate to poor anti-*Candida* properties. The photo-stable silver(I) benzimidazole complexes (51) – (69) were tested over a concentration range of 2 $\mu\text{g}/\text{cm}^3$ to 0.1 $\mu\text{g}/\text{cm}^3$ and found to be excellent antimycotic agents. These compounds will be screened for cytotoxicity and may have potential for application as topical anti-fungal agents.

REFERENCES

-
- ¹ J. Lee, *Concise Inorganic Chemistry*, 3rd edn., Van Nostrand Reinhold, UK, 1977.
- ² E. Hart, H. Steenbock, J. Waddell, C. Elvehjem, *J. Biol. Chem.*, 1928, **77**, 777.
- ³ J. Turnlund, K. Scott, G. Peiffer, A. Jang, W. Keyes, C. Keen and T. Sakanashi, *Am. J. Clin. Nutr.*, 1997, **65**, 72.
- ⁴ D. Winge and R. Mehra., *Int. Rev. Exp. Pathol.*, 1990, **31**, 47.
- ⁵ W. Klein, E. Mete and A. Price, *Arch. Inter. Med.*, 1972, **129**, 578.
- ⁶ D. Beshgetoor and M. Hambidge, *Am. J. Clin. Nutr.*, 1998, **67**, 1017.
- ⁷ F. Cotton and G. Wilkinson, *Advanced Inorganic Chemistry*, 5th edn., Wiley, 1988.
- ⁸ F. Odds, A. Brown and N. Gow, *Trends Microbiol.*, 2003, **11**, 272.
- ⁹ A. Groll, A. De Lucca and T. Walsh, *Trends Microbiol.*, 1998, **6**, 117.
- ¹⁰ M. Klepser, E. Ernst and M. Pfaller, *Trends Microbiol.*, 1997, **5**, 372.
- ¹¹ S. Wirsching, S. Michel, G. Kohler and J. Morschhauser, *J. Bacteriol.*, 2000, **182**, 400.
- ¹² C. Farah, R. Ashman and S. Challacombe, *Clinics in Dermatology*, 2000, **5**, 553.
- ¹³ N. Georgapapadakou and T. Walsh, *Antimicrob. Agents Chemother.*, 1996, **40**, 547.
- ¹⁴ N. Georgapapadakou, *Curr. Opin. Microbiol.*, 1998, **1**, 547.
- ¹⁵ A. Mastrolorenzo, A. Scozzafava and C. Supuran, *Euro J. Pharma Sci.*, 2000, **11**, 99.
- ¹⁶ G. McDonnell and A. Russell, *Clinical Microbiology Reviews*, 1999, 147.
- ¹⁷ H. Brown, A. Matzuk, I. Ilvues, L. Peterson, S. Harris, L. Sarett, J. Edgerton, J. Yaktis, W. Campell and A. Cuckler, *J. Am. Chem. Soc.*, 1961, **83**, 1764.
- ¹⁸ A. Baker, *J. Hosp. Pharm.*, 1972, **30**, 45.
- ¹⁹ P. Allen and D. Gottlieb, *J. App. Micro.*, 1970, **20**, 919.
- ²⁰ C. Kowala and J. Wunderlich, *Inorg. Chim. Acta.*, 1972, **7**, 331.
- ²¹ M. Devereux, M. McCann, D. O'Shea, R. Kelly, D. Egan, C. Deegan, K. Kavanagh, V. McKee and G. Finn, *J. Inorg. Biochem.*, 2004, **98**, 1023.
- ²² M. McCann, B. Coyle, J. Briody, F. Bass, N. O'Gorman, M. Devereux, K. Kavanagh and V. McKee, *Polyhedron*, 2003, **22**, 1595.
- ²³ S. Abuskhuna, J. Briody, M. McCann, M. Devereux, K. Kavanagh, J. Fontecha and V. McKee, *Polyhedron*, 2004, **23**, 1249.
- ²⁴ S. Abuskhuna, M. McCann, J. Briody, M. Devereux and V. McKee, *Polyhedron*, 2004, **23**, 1731.

-
- ²⁵ M. Geraghty, M. McCann, M. Devereux and V. McKee, *Inorg. Chim. Acta*, 1999, **293**, 160.
- ²⁶ M. Devereux a, M. McCann, V. Leon, M. Geraghty and V. McKee, J. Wikaira, *Polyhedron*, 2000, **19**, 1205.
- ²⁷ B. Coyle, M. McCann, K. Kavanagh, M. Devereux, V. McKee, N. Kayal, D. Egan, C. Deegan and G.J. Finn, *J. Inorg. Biochem.*, 2004, **98**, 1361.
- ²⁸ B. Coyle, P. Kinsella, M. McCann, M. Devereux, R. O'Connor, M. Clynes and K. Kavanagh, *Toxicol. in Vitro*, 2004, **18**, 63.
- ²⁹ B. Coyle, K. Kavanagh, M. McCann, M. Devereux and M. Geraghty, *Biometals*, 2004, **17**, 415.
- ³⁰ C. Deegan, M. McCann, M. Devereux, B. Coyle and D. Egan, *Biometals*, in press (manuscript No. BIOM-S-00055).
- ³¹ M. Valko, D. Leibfritz, J. Moncol, M.T.D. Cronin, M. Mazur and J. Telser, *Inter. J. Biochem. Cell Biol.*, (and references therein), 2007, **39**, 44.
- ³² J. McCord, *Science*, 1974, **185**, 529.
- ³³ J. McCord and S. Fridovich, *J. Biol. Chem.*, 1969, **244**, 6049.
- ³⁴ S. Liochev and S. Fridovich, *Redox Rep.*, 2002, **7**, 55.
- ³⁵ T. Rae, P. Schmidt, R. Pufahl and T. O'Halloran, *Science*, 1999, **284**, 805.
- ³⁶ C. Walling, *Accounts of Chemical Research*. 1975, **8**, 125.
- ³⁷ S. Henke, *Expert. Opin. Ther. Pat.*, 1999, **9**, 169.
- ³⁸ S. Goldstein, C. Michel, W. Bors, M. Saran and G. Czapski, *Free Radical Biol. and Med.*, 1998, **4**, 295.
- ³⁹ Y. Morgan, P. Turner, B. Kennedy, T. Hambley, P. Lay, J. Biffin, H. Regtop and B. Wrick, *Inorg. Chim. Acta*, 2001, **324**, 150.
- ⁴⁰ M. Baudry, S. Etienne, M. Palucki, E. Jascobsen and B. Malfroy, *Biochem. Biophys. Res. Comm.*, 1992, **192**, 964.
- ⁴¹ Z. Liao, X. Zheng, B. Luo, L. Shen, D. Li, H. Liu and W. Zhao, *Polyhedron*, 2001, **20**, 2813.
- ⁴² D. Riley, P. Lennon, W. Neumann, and R. Weiss, *J. Am. Chem. Soc.*, 1997, **119**, 6522.
- ⁴³ A. Fisher, S. Maxwell, and D. Naughton, *Biochem. Biophys. Res. Comm.*, 2004, **316**, 48.

-
- ⁴⁴ Z. Durackova, J. Labuda, *J. Inorg. Biochem.*, 1995, **58**, 297.
- ⁴⁵ M. Younes, U. Weser, *FEBS Lett.*, 1976, **61**, 209.
- ⁴⁶ F. Sączewski, E. Dziemidowicz-Borys, P.J. Bednarski, R. Grünert, M. Gdaniec and P. Tabin, *J. Inorg. Biochem.*, 2006, **8**, 1389.
- ⁴⁷ M. Devereux, D. O' Shea, A. Kellett, M. McCann, M. Walsh, D. Egan, C. Deegan, K. Kędziora, G. Rosair and H. Müller-Bunz, *J. Inorg. Biochem.*, 2007, **101**, 881.
- ⁴⁸ C. Young and S. Lippard, *J. Am. Chem. Soc.*, 1980, **102**, 4920.
- ⁴⁹ U. Weser, C. Richter, A. Wendel and M. Younes, *Bioinorg. Chem.*, 1978, **8**, 201.
- ⁵⁰ A. Abuhijleh and C. Woods, *Inorg. Chem. Commun.*, 2002, **5**, 269.
- ⁵¹ U. Weser, K. Sellinger, E. Lengfelder, W. Werner and J. Strahle, *Biochem. Biophys. Acta*, 1984, **91**, 285.
- ⁵² C. Dillon, T. Hambbley, B. Kennedy, P. Lay, Q. Zhou, N. Davies, J. Biffin and H. Regtop, *Chem. Res. Toxicol.*, 2003, **16**, 28.
- ⁵³ D. Demertzi, A. Galani, M. Demertzis, S. Skoulika and C. Kotoglou, *J. Inorg. Biochem.*, 2004, **98**, 358.
- ⁵⁴ A. Bury, A. Underhill, D. Kemp J. Smith P. Gomm, *Inorg. Chim. Acta*, 1988, **138**, 85.
- ⁵⁵ D. Jay, E. Jay and M. Medina, *Archives of Medical Research*, 1999, **30**, 93.
- ⁵⁶ C. Marzano, A. Trevisan, L. Giovagnini and D. Fregonal, *Toxicol. In Vitro*, 2002, **16**, 413.
- ⁵⁷ P.S. Fricker, *Metal Compounds in Cancer Therapy*, Chapman and Hall, London, 1994.
- ⁵⁸ Editorial, *Critical reviews in Oncology*, 2002, **42**, 1.
- ⁵⁹ M. Mates, *Toxicology*, 2000, **153**, 83.
- ⁶⁰ B. Thati, A. Noble, B. Creaven, M. Walsh, M. McCann, K. Kavanagh, M. Devereux, D. Egan, *Cancer Lett.*, 2007, **250**, 128.
- ⁶¹ L. Parks and W. Casey, *Am. Rev. Microbiol.*, 1995, **49**, 95.
- ⁶² C. Deegan, M. McCann, M. Devereux, B. Coyle and D. Egan, *Cancer Lett.*, 2007, **247**, 224.
- ⁶³ C. Deegan, B. Coyle, M. McCann, M. Devereux and D. Egan, *Chemico-Biological Interactions*, 2006, **164**, 115.
- ⁶⁴ H. Robins, H. Stoerk and O. Graesle, *Toxicol. Appl. Pharmacol.*, 1965, **7**, 55.

-
- ⁶⁵ C. Tomlin, *The Pesticide Manual*, 10th ed., Crop Protection Publications The Royal Society of Chemistry, 1994, 972.
- ⁶⁶ R. Mehrotra and R. Bohra, *Metal Carboxylates*, Academic Press, London, 1983.
- ⁶⁷ R. Reardon, W. Tolman and S. Lippard, *New J. Chem.*, 1991, **15**, 417.
- ⁶⁸ X. Chen, Z. Xu, X. Yu and T. Mak, *Polyhedron*, 1994, **13**, 2079.
- ⁶⁹ A. Carvill, *Ph.D. Thesis*, National University of Ireland, 1992.
- ⁷⁰ M. Devereux, M. McCann, M. Casey, M. Curran, G. Ferguson, C. Cardin, M. Convery and V. Quillet, *J. Chem. Soc., Dalton Trans.*, 1995, 771.
- ⁷¹ G. Deacon and R. Phillips, *Coord. Chem. Rev.*, 1980, **33**, 227.
- ⁷² K. Nakamoto, *Infrared and Raman Spectra of Inorganic and Coordination Compounds*, 5th edition, John Wiley and Sons, 1997.
- ⁷³ P. Guinan, M. McCann and H. Ryan, *Polyhedron*, 1992, **11**, 205.
- ⁷⁴ W. Bryska, A. Krol and B. Brandel, *Polish J. Chem.*, 1992, **66**, 587.
- ⁷⁵ A. Ross, *Virology*, 1961, **14**, 340.
- ⁷⁶ G. Morgan, *Gut*, 1996, **38**, 646.
- ⁷⁷ B. Bellosillo, *Blood*, 1998, **92**, 1406.
- ⁷⁸ B. Amborabe, P. Lessard J. Chollet and G. Roblin, *Plant Physiol. Biochem.*, 2002, **40**, 1051.
- ⁷⁹ J. Sorenson, *Metal Ions In Biological Systems*, 1982, **14**, Marcel-Dekker Inc., New York.
- ⁸⁰ M. Chenoworth, *Pharmacol. Revs.*, 1956, **8**, 57.
- ⁸¹ J. Sorenson, *J. Med. Chem.*, 1984, **27**, 1747.
- ⁸² J. Sorenson, *Prog. Med. Chem.*, 1978, 1541.
- ⁸³ F. Hanic and J. Michalov, *Acta Crystallogr.*, 1959, **13**, 299.
- ⁸⁴ J. Ploquin, *Bull. Soc. Chim. Fr.*, 1951, 757.
- ⁸⁵ M. Inoue, M. Kishita, M. Kubo, *Inorg. Chem.*, 1964, **3**, 239.
- ⁸⁶ K. Yoneda, K. Uchiyama, B. Boettcher and Y. Inouye, *Bull. Chem. Soc. Jpn.*, 1993, **66**, 3815.
- ⁸⁷ G. Morgant, H. Dung, J. Daran, B. Viossat, X. Labouze, M. Roch-Arveiller, F. Greenway, W. Cordes, J. Sorenson, *J. Inorg. Biochem*, 2000, **81**, 11.
- ⁸⁸ D. Valigura, M. Melnik, M. Koman, L. Martiška, M. Korabik, J. Mrozinski and T. Glowiak, *Inorg. Chem. Commun.*, 2004, **7**, 548.

-
- ⁸⁹ A. Abuhijleh and C. Woods, *Inorg. Chem. Commun.*, 2002, **5**, 269.
- ⁹⁰ A. Abuhijleh and C. Woods, *Inorg. Chem. Commun.*, 2001, **4**, 119.
- ⁹¹ M. Geraghty, V. Sheridan, M. McCann, M. Devereux and V. McKee, *Polyhedron*, 1999, **18**, 2931.
- ⁹² N. Palanisami, G. Prabusankar and R. Murugavel, *Inorg. Chem. Commun.*, 2006, **9**, 1002.
- ⁹³ M. Devereux, M. Curran, M. McCann and M. Casey, 1996, *Polyhedron*, **15**, 2029.
- ⁹⁴ P. Lemoine, B. Viossat, G. Morgant, A. Tomas and J. Sorenson, *J. Inorg. Biochem.*, 2002, **89**, 18.
- ⁹⁵ L. Zhu and G. Cai, *Chin. J. Chem.*, 2002, **20**, 990.
- ⁹⁶ J. Ranford, P. Sadler and D. Tocher, *J. Chem. Soc. Dalton Trans.*, 1993, 3393.
- ⁹⁷ B. Coyle, M. McCann, K. Kavanagh, M. Devereux, V. McKee, N. Kayal, D. Egan, C. Deegan and G. Finn, *J. Inorg. Biochem.*, 2004, **98**, 1361.
- ⁹⁸ R. Rowan, T. Tallon, A. Sheahan, R. Curran, M. McCann, K. Kavanagh, M. Devereux and V. McKee, *Polyhedron*, 2006, **25**, 1771.
- ⁹⁹ S. Podunavac-Kuzmonovic, L. Leovac, N. Perisic-Janjic, J. Rogan and J. Balaz, *J. Serb. Chem. Soc.*, 1999, **64**, 381.
- ¹⁰⁰ I. Ahuja and I. Prasad, *Inorg. Nucl. Chem. Lett.*, 1976, **12**, 777.
- ¹⁰¹ M. Pujar, T. Bharamgoudar and N. Sathyanarayana, *Trans. Met. Chem.*, 1988, **13**, 423.
- ¹⁰² C. Piguet, B. Bocquet, F. Müller and A.F. Williams, *Helv. Chim. Acta*, 1989, **72**, 323.
- ¹⁰³ B. Bocquet, C. Piguet, F. Müller and A.F. Williams, *Helv. Chim. Acta*, 1993, **76**, 372.
- ¹⁰⁴ E. Bouwmann, W. Driessen and J. Reedijk, *Coord. Chem. Rev.*, 1990, **104**, 143.
- ¹⁰⁵ J. El-On, *Acta Tropica*, 2003, **85**, 243.
- ¹⁰⁶ Wikipedia, online encyclopedia, <http://en.wikipedia.org/wiki/Echinococcosis>.
- ¹⁰⁷ U. Sheth, *Prog. Drug Res.*, 1975, **19**, 147.
- ¹⁰⁸ E. Lacey, *Int. J. Parasitol.*, 1988, **18**, 885.
- ¹⁰⁹ E. Lacey, J. Gill, *Acta Tropica*, 1994, 245.
- ¹¹⁰ M. Roos, *Parasitol. Today*, 1995, **11**, 148.
- ¹¹¹ E. Lacey, K. Snowdown, *Vet. Parasitol.*, 1988, **27**, 309.

-
- ¹¹² I. Tamm, K. Folkers and F. Horsfall, *Yale J. Biol. Med.*, 1952, **24**, 559.
- ¹¹³ C. Xia, C. Lu, X. Wu, L. Chen, Q. Zhang, J. Zhang, and D. Wu, *Inorg. Chim. Acta*, 2006, **359**, 4639.
- ¹¹⁴ E. Şahin, S. İde, M. Kurt, Ş. Yurdakul, *J. Mol. Struct.*, 2002, **616**, 259.
- ¹¹⁵ M. Goodgame, L. Haines, *J. Chem. Soc.*, 1966, (A), 174.
- ¹¹⁶ K. Müller-Buschaum and C. Quitmann, *Inorg. Chem.*, 2003, **42**, 2742.
- ¹¹⁷ J. Grevy, F. Tellez, S. Bernes, H. Noth, R. Contreras and N. Behrens *Inorg. Chim. Acta*, 2002, **339**, 532.
- ¹¹⁸ M. Devereux, M. McCann, D. O'Shea, R. Kelly, D. Egan, C. Deegan, K. Kavanagh, V. McKee and G. Finn, *J. Inorg. Biochem.*, 2004, **98**, 1023.
- ¹¹⁹ T. Wu, D. Li, X. Feng and J. Cai, *Inorg. Chem. Commun.*, 2003, **6**, 886.
- ¹²⁰ C. Su, X. Yang, S. Liao T. Mak and B. Kang, *Inorg. Chem. Commun.*, 1999, **2**, 383.
- ¹²¹ C. Xia, C. Lu, X. Wu, Q. Zhang J. Zhang and D. Wu, *Polyhedron*, 2007, **26**, 941.
- ¹²² B. Visossat, J. Daran, G. Savouret, G. Morgant, F. Greenway, N. Dung, V. Pham-Tran, J. Sorenson, *J. Inorg. Biochem.*, 2003, **96**, 375.
- ¹²³ G. G. Mohamed, *Spectrochim. Acta (Part A)*, 2001, **57**, 411.
- ¹²⁴ D. O' Shea, *Ph.D. Thesis*, Dublin Institute of Technology, Dublin, Ireland, 2004.
- ¹²⁵ M.T. Casey, M. McCann, M. Devereux, M. Curran, C. Cardin, M. Convery, V. Quillet and C. Harding, *J. Chem. Soc., Chem. Commun.*, 1994, 2643.
- ¹²⁶ J.D. Scandalis(Ed), *Oxidative Stress and the Molecular Biology of Antioxidant*
- ¹²⁷ S.M. Cardoso, C. Pereira, C.R. Oliveira, *Biochem. Biophys. Res. Commun.*, 1998, **83**, 246.
- ¹²⁸ M. Mates, *Toxicology*, 2000, **153**, 83.
- ¹²⁹ D.M. Miller, G.R. Buettner, S.D. Aust, *Free, Radic. Biol. Med.*, 1990, **8**, 95.
- ¹³⁰ P. Huang, L. Feng, E.A. Oldam, M.J. Keating W. Plunkett, *Nature*, 2000, **407**, 390.
- ¹³¹ L.W. Oberley, *Antioxid. Redox Signalling*, 2001, **3**.
- ¹³² C. Muscoli, S. Cuzzocrea, D. Riley, J. L. Zweier, C. Thiemerman-Salvemini, *Brit. J. Pharmacol.*, 2003, **140**, 445.
- ¹³³ C.J. Darby Weydert, B.B. Smith, L. Xu, K.C. Kregel, J.M. Ritchie, C.S. Davis, L.W. Oberley, *Free Radic. Biol. Med.*, 2003, **34**, 316.

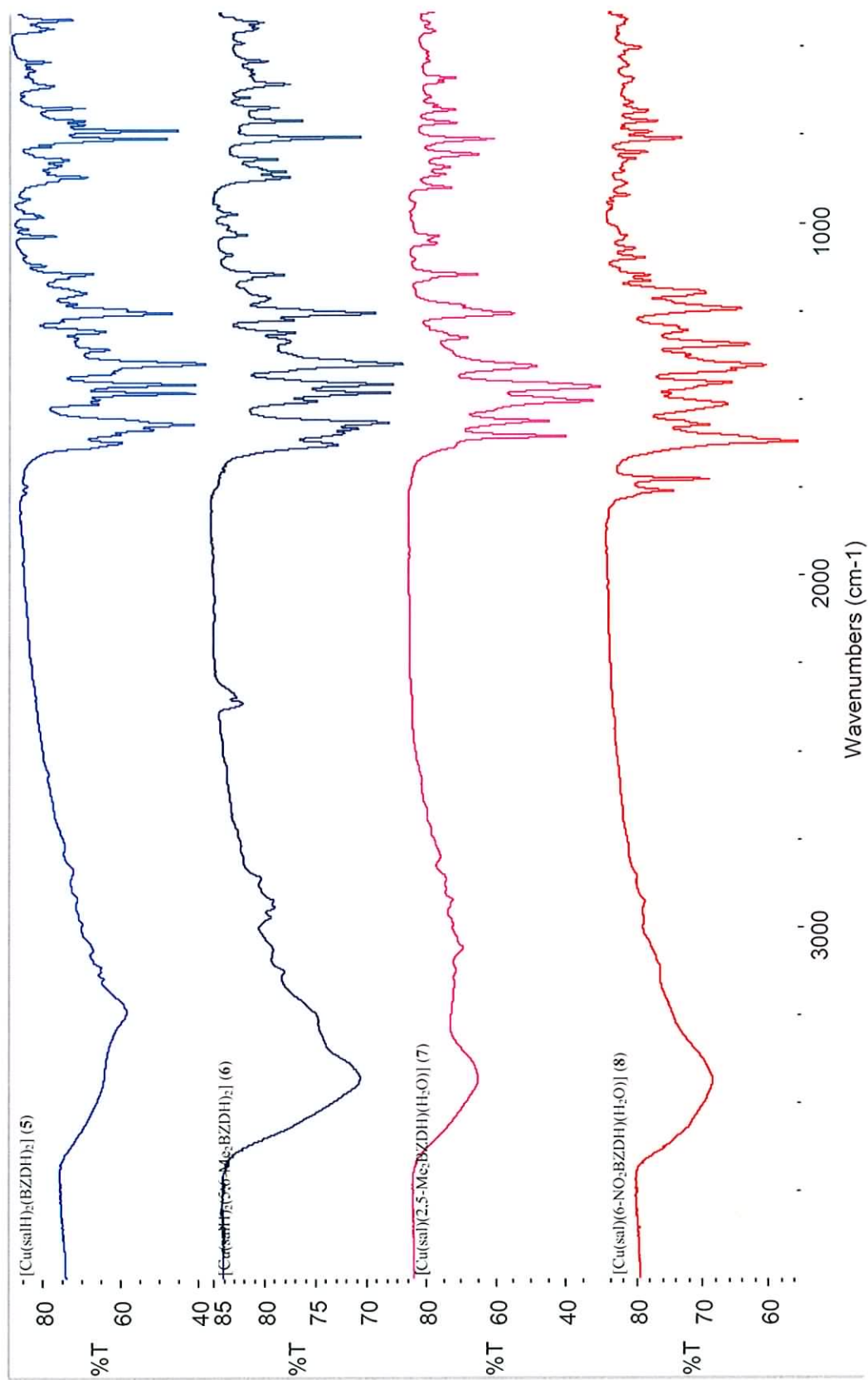
-
- ¹³⁴ E.W.N. Lam, H.M. Hammand, R. Zwacka, C.J. Darby K.R. Baumgardner, B.L. Davidson, T.D. Oberley, J. F. Engelhardt , L.W. Oberley, *Cancer Res.*, 1997, **57**, 5550.
- ¹³⁵ C.J. Weydert, T.A. Waugh, J.M. Ritchie, K.S. Iyer, J.L. Smith, L. Li, D.R. Spitz, L.W. Oberley, *Free Radic. Biol. Med.*, 2006, **41**, 226.
- ¹³⁶ J. Kaiser, R. Csonka, G. Speier, M. Giorgi, M. Reglier, *J. Mol. Catal. A: Chem.* 2005, **236**, 12.
- ¹³⁷ J. Kaiser, T. Csay, G. Speier, M. Reglier, M. Giorgi, *Inorg. Chem. Commun.*, 2006, **9**, 1037.
- ¹³⁸ M. Devereux, M. McCann, D. O Shea, R. Kelly, D. Egan, C. Deegan, V. McKee, *J. Inorg. Biochem.*, 2004, **98**, 1023.
- ¹³⁹ M. Devereux, M. McCann, D. O Shea, M. O Connor, E. Kiely, V. McKee, D. Naughton, A. Fisher, A. Kellett, M. Walsh, D. Egan, C. Deegan, *Bioinorganic Chemistry and Applications*, 2006, Article ID: 80283.
- ¹⁴⁰ A. Kellett, *Ph.D. Thesis*, The Institute of Technology Tallaght Dublin, Ireland, 2006.
- ¹⁴¹ B. Coyle, P. Kinsella, M. McCann, M. Devereux, R. O'Connor, M. Clynes, K. Kavanagh, *Toxicol. In Vitro*, 2004, **18**, 63.
- ¹⁴² M.T. Casey, M. McCann, M. Devereux, M. Curran, C. Cardin, M. Convery, V. Quillet, C. Harding, *J. Chem. Soc., Chem. Commun.*, 1994, 2643.
- ¹⁴³ M. Devereux, M. McCann, V. Leon, V. McKee, R.J. Ball, *Polyhedron*, 2002, **21** 1063.
- ¹⁴⁴ M. Devereux, M. McCann, M.T. Casey, M. Curran, *International Patent*, 1994, IPA No. S940892.
- ¹⁴⁵ Y. Naruta and K. Maruyama, *J. Chem. Soc., Chem. Comm.*, 1994, 2667.
- ¹⁴⁶ M. Curan, *Ph.D. Thesis*, National University of Ireland, 1996.
- ¹⁴⁷ S. Goldstein, G. Czapski, Superoxide Dismutase. In: PUNCHARD N. A. and KELLY F. J., Eds., *Free Radicals-A practical approach*. Oxford University Press, UK, 252 (1996).
- ¹⁴⁸ U. Weser, K.H. Sellenger, E. Lengfelder, W. Werner and J Strähle, *Biochimica et Biophysica Acta*, 1980, **631**, 232.

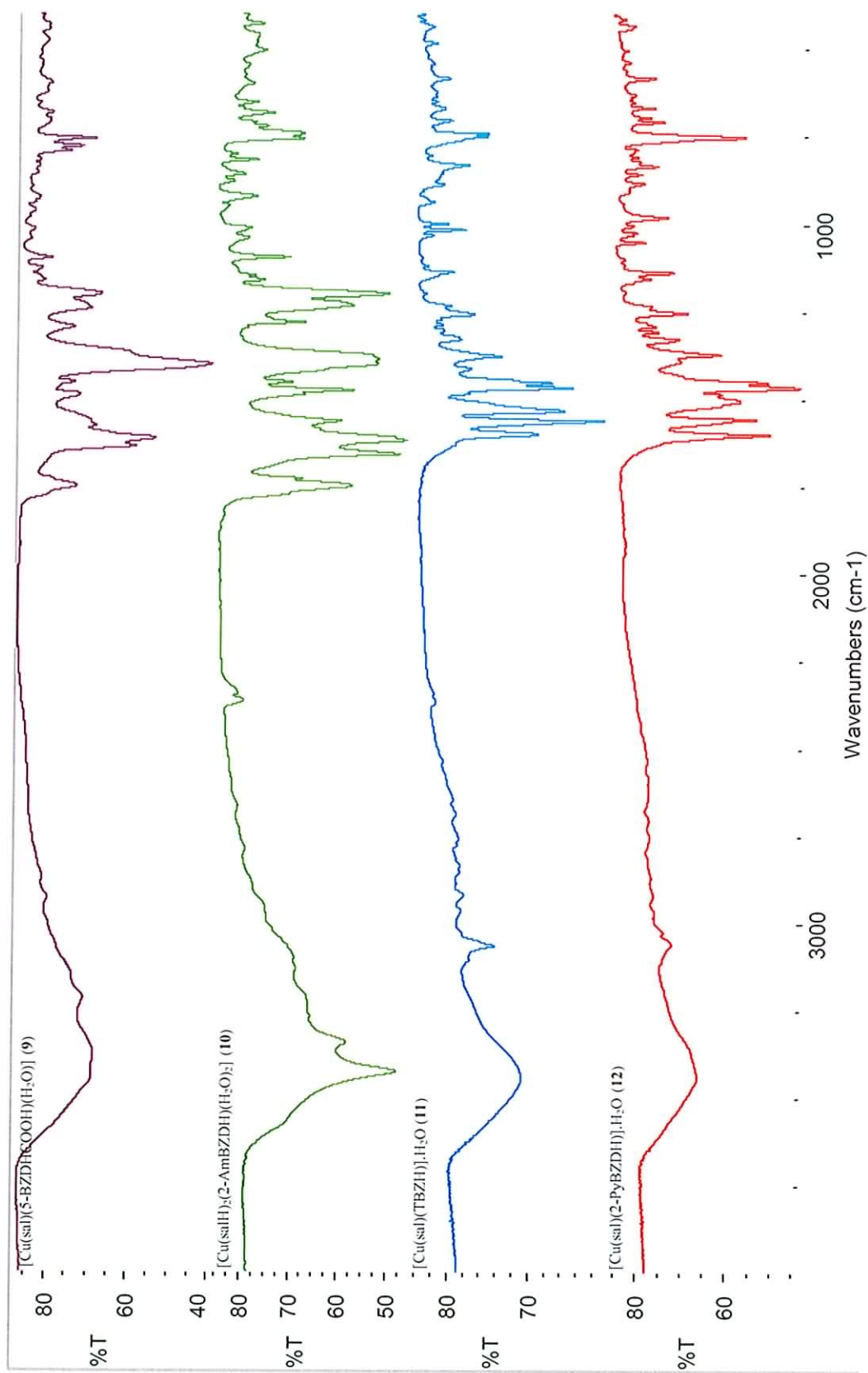
-
- ¹⁴⁹ J.F. Weder, C.T. Dillon, T.W. Hambley, B.J. Kennedy, P.A. Lay, J.R. Biffin, H.L. Regtop, N.M. Davies, *Coord. Chem. Rev.*, 2002, **232**, 95.
- ¹⁵⁰ IVS Annual; MIMS Publishing, Crows Nest, NSW, Sydney, 1997, p. 145, 276.
- ¹⁵¹ J. Weder, T. Hambley, B. Kennedy, P. Lay, D. Maclachlan, R. Brambley, C. Delfs, K. Murray, B. Moubaraki, B. Warick, J. Biffin and H. Regtop, *Inorg. Chem.*, 1999, **38**, 1736.
- ¹⁵² A. Abuhijleb, *J. Inorg. Biochem.*, 1997, **689**, 167.
- ¹⁵³ Z. Durackova, J. Labuda, *J. Inorg. Biochem.*, 1995, **58**, 297.
- ¹⁵⁴ Z. Travnycek, M. Malon, Z. Sindelar, K. Dolezal, J. Rolcik, V. Krystof, M. Strnad and J. Marek, *J. Inorg. Biochem.*, 2001, **84**, 23.
- ¹⁵⁵ M. Belichi-Ferrari, S. Capacchi, G. Pelosi, G. Reffo, P. Tarasconi, R. Albertini, S. Pinelli and P. Lunghi, *Inorg. Chim. Acta*, 1999, **286**, 134.
- ¹⁵⁶ C.P. Raptopoulou, S. Paschalidou, A.A. Pantazaki, A. Terzis, S.P. Perlepes, T. Lialiaris, E.G. Bakalbassis, J. Mrozinski and D.A. Kyriakidis, *J. Inorg. Biochem.*, 1998, **71**, 15.
- ¹⁵⁷ J.A. Khanam, S.P. Bag, B. Sur and P. Sur, *Indian J. Pharmacol.*, 1997, **29**, 157.
- ¹⁵⁸ C.X. Zhang and S.J. Lippard, *Curr. Opin. Chem. Biol.*, 2003, **7**, 481.
- ¹⁵⁹ I. Gracia-Mora, L. Ruiz-Ramirez, C. Gomez-Ruiz, M. Tinoco-Mendez, A. Marquez-Quinones, L. Romero de Lira, A. Marin-Hernandez, L. Masias-Rosales and M.E. Bravo-Gomez, *Metal Based Drugs*, 2002, **8**, 19.
- ¹⁶⁰ A. De Vizcaya-Ruiz, A. Rivero-Mueller, L. Ruiz-Ramirez, G.E.N. Kass, L.R. Kelland, R.M. Or and M. Dobrota, *Toxicol. In Vitro*, 2000, **14**, 1.
- ¹⁶¹ B. Coyle, P. Kinsella, M. McCann, M. Devereux, R. O'Connor, M. Clynes, K. Kavanagh, *Toxicol. In Vitro*, 2004, **18**, 63.
- ¹⁶² B. Coyle, K. Kavanagh, M. McCann, M. Devereux, M. Geraghty, *Biometals*, 2003, **16**, 321.
- ¹⁶³ A. Marin-Hernandez, I. Gracia-Mora, L. Ruiz-Ramirez and R. Moreno-Sanchez, *Biochem. Pharmacol.*, 2003, **65**, 1979.
- ¹⁶⁴ T. Hirohama, Y. Kuranuki, E. Ebina, T. Sugizaki, H. Arii, M. Chikira, P.T. Selvi, M. Palaniandavar, *J. Inorg. Biochem.*, 2005, **99**, 1205.
- ¹⁶⁵ R. S. So, A. A. Adjei, *J. Clin. Oncol.*, 1999, **17**, 409.
- ¹⁶⁶ B. Rosenberg, *Metal Ions Biol. Syst.*, 1980, **11**, 127.

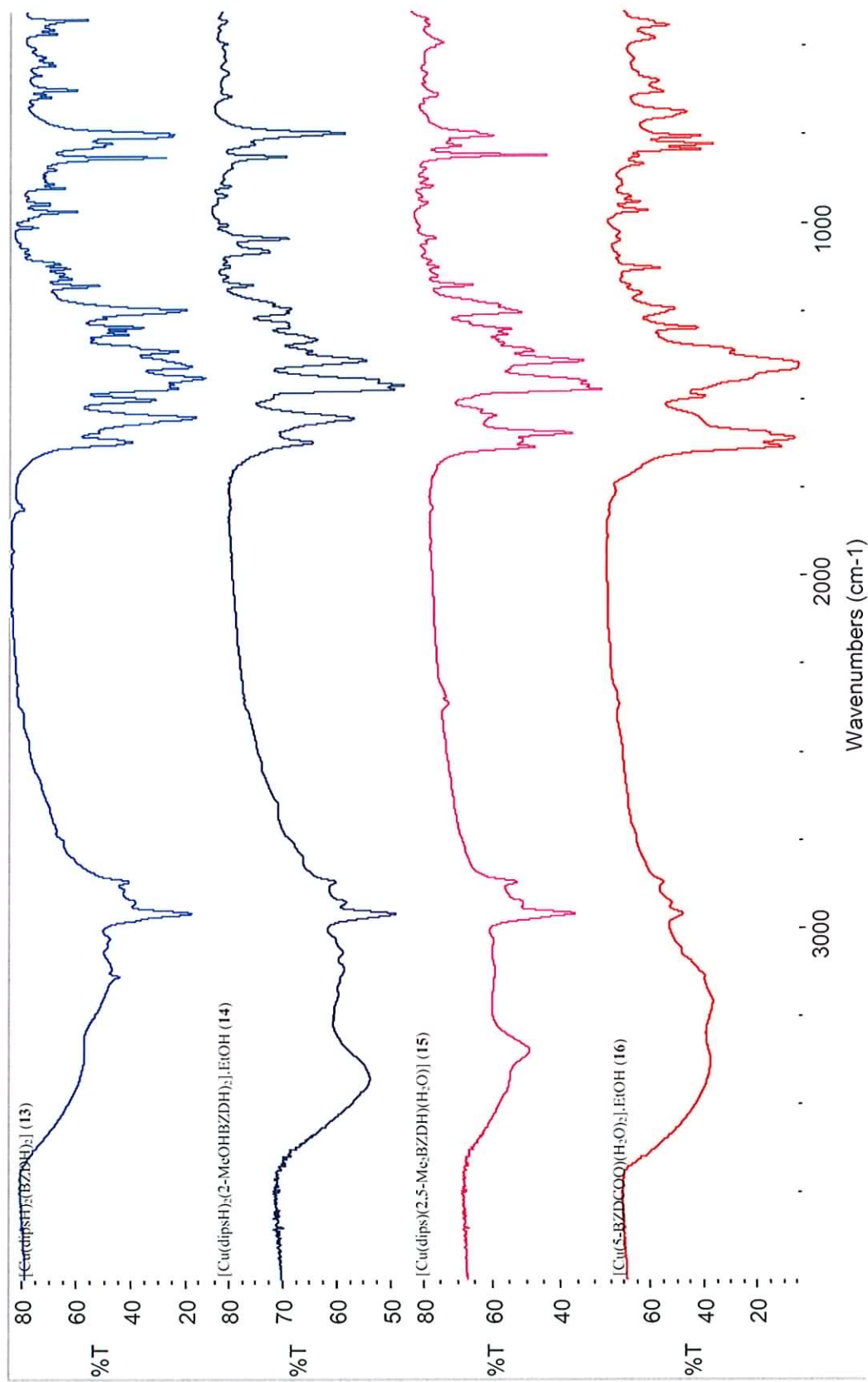
¹⁶⁷ T. Hirohama, Y. Kuranuki, E. Ebina, T. Sugizaki, H. Arai, M. Chikira, P.T. Selvi, M. Palaniandavar, *J. Inorg. Biochem.*, 2005, **99**, 1205.

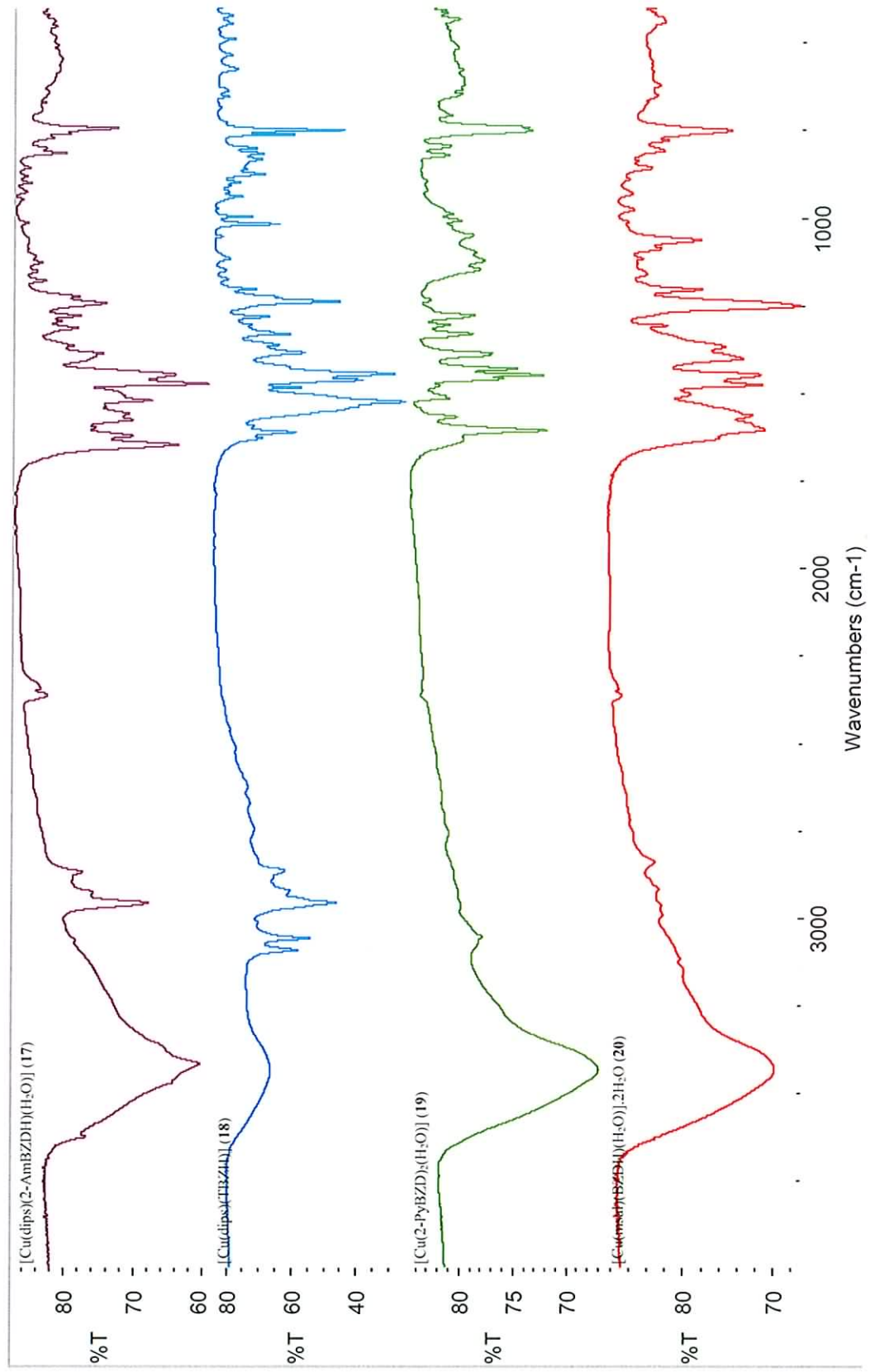
¹⁶⁸ A. Rivero-Müller, A. De Vizcaya-Ruiz, N. Plant, L. Ruiz, M. Dobrota, *Chemico-Biological Interactions*, 2007, **165**, 189.

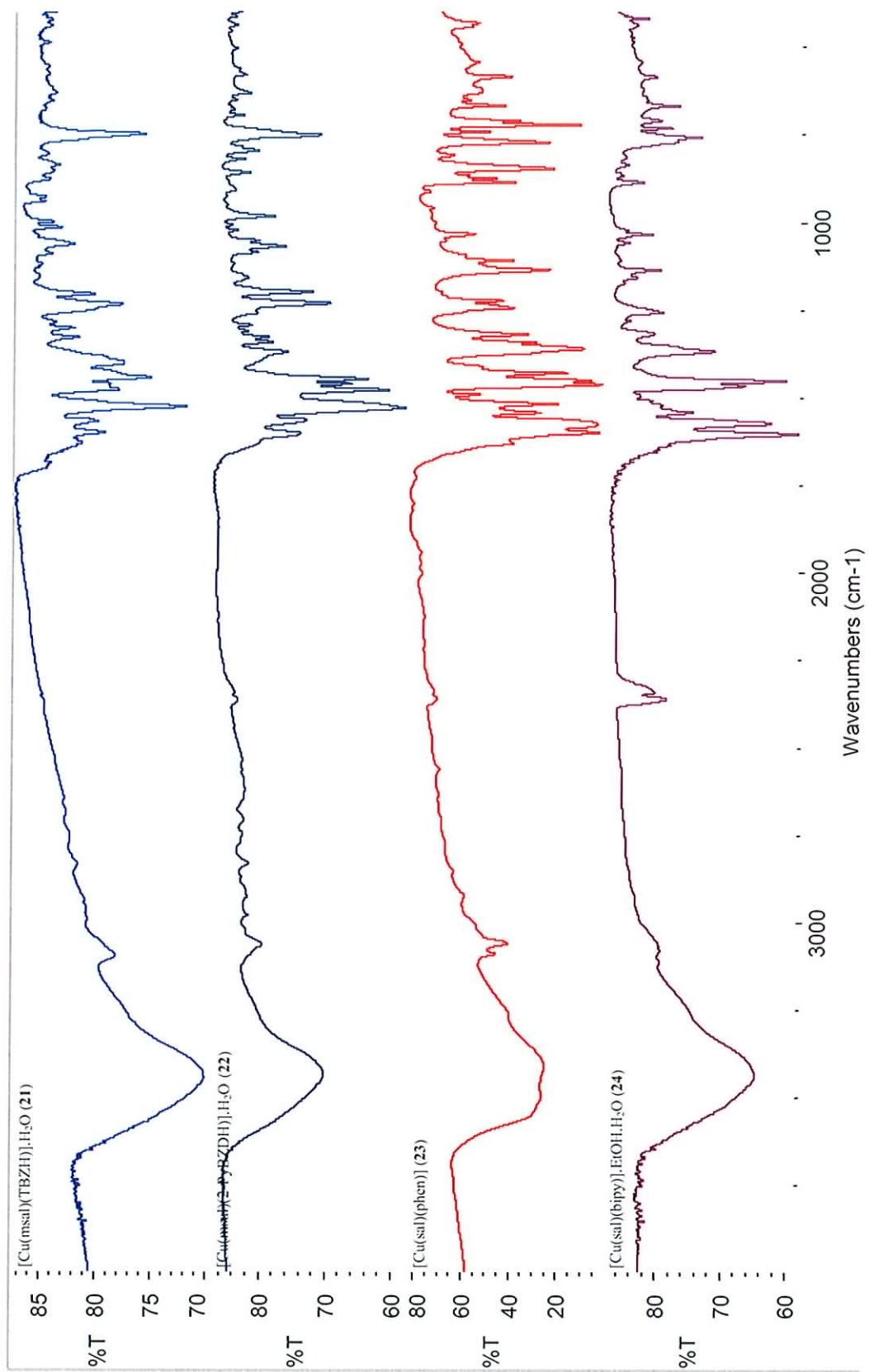
APPENDICES

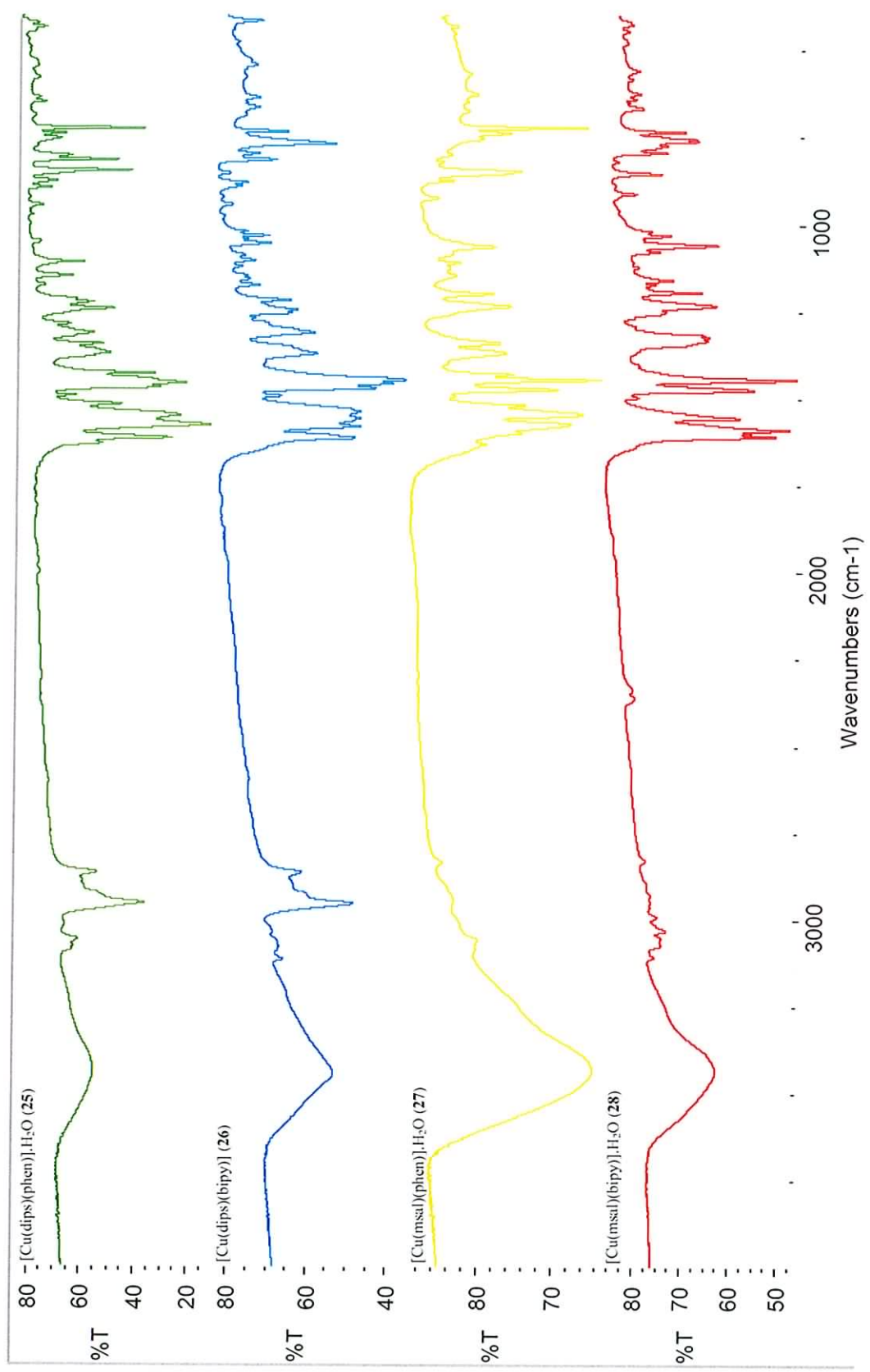


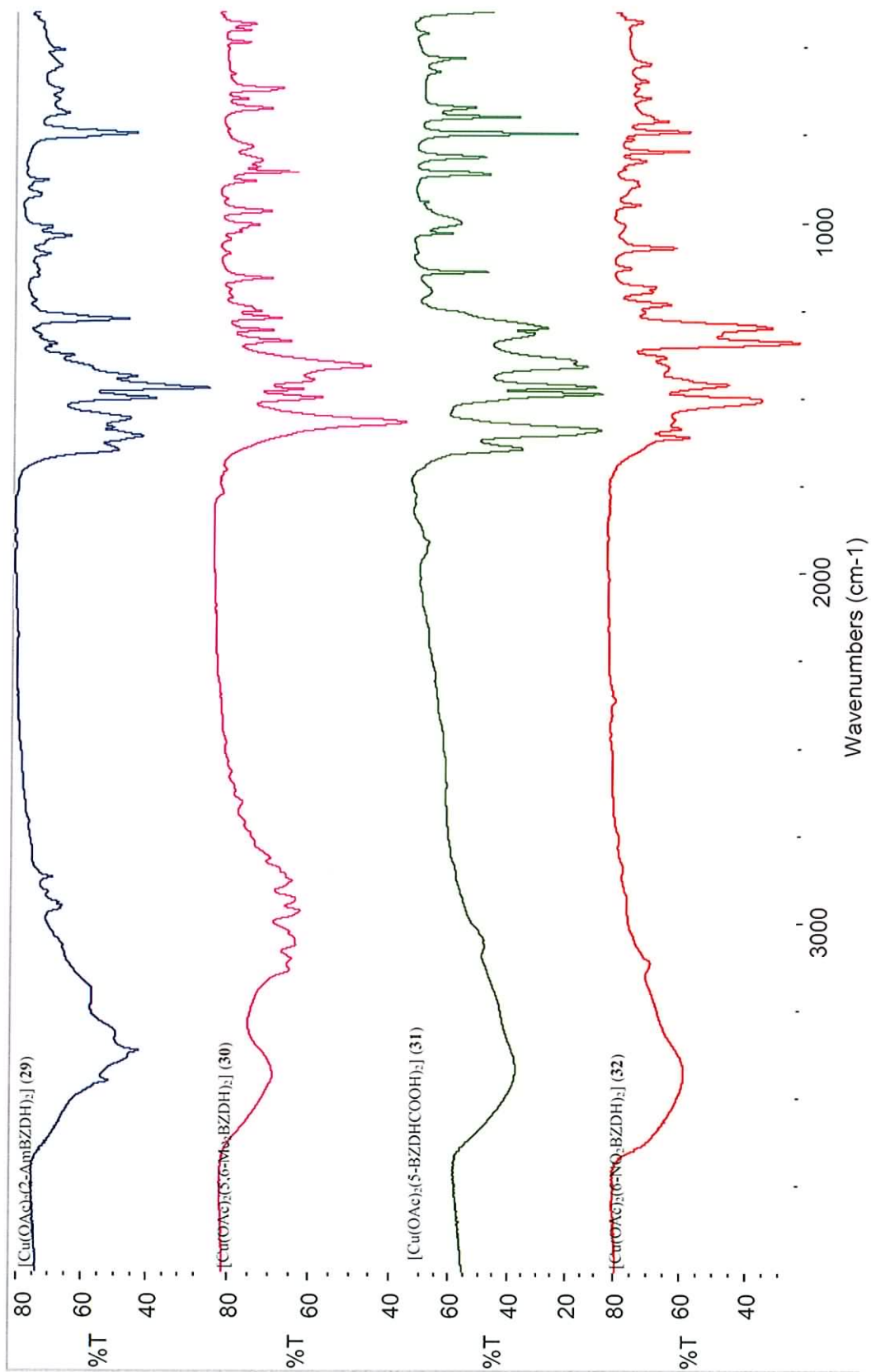


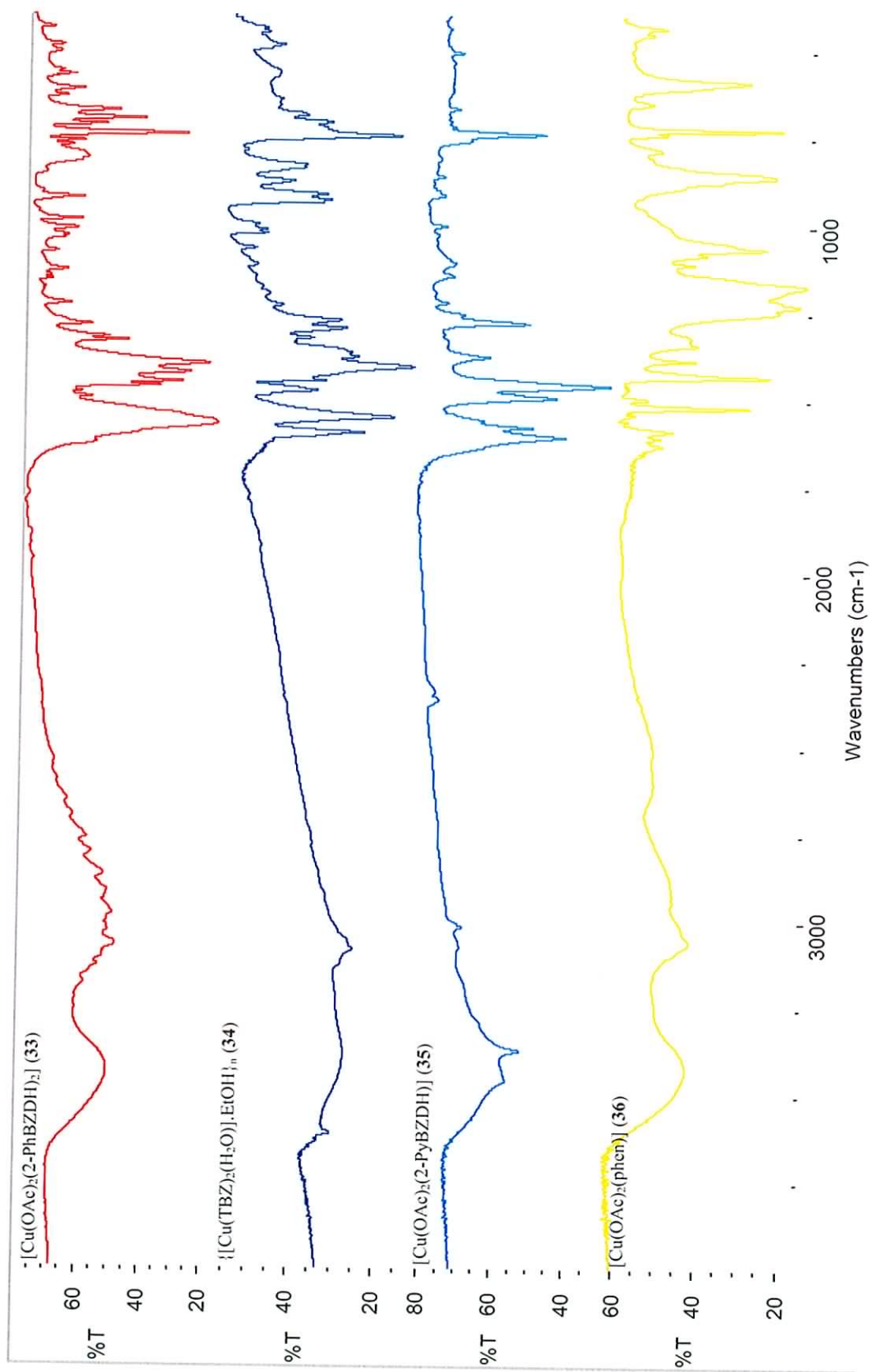


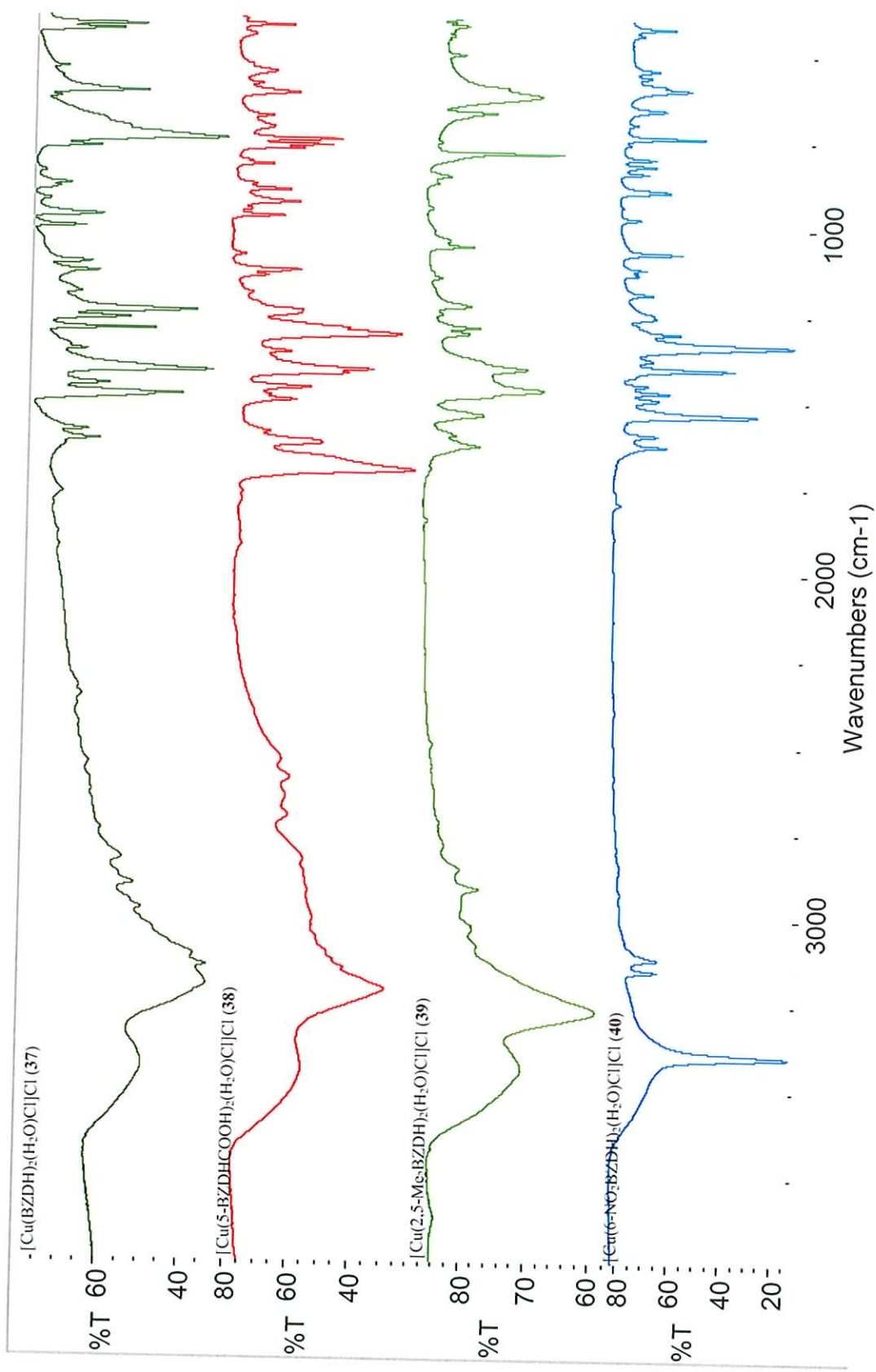


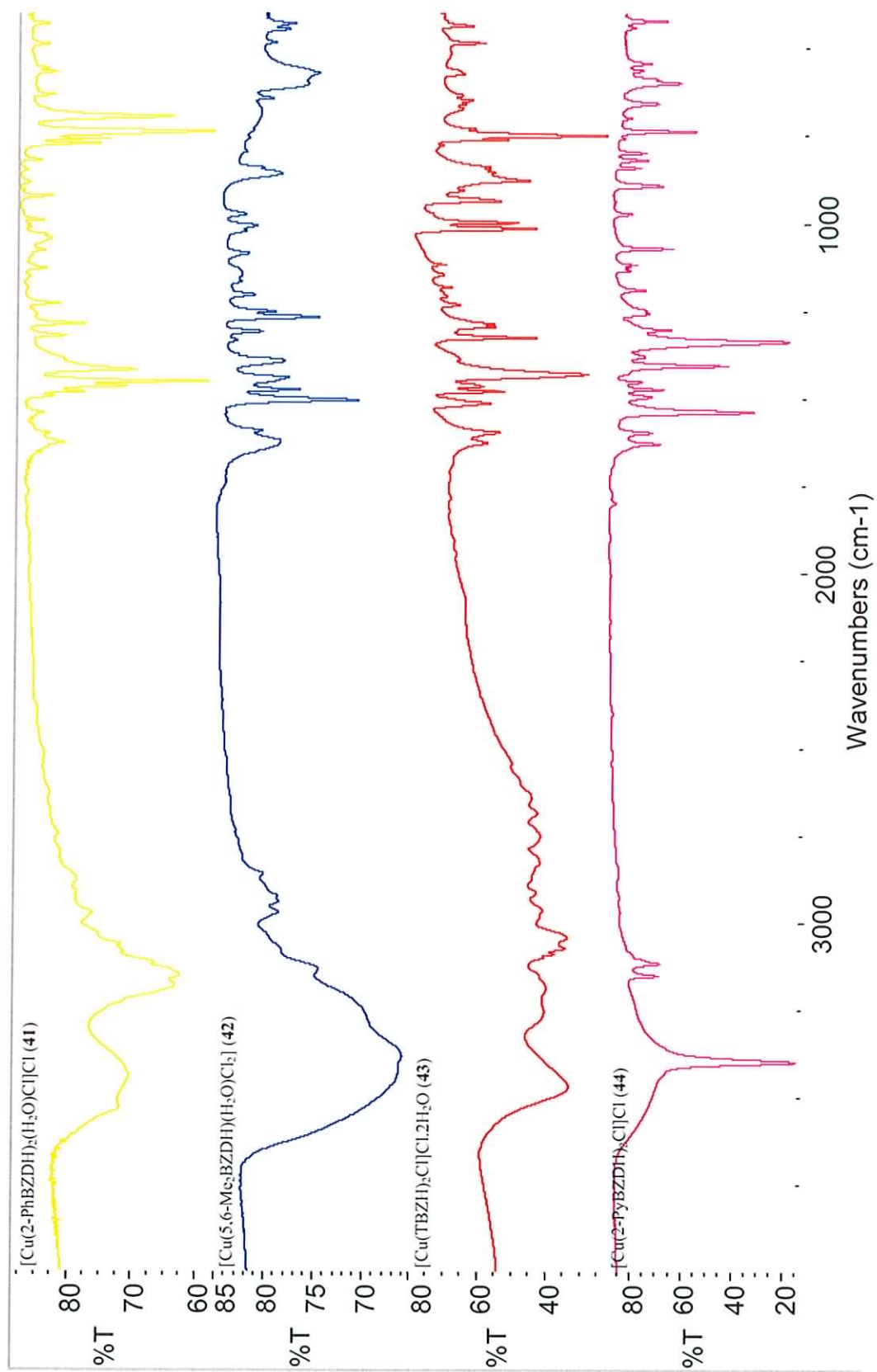


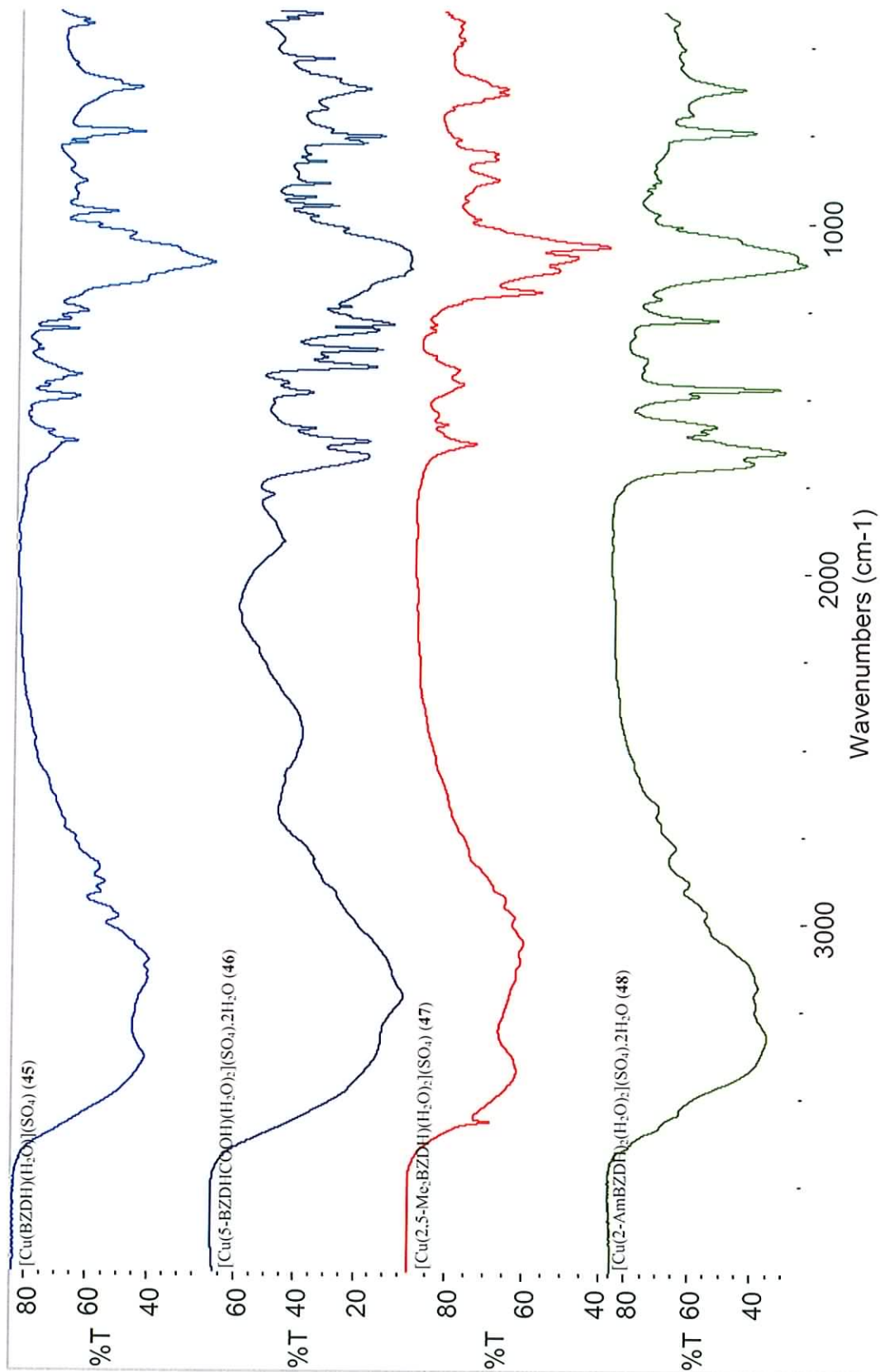


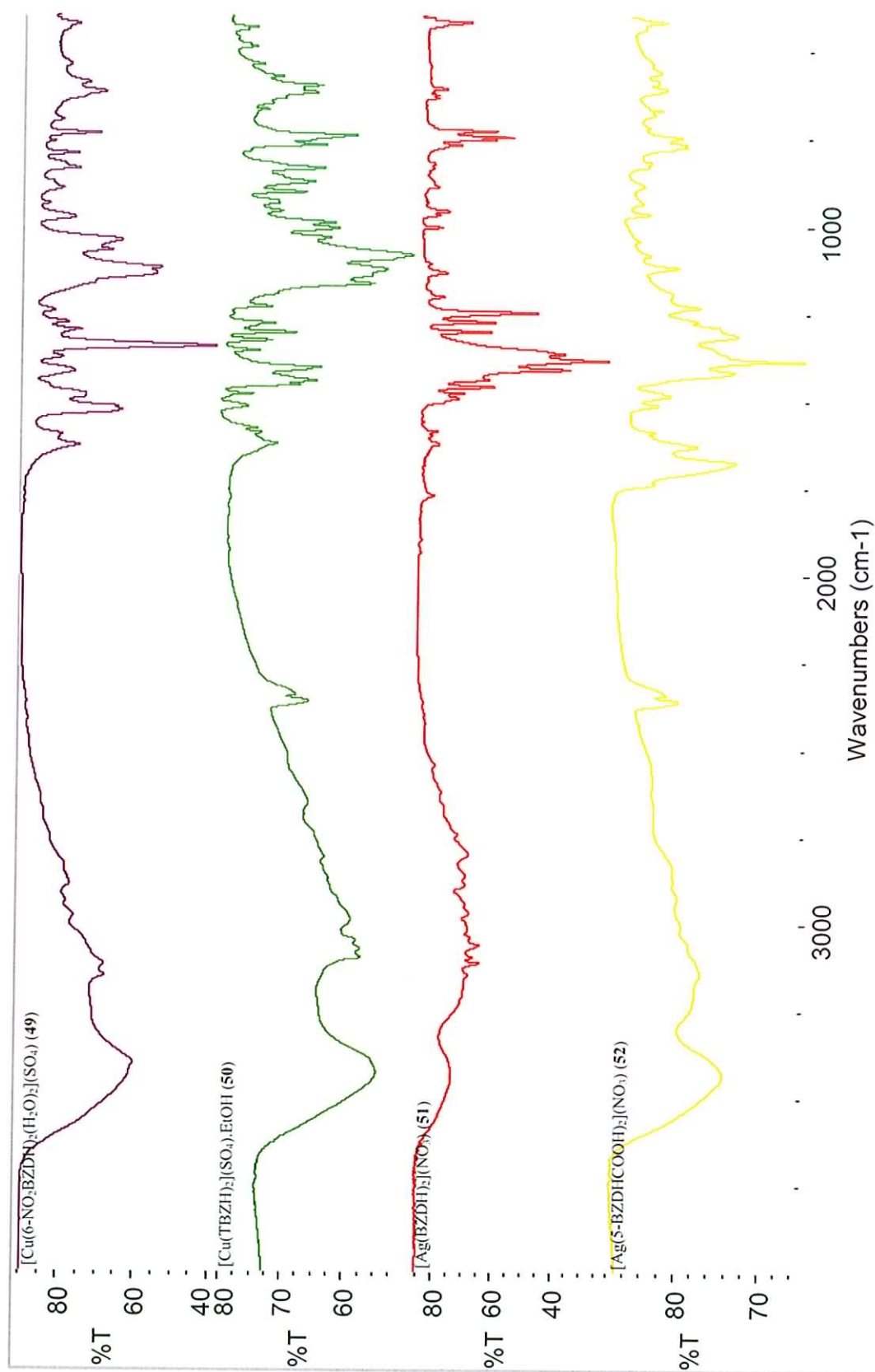


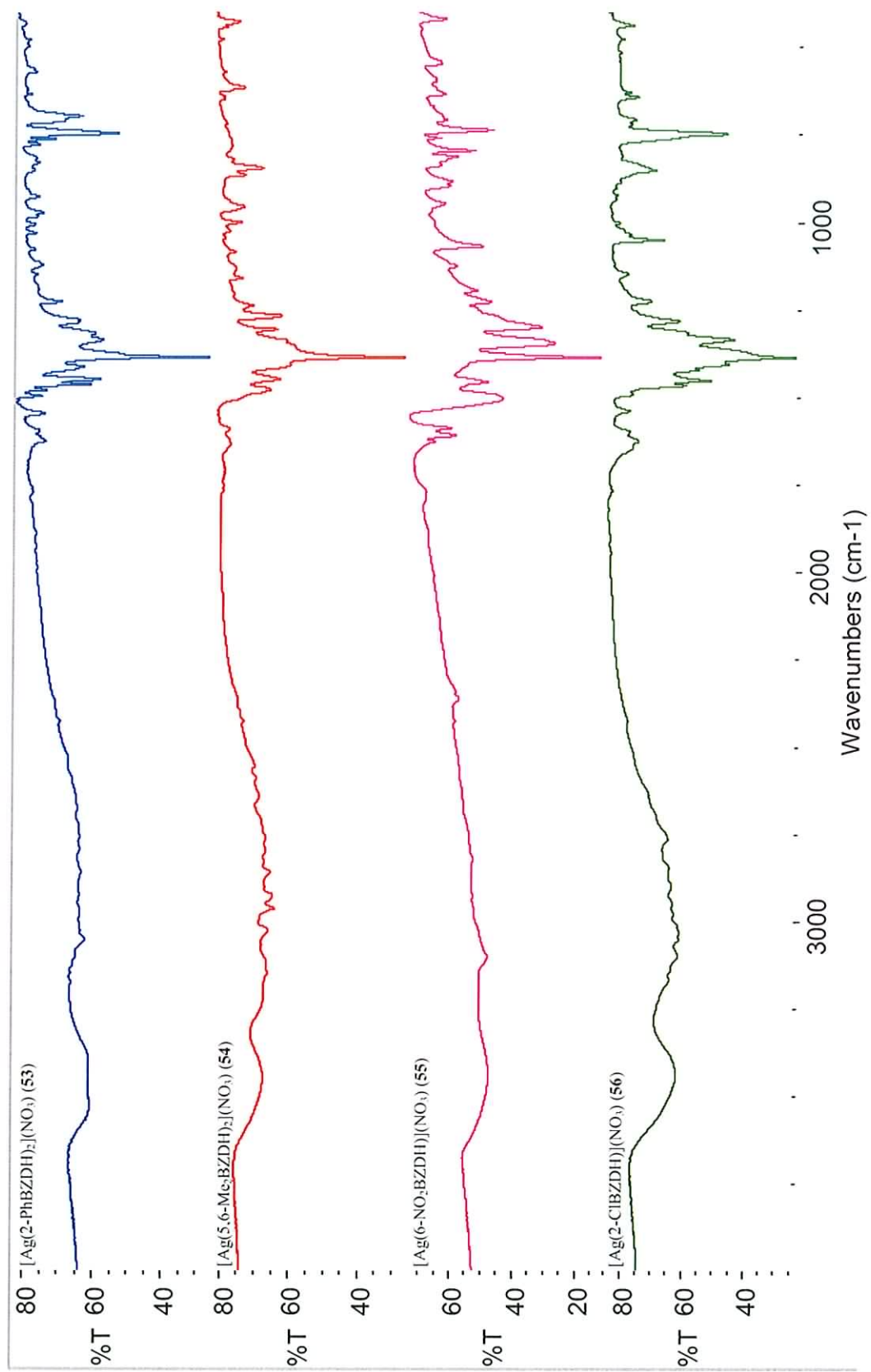


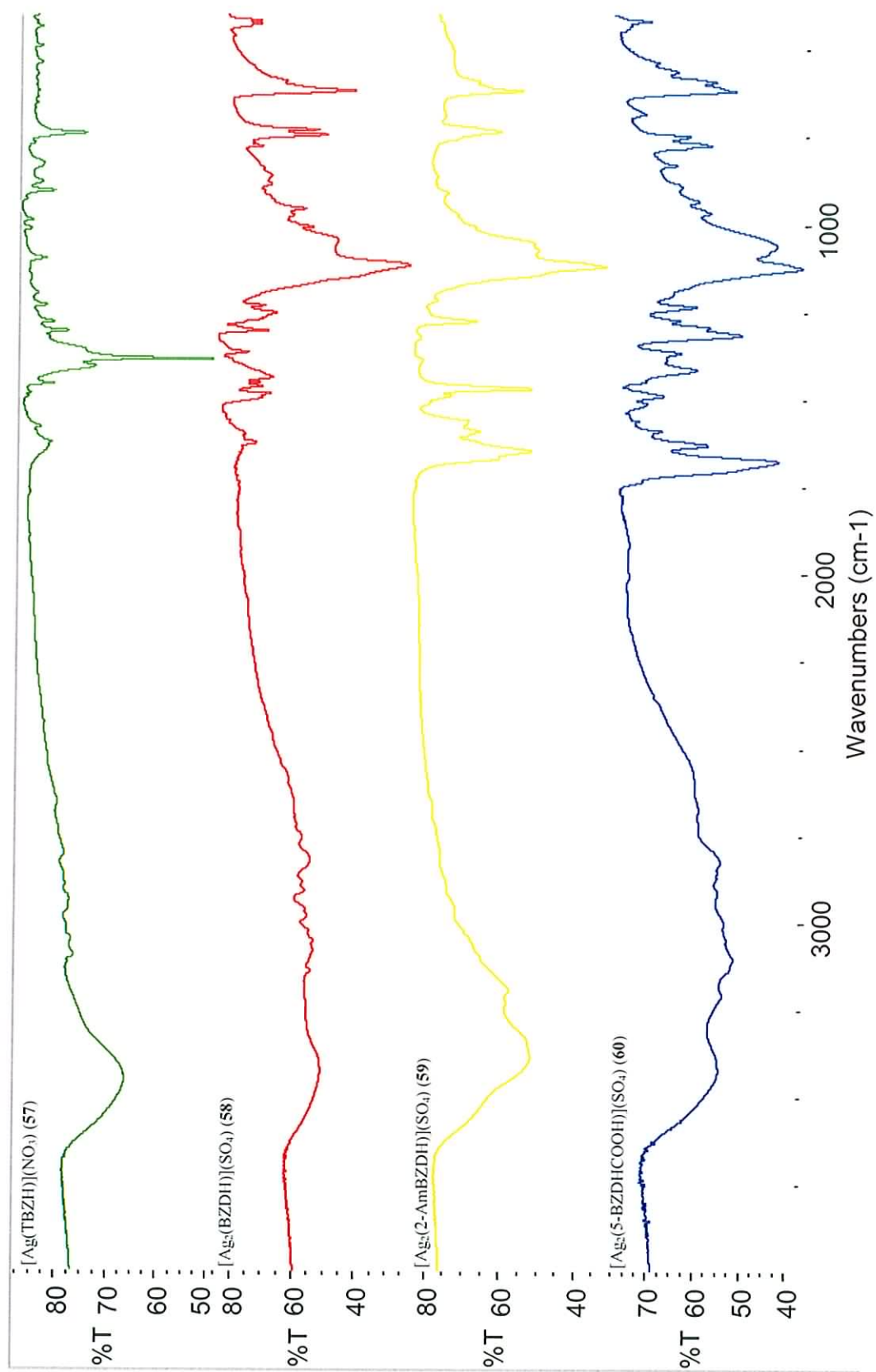


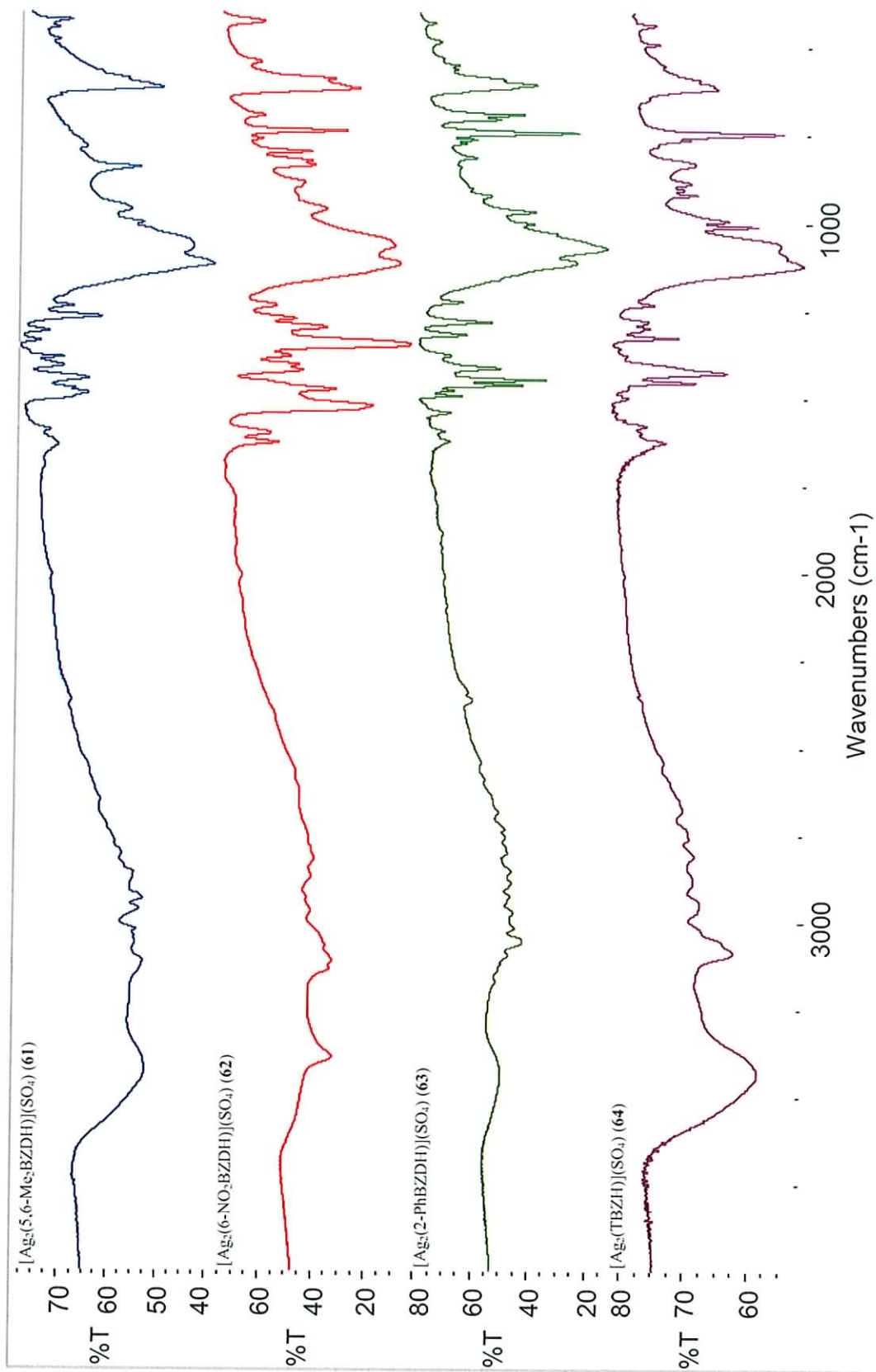


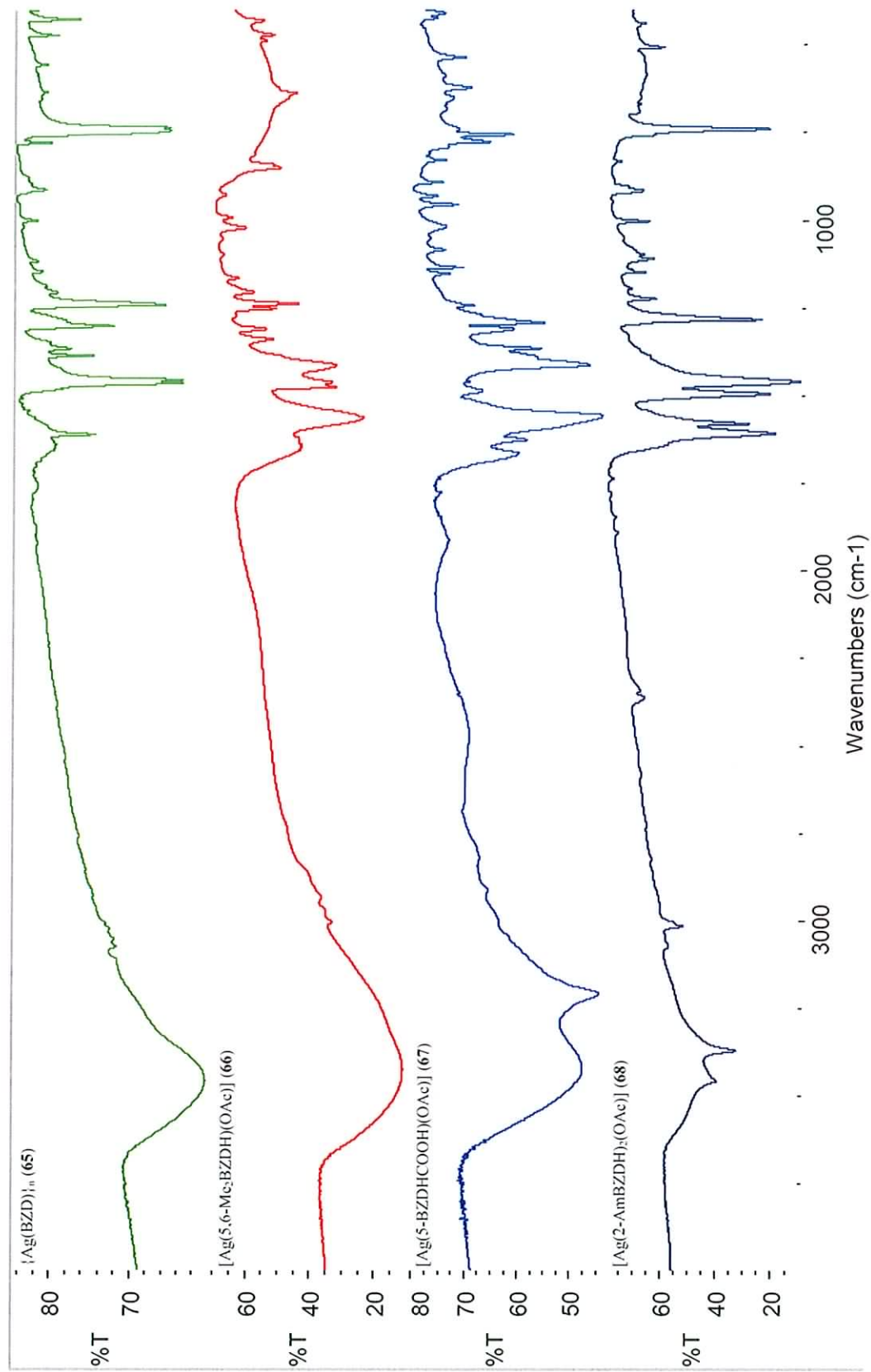


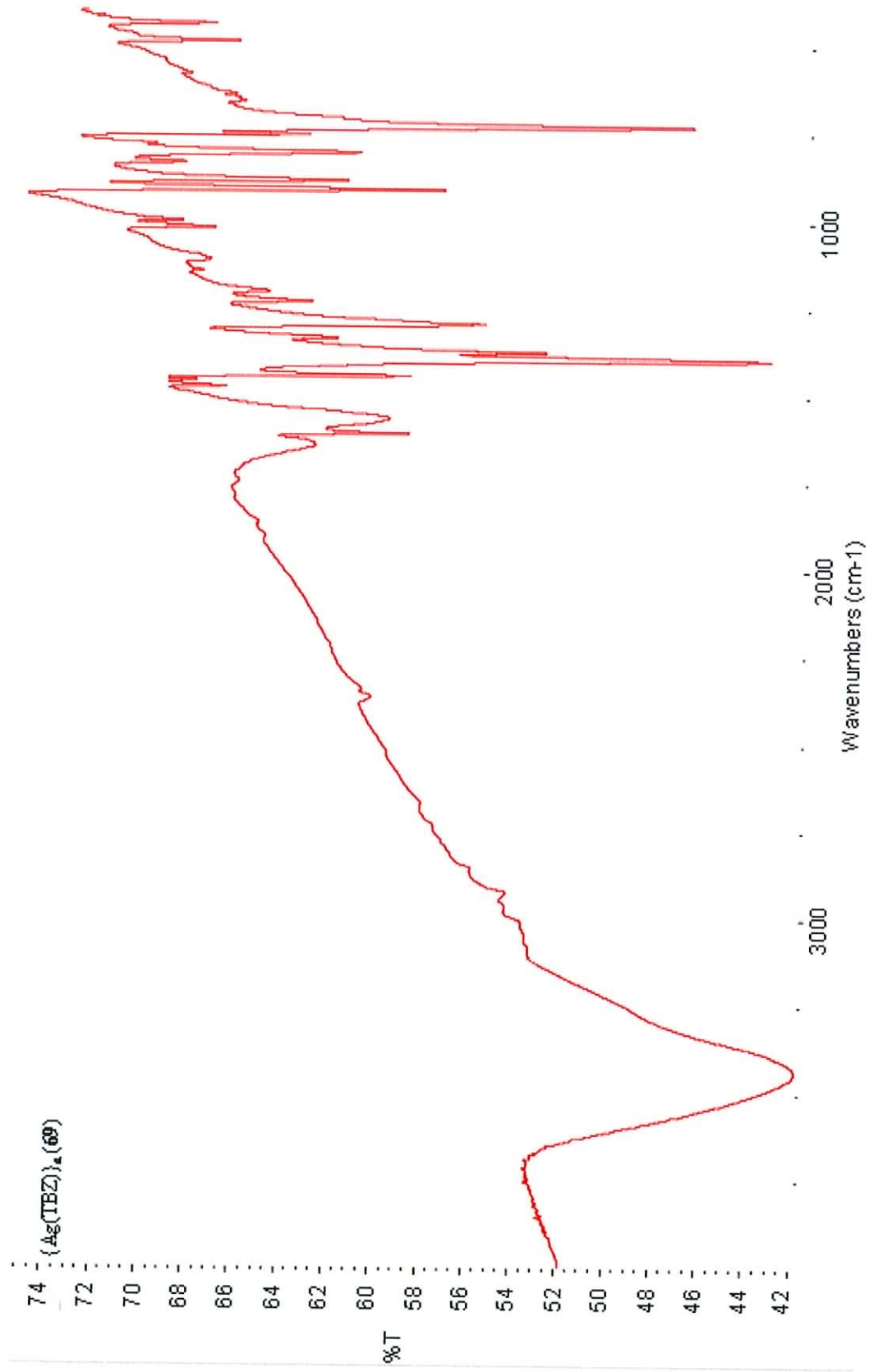












PUBLICATIONS

Papers:

Synthesis, X-ray crystal structures, catalase and superoxide dismutase activities of Copper(II) carboxylate complexes incorporating benzimidazole ligands.

M. Devereux, D. O'Shea, M. O'Connor, V. Dixit, M. McCann, G. Rosair Article in preparation for submission to *Polyhedron*,

Synthesis, catalase, superoxide dismutase and antitumour activities of Copper(II) carboxylate complexes incorporating benzimidazole, 1,10-phenanthroline and bipyridine ligands: X-ray crystal structures of $[\text{Cu}(\text{BZA})_2(\text{bipy})(\text{H}_2\text{O})]$, $[\text{Cu}(\text{SalH})_2(\text{BZDH})_2]$ and $[\text{Cu}(\text{CH}_3\text{COO})_2(5,6\text{-DMBZDH})_2]$ (SalH₂ = salicylic acid; BZAH = benzoic acid; BZDH = benzimidazole and 5,6-DMBZDH = 5,6-dimethylbenzimidazole).

M. Devereux, D. O'Shea, M. O'Connor, H. Grehan, G. Connor, M. McCann, G. Rosair, F. Lyng, A. Kellett, M. Walsh, D. Egan and B. Thati, *Polyhedron*, DOI: 101016/j.poly.2007.05.006

Synthesis, superoxide dismutase mimetic and anticancer activities of metal complexes of 2,2-dimethylpentanedioic acid(2dmepdaH₂) and 3,3-dimethylpentanedioic acid(3dmepdaH₂): X-ray crystal structures of [Cu(2dmepda)(bipy)₂] \cdot 7.5H₂O and [Cu(3dmepda)(bipy)₂] \cdot 5H₂O (bipy = 2,2'-bipyridine)

M. Devereux, M. McCann, D. O Shea, M. O Connor, E. Kiely, V. McKee, D. Naughton, A. Fisher, A. Kellett, M. Walsh, D. Egan and C. Deegan, *Bioinorganic Chemistry and Applications*, 2006, Article ID: 80283.

Conference Presentations:

Copper(II) Superoxide Dismutase Mimetics as Potential Anticancer Drugs.

M. Devereux, D.O Shea, M.O Connor, H. Grehan, G. Connor, M. McCann, D. Egan, B. Thati, F. Lyng and G. Rosair A poster presentation at the 59th University Chemistry Research Colloquium, Dublin City University June 2007.

Copper(II) and silver(I) complexes incorporating benzimidazole ligands: Synthesis and antimicrobial activity.

M. Devereux, D. OShea, M. O Connor, M. McCann, and G. Rosair. A poster presentation at The Chemical Synthesis and Chemical Biology Conference, University College Dublin, December, 2005.